Fabrication of Porous Particulate Scaffolds Using Electrohydrodynamics and Thermally Induced Phase Separation for Biomedical Engineering Applications

A thesis submitted in partial fulfilment of the requirements for the degree of

Doctor of Philosophy

By

Hanif Ghanbar

Department of Mechanical Engineering

University College London

Torrington Place, London WC1E 7JE

U.K

July, 2014

Declaration

I, Hanif Ghanbar, confirm that the work presented in this thesis is my own. Where information has been derived from other sources, I confirm that this has been indicated in the thesis.

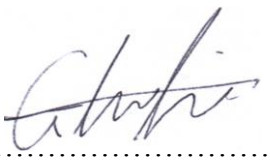

……..

Hanif Ghanbar

Abstract

The availability of forming technologies able to mass produce porous polymeric microspheres with diameters ranging from 150 to 300 μm is significant for some biomedical applications where tissue augmentation is required. Moreover, appropriate assembly of microspheres into scaffold is an important challenge to enable direct usage of the scaffolds in chronic wound treatments. In this thesis, the feasibility of the electrohydrodynamic (EHD) atomization forming combined with thermally induced phase separation (TIPS) for production of such drug delivery carriers, using biodegradable polymers (poly (lactic-co-glycolic acid) and poly (ε-caprolactone)) was explored. To achieve this goal, the first part of the thesis describes comprehensive parametric mode mappings of the diameter distribution profiles of the microspheres obtained over a broad range of key processing parameters and correlating this with the material parameters of five different polymer solutions of various concentrations. Based on the mode mapping studies, combination of poly (lactic-co-glycolic acid) (PLGA) and dimethyl carbonate (DMC) was found to be ideal for generating the microspheres within the targeted diameter range (150-300 μm). Surface porosity was achieved by electrospraying the PLGA/DMC solution and collecting the required size of the polymer particles in liquid nitrogen followed by lyophilisation. The second aim of this thesis was the *in vitro* release studies. In order to conduct this part of the study, the single needle and co-axial needle EHD/TIPS methods were used to generate the dye loaded microspheres of the required size. Three different dyes (Erythrosin B, Pyronin B and Reichardt's) were selected as model drugs to be encapsulated separately in the produced microspheres. The purpose of selecting three different dyes was to have a prediction on the release profile of immunosuppressants with high toxicity used for treatment of chronic wounds such as perianal fistulae. The *in vitro* release studies showed that the dyes were released with the high initial burst release phase in 3.5-5.5 hours followed by a long and sustained release phase (in 30-360 hours). Systematic investigations using different external stimuli such as temperature, fresh media and sonication exposure was also carried out to observe their effects on the release rate of the encapsulated materials from the produced microspheres. The results acquired from the *in vitro* release studies showed that the temperature variations and the sonication with different frequencies have significant effects on the release rates of the incorporated materials from the polymeric microspheres. Moreover, the results demonstrated that the products collected by the single needle EHD/TIPS method is more capable of releasing the payload in a longer period of time with more sustained manner compared to their counterparts obtained from the co-axial needle method.

Publications

Refereed Journal Papers

- Ghanbar, H., Luo, C. J., Bakhshi, P., Day, R., & Edirisinghe, M. (2013). Preparation of porous microsphere-scaffolds by electrohydrodynamic forming and thermally induced phase separation. *Materials Science & Engineering. C, Materials for Biological Applications*, *33*(5), 2488–98.

- Ghanbar. H., Deb S., Day R., Edirisinghe M., (2014). *In vitro* release studies of porous microsphere-scaffold formed by electrohydrodynamic forming and thermally induced phase separation (in preparation)

- Ghanbar. H., Day R., Edirisinghe M., (2014). The effect of modifications of the electrohydrodynamic forming and thermally induced phase separation on the *in vitro* release studies of the loaded microspheres (in preparation)

Conference Presentations

- Ghanbar H., Ahmad Z., Day R., Edirisinghe M., (2011). Preparation of coarse biodegradable polymeric microspheres for application in medicine, PhD Forum, Department of Mechanical Engineering, UCL, London, May 2011 (oral presentation and poster preparation)

- Ghanbar H., Day R., Edirisinghe M., (2012). Preparation of coarse biodegradable polymeric microspheres in form of scaffold for treatment of fistula. PhD Forum, Department of Mechanical Engineering, UCL, London, May 2012 (oral presentation and poster preparation)

- Ghanbar H., Day R., Edirisinghe M., (2013). Porous Microsphere-Scaffold for Chronic Wound Treatment. Material Research and Society Conference (MRS), San Francisco, USA (2014)

Participating in symposia

- Bubbles and Encapsulation, University College London, UK, April 2012

Acknowledgements

At the very outset my wholehearted thanks go to my primary supervisor, Professor Mohan Edirisinghe, for first of all accepting me under his wings as a research student at UCL and then for his continuous guidance, constructive criticism, confidence building and valuable support during the period of my study. I am delighted to have realised my ambition of doing this research under his mentorship.

My thanks are equally due to my second supervisor Dr. Richard Day for his trust, guidance, advice and great support throughout this research work. He is extremely patient, and always enthusiastic to teach with his great level of knowledge, and listen to my views. I feel extremely privileged to be jointly supervised by Prof. Edirisinghe and Dr. Day.

Continuous and invaluable support provided by my colleagues, Ms. Maryam Parhizkar, Mr. Panagiotis Sofokleous, Dr. Chaojie Luo, Dr. Zeynep Ekemen, Dr. Bhairav. Patel, Dr. Marjan Enayati, Dr. Muhammad-Rafique Nangrejo, Dr Poonam Bakhshi and Ms. Sumeyra Gun is unforgettable and many thanks to them. The lovely memories I have with these peoples will always be cherished. My dream of doing this research study wouldn't have been possible if not for the unparalleled understanding, love and support extended to me.

Last but not least, I would like to give a special thank to my parents, Dr. Khosro Ghanbar and Mrs Maryam Ghochkanlou, and my lovely sister, Ms Farinaz Ghanbar for their love, belief, support and help in the past years, without which I would not be brave enough to face this challenge in my life.

I would like to appreciate my beloved Fiancée who also supported, encouraged and guided me emotionally with her supreme peaceful and warm opened heart through this path of life. She is been one of the main motivations that I got this achievement.

Without these important people in my life, I cannot have these achievements.

Thank you all.

DEDICATION

To

My Parents;

Khosro and Maryam

And

my lovely sister; Farinaz

And Also

My beloved Fiancée; Saba

for their sacrifices and supports during the time of this research

Glossary of Abbreviations and Definitions

Cys A	Cyclosporine A
DMAc	Dimethyl Acetomide
DMC	Dimethyl Carbonate
DMF	Dimethyl Formamide
EDX	Energy Dispersive X-ray
EHD	Electrohydrodynamic
FTIR	Fourier Transform Infrared
KBr	Potassium Bromide
IM	Intramuscular
IV	Intravenous
PCL	Poly (ε-caprolactone)
PDI	Polydispersity Index
PEG	Polyethylene glycol
PEO	Poly (ethylene Oxide)
PGA	Poly Glycolic Acid
PLA	Poly Lactic Acid
PLGA	Poly (Lactic-Co- Glycolic Acid)
PMSQ	Polymethylsilsesquioxane
SBF	Simulated Body Fluid
SC	Subcutaneous
SEM	Scanning Electron Microscopy
TIPS	Thermal Induced Phase Separation
UV	Ultraviolent
W/O	Water-in-Oil
W/O/W	Water-in-Oil-in-Water

Monodisperse	Uniform Size
Polydisperse	Non-Uniform Size
Particle	Sphere
Capsule	Hollow Sphere

Tables of Contents

Chapter 1

Introduction and Background

Chapter 2

Literature Review

Chapter 3

Experimental Work

Chapter 5

Conclusions and Future Work

List of Figures

List of Tables

Chapter 1

Introduction and Background

1.1 Background

The first procedure of microencapsulation was conducted in 1931 by Bungenburg de Jong and Kaas for the preparation of gelatin microspheres (Bungenburg de Jong and Kaas, 1931). Later on, in 1950s, Green *et al.* of National Cash register Co., Dayton Ochio developed a microencapsulation dye for the manufacture of carbonless copying paper which ultimately resulted in several patents and made the microencapsulation more common (Green and Schleicher, 1957; Green, 1955). Since then, and particularly since mid-1970's microencapsulation has become more effective and popular in the pharmaceutical industry as well as for many other products and processes in daily use such as food production. Encapsulated products now available include liquid crystals, adhesives, perfumes and fragrances, cosmetics, insecticides, algaecides, fertilizers, washing powders as well as animal feed stocks, tissue mimicking materials and medicinal products, and insulation materials (Arshady, 1990; Schmidt and Roessling, 2006). Such products have diameters varying between 50 nm and 1mm with a solid, liquid or gaseous phase. The wall material can be constructed from surfactants, glasses, oxide ceramics, polymers, mixed oxides or even metals (Bertling et al., 2004; Gaponik et al., 2004). The main motivating factors for encapsulation are taste and odour masking, separation of incompatible components, protection from immediate environment, modification of impact strength, alteration of colloidal and surface properties, prolonged action or sustained release of drug/agent, targeted release and enhanced biocompatibility (Arshady, 1989).

For applications in medicine and pharmaceuticals, there is a growing interest in the use of particles as drug delivery carriers and in the synthesis of artificial cell structures (Bertling et al., 2004; Botchwey et al., 2004). Both micro- and nano-particles can be used therapeutically. For instance, particles loaded with an entrapped therapeutic agent can transport the substance through blood vessels and then release their load at a target area (Panyam and Labhasetwar, 2003). However, the preparation of effective and operative drug delivery systems still represents an important continuing challenge in biomedicine (Mathiowitz et al., 1997). The

purpose in designing an ideal drug carrier is to attain sustained and controlled release which can decrease the fluctuation and variation of drug dosage and maintain the concentration of drug to a constant level over the designated treatment period in order to optimize the effectiveness of the therapeutic agent (Luan et al., 2006; Yang et al., 2001). In particular, the aim in designing an ideal drug delivery system is to minimize the drug degradation and loss, to prevent harmful adverse-side effects and to maximise drug biological activity and the percentage of the drug accumulated in the required zone. Therefore, various preparation methods have been investigated over the years with a view to generate drug carriers which can be tailored to achieve these goals (Freitas et al., 2005; Yang et al., 2001).

Spherical particles play a crucial role in encapsulation of various materials and have been used for a wide range of biomedical applications (Li et al., 2004; Peng and Zhang, 2005). Polymeric spheres are of particular interest, since they provide characteristics such as high surface-to-volume ratio, low density, and low coefficient of thermal expansion (Lou et al., 2008). Control of the internal and external morphology of the spheres can be used to influence their interactions with the encapsulated drug as well as the microenvironment after their delivery into the body (Moon and Jeong, 2008). Encapsulation of drug in biodegradable polymer carriers offer the possibility of drug to be released in a controlled manner which can help to maintain a constant therapeutic concentration between the toxic and minimum levels in body fluids over the period of treatment following administration (Sinha and Trehan, 2003). Recently near monodisperse microspheres with surface porosity have received much attention and been classified as a new category of particles on the account of their higher effective diffusivity and available surface area compared to their counterparts with smooth morphology of same size (Jeong et al. 2007; Yow and Routh 2008; Yin and Yates 2008). Porous microspheres have also showed a higher rate of *in vitro* drug release owing to the porous membrane, which is more suitable for targeted delivery and chronic wound therapy (Enayati et al., 2010a; Setterstrom et al., 1984).

Common methods able to generate drug-encapsulated polymeric microspheres include emulsion polymerization, phase separation and spray-drying. However, there are some definite disadvantages with these methods (Kissel et al., 1996; Konishi et al., 2003; Okubo et al., 1998; Zhang et al., 2003). For example, emulsion polymerization produces polydisperse microspheres with a broad size distribution profile (Fujiwara et al., 2012; Kissel et al., 1996). Non-degradable additives such as surfactants or polymers are also typically required as emulsifiers (Freitas et al., 2005). Residual solvent toxicity is another issue and the purifying

process to separate the microspheres from the solvent is slow and costly for pharmaceutical applications (Luan et al., 2006). Most importantly, due to exposure of drug, for instance, to elevated temperatures and high shear stresses in the emulsion method, the biological activity of the drug can be significantly reduced during processing (Kohane et al., 2006; Rasiel et al., 2002; Vandervoort and Ludwig, 2002). Phase separation technique can also generate microspheres with rigid outer surfaces and a long shelf life. However, the method requires time-consuming multiple processing stages, and suffers from poor control over the diameter distribution of the fabricated spherical particles. In addition, the particles often stick to each other during formation and before the completion of the processing stages, resulting in large aggregates (Arshady, 1990; Nihant et al., 1995). Spray-drying is another robust particle generation method, and the processing conditions to control the generated microsphere diameters are relatively straightforward. However, solvent removal is an issue in spray-drying, which often results in producing large aggregates. In addition, a large number of spherical particles are often lost during production due to sticking to the walls of the spray drier (Blanco-Príeto et al., 2004; Burke et al., 2004; Murillo et al., 2002).

Electrohydrodynamic (EHD) atomisation is an attractive, alternative method for the generation of near monodisperse micro- and nano-spheres for applications in drug delivery systems (Ding et al., 2005; Pareta and Edirisinghe, 2006). A versatile method able to process multiple solutions and emulsions of different polymers and/or therapeutic agents under ambient conditions, it is a single-stage production process for drug encapsulation with the flexibility to monitor the product quality at any time without delay during the production stage, without affecting the continuity of the process or having to wait for a multi-stage production process to complete before inspection (Enayati et al., 2010a; Wu and Clark, 2007; Xu et al., 2006).

The EHD process subjects a liquid to a high electric field (potential in range of kilovolts), which causes charges to build up within the liquid. When the applied electrostatic force overcomes the surface tension of the liquid, the meniscus of the liquid held at the tip of a nozzle elongates into a conical shape and a fine jet generates from the apex of the cone. The jet subsequently breaks up and deposits on an electrically grounded collector as fine spherical particles (Luo et al., 2011). Stable cone-jet is the most desirable electrohydrodynamic jetting condition for production of near monodisperse spherical particles (Luo et al., 2011). The mean sphere diameter generated can be varied from tens of nanometres up to hundreds of micrometres by changing the EHD processing parameters such as nozzle diameter, flow rate and applied voltage as well as solution properties, e.g. viscosity, surface tension and electrical

conductivity of polymer solution (Ahmad et al., 2008; Samarasinghe et al., 2007; Xie et al., 2008; Yeo et al., 2005). To maintain a stable cone-jet, the rate of mass transfer to the nozzle exit (controlled by the liquid flow rate) should be coupled and balanced by that out of the nozzle (controlled by the applied voltage, which is responsible for the force causing jet formation). Therefore, the flow rate and the applied voltage used for each polymer liquid should be carefully coupled within a defined range (Xie et al., 2008).

Biodegradability is one of the key features of drug delivery carriers (Burton et al., 2000). The elimination of an inactive material by a natural process is preferred over surgical removal of a drug delivery system which may lead to presence of non-biodegradable foreign debris inside the body for an indeterminate period of time. Biodegradable polymers are suggested as the most promising materials for drug encapsulation in developing drug delivery systems for sustained and controlled release of drugs. A number of polymers with different properties have been investigated in EHD for their potential applications in drug delivery systems. However, only a few of them such as poly (ε-caprolactone) (PCL) and poly (lactic-co-glycolic acid) (PLGA) have been extensively used due to their biocompatibility, biodegradability and versatile degradation kinetics (Burton et al., 2000; Körber and Bodmeier, 2008). PLGA co-polymers have higher rate of bio-erosion by hydrolysis under physiological conditions compared with PCL as they contain more ester groups per polymer molecular chain (Chen, 2010). The biodegradation products of these two polymers have been shown to be non-toxic, non-immunogenic (not causing immune response), non-teratogenic (not causing malfunction of foetus or embryo) and non-carcinogenic (not causing cancer) (Ravivarapu et al., 2000). Furthermore, the composition of these polymers can be changed in order to obtain a desirable release profile based on the rate of hydrolytic degradation. For these reasons, these two polymers have attracted significant research in the development of drug delivery systems (Jain, 2000) and are selected in this investigation.

Over the past decade, the drug release characteristics of polymeric carriers encapsulating various drugs using different techniques have been studied (Avgoustakis, 2004). However, there are still relatively few attempts to modulate and manipulate the drug release profiles. There are two features of polymeric drug delivery systems that require particular attention. First is the initial burst release phase which can be both desirable and/or undesirable depending on biomedical applications. This phase, which mostly relies on the morphology of generated particles, occurs during the first 24 hours of the administration. Second is the ability to modify the *in vitro* release profile in order to achieve a stable manner of drug release. This type of

release profile can be achieved by controlling the drug release through external stimuli for example exposure to sonication, or applying different temperatures.

Sonication and temperature have many applications in medicine. Sonication in form of ultrasound is mostly adopted for diagnostic imaging (Moore and Promes, 2004). However, recently, it has been used in drug delivery systems for stimulating drug release process (Mitragotri et al., 1995). In ultrasonically stimulated systems, the acoustic waves enhance the degradation of the loaded polymeric carrier in order to stimulate the drug release. For example, in the work conducted by Miyazaki *et al.*, it was found that ultrasonic waves could cause a sharp drop in blood glucose level right after it was administered to an insulin loaded ethylene vinyl alcohol copolymer system (Miyazaki et al., 1988). Temperature is another effective factor in release studies and has been used for stimulating drug release processes. In the study conducted by Reddy *et al.* it was found that the drug release rate is dependent on temperature of the medium (Umamaheswara Reddy et al., 2007). Variations in temperature can lead to more controlled manner of drug release depending on the chemical properties of drug and its carriers. For example, in the study of Shi *et al.*, more controlled release of the encapsulated agents (Ca-alginate and poly(N-isopropylacrylamide)) in hydrogel beads was observed at lower temperature (25^{o}C) compared to higher degrees (37^{o}C) (Shi et al., 2006), whereas in the study of Lin *et al.*, more controlled release of the drug from the ethylene vinyl acetate (EVA) was found at higher temperature (37^{o}C) compared to lower temperature (24^{o}C) (Lin et al., 2003).

1.2 Objectives of the Project

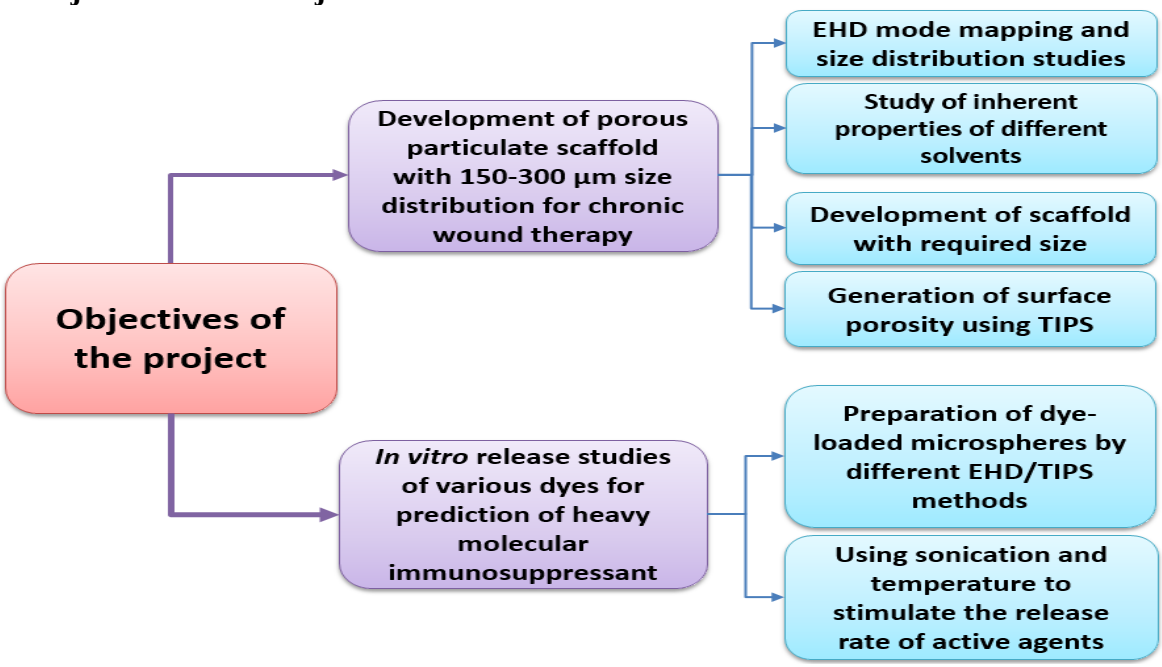

Figure 1.1: Objectives of the research presented in this thesis

The flow chart in **Figure 1.1** displays the key objectives of this thesis. The details regarding each objective is briefly discussed below.

1.2.1 Production of Polymeric Particles Using Single Needle EHD Method

The first main objective of this project was to generate microspheres with porosity on the outer surface in order to develop free flowing scaffold for treatment of chronic wounds. The size distribution of spheres for the formation of scaffold structure was in the range between 150 µm and 300 µm. To meet this objective, the feasibility of the single needle EHD method for fabricating the required size distribution of the microspheres via a single step was investigated as follows:

1.2.1.1 EHD Mode Mapping and Size Distribution Studies

The first aim was to investigate the fundamental ability of the single needle EHD processing in having the control over the particle size, size distribution and shape of the products for preparation of polymeric carriers. It was determined how the size and size distribution of the particles fabricated can be systematically controlled through a range of various operating parameters: flow rate, applied voltage and the inherent properties of the solution such as viscosity, surface tension and electrical conductivity. It was demonstrated that how variations in these parameters affect the jetting mode and the desired stable cone-jet mode can be obtained. For this part of study, different biodegradable polymers (PLGA (33000 g/mole) and PCL (10000 and 45000 g/mole)) were used, and their polymer solutions were electrosprayed at different flow rates and the applied voltages, and the spherical particles with various size distributions were prepared. After these extensive studies, the ideal set of processing parameters for obtaining the required size distribution of PLGA polymer particles were obtained.

1.2.1.2 Fabrication of Porous PLGA Microspheres

Based on the results acquired from the EHD mode mapping and size distribution studies, the ideal set of processing parameters were determined for production of the PLGA microspheres with the required size distribution (150-300 µm). Then, surface porosity was generated by electrospraying the required size of the microspheres in liquid nitrogen followed by freeze drying process. The purpose of surface porosity was to obtain higher rate of drug release for

this particular biomedical application. Although, this has been a challenge in drug delivery system to control the initial burst release phase, this can have a significant application, in particular, in chronic wound therapy (Setterstrom et al., 1984). There is increasing evidence that particles with varying shape and size may play a significant role in the effectiveness of drug delivery and other biomedical interventions (Champion and Mitragotri, 2006; Gratton et al., 2007). However, in this study, the most work has focused on producing near monodisperse microspheres, as this type of microspheres has been considered to provide free flowing scaffold with large enough interstices between them for treatment of chronic wound.

1.2.2 Production of Loaded PLGA Microspheres

Production of particles with narrow size distribution is of particular interest in biomedical engineering (Kissel et al., 1996; Vonarbourg et al., 2009; Zhu et al., 2000). Research on the encapsulation of various therapeutic agents by efficient methods is significant for fabrication of advanced products with different core, targeting behaviour and release profiles (Luan et al., 2006). Since, the EHD method has shown to be a promising technique for fabrication of drug delivery carriers with a required size range, the next objective of the project was to encapsulate therapeutic materials into the PLGA particles.

Cyclosporine A (Cys A) and Tacrolimus are usually prescribed as antimicrobial agent for treatment in early stage of chronic wounds such as Crohn's disease-associated fistula (Ptachcinski et al., 1986; Sheng-Tanner et al., 2000). Since, this type of drugs has huge side effects such as neuro- and nephrotoxicity in the human body, they could not be used for *in-vitro* drug release studies in the first and/or second class laboratories. Thus, in order to fulfil this objective, Reichardt's dye, erythrosin B and pyronin B were selected as model encapsulated materials to show the feasibility of the encapsulation process. The selection criteria was based on covering the range of molecular weight and water solubility of the actual drugs, as these two properties play important role in *in vitro* release profile.

The encapsulation process was carried out via the single needle and the co-axial needle EHD/TIPS methods. The results obtained from both methods were then compared in order to find a suitable EHD process for drug encapsulation. This study successfully confirmed the feasibility of EHD processing (the single needle and the co-axial needle) as a technique for producing drug-loaded particles.

1.2.3 *In Vitro* Release Studies

As discussed in **Section 1.2.1**, the main objective was the fabrication of drug loaded microspheres with required size and surface porosity. Single needle and co-axial needle EHD methods showed the ability for generation of such microspheres, and then combined with thermally induced phase separation (TIPS) process, the surface porosity was achieved. The second main objective was an in-depth study of the release profile of these carriers based on the effect of different parameters such as temperature and the sonication exposure on the release characteristics. However, the overall aim was to predict the release profile of immunosuppressants that have high molecular weight and low water solubility.

1.2.3.1 Temperature Stimulated Release

The final objective was to observe the release characteristics of the model drugs at various temperatures. Since, initial burst release can be an advantage in drug delivery systems for chronic wound treatments, the effect of heat on this release phase of the model drugs was also investigated. The results showed that heat may affect the release characteristics of the incorporated materials, and depending on the chemical properties such as evaporation and degradation rates, it can lead to either higher or lower release rate.

1.2.3.2 Sonication Stimulated Release

The other final objective was to observe the release characteristics of the encapsulated dye upon sonication exposure. As discussed before, the initial burst release of the encapsulated agents in conjunction with the application of sonication was also studied. The results showed that sonicator responsive drug delivery has great potential in releasing the payload from their carriers with higher rate. Systematic investigations were carried out to determine the effect of sonication exposure parameters such as duty cycle and exposure time on the release rate of the encapsulated agents from the PLGA microspheres.

1.3 The Structure of the Thesis

Chapter 1 provides the background information about the research project and gives an overview about the basics of electrohydrodynamic atomization and other related techniques which are adopted for generation of micro- and nano-spheres for drug encapsulation. The

objectives of the research are then stated and the organization of this thesis and the scope of the research are outlined.

Chapter 2 presents a detailed literature review. Since, the aim of the project is to prepare porous microspheres using combination of EHD and thermally induced phase separation (TIPS) method, an extensive collection of literature reviews has been surveyed to understand the principles of electrohydrodynamic atomization, the procedure and its usage, as well as materials and other methods adopted for the preparation of polymeric carriers. Furthermore, a literature review has been presented on micro and nano particulate drug delivery systems for applications in medicine and treatment of chronic wounds such as fistulae using different methods of product fabrication.

Chapter 3 describes the experimental setup, modification process, materials adopted, experiment and characterization procedures conducted, and a detailed description of the experimental tools employed.

Chapter 4 explains the results acquired from the experimental work. This chapter contains two main parts: 1) the EHD mode mapping and size distribution studies, and 2) the *in vitro* release studies. The results in this chapter is discussed in detail in conjunction with the existing literature review. The EHD mode mapping and size distribution studies has three main sections. In **Section 4.1**, different concentrations of PCL and PLGA solutions are used to show the feasibility of the single needle EHD method in fabrication of polymeric microspheres with different size ranges. Different modes of EHD processing are also studied and classified. Furthermore, the effect of different parameters such as applied voltage, flow rate, viscosity and electrical conductivity are studied on the size, size distribution of spheres, polydispersity index and also the mode of cone-jet. **Section 4.2** demonstrates micrographs of the produced spherical particles for EHD mode mapping and size distribution studies. **Section 4.3** of this chapter states how the combination of single needle EHD and thermally induced phase separation (TIPS) method can be adopted for mass production of the required size distribution of microspheres with porosity on the outer surface for treatment of chronic wounds such as perianal fistulae.

Chapter 4 also describes the release profiles of the dye loaded PLGA microspheres obtained from the single needle and the co-axial needle EHD/TIPS processes. The *in vitro* release studies has five main sections. **Section 4.5** focuses on the internal and morphological structure of the products collected from the single needle EHD/TIPS process, and then they are compared to those obtained from the co-axial needle EHD/TIPS method. **Sections 4.6** and **4.7** are provided

to show the presence of the dyes encapsulated in the microspheres produced by different EHD/TIPS methods. **Section 4.8** focuses on the yield of the process based on the collection of the products. In this section, the percentage yield of the modified co-axial process in comparison with the modified single needle process is briefly discussed. In the next section (**Section 4.9**) of this chapter, the *in vitro* release profile of loaded microspheres from the co-axial needle technique are described and then they are compared to those obtained from the single needle method in order to discover the suitable process for encapsulation and drug delivery. This section also provides a prediction for the release profile of immunosuppressive agents with high molecular weight and low water solubility based on the release profiles obtained from using model drugs with various chemical and physical properties. The final section of this chapter is also dedicated to the effect of external stimuli such as temperature and sonication exposure on the release rate of the encapsulated materials from their polymeric shell for obtaining more efficient release profile.

Chapter 5 is divided into two sections. **Section 5.1** summarizes the experimental results and presents the conclusions of the work, whereas **Section 5.2** discusses some recommendations for future work, employing EHD combined with TIPS processing and beyond, to continue the research presented in this thesis in new directions. Eventually the literature referred to throughout the thesis is listed in the References section.

Chapter 2

Literature Review

2.1 Introduction

The objective underlying the research described in this thesis is to study electrohydrodynamic forming as a technique for preparation of micro- and nanoparticles which can satisfy the requirements for the spheres that are adopted principally for applications in biomedical engineering, targeted for drug delivery and controlled release systems.

In order to accomplish this objective, the relevant literature will be reviewed as follows:

- **Fundamental concepts of drug delivery systems, routes of drug delivery and the mechanism of drug release:** the aims of drug delivery systems, variety of drug administration routes and the mechanisms which control the drug release including the degradation and erosion of the polymeric carriers are presented. Furthermore, a comprehensive description of various particulate drug carriers with different structures will be explained.

- **Methods for polymeric microsphere preparation:** different techniques for the fabrication of drug loaded polymeric carriers such as emulsion-solvent evaporation (conventional), coacervation (aggregation of colloidal droplets) phase separation and spray drying are discussed, and then they are compared with the electrohydrodynamic forming process, which is adopted in this study, in order to find out the advantages and disadvantages of this forming process.

- **Electrohydrodynamic forming process:** the theory of this processing method and the previous work based on using electrohydrodynamic (EHD) atomization are reviewed and briefly discussed. Various modes of EHD processing and all the parameters such as processing factors (applied voltage and flow rate) and solution properties (surface tension, electrical conductivity, density and viscosity) involved in this process are well explained. The applications of single needle and co-axial needle electrohydrodynamic atomization methods in preparation of various drug carriers such as microspheres,

capsules, aerosols, porous particles and microbubbles are also reviewed in order to understand how this unique processing technique offers great opportunities in health improvement and further research.

- **Polymeric based drug delivery systems:** numbers of different polymers have been extensively adopted for preparation of drug delivery carriers using EHD. In this section, a detailed examination of synthetic biopolymers such as poly (ε-caprolactone) (PCL) and poly (lactic-co-glycolic acid) (PLGA) will be made.

- **Controlling the drug release profile:** The main purpose of such drug delivery system is to have a regulated and sustained release profile from the drug loaded carriers. In this part, the role of sonication and temperature in biomedical engineering, in particular, in drug delivery system and drug release profiles will be explained.

- **An overview of chronic wounds and the treatments with application of biomaterials:** the aetiology of chronic wounds and how they can later on develop into non-healing cavities in human body tissues are reviewed. The previous work conducted for the treatment of perianal fistulae which are a severe type of chronic wounds is also revised. Then, the new approach for therapy of such disease by application of biomaterials using EHD method is described.

2.2 The Drug Delivery Concept and Goal of Drug Delivery Systems

The goal of drug therapy is to prevent, cure or control various states of a disease. To achieve this goal, adequate drug doses must be delivered to targeted area in the human body over the appropriate length of time so that therapeutic yet nontoxic levels are obtained. Pharmacological and toxicological actions of drugs are primarily related to the plasma concentrations of drugs (Finkel et al., 2009). Therefore, clinicians must be able to recognize that the speed of onset of drug action, the intensity of drug's effect and the duration of drug action are controllable by the following four fundamental pathways of drug movement and modification in the body: 1) drug absorption from the site of administration which allows entry of the therapeutic agent either directly or indirectly into plasma; 2) drug distribution which the drug may then reversibly leave the blood stream and distribute into the intestinal and intracellular fluids; 3) drug metabolism, that the drug may be metabolised by liver, kidney, or other tissues; and 4) drug

elimination, that the drug and its metabolites are removed from body by urine, bile or faeces (Finkel et al., 2009). Therefore, biocompatibility, biodegradability and pharmokinetics of the drug must be considered before administration.

The concentration level of the therapeutic agent (drug), in conventional drug delivery system such as tablets or injections, decreases significantly after administration. It is fundamentally hard to keep the drug concentration in the blood stream at a therapeutic level for extended periods of time; therefore, multiple administrations are usually required to attain the desired therapeutic outcome (Cohen et al., 1991). In such drug delivery system, high concentrations of drugs, especially those with more side effects, may induce more adverse toxic effects, as delivering the therapeutic agent is only dependant on diffusion or partition from the blood stream to the action site. The only advantage of this system over the controlled release system is its low processing and administration cost. The drug level in the blood stream rises after administration of the drug and then decreases with time until the next administration (**Fig. 2.1a**). The concentration of a therapeutic agent obtains two limits in blood stream; the toxic level of the therapeutic agent (upper limit) and the effective therapeutic level (lower limit). Thus, the key point with the traditional administrations of drug is to maintain the level of the drug between the two limits during the period of treatment (Park et al., 1998).

The limitation with the traditional administration of drugs was improved by the contemporary drug delivery systems which can release the drug over the long periods of time with remaining the level of drug at the constant stage in the blood stream (**Fig. 2.1b**), between the toxic and effective level of therapeutic agent for a specific time (Brannon-peppas, 1997). For treating the imbalance of biological homeostasis, drug releases only when it is needed. For instance, insulin releases from a polymer matrix only in response to an enhanced glucose concentration of diabetic patients. This type of release profile is typically known as pulsatile release (**Fig. 2.1c**). Highly localised drug release which is another route of drug release, can be attained by various targeting strategies (**Fig. 2.1d**). In this drug delivery system, release is restricted to a target site at a high local concentration for an extended time, and multiple drug components are planned to be sequentially released only when they are needed. For instance, ischemic brain leads to numerous cellular events including provocation of excitatory amino acids and reactive oxygen species within an hour, formation of polymorphononuclear leukocytes within a day, and macrophages activation within a week. Therefore, a temporally programmed drug release system is an outstanding solution to supply multiple drugs. Therapeutic efficiency in these two

introduced systems is very high while the side effects are significantly reduced compared with the traditional administrations (Kim et al., 2009).

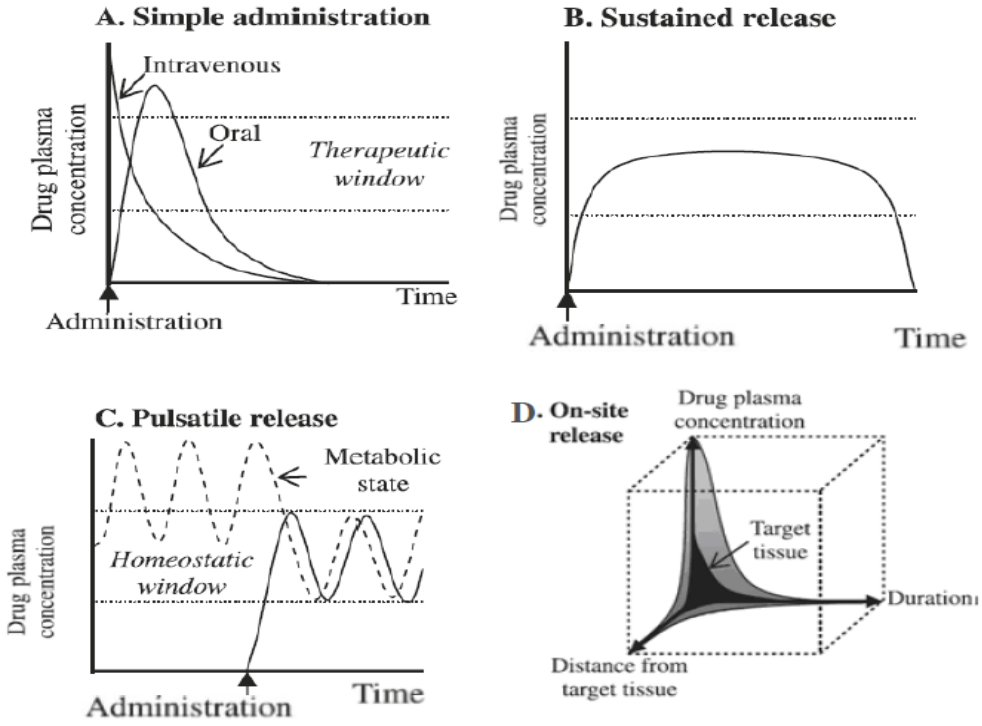

Figure 2.1: Different types of controlled release systems: (a) Drug delivery based on simple diffusion and partition; (b) Sustained release to prolong the therapeutic period; (c) Pulsatile release to tightly maintain homeostasis; (d) On-site release to maximize therapeutic efficiency and to minimize the side effect (Kim et al., 2009).

2.3 Routes of Drug Delivery Using Micro and Nano Spheres

There are number of potential routes for administration of drug loaded micro- and nano-particles, ranging from parenteral, i.e. intramuscular and subcutaneous, to nasal, pulmonary, oral, ophthalmic, transdermal, etc. In this part, a short description of the most popular drug delivery routes is provided.

Oral drug delivery: this is the most common method of drug delivery as it is convenient, easy to use and can be controlled by patient. However, there are some drawbacks associated with this method. For instance, the oral course is very variable, so that there is a noticeable potential for bio-inequivalence between orally administrated drugs (Zhang et al., 2002).

Parenteral drug delivery: this technique is used if drugs cannot be given by the oral route due to two reasons, firstly poor absorption properties of drug, secondly, propensity to degrade in the gastrointestinal tract. In this technique, drugs are delivered by injection to the target sites

in the body. The aim of using this method is to deliver the drug to specific body tissues. The most common ways of administrating drug to the targeted area in this method are intramuscular (IM), intravenous (IV) and subcutaneous (SC) (Sinha and Trehan, 2005).

Pulmonary drug delivery: inhalation is another effective route of drug delivery for some of the therapeutic agents. In this route of drug delivery, the therapeutic agents are directly delivered to lungs (Clark, 1995). The physical characteristics of the drug carriers are crucial for successful pulmonary drug delivery. The desired range of spheres for transporting the drug to the lungs must be within 1-5 μm (Grossman, 1994; Schreier et al., 1993). In this route of drug delivery, biodegradable polymeric carriers can help the inhalation treatment to have a sustained release of the drug (Kawashima et al., 1998). Gradual release from inhaled drug loaded microspheres can increase the residence of the drug in the airway, and therefore can reduce the percentage of the therapeutic agent in the blood stream. This method would also be more convenient for patients compared with the oral administrations due to reduction in the dosage frequency (Schreier et al., 1993).

Transdermal drug delivery: this technique utilises an adhesive patch containing drug, which passively diffuses through the dermal system (skin). The skin is formed to act as a potent barrier against external damage; therefore, transdermal delivery systems have been developed to overcome this resistance, and by far number of different drugs have been delivered transdermally such as contraceptives, nicotine and oestrogen (Prausnitz et al., 2004; Singh and Roberts, 1989).

2.4 Particulate Drug Carriers

The development of drug delivery in the form of polymeric carriers is a relatively new area of scientific research, as the technology to work at atomic, molecular and supramolecular levels have only become extensively available in recent years. Particulate drug carriers include different types of structures such as micro/nano spheres (micro/nano particles), liposomes, vesicles, micelles and dendrimers (**Fig. 2.2**). Microspheres are small spherical units, composed of various combinations of natural and synthetic materials with diameters in the micrometre range. The therapeutic agents can be dispersed or dissolved in the matrix of spheres. However, nanospheres are spherical nano-sized unit, where active compounds can be firmly adsorbed at their surface, entrapped or dissolved in the matrix. Nanocapsules are the nano-scale capsules

with a polymeric shell and an inner core. In this case, the active substances are dissolved in the core (Mainardes et al., 2006).

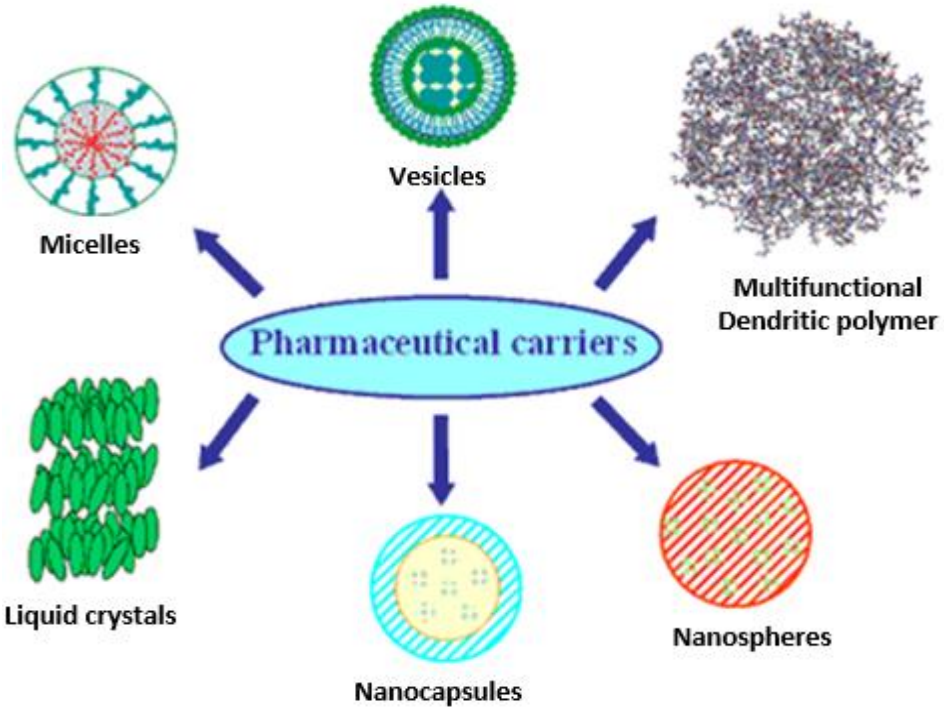

Figure2.2: Pharmaceutical carriers (Kaparissides et al., 2006)

Liposomes contains a lipid biolayer surrounding an aqueous core, which can be produced in sub-micron size. They are capable of carrying drugs either in their lipid biolayer or aqueous core (Bangham et al., 1965). **Micelles** are another type of drug carriers which are a collection of amphiphilic surfactant molecules that spontaneously aggregate to form a spherical vesicle in water. The core of each micelle is hydrophilic which can sequester hydrophobic drugs until they are released by some drug delivery mechanisms. Micelles are usually formed from small molecules, which have a hydrophilic or polar head group and hydrophobic tail, and are often composed of the hydrocarbon portion of long fatty acids. Geometrical features such as molecular size of the surfactants determine the micelle size (Nishiyama and Kataoka, 2003; Savic et al., 2003). A **dendrimer** is commonly described as macromolecule which is characterised by its highly branched 3D structure, and has the ability to provide a high degree of surface functionality and versatility. Dendrimers have been often referred to as the "Polymers of the 21st century" (Lee et al., 2005; Pushkar et al., 2006). The unique architectural design of this type of macromolecules provides high degree of branching, multivalency, globular architecture and well-defined molecular weight that clearly distinguishes their structures from other types of drug carriers in medical applications such as gene transfection, tumour therapy, drug delivery, diagnostics, etc. Synthetic approaches induce a dendritic

architecture with characteristics amenable to modifications of size, polarity, morphology as well as internal structure (Boas and Heegaard, 2004).

2.5 Mechanisms of Drug Release

Mechanism of drug release from synthetic degradable polymeric carriers involves a series of steps: diffusion, chemical reaction and solvent activation. The classification of controlled release systems is based on the means which controls the drug release that requires dissolution of the drug followed by diffusion through the structure of polymeric particles in order to reach the release medium. So far, two different types of diffusion-controlled mechanisms have been developed: the first is the reservoir system, and the second is the matrix system (Huang and Brazel, 2001).

In the reservoir system, the drug is physically captured inside a polymeric device that can be then injected or implanted in the body. In this mechanism, the drug diffuses through the polymer membrane which entraps and protects the drug from the outer environment (**Fig. 2.3a**). Early forms of this mechanism involved using non-degradable polymers such as silicone rubber, that could release drugs with low lipophilic molecular mass over extremely long time periods (Folkman and Long, 1964). This approach led to the development of small silicone capsules such as Norplant containing contraceptives that can be slowly released by diffusion through the polymeric shell for 5 years. The process of diffusion is described by a series of equations managed by Fick's first low of diffusion:

$$J = -D \frac{\partial c}{\partial X} \qquad \textbf{(2.1)}$$

Where J, known as flux density, is the amount of drug crossing the membrane per unit time and is typically expressed in units such as moles of particles per m^2 per second. D is the diffusion coefficient of the drug in the membrane that reflects a drug molecule ability to diffuse through the polymeric matrix. This coefficient is also dependent on factors such as molecular size and charge. $\frac{\partial c}{\partial X}$ represents the rate of change in concentration where c is relative to distance x in the membrane.

In the matrix mechanism, drug is physically embedded and distributed in a polymeric carrier (**Fig. 2.3b**) through which the entrapped drug consequently diffuses out (Langer and Folkman, 1976; Langer, 1990). The matrix systems are the most common mechanisms for controlling

the release rate of drugs. This is due to relatively easy fabrication of devices compared with reservoir systems, and less risk of an accidental high dosage that could result from the membrane rupture of reservoir device.

Mechanism of drug release in some of other drug delivery systems is based on a combination of diffusion and polymeric degradation processes. In those systems, biodegradable (or bioerodible) polymers are adopted for fabrication of the drug carriers. The concept behind using biodegradable polymers is that they can be finally absorbed by the body due to their biocompatibility, and hence there is no need for surgical removal.

Bioerosion of a polymer can be defined as the conversion of a material that is insoluble in water into one of the form which is water-soluble. In a mechanism of bioerosion, the drug is preferably distributed uniformly throughout a polymer matrix in the same way as in monolithic systems. In this form, the drug releases as the polymer surrounding the drug is eroded (**Fig. 2.3c**).

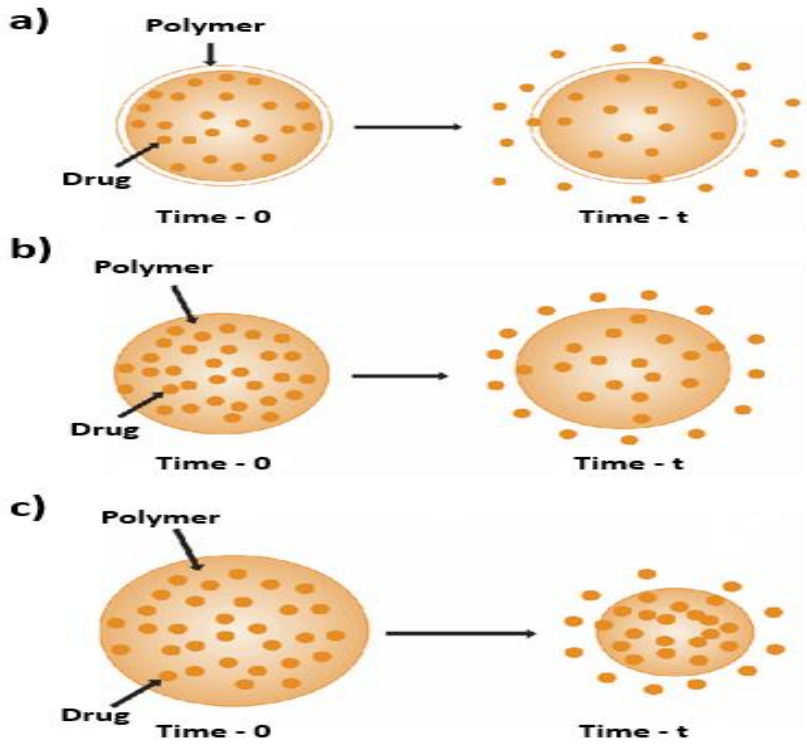

Figure 2.3: Schematic representation of (a) Reservoir diffusion controlled, (b) Matrix diffusion controlled and (c) Biodegradable drug delivery devices (Salamone, 1996)

2.6 Polymer Degradation and Erosion

Although classification of the biopolymers adopted in drug delivery systems is difficult due to the inherent diversity of their structures, it is helpful to categorise them in order to emphasise

common properties within groups of polymers. There are number of different descriptions for degradation and erosion in the literature review (Vert et al., 1992). However, the following definitions are adopted in this study: **Degradation** is based on a chemical process and exclusively refers to bond cleavage and the chain scission process during which polymer chains are sliced to form oligomers and monomers, whereas, **erosion** is fundamentally a physical phenomenon dependent on dissolution and diffusion processes leading to reduction of material (Tamada and Langer, 1993).

Polymer Degradations: degradation is one of the important procedures that leads to drug release in drug delivery system. Polymeric biomaterials, depending on the mode of degradations can be classified further into two categories of hydrolytically degradable and enzymatically degradable polymers.

Hydrolytical degradation is the main type of degradation for synthetic polymers. There are number of different variables influencing this process, such as the type of chemical bond, copolymer composition, water uptake and pH. During the process of degradation, one or some of these factors can occur to have a significant effect on the degradation of polymer. One of the most crucial parameters for monitoring degradation is molecular weight. Apart from loss of molecular weight, other factors have been proposed as a measure of degradation including: loss of mechanical strength and complete degradation into monomers or monomer release (Huang and Brazel, 2001).

Enzymatic degradation of polymer is another type of degradations, and mainly occurs in natural biopolymers such as proteins (gelatine and collagen), polysaccharides and poly (β-hydroxy acids), where appropriate enzymes are obtainable (Huang and Brazel, 2001).

Polymer Erosion: this mechanism basically has two different types: first; surface erosion and second, bulk erosion (Göpferich, 1996). When the surface erosion occurs, polymers lose material from the surface; therefore, they become smaller in terms of size but keep their original geometric shape (**Fig. 2.4b**). With surface eroding polymers, the rate of erosion exceeds the rate of water permeation into the bulk of the polymer. Due to kinetics of erosion, the mechanism of surface erosion is often considered to be desirable in drug delivery systems, and hence the rate of drug release is highly reproducible and predictable. Also, the magnitude of the erosion rate may change by simply altering the surface area of the drug delivery carrier. The slow rate of water permeation into surface eroding polymers has further beneficial influence on protecting water labile drugs from quick release up to the time of drug release (Göpferich,

1996). Poly (anhydrides) and poly (orthoesters) are the examples of surface eroding polymers, which in both classes, the biodegradable polymers possess highly labile groups that ensure rapid hydrolysis of polymer chains encountering water molecules. Permeation of water is retarded by designing the polymer chains with hydrophobic monomer units. Alternatively, hydrophobic excipients can be added to stabilise the polymer bulk (Lee et al., 2004; Modi et al., 2005). The ideal surface erosion can occur when the erosion rate is directly proportional to external surface area. This can result in zero-order drug release (a steady amount of drug release over time) provided that diffusional release is restricted and the overall shape remains constant.

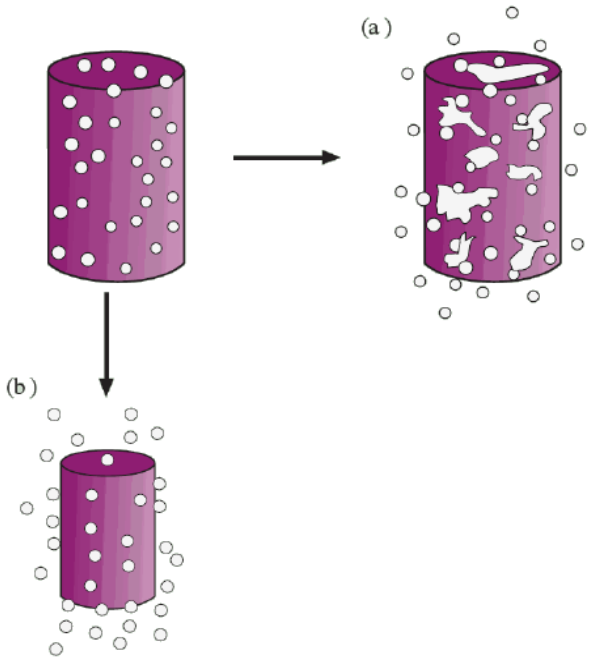

Figure 2.4: Schematic illustration of the biodegradation of a polymeric drug delivery system: (a) Bulk erosion and (b) Surface erosion

In the case of bulk eroding polymers, erosion is not limited to the surface of the polymer or the device. Therefore, the size of device may remain constant for a substantial period of time during its application (**Fig. 2.4a**). Bulk erosion occurs when the rate of water permeation into the bulk of the polymer exceeds the rate of erosion. As a result, polymer molecules in the bulk are hydrolysed. The kinetics of polymer bulk erosion is more complicated than for surface eroding polymers and the majority of biodegradable polymers adopted in controlled drug delivery for release of drug undergo bulk erosion rather than surface erosion (Lee et al., 2004).

Surface and bulk erosion mechanisms occur for most biodegradable polymers; however, relative extent of the mechanisms varies completely with chemical structure of the polymer

backbone. Polymer erosion is more complex compared with degradation, as it depends on many factors including swelling, the dissolution and diffusion of oligomers and monomers, and also morphological changes (Kwon et al., 1991).

2.7 Methods for Preparation of Micro and Nano Polymeric Spheres

A number of different methods are available for fabrications of micro- and nano-spheres and also encapsulation of therapeutic agents in the polymeric carriers: emulsion solvent evaporation/extraction, spray drying, phase separation, suspension cross-linking and electrohydrodynamic atomization. Each technique has its own advantages and disadvantages, depending on the polymer and the solvent used, the drug and the site of its action and also the duration of therapy (Fukushima et al., 2000; Jain, 2000; Okada and Toguchi, 1995). Generally, there are few requirements needed for successful and effective preparation of polymeric spheres:

- The chemical stability and biological activity of the therapeutic agent should be preserved during the whole process of drug delivery.
- The encapsulation efficiency and the yield of the process should be high enough for mass production of micro- and/or nano-spheres.
- Spheres should be within certain range of size and they should also be almost monodisperse (uniform size).
- Spheres should also have a controlled release profile without high initial burst release.

2.7.1 Emulsion-Solvent Evaporation/Extraction Methods

2.7.1.1 Single Emulsion Method

This technique is adopted for loading the hydrophobic drugs in carriers via oil-in-water (o/w) emulsification method. In the first step for the preparation of the drug-loaded spheres, the polymer is dissolved in a water-immiscible solvent and then the drug is dissolved into the polymer solution. The resulting solution is emulsified in water using an emulsifier (Hombreiro Pérez et al., 2000; Jain, 2000). In this technique, the amount of solvent in the emulsion is usually reduced by increasing the temperature for evaporation of the residual solvent (Arshady, 1991). Although with this technique, the drug loaded spheres can be simply fabricated, it is only suitable for hydrophobic drugs. The encapsulation efficiencies for hydrophilic drug are

very low since drug may diffuse out from the dispersed oil phase into the aqueous phase (Arshady, 1991; Hombreiro Pérez et al., 2000).

2.7.1.2 Double Emulsion Method

Most water-soluble drugs are encapsulated by the water-in-oil-in-water (w/o/w) mechanism (Crotts and Park, 1998; Okochi and Nakano, 2000). In this technique, first, the polymer is dissolved in an organic solvent and then the aqueous solution of the drug is emulsified to form a water-in-oil (w/o) emulsion. Subsequently a w/o/w emulsion is formed by enhancing the w/o emulsion into an excess amount of water containing an emulsifier under strong stirring (**Fig. 2.5**). Finally, the residual solvent from the solution is removed by evaporation or another extraction method. Advantage of this method compared to the single emulsion technique is the high encapsulation efficiency for hydrophilic drugs (Crotts and Park, 1998; Okochi and Nakano, 2000).

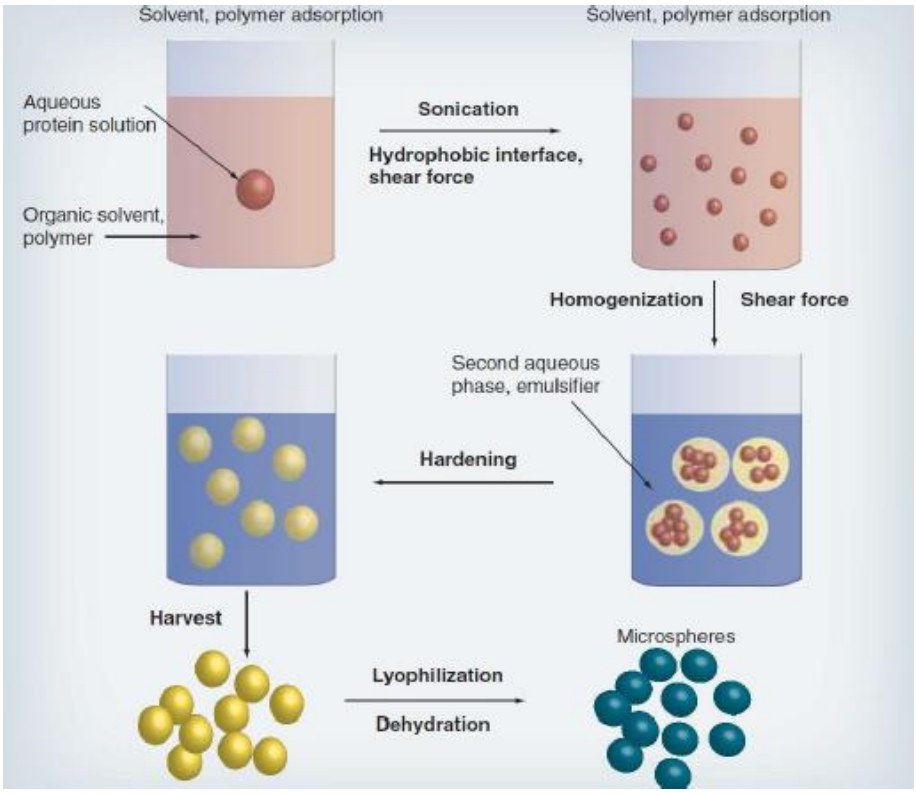

Figure 2.5: Processing scheme for microsphere preparation by double emulsion system (Chiellini et al., 2008)

2.7.2 Coacervation and Thermally Induced Phase Separation (TIPS) Methods

The term, coacervation is derived from the Latin word “acervus”, meaning aggregation and the prefix co indicates union of colloidal particles. This process, which is illustrated in **Figure 2.6**,

has three steps and is carried out under continuous agitation. The first step is the formation of three immiscible chemical phases. The second stage is the deposition of the coating and the final step is the rigidization of the coating (Carrasquillo et al., 2001; Mallardé et al., 2003).

Formation of three immiscible chemical phases: the three phases include one liquid vehicle phase, one core material and one coating material phase. These three phases are formed by dispersing the core material in a solution of coating polymer. The vehicle phase is adopted as a solvent for the polymer. For the coating material phase, an immiscible polymer in liquid state is formed by (i) altering the temperature of polymer solution, (ii) addition of salt, (iii) addition of non-solvent or (iv) addition of incompatible polymer to the polymer solution (Madan, 1978).

Deposition of the coating phase: this phase includes the deposition of the liquid polymer coating upon the core material. This occurs when the polymer is adsorbed at the interface formed between the core material and the liquid vehicle phase. This adsorption phenomenon is a required condition for an effective coating.

Rigidization of the coating phase: the rigidization of the polymer coating is generated when the continued deposition of the coating material is promoted by a reduction in the total free interfacial energy of the system. This phase can be carried out using thermal cross linking or desolvation techniques.

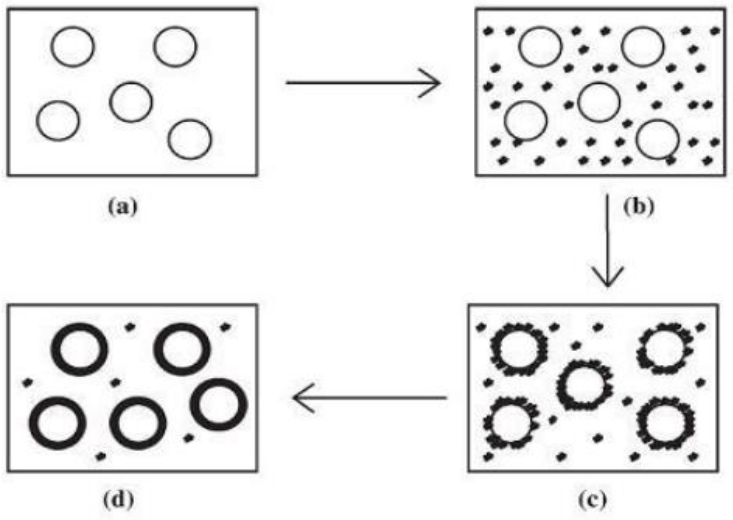

Figure 2.6: Schematic representation of the coacervation process: (a) Dispersion of core material in a shell polymer solution, (b) Separation of coacervation from solution, (c) Coating of the core material by coacervation microdroplets, (d) Coalescence of coacervation to form continuous shells around the core particles

The processing setup for this technique is fairly simple. It contains jacketed tanks with variable speed agitators. However, the significant disadvantage of this method is that when the spheres are formed, they stick to each other prior to the completion of the process and produce large aggregates.

Thermally induced phase separation (TIPS) is a supplementary fabrication method which has been used lately in polymer particle formation to produce porous surface microspheres for applications in wound therapy, drug delivery and also tissue engineering (Blaker et al., 2008a, 2008b; Keshaw et al., 2010; Martínez-Pérez et al., 2011). This technique requires the use of solvent such as dimethyl carbonate with a low melting point that is easy to sublime. Then, by collecting the products in an immiscible liquid to the polymer solution with a melting point of lower than the solvent, such as liquid nitrogen, a polymer-rich and a polymer-poor phases are formed. Following cooling below the solvent melting point, using a vacuum-drying to sublime the solvent, a porous structure of the products is obtained.

2.7.3 Suspension Cross-Linking

Suspension cross-linking process prepares the polymeric microspheres by forming a stable droplet suspension of the polymer solution in an immiscible liquid, gradual hardening of the droplets by covalent cross-linking, and finally, recovery of the resulting cross-linked polymeric spheres. For the preparation of polymeric products, the core material remains entirely within droplets. This is because the core material has significantly a higher affinity for droplet phase than suspension medium. In this technique, the average size of the droplets must be around one order magnitude larger than that of the core spheres to ensure entire encapsulation (Arshady, 1989).

2.7.4 Spray Drying

In this technique, dried spherical particles are produced from liquid polymer solution by rapidly drying the processing solution with a hot gas. This method offers number of advantages compared with the other methods described above. It has improved the reproducibility of microspheres, and the processing conditions are relatively easy which facilitates to control the sphere size. However, this technique (**Fig. 2.7**) has two main disadvantages: first, loss of a large number of products due to sticking to the wall of the spray drier, and second, production of

large aggregates prior to the complete removal of the solvent (Blanco-Príeto et al., 2004; Burke et al., 2004; Murillo et al., 2002).

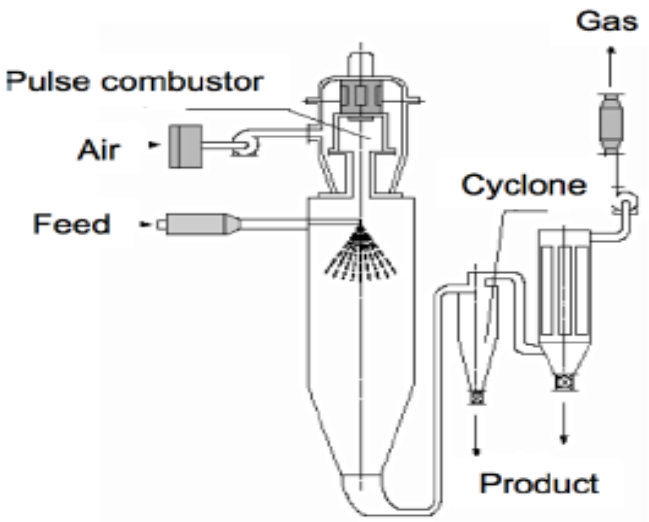

Figure 2.7: Schematic process for preparation of microspheres by spray drying (Zbicinski et al., 2000)

2.7.5 Electrohydrodynamic (EHD) Atomization

Over the past decade, electrohydrodynamic (EHD) atomization is recognised and appreciated as an attractive and alternative method for the generation of micro- and nano-spheres suitable for application in drug delivery systems (Ding et al., 2005; Pareta and Edirisinghe, 2006). As discussed earlier, emulsion polymerization, phase separation and spray-drying are the common fabrication methods for generating a variety of drug-loaded hollow polymeric structures (Yang et al., 2001; Zhang et al., 2008; Zhu et al., 2000). However, there are some certain drawbacks with these approaches. For instance, emulsion method results in a broad size distribution of sphere (Kissel et al., 1996). Moreover, non-degradable additives such as polymers or surfactant are generally adopted in this method as emulsifiers (Freitas et al., 2005) and the separation of products from solvent can be expensive and time-consuming but requires to be conducted in order to decrease the volume of residual solvent to a safe level for application in medicine and pharmaceuticals. Most importantly, due to exposure of drug to elevated temperatures and high shear stresses in the emulsion method, the biological activity of drugs can be greatly reduced during processing (Kohane et al., 2006; Rasiel et al., 2002).

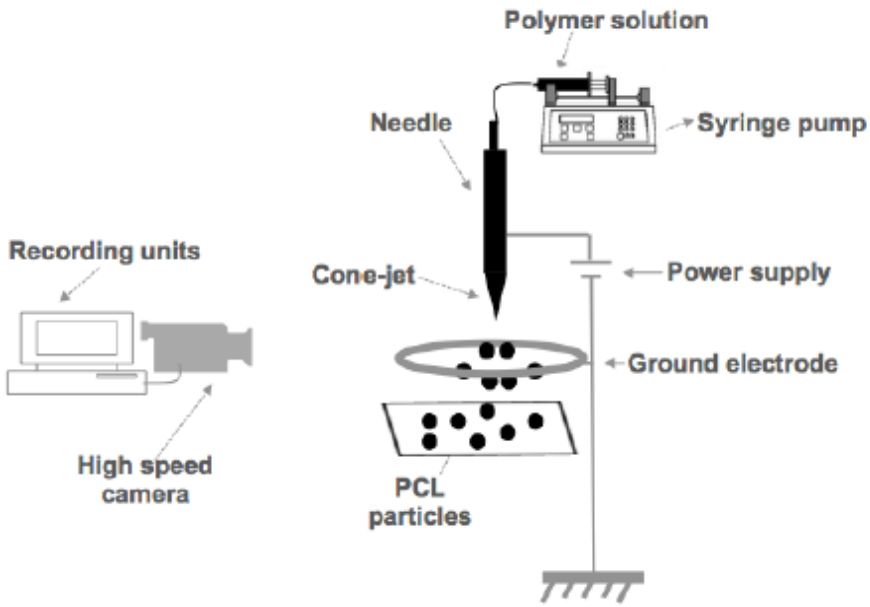

Figure 2.8: Schematic representation of the single-needle EHD setup adopted for fabrication of polymeric carriers (Enayati et al., 2010b)

In the EHD method (**Fig. 2.8**), spheres are fabricated at ambient temperature and pressure. Therefore, this method simply overcomes the complications associated with defunctionalisation of drugs under extreme processing conditions in the emulsion method. Furthermore, this method is cable of producing spheres with a narrow size distribution and a mean diameter which can be varied from tens of nanometres to hundreds of micrometres by controlling the processing parameters such as flow rate(s), needle diameter(s) and applied voltage. Besides, with the application of voltage in production of microspheres, the problems with the large aggregates of products in the phase separation and spray-drying techniques have been easily overcome (Ahmad et al., 2008; Samarasinghe et al., 2007; Xie et al., 2008).

The single needle EHD (**Fig. 2.8**) describes a method in which a liquid is passed at a controlled flow rate through a silicone tube to the nozzle maintained at several kilovolts relative to a ground electrode a few centimetres away.

2.8 Principles and Theoretical Aspects of EHD Process

The effect of an applied electrical field on a liquid with certain conductivity was described in 1600, when William Gilbert stated that electrostatically charged amber could produce a jet of liquid from a droplet (Gilbert, 1600). Electrohydrodynamic research was initially presented in the technical literature by Lord Rayleigh, who also studied the influence of an electric field on liquid drops. It was concluded by Rayleigh that the stability of a drop suspended from capillary

is dependent upon a balance of forces such as the electrical stresses, owing to the presence of an electric field and the surface tension forces (Rayleigh, 1882). He also observed a conical shape of the deformed liquid and a thin jet evolving from the tip of a cone. Later, Theoretical discussions of a mathematical model for the conical shape of the droplet under the influence of an electric field were supplied by Taylor, showing that a conducting fluid could exist in equilibrium in the form of a cone under the action of an electric field but only when the semivertical angle was close to 49.3°, which is a material-dependent value (Taylor, 1969, 1964). The critical voltage V_k in kilovolts applied to transform a spherical droplet to a cone-shape at the end of a cylindrical capillary connected to one of the electrodes can be predicted based on the semivertical angle of 49.3° (Taylor, 1969):

$$V_k^2 = \frac{4H^2}{L^2}\left(\ln\frac{2L}{R} - 1.5\right)((2\cos 49.3°)\pi RT)(0.09) \quad \textbf{(2.2)}$$

Where H is distance between the electrodes, L is the length between the end of the cylindrical capillary and the contacting point of the electrode on the capillary, R is the inner radius of the capillary, T is the surface tension, and θ is the semivertical angle. Because this semivertical angle has been found to vary with different polymer solutions and melts (Rangkupan and Reneker, 2003), the critical voltage to generate a cone-shape from a droplet varies with different electrosprayed materials.

The cone jet mode is the most desirable and the used mode for producing fine spheres for application in drug delivery. In this EHD jetting mode, the liquid derives from the capillary in the form of a regular, symmetric cone with a thin jet at its apex (**Fig. 2.9a**), stretching along the capillary axis and breaking up into fine particles. To achieve this mode, the liquid is pumped through a nozzle at a known flow rate and a droplet is formed at the tip of this nozzle. Then, an electric field (potential) is introduced which in turn induces a surface charge to the droplets. As a result of this electric stress, the droplet is transformed into a conical shape. The liquid acceleration and the conical shape of the liquid results from the balance of several forces applied to the surface of droplets formed on the tip of the nozzle. These forces consist of liquid pressure, liquid surface tension, gravity and electric strength in the liquid surface. The conical shape is sometimes referred to as Taylor cone that forms when the outward stress owing to an electric field is equal to the inward stress due to the liquid surface tension. The forces involved in the formation of cone jet are illustrated in **Figure 2.9b** (Hartman et al., 1999). Further investigation shows, when the applied voltage accelerates the surface charge towards the cone

apex, the jet breaks up into a number of primary or main droplets and a number of secondary droplets and satellites (Jaworek and Krupa, 1999a, 1999b).

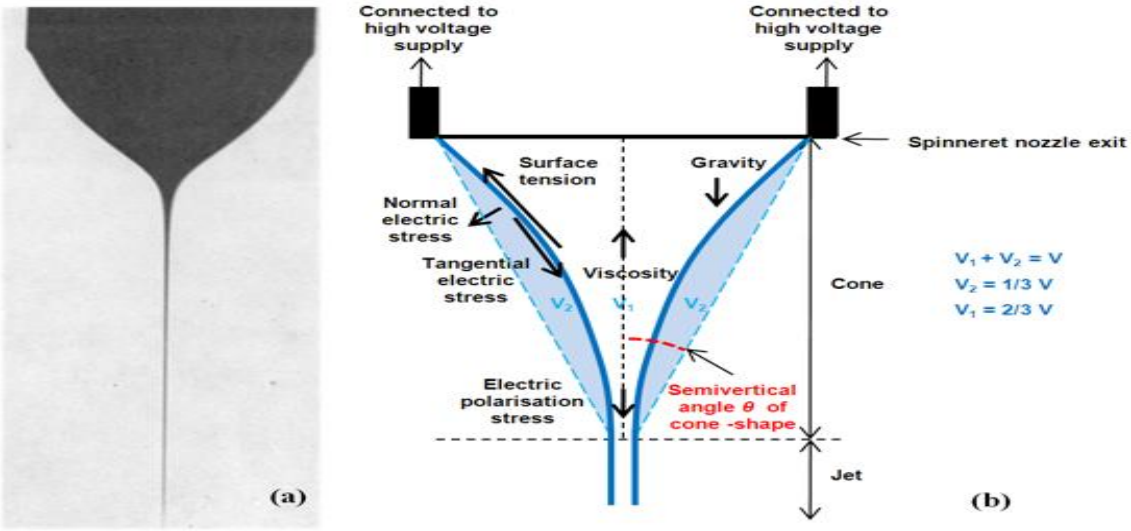

Figure 2.9: (a) A stable cone-jet (Taylor, 1969). (b) A geometric diagram of an axisymmetric liquid cone with a thin jet at its apex depicting forces acting on a cone-jet (Hartman et al., 1999)

V is the volume of the conical frustum and V_1 is the jet volume, V_2 is the space in which the jet is not occupying in the conical frustum. Upon the establishment of a conical shape of the droplet at the capillary end, at a sufficiently high-applied voltage, additional surface area needs to be created by some means to accommodate the charge build-up on the conical surface (**Fig 2.9**) (Hartman et al., 1999). The electrostatic force and viscous drag force are the two main forces acting on an ion moving in horizontal under the application of electric field. The sum of electric field related forces is:

$$\sum F_{electrostatic} = \vec{F}_{qpi} + \vec{F}_{dpi} + \vec{F}_{qni} + \vec{F}_{dni} \quad \textbf{(2.3)}$$

Where $\vec{F}_{qpi}$ and $\vec{F}_{dpi}$ are respectively the electrostatic force and the viscous drag force acting on a positive ion; $\vec{F}_{qni}$ and $\vec{F}_{dni}$ are respectively the electrostatic and the viscous drag force acting on a negative ion. Electrostatic force and viscous drag force can be respectively expressed as qE and $6\pi\eta r\mu E$, where q is the amount of charge on the ion, E is the electric field strength, η is the solution viscosity, r is the hydrodynamic radius of the ion and μ is the ion mobility. Hence, equation (2) can also be expressed as the following:

$$\sum F_{electrostatic} = (n_1 qE) - (n_1 6\pi\eta r_{pi}\mu_{pi}E) - [n_1 (1-y)qE] + [n_1(1-y)6\pi\eta r_{ni}\mu_{ni}E] \quad \textbf{(2.4)}$$

Where n_1 is the number of ions in a solution of mass m, μ_{pi} and μ_{ni} are the ion mobility of positive and negative ions. When the solution becomes charged at the electrode, a fraction of the negative ions, y, is neutralized due to limited contact between the solution and the charged electrode. The solution thus still contains $n_1(1-y)$ negative ions and n_1 positive ions.

Zeleny (1917) was the first person who studied this mode of interest. Later on, Taylor successfully examined the cone-jet profile and the angle based on the liquid in the cone-jet. Based on the assumption that the jet is thinner than the capillary tube for a liquid with relatively high conductivity, Mora and Loscertales (1994) stated the scaling laws of droplet size and spray current (the two ratios below) related to the flow rate and liquid properties (De La Mora and Loscertales, 1994; Zeleny, 1917):

$$r^* \sim (\varepsilon\varepsilon_0 Q/K)^{1/3} \quad \textbf{(2.5)}$$

$$I \sim f(\varepsilon)(rQK/\varepsilon)^{1/2} \quad \textbf{(2.6)}$$

Where r^* is the radius of the scaled jet, ε_0 is the permittivity of vacuum, ε is the permittivity of liquid, Q is the flow rate, K is the conductivity of the liquid, I is the spray current and $f(\varepsilon)$ is the dimensionless function of ε.

However, according to the experimental work, the use of scaling laws for the prediction of resultant relics (particles with different shapes and sizes) is still controversial. This is because experimental errors in the reported measurements do not allow adequate distinction between various types of relics (Gañán-Calvo, 1997; Gañán-Calvo et al., 1997). In addition, there is a range of different combinations (processing parameters and physical properties of the injected liquid) that affects the stability of EHD and the size of produced particles. For instance, Mei and Chen (2007) demonstrated that enhancement in flow rate of the flowing liquid results in an increase in particle size for certain value of liquid flow rate (Mei and Chen, 2007). However, over a certain range of material combinations and processing parameters, size of particles decreases with an increase in the magnitude of the following parameters: voltage, electrical conductivity, and surface tension of the electrosprayed solution. In contrast, an increase in particle size can also be obtained by means of increasing the flow rate, density and also viscosity of the sprayed solution (Zhang et al., 2006).

2.8.1 Modes of EHD Process

There are various modes in which the jet can form from nozzle tip in electrospraying. These modes are typically defined by geometrical features of the liquid at the apex of the nozzle and the behaviour and disintegration of the jet into droplets (**Fig. 2.10**). The various spraying modes are all of interest, because each of them has different stability and provides different size, size distribution and shape (Cloupeau and Prunet-Foch, 1990). Different parameters such as physical properties of the liquid (e.g. surface tension, electrical conductivity and viscosity) and processing parameters (e.g. flow rate and applied voltage) have significant influences on generating different modes of EHD (Paine et al., 2007). The spraying modes can be basically divided into two major groups; those in which small fragments of the liquid are ejected from the nozzle, and those which produce a long continuous jet that disintegrates further downstream of the jet (Jaworek and Krupa, 1999a, 1999b). The first set includes dripping, micro-dripping, spindles and ramified meniscus modes, whereas the latter includes cone-jet, multi-jet, oscillating jet, ramified-jet and precession modes (**Fig. 2.10**). Electrospraying at low voltage creates the modes such as dripping, microdripping, rapid dripping and spindle. However, at high applied voltage, the modes of a sustained and continuous jet can be formed such as stable cone-jet, multi-jet, ramified-jet and precession. In the modes under the application of high voltage, the jet usually breaks up into droplets a few millimetres away from the nozzle exit. The meniscus and the jet can be either stable or spin around the needle axis or rotate irregularly (Cloupeau and Prunet-Foch, 1994; Hayati et al., 1987a, 1987b).

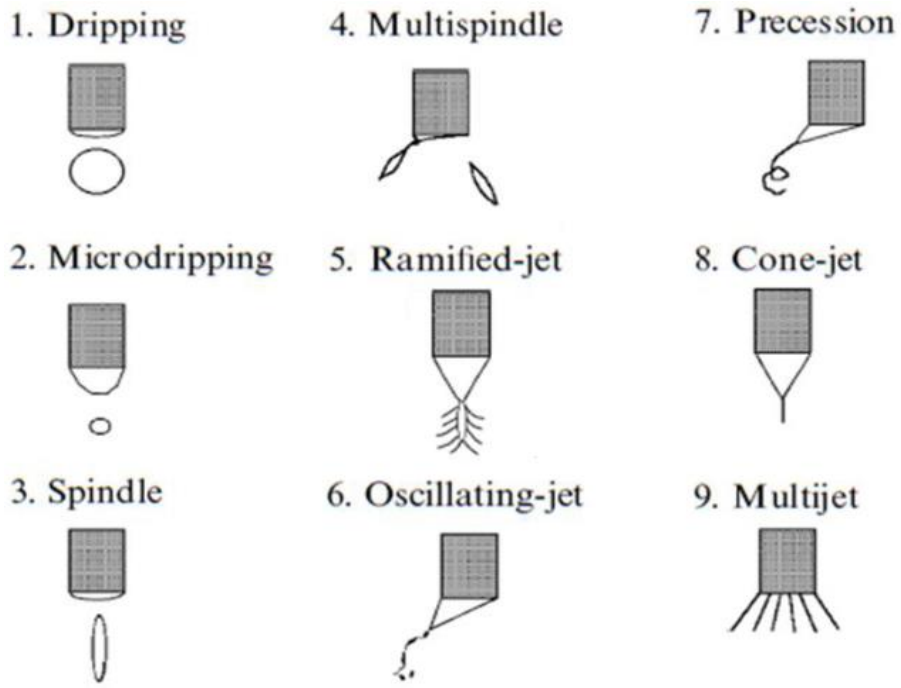

Figure 2.10: Various modes of electrospraying (Jaworek and Krupa, 1999b)

2.8.2 Effect of Liquid Flow Rate on the Cone-Jet Mode

The size distribution of spherical particles generated by the EHD process in the mode of the cone-jet is varying and depending on the diameter of the jet flowing out of the nozzle, and on the break-up of this jet into droplets. Every liquid has a minimum flow rate below which a stable cone-jet mode cannot be produced for a given voltage. At this minimum flow rate, the jet breaks up with the application of applied voltage due to asymmetric instabilities. These instabilities are also known as varicose instabilities (Hartman et al., 2000). At higher flow rate, when the current through the liquid cone increases, the surface charge on the jet grows. Therefore, above a certain surface charge the jet break-up will also be influenced by lateral or azimuthal instabilities of the jet mode. These instabilities are also called kink. When the influence of these kink instabilities enhances, the size distribution of main droplets also swells (Hartman et al., 2000).

2.8.3 Effect of Applied Voltage on the Cone-Jet Mode

Electric field strength between the capillary and the ground electrode is a crucial factor in controlling the mode of jet in the EHD process. This is determined largely by tuning the applied voltage and the configuration of the ground electrode. Within a well-defined range of voltage, the meniscus of liquid gives the shape of cone and becomes stationary. However, below this range, the spray always operates in pulsating mode (Gañán-Calvo, 1997; Gañán-Calvo et al., 1997). With a given inter-electrode spacing, various modes of atomization can be observed from dripping to the multi-jet if the voltage is gradually increased from low to high values. Applied voltage is a key parameter in generating the cone-jet mode and this mode can be successfully achieved within a specific range of applied voltage (Tang and Gomez, 1994). Within this range, particle size reduces with increasing applied voltage. Therefore, it is necessary to select the appropriate flow rate and voltage to obtain the stable cone-jet mode for fabrication of the required size of spherical particles (Jayasinghe and Edirisinghe, 2004).

2.8.4 Liquid Properties

Different modes of EHD are also influenced by the liquid properties such as viscosity, electrical conductivity, surface tension, relative permittivity and density (Gañán-Calvo, 1997; Gañán-Calvo et al., 1997; Hartman et al., 1999).

2.8.4.1 Viscosity

Viscosity is a property of liquid which plays a crucial role in the process of jet break-up and influences the size of the generated products (López-Herrera et al., 2003). Increase in viscosity will lead to an enhancement of particle size in EHD processing (Weber, 1931). Jayasinghe and Edirisinghe (2002) conducted a study to show the effect of viscosity on the size of relics produced by EHD forming. They found that an enhancement in viscosity over three orders of magnitude had a significant influence on the size of generated particles (Jayasinghe and Edirisinghe, 2002).

2.8.4.2 Electrical Conductivity

Electrical conductivity is another most crucial property affecting the mode of cone-jet for electrospraying. Sufficient electrical conductivity is needed for the liquid droplet at the capillary exit to be transformed into a conical shape. However, if the electrical conductivity is extremely high, EHD forming will be impossible owing to corona discharge occurring before the required applied voltage for the stable cone-jet mode is obtained. On the other hand, liquids with low electrical conductivity such as olive oil cannot be subjected to EHD processing; however, they can be electrosprayed in the cone-jet mode by artificially enhancing their conductivity with additives such as ethanol (López-Herrera et al., 2003). The electrical conductivity for different liquids influences the morphology of the liquid issued in the stable cone-jet mode. Based on experimental research, by increasing the conductivity, the filament width, length, flow rate for the cone-jet mode and particle size will all decrease (Gañán-Calvo, 1997; Gañán-Calvo et al., 1997).

2.8.4.3 Surface Tension

For the formation of the stable cone jet in producing spherical particles, the surface tension has to be overcome by the applied electric stresses. The higher the surface tension, the greater is the electric field (potential) required for break up. According to the experimental results obtained by Smith in 1986, the threshold voltage for the stable cone-jet will increase with the liquid surface tension (Smith, 1986). However, if the liquid surface tension is extremely large, the stable cone-jet may not be established, because the required electric field (potential) exceeds that for the electric breakdown in the gas surrounding the cone. In 1995, Tang and

Gomes adopted gases with higher electrical breakdown strength as a surrounding fluid instead of air to achieve the stable cone-jet mode for water (Tang and Gomez, 1995).

2.8.4.4 Relative Permittivity

Dielectric constant, known as relative permittivity, is a measure of the polarizability of material in an electric field, which is related to the ability of solutions in formation of the cone-jet and production of particles. Polarisation leads to reduction in the magnitude of the electric field (potential) inside the liquid. The three parameters of dielectric constant, vacuum permittivity and conductivity determine the electrical relaxation time:

$$t_e = \beta\varepsilon_0/K \quad \textbf{(2.7)}$$

Electrical relaxation time is the time required to smooth a perturbation in the electric charge, where β is the relative permittivity, ε_0 and K are the vacuum permittivity and electrical conductivity respectively (Gañán-Calvo, 1997; Gañán-Calvo et al., 1997).

2.8.4.5 Density

Density is another parameter that plays an important role in determining the jet characteristics in the cone-jet mode. When the viscosity and the conductivity of a liquid are large enough, the electrical charge is efficiently transmitted across the jet section by viscous forces. However, these viscous forces depend on the density of the liquid (Gañán-Calvo, 1997; Gañán-Calvo et al., 1997). Furthermore, the liquid density is of some importance, owing to the influence of gravity on the cone shape. For large capillaries with diameter greater than 1mm, gravity affects the shape of the cone strongly (Hartman et al., 1998).

2.8.4.6 Nozzle Size and Electrode Configuration

There are still some differences of opinion among researchers with regard to needle size. In 1990, Cloupeau and Prunet-Foch illustrated that for a given liquid, the flow rate changes with respect to the change of needle size (Cloupeau and Prunet-Foch, 1990). However, later on in 1996, Tang and Gomez found that the particle size is independent of the nozzle size. They showed that the needle size significantly influenced the stable cone-jet mode domain of electrospraying. As the needle size increases, the maximum liquid flow rate needed for the stable cone-jet electrospray decreases dramatically. This illustrates that in the voltage-flow rate

graph, the stable cone-jet domain of the electrospray becomes narrower as the needle size increases (Tang and Gomez, 1996).

In 2002, the study conducted by Jayasinghe showed that the droplet trajectories depend on the configuration of the ground electrode. For a point like ground electrode, the smaller the diameter of the point, the higher configuration of the droplets generated in the spraying pattern. They pioneered the use of a point-like ground electrode, and this configuration of the ground electrode was the key to their innovation of electrostatic atomization printing (Jayasinghe et al., 2002).

2.9 Co-axial Electrohydrodynamic Atomization

Further development of the EHD process led to the co-axial electrohydrodynamic atomization. In this technique, electrohydrodynamic forces generate co-axial jets for immiscible liquids or suspensions. A schematic of the basic experimental setup for the co-axial EHD process is provided in **Figure 2.11**, where the two immiscible liquids or suspensions (yellow for outer liquid and blue for inner liquid) are passed through the two concentrically arranged capillaries. The outer and inner needles in the co-axial arrangement are coupled to the same electrical potential of several kilovolts relative to an earthed ring electrode.

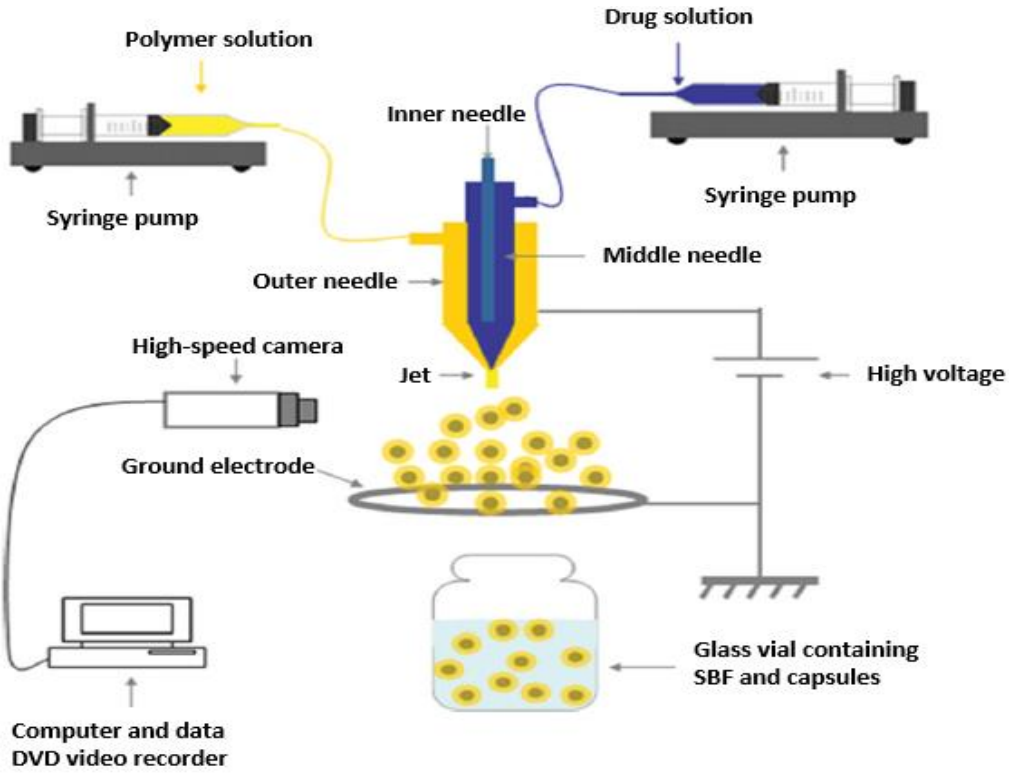

Figure 2.11: Schematic representation of the co-axial EHD setup (Enayati et al., 2010a)

2.9.1 Co-axial Electrohydrodynamic Atomization Mechanism

For a certain range of flow rates and applied voltages which depends on the physical properties of suspensions, a cone-jet is formed at the exit of needles with an outer meniscus surrounding the inner one (**Fig. 2.12b**). A liquid thread is distributed from the vortex of each one of the two menisci, leading to a compound jet of the two co-flowing suspensions (**Fig. 2.12c**) (Loscertales et al., 2002).

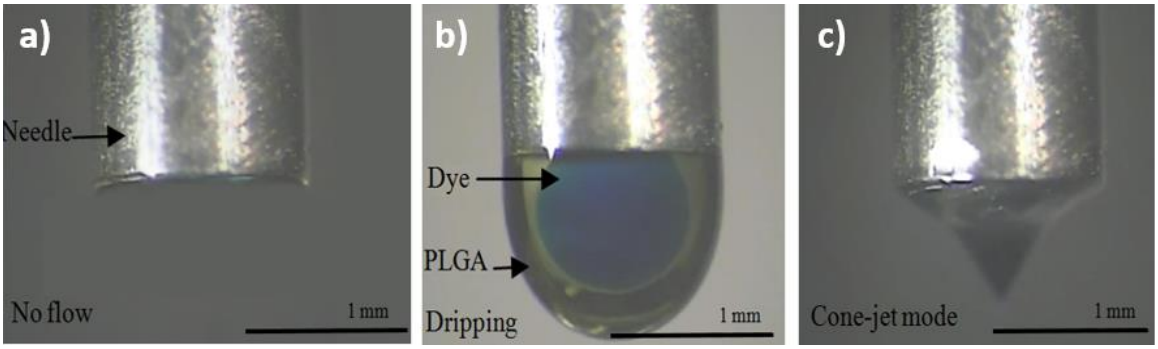

Figure 2.12: The co-axial EHD process: a) Needle, b) Dripping mode and c) Formation of a compound cone-jet

2.9.2 The Driving Liquid Concept

For obtaining a structured and stable cone-jet, the electrohydrodynamic forces in terms of voltage supply must act on at least one liquid, although they may act on both. In the co-axial EHD process, the liquid/suspension which the electrohydrodynamic forces act predominantly to form a cone-jet is called the driving liquid. The driving liquid can be determined by comparing the electrical relaxation time of the two liquids. The electrical relaxation which was introduced in **Section 2.8.4.4** on relative permittivity, is the time required to smooth a perturbation in the electric charge. The driving character of one of the liquids can be neglected in favour of the other one if the electrical conductivity is sufficiently enhanced by adding a suitable additive to it (López-Herrera et al., 2003). By applying voltage as an electrical force, when charges are located at the outer surface, the tangential electrical stresses which point towards the vortex of the conical interface must be efficiently transmitted throughout the liquid bulk by viscous diffusion. This requires the viscosity of the outer liquid to be high enough to play a crucial role in the liquid motion. Furthermore, the use of low viscous liquid in the outer needle would lead to intense re-circulation in the electrified meniscus and these re-circulatory motions are incompatible with the stable compound jets. However, when the liquids with lower viscosity is adopted as drivers in the inner needle, even a non-conductive liquid such as olive

oil can be used in the outer needle. This is one way of electrospraying non-conductive liquids such as insulators (Loscertales et al., 2002).

2.10 Applications of EHD Methods in Preparation of Various Drug Carriers

2.10.1 Single Needle EHD Method

In the single needle EHD processing, a therapeutic agent is encapsulated in the particles, e.g. dispersed in a polymeric matrix (Ciach, 2007). The processing parameters and the inherent physical properties of the solutions adopted perform a crucial role in determining the characteristics of the drug carriers. It has been demonstrated that the parameters such as needle size, collection distance, flow rate and the applied voltage enables carriers to be generated with different size, shape and morphology for various applications (Berkland et al., 2004; Xie et al., 2006a, 2006b). The first part of the experimental work in this thesis concentrates on controlling the size of the fabricated spheres via processing parameters. Then, a detailed description of various structures such as spherical particles with smooth and porous surface made by the single needle EHD is given. Furthermore, the single needle EHD setup followed by TIPS process was then applied for fabrication of the polymeric microspheres loaded with the model drugs.

2.10.1.1 Spherical Particles

One of the most essential challenges in the current pharmaceutical and medical research is the generation of drug loaded carriers with high encapsulation efficiency and a well-defined and controllable size distribution (Langer, 1998). In 2009, Wu adopted the EHD technique for production of spherical nanoparticles with mean size ranging 300-400 nm which were composed of genetically engineered elastin-like polypeptides (ELPs), a biodegradable and bioresponsive polymer. In this study, doxorubicin was successfully loaded into the particles and the loading of the drug at 20 wt% did not influence the product morphology. However, the particle size, polydispersity and morphology were significantly affected by solvent concentration, spraying voltage and the polymer molecular weight. The release rate of the drug was also influenced by the pH and solubility of ELPs (Yiquan Wu et al., 2009). Xu and Hana Similarly prepared bovine serum albumin (BSA)-loaded tripolyphosphate (TPP) cross-linked chitosan particles with size which was found to be hugely influenced by flow rate (Xu and Hanna, 2007). In another study, BSA loaded spherical particles was fabricated by

electrospraying an emulsion of BSA in polylactide (PLA) solutions. The spherical particles ranging from 0.8-4 μm were produced with smooth surface (Xu et al., 2006). The encapsulation efficiency and the yield of the process were varied 22-80% and 64-80% respectively. However, the *in vitro* release profile of the loaded material did not show a steady state during the time of observation owing to quick PLA erosion (Xu et al., 2006).

It has been illustrated that EHD processing can be adopted for preparation of polymeric micro- and nano-spheres encapsulating both hydrophilic and hydrophobic drugs (Pareta et al., 2005; Valo et al., 2009), which the biofunctionality of the drug is unaffected and also the high encapsulation efficiencies can be obtained. For example, Xie *et al.* generated spheres by EHD processing for sustained delivery of the anticancer drug paclitaxel to treat C6 glicoma with an encapsulation efficiency up to 80% (Xie et al., 2006b). Same values were stated for the case of ampicillin loaded chitosan micro/nano-spheres with a mean size of 520 nm (Arya et al., 2009), and by Ding *et al*. for taxol-loaded poly (ε-caprolactone) (PCL) which showed great sustained release profiles for a month (Ding et al., 2005).

Furthermore, varying the properties of the solvents and solutions employed in EHD forming also provided a means of tailoring the morphology and different structures of the spherical particles (Farook et al., 2009a). In 2004, Berkland presented that specific structural types such as tapered shapes, porous surface, and blood cell-shaped particles could be obtained by changing the properties of the polymer and solvent adopted (Berkland et al., 2004). Decrease in the size of the generated particles was demonstrated by increasing the conductivity of the polymer solutions. Also, the morphology of the fabricated particles can be considerably varied by adopting different combinations of polymers such as poly caprolactone, poly lactic-co-glycolic acid and poly-L-lactic acid and solvents (Yao et al., 2008).

2.10.1.2 Porous Particles

Recently, near monodisperse (uniform size) microspheres with surface porosity have received much attention and been classified as a new category of particles on the account of their higher effective diffusivity and available surface area compared to their counterparts with smooth morphology of same size (Jeong et al., 2007; Yow and Routh, 2008; Yin and Yates, 2008). The bioactive agents can be arranged in a specific order to make this structure have a unique architecture for particular applications in pharmaceutical and biomedical research (Jiang et al., 1999). In 2007, Wu and Clark collected porous particles by electrospraying the PCL different

solutions into water bath. They had the different concentrations of PCL solutions dissolved in chloroform. Solvent evaporation and phase separation are the two main mechanisms for the formation of pores on the surface of particles. They demonstrated that solvents with low boiling points generate pores with irregular morphologies and large dimensions. Moreover, Wu and Clark illustrated that solvents with internal property of high evaporation rate has key role in the formation of porous particles via EHD processing (Wu and Clark, 2007). Also, in 2009, Enayati *et al.* conducted a study using EHD process for evaluating the release profile of oestradiol from the polymeric particles. The results illustrated that the porous membrane in the PLGA particles which was induced by sonication could lead to a higher rate of drug release with more controllable release manner compared to their counterparts with the smooth surfaces (Enayati et al., 2010a). Moreover, the porous morphological particles can lead to a higher initial burst release due to the surface porosities which can be more suitable for targeted delivery and chronic wound therapy (Setterstrom et al., 1984).

2.10.1.3 Aerosol

Aerosol is another type of pharmaceutical carrier which can be generated using the single needle EHD process. In 1990, the first aerosol carriers were produced for pulmonary disease therapy. The aerosols which are adopted in an inhaled drug delivery system for pulmonary disease therapy must have some critical characteristics. For example, for an effective drug delivery of the aerosol to the lower airway, the aerodynamic size distribution of the particles should be varied between 2-5 μm with near monodisperse (uniform size) property (Ijsebaert et al., 2001). Based on the final aerosols collected in this study, EHD processing was shown to meet these requirements for fabrication of the required products. The resulting microspheres were nearly monodisperse, and the size distribution of particles could be simply varied by controlling the processing parameters such as the applied voltage and flow rate. In another study in 2000, Zimlich *et al.* developed a hand-held prototype of pulmonary drug delivery nebulizer using the single needle EHD process. In this study, 78% of the aerosols with a size of 1-6 μm were found in the respiratory tract, which were approximately four times greater than that attained using some other commercially tested devices (Zimlich et al., 2000).

2.10.2 Co-axial EHD Method

The co-axial EHD processing is a powerful technique for the fabrication of capsules in the range of micrometre and nanometre size. It facilitates encapsulation of sensitive materials such as cells, enzymes, dye and/or drug in the core of a protective shell. A range of different polymeric materials including polyurethanes, polysiloxanes, polylactides, polyglycolides, poly(lactic-co-glycolic) acid are employed as shell materials of the capsule/bubble production. The polymers mentioned above are the most desirable materials for encapsulations, owing to their physical properties, such as elasticity, insulating ability, physical strength, toughness and freedom from leachable impurities. Many of these polymers in particular, polylactide (PLA), polyglycolide (PGA) and poly(lactide-co-glycolide) (PLGA) are designed to degrade within the body environment (Brannon-peppas, 1997; Langer, 1998). These biodegradable polymers have been widely adopted in research and pharmaceutical applications as they have shown no adverse tissue reaction when carrying bio-active agents. They can be hydrolysed in human body to form products which can be easily eliminated without the need to remove the implants by surgery. Also, the co-axial EHD method has the ability for microbubble productions in which they have shown great potential in therapeutic applications such as targeted drug delivery, diagnostic imaging, focused ultrasound surgery, and also gene therapy (Mizushige et al., 1999; Poliachik et al., 1999; Schmidt and Roessling, 2006; Unger et al., 2001). In this study, the co-axial EHD combined with TIPS process was also used for fabrication of the loaded microspheres and comparison of the data obtained from the single needle EHD/TIPS method.

2.10.2.1 Capsules

Using the co-axial EHD method for micro/nano encapsulation is of particular interest in drug delivery (Barisci et al., 2000; Xie et al., 2008), food industry (Yoshii et al., 2001), and specific material processing (Burlak et al., 2001; Lee et al., 2001). Loscertales *et al.* conducted a study in 2002 in order to demonstrate the fabrication and control of near monodisperse capsules in varying size ranges from 0.15 to 10 micrometres. This study showed that the capsule diameters were affected by experimental parameters including applied voltage and the flow rates, the physical properties of the solution and also the interaction between inner and outer solutions during the electrospray (Loscertales et al., 2002). A year later, an investigation was conducted by Lopez-Herrera *et al.* to study the electrified co-axial jets of two solutions progressed from a structured cone-jet. This group presented the concept of driving liquid and also studied the linear scaling law for predicting the jet diameters as described in **Section 2.8**. However, their

work did not involve the specification of criteria that determines the structure of the capsules (López-Herrera et al., 2003). Chen *et al.* conducted another study to investigate the co-axial jet electrospraying using an ethanol/glycol/TWEEN mixture and cooking oil as two solutions. In this study, they discovered that the physical properties of the outer liquid with higher viscosity and more electrical conductivity play important role in controlling the process (Chen et al., 2005).

Number of studies have been conducted in this category for encapsulation of bioactive agents. Paclitaxel as a hydrophobic anticancer drug was encapsulated in biodegradable polymer via the co-axial EHD process (Ding et al., 2005). The size distribution of the capsules in this study was between 1 and 15 µm. Another study related to microencapsulation was conducted by Pareta and Edirisinghe to demonstrate the ability of the co-axial EHD setup for preparation of polymer-coated starch/bovine serum (BSA) capsules. The mean diameter of the products was found to be 5-6 µm and more than 75% of the BSA in the *in-vitro* studies was released over a 7 days period (Pareta and Edirisinghe, 2006). In 2009, Wu *et al.* produced oligodeoxynucleotide encapsulated lipoplex nanocapsules via co-axial jetting (Yun Wu et al., 2009). In this study, the products diameter was about 190 nm which they provided an efficient medium for gene therapy. In another study in 2010, Enayati *et al.* used the co-axial needle EHD method to produce oestradiol encapsulated in the biodegradable poly (lactide-co-glycolide) shells ranging from 120 nm to a few micrometres (Enayati et al., 2010a). The *in vitro* studies of this investigation showed a sustained release of the drug for a period of over 20 days with entrapment efficiency of 70%. Capsules with micro- and/or nano-scale anisotropy have received additional attention owing to their ability to instantaneously show different physical and chemical properties. In Lim *et al.* study, gold nanocrystals (NC) was encapsulated into one compartment of anisotropic polymeric particles via EHD co-jetting of aqueous nanoparticles suspensions followed by thermal cross-linking (Lim et al., 2010). Biocompartmental capsules with varying nanocrystal densities were acquired by changing the NC concentration in the jetting suspension. This investigation demonstrated a new approach for preparing organic/inorganic composite products with precisely engineered, anisotropic micro- and/or nanocapsules, and may contribute to advanced progress in developing scientific areas such as smart materials or particle-based diagnostics.

2.10.2.2 Microbubbles

Another versatile application of the co-axial EHD principle is to produce microbubbles with near monodisperse size distribution (Ekemen et al., 2013; Farook et al., 2007). Since EHD method can provide distinctive advantages compared with e.g. microfluidic devices and simple agitation (Pancholi et al., 2008), preparation of microbubbles via co-jetting has opened a new window in a range of different biomedical applications from use as contrast agents for ultrasound imaging to drug delivery. In 2007, Farook *et al.* was pioneered to show that the co-axial EHD system could be used for preparation of microbubbles less than 10 μm. In this investigation, glycerol was pumped through the outer needle of the co-axial needle arrangement, while air was simultaneously flown through the inner needle (Farook et al., 2007). This procedure was then adopted to fabricate phospholipid-coated microbubbles with a high yield of 10^9 bubbles per minute (Farook et al., 2009b). In this study, phospholipid-coated microbubbles were found to be highly stable at ambient temperature with size distribution of 6.6 ± 2.5 μm. However, at biological temperature (37^{o}C), the mean diameter of the bubbles rapidly decreased to 1-2 μm within 20 minutes (Farook et al., 2009a). Farook *et al.* also demonstrated that the stability of the microbubbles prepared by the co-jetting can be further improved and the polydispersity index controlled by adding a dispersant such as Tween to the phospholipid solution (Farook et al., 2009a). Producing bubbles by the co-axial EHD process demonstrates three characteristic spray modes: bubble dripping, coning and continuous bubbling as the latter mode is the most suitable mode for microbubble preparations for applications in biomedicine. In another study, Ekemen *et al.* used silk fibroin (SF) to produce hallow spherical structure of SF in single step by utilizing the co-axial EHD process. The produced bubbles had size distribution of 240-1000 μm and their characteristics could be easily controlled through simple adjustments of the processing parameters (Ekemen et al., 2013). FTIR characterizations of the samples confirmed that the rate of air infused into the SF bubbles during the processing was enhanced at higher flow rates. Ekemen *et al.* also showed that the resultant bubbles can serve as pore generator when dehydrated (Ekemen et al., 2013). The results acquired from tensile strength test presented that the electrohydrodynamically fabricated SF and their composite bubbles can be used as new tools for generating porous structures in a controlled manner with a range of potential applications in biocoatings and tissue engineering scaffolds.

2.10.2.3 Hollow Spheres

Many studies have recently focused on the versatility of co-jetting in production of hollow micro- and nano-spheres. Chang *et al.* (2009) conducted a study using volatile liquid such as perfluorohexane (PFH) instead of air at inner needle to produce hollow spheres. In this study, polymethylsilsesquioxane (PMSQ) capsules were generated using the co-axial EHD process with an even higher degree of control over their characteristics. It provided a mean of controlling the content of the capsules by heating the suspension to the boiling point of the PFH. Experimental results showed that using more volatile liquid leads to higher near monodisperse products at the cone-jet mode, compared to those with less volatile solvent (**Fig. 2.13**) (Chang et al., 2009). This is due to the inherent properties such as high evaporation rate, moderate conductivity and low surface tension of the solvent used during the EHD process.

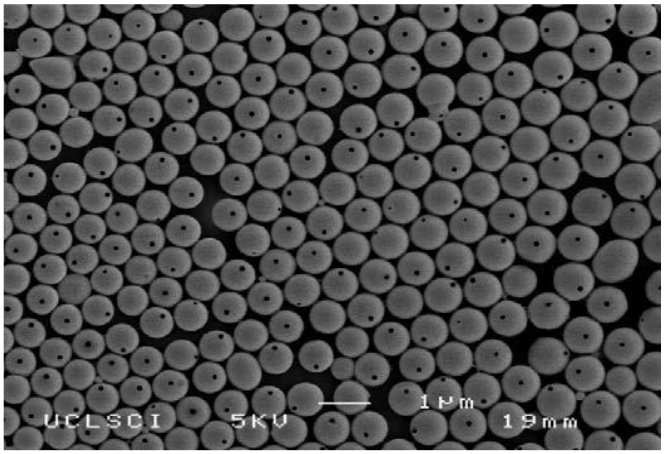

Figure 2.13: SEM image of the one-hole microspheres (flow rates for PFH at 300 μl min^{-1} and for PMSQ at 600 μl min^{-1}) (Chang et al., 2010).

Unlike traditional methods such as emulsification, fabrication of core-shell capsules via the co-axial EHD forming was obtained in a single step, which is clearly more preferable. In this study, dye encapsulation was obtained by PFH core evaporation to enable inward diffusion of the liquid (Chang et al., 2009). This procedure was further developed for fabrication of monoporous hollow spheres (Chang et al., 2010) which in turn could provide higher effective diffusivity (Guan et al., 2007). Chang *et al.* (2009) also showed that the geometry and the porosity of these nanocapsules with and without a single surface pore could be controlled by changing the processing parameters of the co-axial EHD setup. Experimental observations demonstrated that flow rate plays the most important factor in the final morphology which could be varied to control the pore size of the hollow nanospheres. The size distribution of the fabricated monoporous hollow spheres is between 275 and 860 nm with the pore size of 35-135 nm. In this study, the formation of surface pore is highly related to evaporation flux of the

PFH solvent during the electrospraying process. This method overcomes some of the challenges related to the existing techniques of producing this type of structure, for instance, requirement for highly specialised equipment, presence of highly controlled processing environment and the use of surfactants and other additives (Guan et al., 2007). Ability for tuning the pore size of the hollow spheres via the co-jetting system is of interest for specific applications in drug/gene delivery vehicles, targeting and catalysis.

2.10.3 Application of Multi-Capillary EHD Processing

2.10.3.1 Three Needles EHD System

Versatile capability of EHD system in encapsulation led to different combination of needles arrangement. The concept of electrified co-jetting was further extended by Roh *et al.* (2006), and triphasic nanocolloids with three different compartments were obtained by simultaneous injection of three separate liquid flows (Roh et al., 2006). Later on in 2008, Ahmed *et al.* exhibited the ability of employing three co-axially arranged needles to form a variety of novel morphological structures (**Fig. 2.14**) (Ahmad et al., 2008).

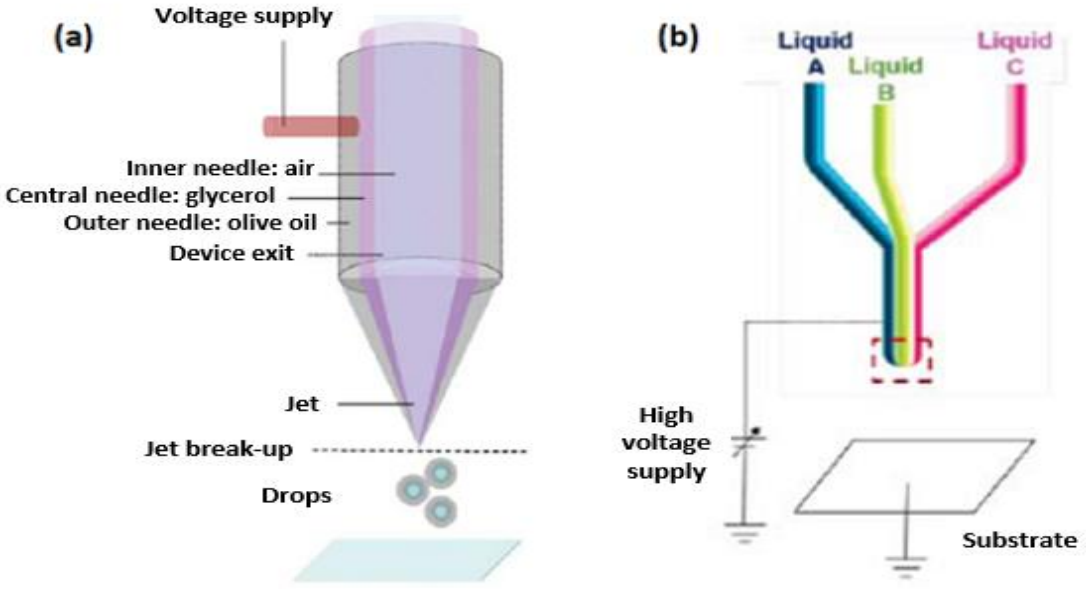

Figure 2.14: Schematic representation of the three needles experimental set up of (a) Concentric arrangement and (b) Co-planar arrangement (Ahmad et al., 2008; Roh et al., 2006)

The resulting documents from Ahmad *et al.* study showed the ability of electrohydrodynamic flow for preparing double layered bubbles, porous encapsulated threads and nanocapsules containing three layers (Ahmad et al., 2008). This capability of EHD system in processing multi-layered structures could provide multistage controlled release (Ahmad et al., 2008), and

in situ encapsulation of nanoparticles, liquid and/or gases (Ahmad et al., 2008; Kalra et al., 2009). In multi-capillary EHD system, it is not imperative to have the needles arranged concentrically (**Fig. 2.15**).

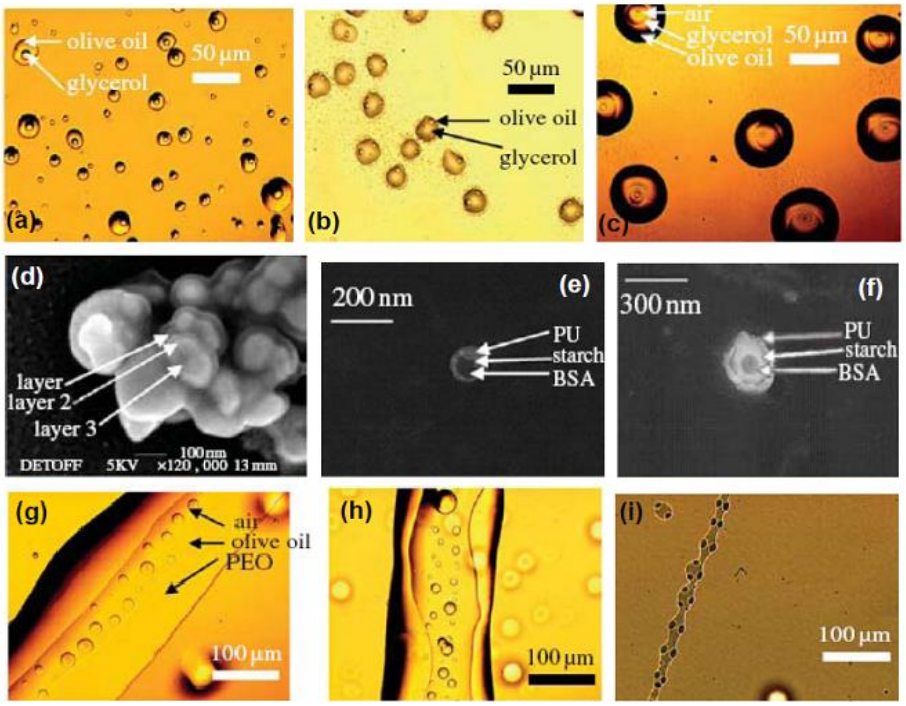

Figure 2.15: Droplet, nanocapsule and thread formation: (a) The co-axial two needles with olive oil and glycerol; (b) Non-concentric co-axial two needle encapsulation; (c) Co-axial tri-needle encapsulation with air, glycerol and olive oil; (d) High magnification scanning electron micrograph of nanocapsules showing different regions (densities); (e) Transmission electron micrograph of nanocapsule with non-concentric multiple layers; (f) Transmission electron micrograph of nanocapsule with concentric multiple layers; (g) Air encapsulation in twin-layered thread with olive oil and PEO solution; (h) Instabilities during thread formation; and (i) Two-needles (third needle switched off) co-axial non-concentric thread encapsulation using olive oil and PEO solution (Ahmad et al., 2008)

Three needles system can also be used as anisotropic imaging probes with short-term biocompatibility by reducing the co-polar distance of two needles (Yoshida et al., 2007).

2.10.3.2 Four Needles EHD System

Great flexibility of the EHD system in microencapsulation of different materials led to more sophisticated arrangement of co-axial four needles. Labbaf *et al.* (2014) pioneered to demonstrate the feasibility of using four co-axially arranged needles in production of nano-particles and fibres with four distinct layers (Labbaf et al., 2014).

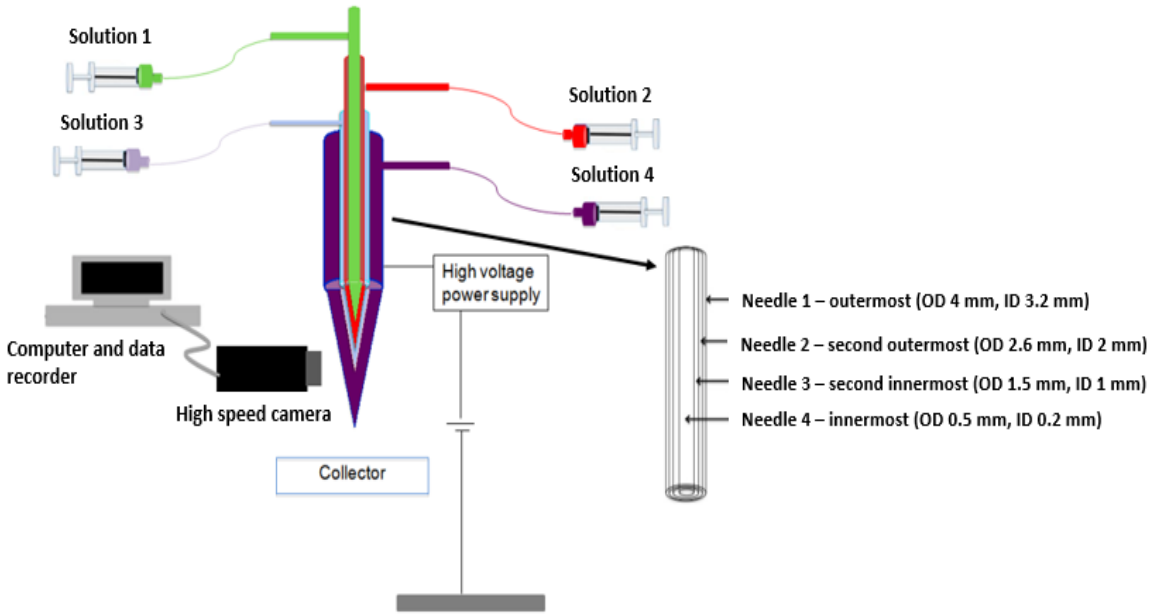

Figure 2.16: Schematic diagram of four needle experimental setup (Labbaf et al., 2014)

Four different polymers, polyethylene glycol (PEG), poly (lactic-co-glycolic acid) (PLGA), poly (ε-caprolactone) (PCL) and polymethylsilsesquioxane (PMSQ) were used for generating the multi-layered polymeric carriers (**Fig. 2.17**). This study showed the great feasibility of EHD forming process in successfully producing the four layered drug delivery vehicles in a single step, which can be hugely beneficial to provide multi-stage controlled release of active agents for particular applications in pharmaceutical and biomedicine (Labbaf et al., 2014).

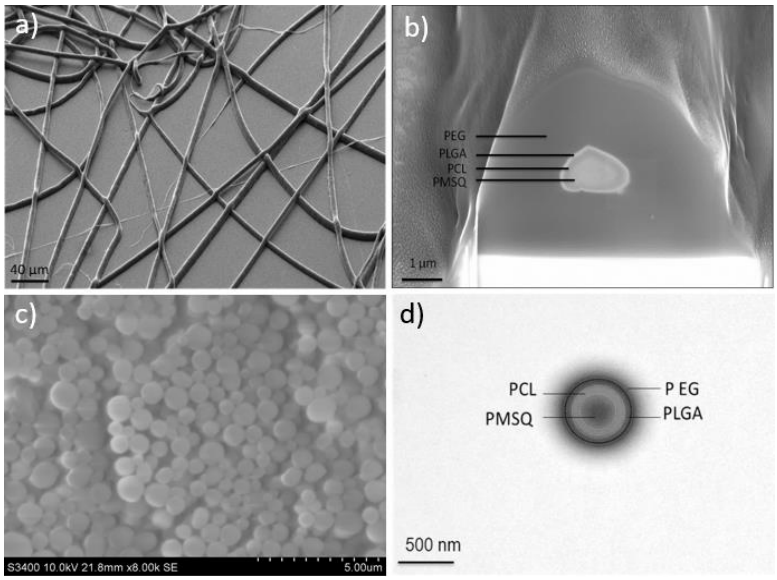

Figure 2.17: Formation of products produced by the four needle EHD process: a) Fibres, b) Fibre cross section, c) Nanoparticles, d) Nanoparticle cross section (Labbaf et al., 2014)

Transmission (TEM) and scanning electron microscopy (SEM) followed by focused ion beams showed that the produced fibres were quite uniform (**Fig. 2.17a**) and possesses four different

layers of 2, 0.07, 0.12 and 1 μm in thickness from outer to inner (**Fig. 2.17b**). The acquired results also presented the four layered spherical nanoparticles with average size distribution of 620 nm ± 150 nm (**Figs. 2.17c** and **2.17d**). Furthermore, *in vitro* release studies were conducted in support of the four layered nanoparticles. Four different dyes were separately loaded in each layer during electrospraying to show the multi-stage controlled release manner of the produced nanoparticles over time (Labbaf et al., 2014).

2.11 Polymers and Drug Delivery Systems

Polymers, as the most versatile class of materials, have been widely adopted for application in drug delivery systems (Li and Vert, 1999). Polymers can be either degradable or non-degradable. Over the past two decades, the use of biodegradable and biocompatible polymers for the administration of therapeutic agents has been rapidly enhanced. This type of polymers can be either natural or synthetic. In general, synthetic polymers have several advantages over the natural ones as their properties can be tailored and have lower level of toxicity. An important key point to consider when selecting a drug carrier is to match the degradation rate to the needs of the application (Uhrich et al., 1999).

Synthetic polymers are broadly used for drug delivery and they often include esters such as poly lactic acid (PLA), poly glycolic acid (PGA), the copolymer poly lactic-co-glycolic acid (PLGA) and poly ε-caprolactone (PCL). These cited polymers are considered as the aliphatic polyesters which have attracted much interest as drug carriers due to their biodegradability and biocompatibility. This class of polymers degrades via the hydrolytic cleavage of the ester bonds in their backbone (Fu et al., 2000; Sinha and Trehan, 2003). More details about the PLGA and PCL, the two polymers adopted in this study, are provided below.

2.11.1 Poly (Lactic Acid-Co-Glycolic Acid) (PLGA)

This type of polymer is amphiphilic. However, the lactic acid is more hydrophobic than the glycolic acid, and hence lactic-rich PLGA copolymers are less hydrophilic. It absorbs less water, and subsequently degrades more slowly (Witschi and Doelker, 1998). The physical properties such as the polydispersity index and the molecular weight influence the mechanical strength of the polymer and its ability to be formulated as a drug delivery vehicle. Furthermore, these properties may control the biodegradation rate and hydrolysis of the polymer. PLGA is basically synthesised by means of random ring-opening co-polymerization of glycolic acid and

lactic acid monomers. During the process of polymerization, successive monomeric units of glycolic and lactic acid are linked together in PLGA by ester linkages; therefore, yielding linear, aliphatic polyesters as products (**Fig. 2.18**). The commercial PLGA polymers are usually characterized in terms of intrinsic viscosity, which is directly related to their molecular weight. The other properties of the copolymer such as mechanical strength, swelling behaviour, capacity to undergo hydrolysis and subsequently the biodegradation rate are directly influenced by the PLGA polymer crystallinity. The resultant crystallinity of PLGA copolymers depends on the type and the molar ratio of the individual monomer components of lactide and glycolide in the copolymer chain (Jalil and Nixon, 1990). The PLGA polymers containing 50:50 ratio of lactic and glycolic acids are hydrolysed much faster than those obtaining higher proportion of either of the two monomers (Sinha and Trehan, 2005).

The glass transition temperature of the PLGA copolymers is above the physiological temperature of 37^{o}C, and hence they are glassy in ambient temperature. Therefore, they obtain a fairly rigid chain structure that provides them with sufficient mechanical strength to be utilized in drug delivery vehicles. In 1988, Jamshidi *et al.* reported that this glass transition temperature of PLGA decreases by decreasing the content of lactide in the copolymer composition and reducing the molecular weight (Jamshidi et al., 1988).

A three phase mechanism for the biodegradation of PLGA copolymer has been reported (Cai et al., 2000) as follows:

1. Random chain scission process, which the molecular weight of the polymer reduces extensively. However, there is no considerable weight loss and no soluble monomer products made.
2. A decrease of molecular weight in the middle phase is accompanied by rapid loss of mass, and soluble oligomeric and monomer products are formed
3. The products of soluble monomer are formed by soluble oligomeric fragments which corresponds to the complete polymer solubilisation

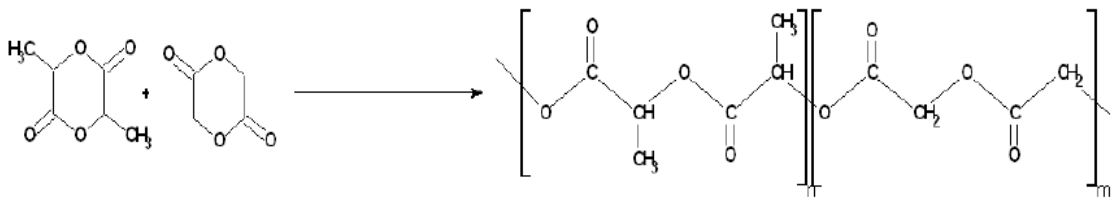

Figure 2.18: Synthesis of poly (lactic-co-glycolic acid) (PLGA)

2.11.2 Poly (ε-Caprolactone) (PCL)

PCL is another type of aliphatic polyester which is synthesised by the ring-opening polymerization of the cyclic monomer ε-caprolactone (**Fig. 2.19**) (Benoit et al., 1999).

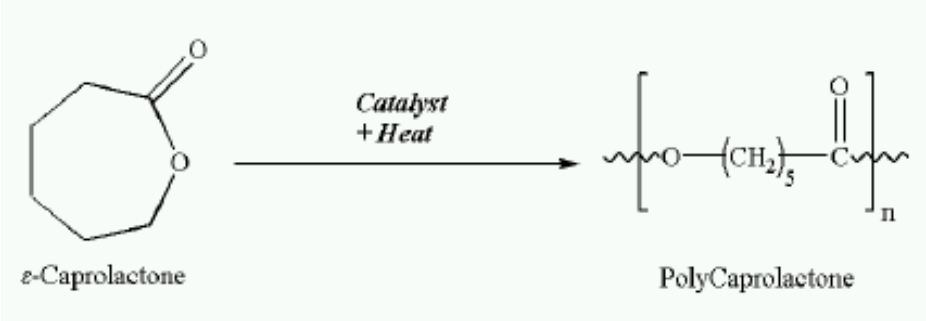

Figure 2.19: Synthesis of poly (ε-caprolactone) (PCL)

There are distinct mechanisms that influence the PCL polymerization and they are categorised as anionic, cationic, co-ordination and radial. Each one influences the molecular weight (M_w), molecular weight distribution, end group of composition and chemical structure of the polymer. PCL with semi-crystalline structure has a glass transition temperature of -60ºC and a melting point ranging between 59-64ºC, depending on the crystalline structure of the polymer. The average molecular weight of PCL samples varies from 10,000 to 45,000, and it is graded according to the molecular weight (M_w). PCL is soluble in hydrophobic solvents such as chloroform, dichloromethane, carbon tetrachloride, benzene, toluene and cyclohexanone in ambient temperature. However, it has low solubility in acetone, 2-butanone, ethyl acetate, dimethyl formamide and acetonitrile and is insoluble in alcohol, petroleum, ether and diethyl ether. PCL can be combined with other polymers in order to improve stress crack resistance, dye ability and adhesion. PCL polymer is adopted in combination with other polymers such as cellulose propionate, cellulose acetate burytate, poly lactic acid and poly lactic-co-glycolic acid for manipulation of the drug release rate from micro- and nanoparticles (Chang et al., 1986).

2.12 Controlling and Regulating Drug Release Profiles

Controlled release systems based on using polymers as a carrier have been widely adopted to decrease the amount of drug required to achieve a given therapeutic effect in patients. The key purpose of these systems is to deliver the pharmaceutical agents to the target site and to release them at specified rate over a defined period of time. There are two strategies to achieve this aim: 1) increase the efficiency of such system in order to modulate the initial burst release phase, which is the period of high release rate in 24 hours following administration; 2) use of

external stimuli such as sonication to non-invasively promote the release from the polymeric carriers. This type of release profile regulation is applicable in pulsatile drug delivery systems. In this project, both strategies are investigated in order to find an ideal pattern in release profile of agents with optimum control in various therapeutic applications. The existing literature relevant to both strategies are discussed in the following sections.

2.12.1 Importance of the Burst Release in Drug Delivery Systems

As discussed earlier in **Section 2.2,** biodegradable polymer particles with loaded drug have been widely investigated in pharmaceutical applications for their potential to release bioactive agents in a sustained pattern. However, these products still suffer from a crucial technical issue which is known as the burst release (**Fig. 2.20**). The burst release usually occurs over a short period of time during the first 24 hours of administration (Huang and Brazel, 2001; O'Donnell and McGinity, 1997; Wang et al., 2002; Zhang et al., 2005).

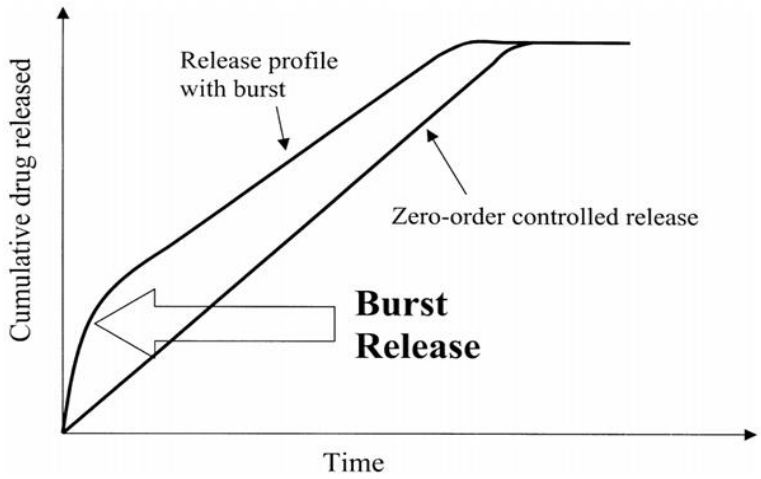

Figure 2.20: The burst release effect in drug delivery systems with a zero-order release pattern (Huang and Brazel, 2001)

Burst release is often regarded as an undesirable and negative phenomenon in drug delivery systems. Because it can be associated with toxicity and decreases the lifetime of the therapeutic systems, making it a major obstacle in the utilization of these types of delivery system. However, there are certain situations which this phenomenon can be desirable. In many pulsatile delivery systems, for example, repeated burst release is one of the purposes for rapid delivery of the active agents at specific time (**Table 2.1**); whereas in some other applications, therapeutic agents need to be administered at different rates. For example, the drugs adopted at the first stage of wound therapy need to have high initial release rates to provide instant pain

relief followed by a sustained and prolong release to help gradual wound healing (Setterstrom et al., 1984).

Table 2.1: Desirable application with positive and negative effects of burst release

Positive burst release situations	Negative burst release effects
Wound therapy (burst release followed by a diminishing need for drug)	Local or systemic toxicity (from high drug concentrations) and short half-life of drugs
Targeted delivery (triggered burst release)	Economically and therapeutically wasteful of drug
Pulsatile release	Shortened release profile; requires more frequent dosing

A few studies have been conducted to investigate the initial burst release mechanism and the control of this phenomenon. Burst release is usually attributed to two main reasons: 1) The heterogeneous distribution of the drug in the polymeric carriers, and 2) morphology of the drug loaded carriers as the drug can escape from their polymeric shell through porous structure which is formed during the fabrication process (Huang and Brazel, 2001; Yang et al., 2001).

In most previous investigations, surface-associated drugs have been identified as the main factor determining the burst release phase (Cohen et al., 1991). This mostly arises due to quick water intake of particle matrix which consequently leads to swelling of polymer chains near the surface. This in turn vastly increases the diffusion process of the therapeutic agent molecules dispersed in this region. Another reason associated with initial burst release could be due to the fact that some drugs become entrapped on the surface of the polymer shell during the fabrication process (Batycky et al., 1997). This usually arises when drug loading for encapsulation process is too high (Brazel and Peppas, 1999). Moreover, diffusion and migration of loaded agents during drying and storage stages may lead to a heterogeneous distribution of drugs. For example, as water moves to the particles' surface, it starts to evaporate and drug may diffuse by convection with water, leading to an uneven drug distribution across the particles, with higher concentration towards the surface (**Fig. 2.21**) (Kishida et al., 1998; Mallapragada et al., 1997).

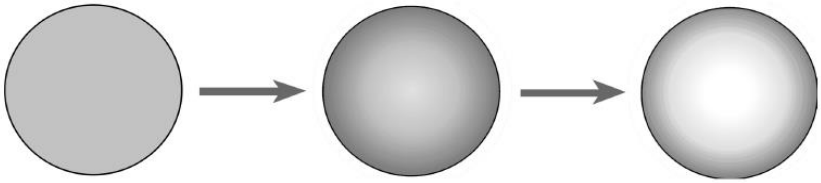

Figure 2.21: Drug redistribution at the surface due to convection during the drying process (Kishida et al., 1998)

2.12.1.1 Controlling the Burst Release Phase

Several strategies can be applied for controlling the burst release in application of drug delivery:

Preventing of drug on the surface of polymeric carriers

Decreasing the rate of water intake which can be achieved by enhancing the hydrophobicity of the drug carrier

Enhancing the diffusional resistance to the drug by increasing the length of the diffusion pathways to the drug molecules

The three strategies mentioned above can be effectively performed by enhancing the polymer concentration in fabricating solution, manipulating carrier size and surface modification (Huang and Brazel, 2001; Ravivarapu et al., 2000; Yamaguchi et al., 2002). There are a variety of surface modification techniques such as:

Surface extraction method, which is effective in decreasing the initial burst release, removes the applied drug from the outer layers of drug loaded carriers. However, the main problem with this technique is the extraction cost and the reduction in the effective use (frequently expensive) of active agents (drugs).

Surface modification via chemical couplings method, a complex procedure that involves two stages: 1) surface activation, 2) coupling reaction

Surface modification via co-incorporation of surface modifying agents into carriers' method, a process that requires surface modifying agents for co-incorporating into the carrier matrix during the fabrication protocol. This method requires overnight stirring, ultracentrifugation and in some cases elevated temperature which may lead to defunctionalisation of the active loaded agent.

Surface modification via additional coating method, is another method of controlling the burst release phase, by providing an outer drug free layer. In this strategy, the amount of drug release is regulated by the dissolution or erosion of the outer coating which is applied to the loaded polymeric carriers (**Fig. 2.22**). Optimising the thickness of the outer shell coating can result in a more controlled, time dependent release of the active agents. Also, the other processing parameters such as the type of the coating materials, their coating concentration as well as the coating techniques should be considered carefully in this strategy.

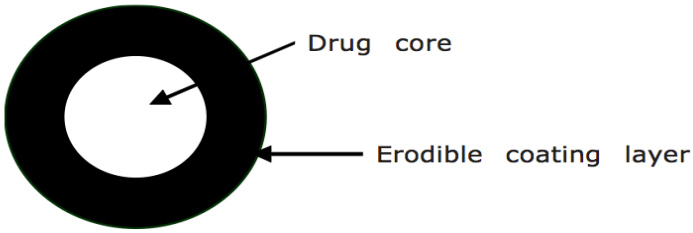

Figure 2.22: Schematic illustration of surface modification with erodible coating layer for drug release system (Rasve et al., 2011)

Although the suggested methods introduced above can be used to prevent burst release, they contain some additional costly phases which can lead to reductions in drug loading percentage and efficiency in such drug delivery systems. The final part of the thesis is allocated to the initial burst release phase, and the positive effect of this phenomenon for the particular biomedical application in chronic wound therapy.

2.12.2 Application of Sonication in Drug Release

Sonication is a subsection of acoustics that relates to sound pressure or stress waves at frequencies greater than the upper limit of the human hearing range i.e., >20kHz (Wu and Nyborg, 2008). Sonication has been adopted for over 30 years in diagnostic imaging of the human body. Also, it has been employed for other therapeutic applications, such as collagen repair promotion (Demir et al., 2004), nerve regeneration (Lazar et al., 2001; Paik et al., 2002), thrombolysis and fracture healing enhancement (Dalecki, 2004; Warden, 2003). In recent years, it has been applied for drug delivery enhancement including facilitating the delivery of drug across the skin and transferring chemotherapeutic drugs into tumours.

In sonication simulated pulsatile systems, the acoustic waves promotes the erosion of the polymer matrix, thereby increasing the drug release. An investigation was conducted by Miyazaki *et al.* to study the influence of sonication at a frequency of 1MHz on the release rate of bovine insulin from ethylenevinyl alcohol copolymer system. The results showed that insulin

release rate was improved with exposure of sonicator, which in turn led to a dramatic reduction in blood glucose level (Miyazaki et al., 1988). In another study, kost *et al.* also investigated the application of sonication on the degradation of biodegradable polymers such as polyanhydrides, polyglycolides as well as the release rate of the molecules integrated into those polymers. In the final outcomes, they observed the feasibility of ultrasonically augmenting of polymer degradation and up to 20-fold increase in the release rate of the incorporated materials (Kost et al., 1989).

Table 2.2: Application of pulsatile drug delivery system with the respective diseases (Rajput et al., 2012)

Disease	Chronological behaviour	Drugs used
Peptic ulcer	High secretion of acid in the afternoon and night	H_2 blockers
Asthma	Precipitation of attacks during night or at early morning hour	β_2 agonist, Antihistaminics
Cardiovascular diseases	Blood pressure is at its lowest during the sleep cycle and rises steeply during the early morning awakening period	Nitroglycerin, Calcium channel blocker
Arthritis	Pain in the morning and more pain at night	NSAIDs, Glucocorticoids
Diabetes mellitus	Increase in the blood sugar level after meal	Sulfonylurea, Insulin
Attention deficit syndrome	Increase in DOPA level in afternoon	Methylphenidate
Hypercholesterolemia	Cholesterol synthesis is generally higher during night than during day time	HMG CoA reductase inhibitors

Further application of sonication is the simulation of drug release in pulsatile systems. **Table 2.2** enumerates the various diseases that requires pulsatile drug delivery system as a more improved way of transferring the active agents within human body. This system has attracted the attention of many researchers for the treatment of various diseases in which the drug requires to release at different time interval.

It is essential to have a good understanding of the disease physiology before designing the pulsatile drug delivery system. Diseases where the circadian rhythm plays a crucial part, pharmacokinetics of the drug cannot be constant within 24 hours. Asthma, for example, is one of the diseases where the pulsatile drug delivery system can be usefully applied. This is because the circadian changes in normal lung function reaches a low point in the early morning hours and the pulsatile drug delivery system can be applied to enhance the dosage of the prescribed drug such as antihistamines at low points of the day.

2.12.2.1 The Physiological Effects of Sonication

There are two main types of physiological effects upon tissue with the application of sonication. Occurrence of its thermal effects is usually accompanied with the non-thermal effects; however by variation of exposure parameters, only non-thermal effects can be obtained.

Thermal bioeffects of sonication where thermal effects occur in tissue with an increased temperature to 40-45^{o}C for more than 5 minutes. These effects can produce number of biological responses including blood flow enhancement, muscle spasm reduction and also improved extensibility of collagen fibres (Barnett et al., 1994). Higher temperature can also result in protein denaturation and tissue ablation.

Non-thermal bioeffects of sonication which are predominantly based on two processes: 1) cavitation and 2) acoustic streaming. Cavitation in particular plays a significant role in delivering therapeutic agents to the targeted tissue.

Cavitation is the formation and successive oscillation of gas and/or vapour filled bubbles which expand and compress due to ultrasonically induced pressure variations in a medium exposed to the sonicator (Barnett et al., 1994). Based on ongoing researches, there are two distinct types of cavitation: stable (non-inertial) and transient (inertial). In the former cavitation, the induced pressure in the medium generates a fairly stable oscillation in bubble size. This oscillation produces a circulating fluid flow (known as acoustic microstreaming) around the bubbles which, in other word, is a unidirectional movement of fluid along the cell membrane (Marmottant and Hilgenfeldt, 2003). The amplitude of the oscillation controls the velocities and shear rates of microstreaming. The investigations show that microstreaming is capable of shearing open red blood cells (Rooney, 1970) as well as drug carriers such as liposomes (Marmottant and Hilgenfeldt, 2003) at high amplitudes. However, when the shear stress exceeds the strength of the vesicle, it will rupture and spill its contents.

Transient cavitation which is also known as collapse cavitation, occurs as a results of increase in the intensity of the sonication. For a given bubble size and sonicator frequency, there is a critical pressure above which the inertia of surrounding fluid cannot be supported by the pressure of the gas inside the bubble during compression. Therefore, the bubbles collapse and produce shock waves as well as high temperature and pressure inside the bubbles. This collapse can have a significant damage upon both cells and drug carriers and may also lead to production of smaller bubbles by fragmentation of the original bubbles. This action can have a further cavitation nucleus growing by more gas absorption from the surrounding area, then the process is repeated (Brennen, 1995). Asymmetrical collapse can also occur in the case of bubbles collapsing near a solid surface. This can produce a high speed fluid jet towards the solid surface (Jenne, 2001) and may be strong enough to penetrate the surface of relatively rigid drug carriers leading to release of additional drug and also damaging the tissue membrane (**Fig. 2.23**).

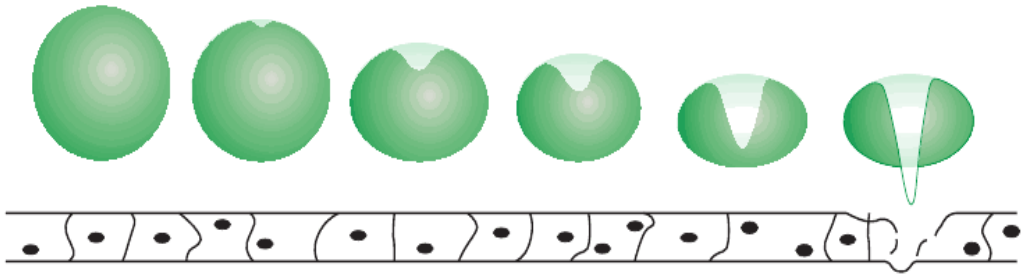

Figure 2.23: Asymmetric collapse of a bubble near a surface, producing a jet of liquid towards the solid surface (Pitt et al., 2004)

The acoustic shock waves caused by collapsed cavitation can also lead to enhancement of drug release rate by damaging the carrier surface. Recently, sonication has been used to efficiently regulate the drug release from the liposomes, micelles and particles by inducing both thermal and non-thermal influences. For instance, the presence of cavitation near the carriers' surface was found to significantly increase drug release rate and gene delivery (Enayati et al., 2010a; Ferrara, 2008; Suzuki et al., 2007; Unger et al., 2001).

Due to increased temperature and decreased pressure upon exposure of particles to sonicator, microbubbles will be formed. These microbubbles will undergo cavitation, causing pores formation on the particles surface, leading to the drug release in the surrounding medium. This action results in the enhanced permeability of the cellular membrane, most likely as a result of microstreaming, leading to enhanced penetration of the drug into the cells (Lentacker et al., 2010).

In this study, the application of sonication in drug release system has two purposes: first to provide a higher release rate of the adopted agents encapsulated in the polymeric particles, and second to evaluate the accuracy for the entrapment efficiency of the loaded ingredient which was calculated with respect to the yield of the process.

2.12.3 Application of Temperature in Drug Release

Temperature can have either positive or negative effects on the polymeric carriers as well as the encapsulated drug. These positive and negative effects on the polymeric carriers are dependent on the critical temperature of the polymer (Jones, 2004). For example, the critical temperature of 50%:50% (lactide:glycolide) PLGA is 37°C; thus the polymer will start to shrink and collapse as the temperature is raised above this point. However below the critical temperature, the polymer is formed crystalline. Since, the PLGA is a biodegradable polymer, in an aqueous solutions, it will shrink and biodegrade at faster rate above the critical temperature compared to that of below the critical temperature. Therefore, the drug release from the PLGA carriers occurs at faster rate due to quicker bulk erosion of the polymer above the critical point compared to that of below the critical point (Jamshidi et al., 1988).

In the study conducted by Reddy *et al.*, it was found that the drug release rate is dependent on temperature of the release medium (Umamaheswara Reddy et al., 2007). Variations in temperature can lead to more controlled manner of drug release depending on the chemical properties such as evaporation or degradation rate of the encapsulated active agents (Deng et al., 2010). Deng *et al.* also demonstrated that more control of the initial burst release phase can be obtained by variations in the temperature of the release medium. However, the changes in temperature for obtaining a more controllable release profile is completely dependent on the chemical structure and degradation rate of active agent in the release medium. For example, in Shi *et al.* study, more controlled release of the encapsulated agents (Ca-alginate and poly(N-isopropylacrylamide)) in hydrogel beads was observed at lower temperature (25^{o}C) compared to higher degrees (37^{o}C) (Shi et al., 2006), whereas in Lin *et al.* study more controlled release of the drug from the ethylene vinyl acetate (EVA) was found at higher temperature (37^{o}C) compared to lower temperature (24^{o}C) (Lin et al., 2003). Thus, the release rate of drug at different temperatures not only depends on the critical temperature of the biodegradable polymer in aqueous solution, it is also dependent on the chemical properties of the incorporated materials. In this Study, temperature as another external stimuli has been also used to

investigate its influence on the release rate of the encapsulated materials from the polymer carriers.

2.13 Application of Biomaterials in Biomedical Research

Although biomaterials have great potential to positively improve the quality of life, at the same time they may be associated with health risk; particularly the inhalation toxicology and pathology of particles have become the important features which affect their wide applications in pharmaceutical and biomedical fields (Williams, 2008). Bio-safety is one of the most crucial requisites for medical devices, including every medically applied particles. Thus, it is essential to develop bio-safe micro- and/or nano-spheres. Different morphological spheres were fabricated earlier and applied in biomedical fields; however, the potential bio-safety problems still exist, since most of them had been generated by metals (Asiyanbola and Soboyejo, 2008; Chen et al., 2006; Gupta et al., 2006), metallic oxides (Liu et al., 2008), inorganic materials (Hilder and Hill, 2008) and non-biodegradable polymers (Bhargava et al., 2006; Hou et al., 2003; Luo and Eisenberg, 2001; Zhang and Eisenberg, 1996). Therefore, these potentially harmful particles may be deposited permanently in the tissues of the body, with possible translocation to major organs, and hence limiting the medical usage of such materials.

Producing the appropriate size of microspheres is one of the main and important features of such drug delivery systems. The appropriate size distribution of spheres will determine their ability to penetrate the structure of tissue *in vivo* (intercellular trafficking), which may become both desirable and/or undesirable in various applications (Sinha et al., 2006). Morphology of spheres is another crucial factor in determining physical and chemical properties which also influences their *in-vivo* applications. Spherical particles with different morphologies and sizes will have distinct surface area to volume ratio, anisotropy and so on, endowing them additional promising advantages for medical and pharmaceutical applications (Chen et al., 2006; Hilder and Hill, 2008; Liu et al., 2008).

2.13.1 Chronic Wound Therapy

Chronic wounds barely heal itself in an orderly set of steps and in an expected time the most wounds do (Mustoe, 2005). The wounds which do not heal within three months are generally considered chronic. In acute wounds, there is a precise stability between production (tissue regeneration) and degradation of collagen, whereas in chronic wounds this balance is disrupted

and degradation plays an excessive role (Edwards et al., 2004). These wounds cause patients severe emotional and physical stress which creates significant burden on the entire healthcare system (Augustin and Maier, 2003). Chronic wounds may only influence the epidermis and dermis or the tissues where is it appeared all the way to the fascia (Crovetti et al., 2004). Chronic wounds are often accompanied with pain, and bleeding to some extent. Lack of treatment of a chronic wound will lead to more pain and possible blood infection, and consequently will induce cancer depending on the location and the severity of the wound in the affected tissue (Reddy et al., 2012).

Perianal fistulae are a severe type of chronic disease with an abnormal connection in the form of hollow track between the anal canal and the perianal skin. The aetiology of perianal fistulae contains anorectal abscess initiated by bacterial infection, Crohn's disease, trauma and anal fissure (Blaker et al., 2008a, 2008b). Although the pathogenesis remains undetermined, there are two key hypotheses: 1) fistulae can initiate in the anus or rectum as deep penetrating ulcers which spread over time as a consequence of faeces being pushed into the ulcer with the defecation forces (Hughes, 1978), 2) fistulae can occur due to infection or frank abscess of the anal glands located at the anal crypts (Hawley, 1975; Parks, 1961; Schuppan and Freitag, 2004). Based on the both hypotheses, fistulae appear when there is no quick compensatory fibrogenic response to fill the caused defect (Kirkegaard et al., 2004; Schuppan and Freitag, 2004). Perianal fistulae are then extended due to bacterial colonization by the commensals of the lower gastrointestinal tract and/or skin (de San Ildefonso Pereira et al., 2002; Nicholls et al., 1990; Seow-Choen et al., 1992; West et al., 2005).

The treatment options are continuing to develop, since perianal fistulae do not heal itself without the need to surgery. For example, in the case of crohn's disease-associated fistulae, there is proven efficacy from the thiopurines, the Infliximab and possible benefits from antibiotics, Cyclosporine A and Tacrolimus (Schwartz and Herdman, 2004). These antimicrobial agents are effective with clinical improvements that are usually observed after 6-8 weeks. However, it results in early deterioration on withdrawal. For full treatment of Crohn's disease-associated fistulae, surgery is very successful; however it can involve several operative procedures and lead to consequence of provoking faecal incontinence (Schwartz and Herdman, 2004).

Lately, for treatment of tissue cavities such as fistulae, biomaterials such as fibrin glue was suggested as an alternative to the cutting seton (a medical procedure for fistulae treatment) and

mucosal advancement flap repair of the complex study (Buchanan et al., 2003). Failure of this study was due to semi-liquid consistency and the disadvantage of the materials to fill in the cavities for promoting the healing process. In another approach, fistulae plugs were fabricated from porcine small intestine submucosa with the aim of plugging the fistulae track (Johnson et al., 2006). The failure of this study was also due to nature of the device to completely fill in the cavities caused by fistulae. Moreover, it was unclear whether the collagen materials employed for preparation of the devices were entirely compatible in fistulae matrix. Still, there is evidently an ongoing need for novel treatment strategies of perianal fistulae, but with more suitable filling biomaterials. It is suggested that the physical properties of filler materials combined with bioactive phases could improve the rate and the speed of the heeling process. Blaker *et al.* (2008) developed a study to produce porous PLGA microspheres containing either antibacterial phosphate glass or metronidazole for use as a potential alternative filler strategy in fistulae treatment (Blaker et al., 2008a, 2008b). Although, the fabricated microspheres had such a good interconnected porous structure and implanted as a cluster, the nature of the wound packet resulted in movement of them subsequent to the implantation site. Failure was due to the large size distribution of microspheres (~1.5 mm), where most of them were destroyed at the event of *in vivo* injection (Blaker et al., 2008b). Besides, due to large polydispersity of the produced particles, no cell migration was occurred into the free flowing microsphere-scaffold for tissue regeneration (Blaker et al., 2008a).

Microspheres have been widely used in medical and pharmaceutical applications as effective carriers of encapsulated drugs (Foy et al., 2004; Li et al., 2004; Peng and Zhang, 2005); therefore, they are considered for *in vitro* studies of the perianal fistulae treatment in this investigation. This type of polymeric particles provide special characteristics such as high surface-to-volume ratio, low density, and low coefficient of thermal expansion (Lou et al., 2008). These characteristics facilitate the manipulation of the surface properties of the interior or exterior of the microspheres to control interactions with various species (Moon and Jeong, 2008). Encapsulation of drug in biodegradable polymer enables the drug to be released in a more controlled manner which in turn helps to sustain a constant therapeutic concentration between the toxic and minimum levels in body fluids over the period of treatment following administration (Sinha and Trehan, 2003).

Based on the literature review conducted on perianal fistulae as a type of chronic wounds, microspheres with surface porosity are considered for two main reasons: 1) porosity on surface will lead to higher initial burst release of loaded agent which is a positive feature in treatment

of such disease (**Table 2.1**) and 2) a more sustained period of drug release will be obtained due to lower water uptake of the biodegradable polymeric carriers (Enayati et al., 2010a).

Failure of the previous research in treatment of such disease was due to the incomplete filling of the fistulae cavitation with the application of biomaterials. This issue could be simply resolved by introducing the EHD method combined with TIPS process to fabricate near monodisperse microspheres in a form of free flowing scaffold. Based on the literature review and research conducted on the perianal fistulae, microspheres in a form of free flowing scaffold with surface porosity and size distribution of 150-300 µm would be more suitable for filling the fistulae cavitation. Furthermore, this range of microspheres would have large enough interstices between them to allow cell migration for wound healing and tissue regeneration (**Fig. 2.24**). The reason behind selecting this range is that the microspheres less than 100 µm may start moving to other parts of the human body by absorption into blood system and result in further complication such as embolism and/or deposition in another organ, and also the microspheres over 350 µm cause blockage of the needle at the events of *in vitro* and/or *in vivo* injection tests.

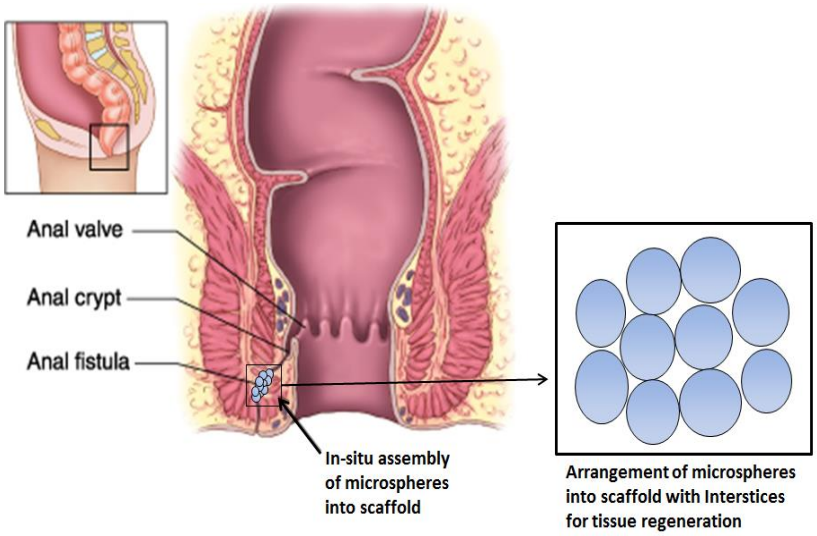

Figure 2.24: Schematic diagram of perianal fistulae with the arrangement of microsphere-scaffold for treatment

The main purpose of this study is to fabricate microsphere-scaffold with the single needle EHD/TIPS process. To ensure robust EHD production, this work mapped EHD parameters using a variety of polymer solutions for controlled generation of near monodisperse microspheres of the targeted diameter. Comprehensive sets of data on the diameter distribution

profile of the spherical particles obtained over a broad range of flow rates and applied voltages are presented.

The *in vitro* release studies are the second purpose of this project. It was aimed to predict the *in vitro* release profile of immunosuppressive drugs such Cyclosporine A and Tacrolimus with high molecular weight and very low water solubility. Since, these drugs have several drawbacks such as marked nephron- and neurotoxicity, three fluorescent dyes (erythrosin B, pyronin and Reichardt's dye) as surrogate drug entity were selected. Selection of these dyes was based on covering the range of molecular weight and water solubility of the actual drugs as these two properties play crucial role in release rate of incorporated materials. The single needle EHD/TIPS process was conducted for encapsulation of each dye into the required size of the microspheres, and then the results were compared with those produced by the co-axial EHD/TIPS technique in order to discover a more suitable method in fabrication of the required drug delivery carriers for the chronic wound therapy.

Chapter 3

Experimental Details

3.1 Introduction

This chapter of the report reviews in details the procedures adopted for the experiments in this thesis. The materials used, the corresponding suppliers and the product details are given. The methods used to characterise the materials and the solutions are also described. A detailed description of the equipment adopted in the single needle EHD and the co-axial needle EHD processes for mode mapping studies and the *in situ* development of scaffold with dye loaded microspheres is also given. Finally, the experiments for the *in vitro* characterization of the dye loaded microsphere-scaffolds are also discussed.

3.2 Materials

The main materials used in the experimental work were as follows:

3.2.1 Poly (Lactic-Co-Glycolic Acid) (PLGA)

PLGA is a copolymer of glycolic and lactic acid which has been approved by the Food and Drug Administration (FDA) for usage in therapeutic devices due to its biocompatibility and biodegradability. Various forms of PLGA can be acquired depending on the ratio of lactide and glycolide monomers and they are usually identified in terms of the monomer ratio adopted. In this research work, the PLGA copolymer 50:50 Resomer RG503H (Boehringer Ingelheim, Germany) was used with the molecular weight of 33000 g/mole composed of 50% lactic and 50% glycolic acid.

3.2.2 Poly (ε-Caprolactone) (PCL)

PCL is another important polymer in the drug delivery systems owing to its mechanical properties, miscibility with a large range of other polymers and biodegradability. This polymer has a high melting point of approximately 60^{o}C with a glass transition temperature of -60^{o}C. The two different molecular weights of PCL used in this work were PCL10,000 (M_w = 10000 g/mole) and PCL45,000 (M_w = 45000 g/mole) and they were both purchased from Sigma Aldrich (Poole, UK).

3.2.3 Dimethylacetomide (DMAc)

DMAc (C4H9NO) is a colourless, water miscible, high boiling point liquid compound. This solvent has a molecular weight of 87.12 g/mole with density of 0.94 g/cm^3 and melting point of -20^{o}C. DMAc was procured from Sigma Aldrich (Poole, UK) and used as a solvent in this study.

3.2.4 Dimethylformamide (DMF)

DMF is an organic compound with formula $(CH_3)_2NC(O)H$. This solvent is colourless with miscibility in water and high boiling point around 154^{o}C. The molecular weight of DMF is 73.09 g/mole with density of 0.95 g/cm^3 and very low melting point of -60^{o}C. DMF was purchased from Sigma Aldrich (Poole, UK) and used as a solvent in this study for dissolution of polymer.

3.2.5 Toluene

Toluene is a clear, water-insoluble liquid with characteristic smell of paint thinner. This liquid with formula C_7H_8 has a molecular weight of 92.138 g/mole and density of 0.90 g/cm^3. Toluene has a high boiling point (110^{o}C) and the melting point of nearly -95^{o}C. This solvent with high level of evaporation rate was purchased from Sigma Aldrich (Poole. UK) and used as a solvent in this study.

3.2.6 Dimethyl Carbonate (DMC)

DMC is an organic compound which is a colourless, flammable liquid with solubility in water and high boiling point of 90^{o}C. This liquid has a molecular mass of 90.08 g/mole and density of 1.07 g/cm^3. This solvent has a melting point of between 2-4^{o}C, and due to low level of toxicity it is often considered as a green reagent. This liquid is used as a solvent for dissolution of polymer and was purchased from Sigma Aldrich (Poole, UK).

3.2.7 Distilled Water

Distilled water is water that has many of its impurities removed through distillation. Distillation involves boiling the water and then condensing the steam into a clean container. It has an electrical conductivity of less than 10 μS/cm and total dissolved solids of less than 10 mg/L. It

was used as a collection media in the particle production and provided by the Biomaterial Lab in Mechanical Engineering Department at UCL (London, UK).

3.2.8 Ethanol

General purpose research grade ethanol with molecular weight of 46 g/mole (C_2H_5OH 99%), density of 0.79 g/cm^3 and viscosity of 1.3 mPa s, was used in this investigation. As described in **Section 3.9.2.3,** ethanol was used as a supplementary liquid in the SBF media for release studies of some packs of loaded microspheres. In addition, ethanol was also used for the calibration of the characterisation apparatus and for cleaning the capillary of the needles which were the essential components of the experimental set-up. This material was purchased from Sigma Aldrich (Poole, UK).

3.2.9 Liquid Nitrogen

Liquid nitrogen is nitrogen in liquid state at an extremely low temperature that is produced industrially by fractional distillation of liquid air. It is a clear liquid with density of 0.81 g/ml, boiling point of -196^{o}C and freezing point of -210^{o}C at atmospheric pressure. Due to its very low melting point, it is used in thermally induced phase separation procedure for removal of solvent or unnecessary materials from systems. Liquid nitrogen combined with freeze drying is widely used to produce solid form of a liquid solution that has high melting point. This liquid was provided by BOC (London, UK).

3.2.10 Erythrosin B

Erythrosin B ($C_{20}H_6I_4Na_2O_5$) with molecular weight of 839.85 g/mole was used as a model drug in *in vitro* release studies to predict the release profiles of Cyclosporine A (1202.61 g/mole) and Tacrolimus (804.018 g/mole). This fluorescent dye has very low water solubility (1 g/mole) and is widely used for applications in food colouring and printing ink (Lin and Brusick, 1986; Lyday, 2005). Also, due to its biocompatibility and biodegradability in physiological environments, it has been used as a biological stain for detection of viable cells in tissue engineering and a dental plaque disclosing in dentistry (Krause et al., 1984). Nowadays, erythrosin B can be found in sweets such as some candies and popsicles, and even more widely used in cake-decorating gels and colouring of pistachio shells (Cantor, 1997; Diamond Foods, 2007). This dye was purchased from Sigma Aldrich (Poole, UK).

3.2.11 Pyronin B

Pyronin B ($C_{42}H_{56}Cl_8Fe_2N_4O_5$) with molecular weight of 1042.28 g/mole was also used as a model drug in *in vitro* release studies for prediction of Cyclosporine A and Tacrolimus release profiles. This dye has low water solubility (20 g/mole) with particular application in cell biology and haematology for detection of the required cells under investigation. The major application of this dye as a stain is identification and analysis of the heamatopoietic stem cells in histology, due to its biocompatibility, biodegradability and non-toxicity in physiological environments (Challen et al., 2009). This agent was procured from Sigma Aldrich (Poole, UK).

3.2.12 Reichardt's Dye

Reichardt's dye ($C_{41}H_{29}NO$, M_w = 551.68 g/mole) was also used as a model drug in *in vitro* release studies to forecast the release profiles of Cyclosporine A and Tacrolimus from the porous microspheres. Unlike the other two fluorescent agents, Reichardt's is a completely hydrophobic dye and has a lower molecular weight. Since, it has both positive and negative charge sides, it is used in characterizing the polarity of certain microenvironments such as cell membrane. Moreover, it is been used for determining the water content of a solvent by changing the colour (Reichardt, 1994). This dye was also procured from Sigma Aldrich (Poole, UK).

3.2.13 Simulated Body Fluid (SBF)

SBF is a mixture of several different chemicals that when combined produce similar composition to human blood plasma (Oyane et al., 2003; Swain and Pattanayak, 2008). The existing chemicals for SBF preparation includes NaCl, KCl, $CaCl_2.2H_2O$, $MgCl_2.6H_2O$, $NaHCO_3$, K_2HPO_4, $NaSO_4.10H_2O$, tris buffer such as Tris-hydroxymethyl-aminomethane, $H_2NC(CH_2OH)_3$ and 1 mole of HCl. The concentration of total ions for SBF preparation is presented in **Table 3.1** (Kokubo et al., 1990). All of these reagents were purchased from Sigma Aldrich (Poole, UK) with analytical grade.

Table 3.1: comparison between ion concentration of SBF and human blood plasma (Kokubo et al., 1990; Ohtsuki et al., 1995)

Ion	SBF (g)	Blood plasma (g)
Na^+	142.0	142.0
K^+	5.0	5.0
Mg^{2+}	1.5	1.5
Ca^{2+}	2.5	2.5
Cl^-	148.8	103.0
HCO^{3-}	4.2	27.0
HPO_4^{2-}	1.0	1.0
SO_4^{2-}	0.5	0.5

For preparation of SBF, 500 mL deionised water was added into 1 L of polyethylene bottle and covered with a transparent glass lid. The reagents were then dissolved one by one in order according to **Table 3.2** with constant stirring. During preparation, the temperature of the solution was maintained at 36.5ºC by being placed in a water bath and the pH of the solution was adjusted to 7.4 by titration with 1 mole of HCl. The total volume of the solution was then made up to 1 L by adding deionised water. The SBF solution is usable for a maximum period of four months. Afterwards, the reagents start to degrade that results in pH changes in the solution (Kokubo et al., 1990; Ohtsuki et al., 1995).

Table 3.2: Chemicals used for SBF preparation (Kokubo et al., 1990; Ohtsuki et al., 1995)

Order	Reagent	Amount
1	NaCl	7.996 g
2	$NaHCO_3$	0.350 g
3	KCl	0.224 g
4	$K_2HPO_4 \cdot 3H_2O$	0.228 g
5	$MgCl_2 \cdot 6H_2O$	0.305 g
6	1M-HCl	40 mL
7	$CaCl_2$	0.278 g
8	Na_2SO_4	0.071 g
9	$(CH_2OH)_3CNH_2$	6.057 g

3.3 Characterisation of the Solutions

3.3.1Viscosity

Dynamic viscosities of the solutions prepared for this study were determined using a U-tube viscometer (BS/U type, Schott Instrument GmbH, Germany). The calibrated U-tube adopted for measurements was size C with nominal constant of 0.03. The time measured for a standard volume of solution to pass through the capillary of the U-tube was noted for five passes, and the mean value and standard deviation were calculated. Then, the total kinematic viscosity (v) was computed by having the nominal constant multiplied with the time (t):

$$v = Ct \quad (m^2/s) \tag{3.1}$$

The dynamic viscosity (η) was then calculated by having the value of density (ρ) of solution multiplied by the kinematic viscosity:

$$\eta = v\rho \tag{3.2}$$

By combining the two equations, (3.1) and (3.2), the dynamic viscosity is calculated:

$$\eta = Ct\rho \quad (Pa\ s) \text{ or } (kg/(m.s)) \tag{3.3}$$

Water was adopted for calibration of the U-tube viscometer. The mean value of five readings was taken as the dynamic viscosity of each sample. It is essential to calibrate the U-tube viscometers, which are not calibrated by manufacturers, by a liquid with known properties and then comparing the values in order to validate the results.

3.3.2 Density

Density of the liquids or the solutions prepared for this study was measured using a 25 ml standard bottle (VWR International, Lutterworth, UK). The mass of the empty bottle (W_1) and the mass of the bottle filled with liquid or the solution (W_2) were measured using an electronic balance device (AND HF-1200G A&D Instruments Ltd, Japan). Density was then calculated as follows:

$$\text{The density of the liquid or the solution} = (W_2-W_1)/25 \quad (kg\ m^{-3}) \tag{3.4}$$

The mean value and standard deviation of the five successive calculations were then taken as the density of liquid or the solution. The characterizations of all the solutions used in this study were carried out at the ambient temperature (~24^{o}C) and pressure.

3.3.3 Surface Tension

The surface tension of the solutions/liquids was calculated using Kruss Tensiometer K9 (Standard Wilhelmy's plate method). The plate was suspended from a hook and a 25 ml beaker containing sample was placed on the platform. The plate was thoroughly immersed into a sample whose surface tension was to be measured. The plate was then gradually lifted and the surface tension value was presented on the reading monitor when the plate was about to detach from the liquid surface. For minimising the errors, the plate was cleaned completely with ethanol and dried before each set of measurement. This procedure was conducted five times for each sample, and the mean value along with the standard deviation were then recorded as the surface tension of the relevant sample.

3.3.4 Electrical Conductivity

Electrical conductivity was measured using pHenomenal PC 5000 H (VWR International, Lutterworth, UK) conductivity probe. The electrode on the conductivity probe was always cleaned with ethanol or distilled water and dried before each set of measurements. The standard conductivity probe was kept immersed in a 20 ml beaker of solution up to the point marked on the electrode for 60 s and then the reading of the meter was recorded. The mean value and standard deviation of the five successive readings were taken as the final value for the electrical conductivity of the sample.

3.3.5 pH

The pH of solution was also measured dipping a standard pH probe (pHenomenal CO11, VWR International, Lutterworth, UK) in solution. The pH probe was held in the solution for 60 s and then the reading shown on the meter was recorded. For accuracy in measurement, the pH probe was needed to be thoroughly cleansed with distilled water or ethanol and then dried before any measurement. The five consecutive measurements were taken and the mean value was calculated as the final value for the pH of the solution.

3.4 Solution Preparation

3.4.1 PLGA Solutions for EHD Mode Mapping and Size Distribution Studies

Clear solution of PLGA with varying concentrations (5%, 10% and 20% w/w) were prepared by having the appropriate amount of the polymer combined with DMAc under mechanical stirring until complete dissolution of PLGA (~2700 s). The same procedure with the similar concentrations was carried out for preparation of the PLGA solutions mixing with DMF. Another PLGA solutions with different concentrations (5%, 10% and 15% w/w) were also prepared by dissolving this copolymer in DMC under mechanical stirring until full dissolution of polymer in the solution (~2700 s).

3.4.2 PCL Solutions for EHD Mode Mapping and Size Distribution Studies

PCL solutions of different concentrations (15%, 20% and 25% w/w for PCL10,000, and 5%, 7% and 10% w/w for PCL45,000) were also prepared by mixing the proper amount of polymer and toluene under mechanical stirring at ambient temperature until clear solution for the total PCL dissolution was obtained (~3600 s). Lower concentrations were used for PCL45,000 to ensure the solutions remain in the dilute concentration regime for the higher molecular weight PCL polymer to be able to generate spheres instead of fibres (Luo et al., 2012) during EHD processing.

3.4.3 Dye Loaded Solutions for *In Vitro* Release Studies

3.4.3.1 Single Needle EHD/TIPS Process

Three separate batches of 17.5% w/w PLGA solutions were prepared by having appropriate amount of the polymer fully dissolved in dimethyl carbonate for 2700 s under ambient conditions. After complete dissolution of PLGA in DMC, 0.16 g of each dye was added to each solution to give a final concentration of 0.6% w/v. Full dissolution of the dyes in the solutions was performed with vortexing. One extra batch of PLGA solution with same concentration (17.5% w/w) was also prepared and used as the control sample during the experimental process.

3.4.3.2 Co-axial Needle EHD/TIPS Process

Three separate batches of same concentration (17.5% w/w) of PLGA solutions were prepared by having appropriate amount of the polymer fully dissolved in dimethyl carbonate for 2700 s under ambient conditions. Also, 0.3 g of each dye with total concentration of 3% w/v was

dissolved in dimethyl carbonate for the encapsulation of agent by the co-axial needle EHD/TIPS process.

3.5 Particle Formation for EHD Mode Mapping and Size Distribution Studies

3.5.1 Single Needle EHD Setup

Needle setup: in the single needle EHD processing, a stainless steel needle (Stainless tube & Needle Co. Ltd, Staffordshire, UK) was coupled to a high power voltage supply in order to provide the electric field on the apex of the needle. The external and internal diameters of the nozzle were 1.34 mm and 1.18 mm respectively.

Syringe pump: the single needle was connected by silicone tubing to a 5 ml plastic syringe (BD Plastic^{TM}, VWR International, Lutterworth, UK) containing the polymer solution. The flow rates of solution through the needle were controlled by high precision syringe pump (Infuse/Withdraw PHD 4400 Hpsi programmable syringe pump, Harvard Apparatus Ltd, Edenbridge, UK). The pump was calibrated with ethanol before each set of experiments conducted. The range of flow rates for PLGA/DMF and PLGA/DMAc solutions was varied from 30 to 200 µl min^{-1}, whereas this range for the solutions of PLGA dissolved in DMC was between 75 and 450 µl min^{-1}, and for both PCL types in toluene varied from 20 to 50 µl min^{-1}.

High voltage power supply: the needle and the ground electrode were coupled to a high voltage DC power supply unit (FC30 P4 12w, Glassman Europe Limited, Bramley, UK) via a high voltage power cable. At each flow rate, when the solution was pumped through the needle, the appropriate range of voltage was used in order to obtain stable cone-jet on the tip of the needle. Therefore, collection of spherical particles from each sample was conducted at specific range of voltage when the stable cone-jet mode was achieved.

Ground electrode: An electrode was connected from the voltage power supply unit to the ground as shown in **Figure 3.1**. The electrical stress is determined by the strength of the electric field between the needle and the ground electrode.

Data recording unit: different modes of jet and particle formation process were monitored using LEICA S6D JVC-colour video camera attached to a zoom lens and a data DVD video recorder MP-600 using CDV Recorder/Editor DN-100 with a video screen for real time monitoring.

In the process of single needle, the spherical particles were collected at a working distance of 80 mm below the nozzle exit directly into 10 ml glass vials containing 5 ml distilled water. Each sample was collected for 600 s and then dispersed on a glass slide by a pipette in order to be dried for analysis under optical microscopy.

3.6 Particulate Scaffold Fabrication

3.6.1 Conventional Single Needle EHD Setup

The single needle EHD setup was used for development of free flowing and non-free flowing scaffold structures (**Fig. 3.1**). The same procedure as explained in **Section 3.5.1** was carried out; however, the collection medium was changed from glass vial filled with water to a beaker contained liquid nitrogen. 15 wt% concentration of the PLGA/DMC combination was selected for the preparation of the particulate scaffold structure, as this concentration of polymer solution from the EHD mode mapping and size distribution studies (**Section 3.5)** provided the required size range of particles. This combination in 20 ml plastic syringe was electrosprayed for 1800 s in a metallic collection vessel filled with liquid nitrogen.

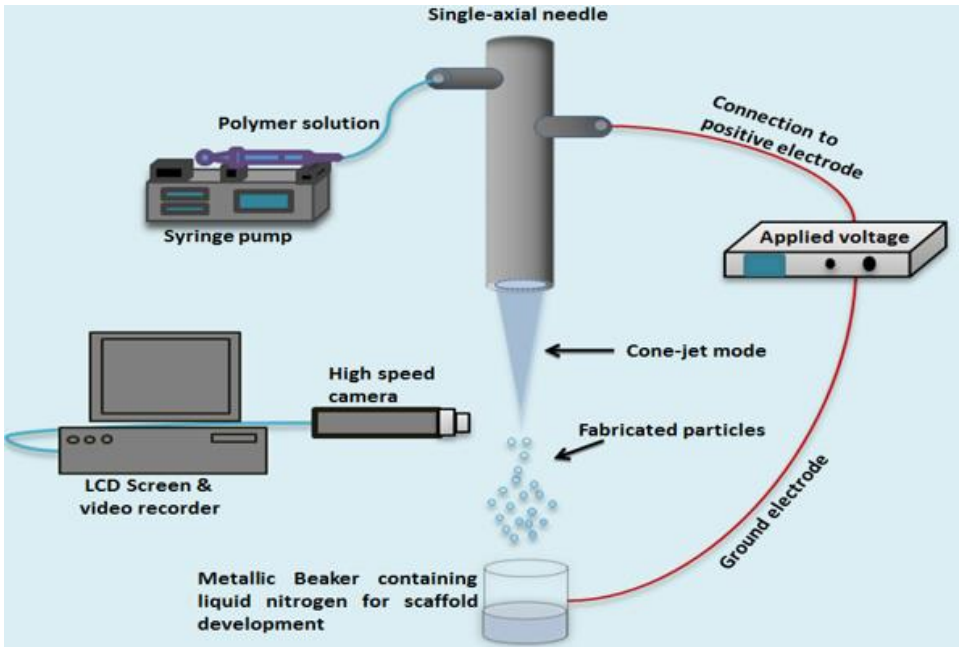

Figure 3.1: Experimental setup of single needle EHD/TIPS for the production of microspheres

Free flowing scaffold structure: for development of the free flowing scaffold, metallic beaker was filled with liquid nitrogen to the top and every 2 minutes it was topped up in order to keep the level of liquid nitrogen constant in the beaker. In this form of scaffold development, when the spherical particles reached the liquid nitrogen, they became solidified and started flowing around due to the lower density of the polymeric microspheres compared to the liquid nitrogen.

Non-free flowing structure: for the formation of rigid (non-free flowing) scaffold structure, only a small amount of liquid nitrogen was poured to the bottom of the metallic beaker to provide a freezing medium for the collection of solid spherical particles. In this arrangement, as soon as the particles entered the beaker started to solidify and aggregate to form a rigid non-free flowing scaffold.

Collection of particles in cold medium using liquid nitrogen led to generation of solid microspheres. For production of the spherical particles, flow rate was set at 225 µl min^{-1}, and in order to obtain the stable cone-jet mode, the applied voltage range varied between 6-7 kV. During the collection of particles, the beaker was placed 80 mm below the tip of the needle with the ground electrode connected to it. The direct grounding of the electric field to the collector resulted in attraction of the charged microspheres and their deposition at the bottom of the metallic container**.**

3.6.2 Freeze Drying

These spherical particles after collection in the metallic beaker containing liquid nitrogen were immediately placed in freeze dryer until the complete extraction of the solvent (DMC) was obtained (~20 hours). The frozen spherical particles after removal from the freeze dryer were completely solidified. These prepared microspheres after freeze drying were subjected to SEM and optical microscopy studies for further analysis.

3.7 Agent Loaded Microspheres Fabrication for *In Vitro* Release Studies

3.7.1 Conventional Single Needle EHD/TIPS Process

The experimental setup for producing the PLGA microspheres with the entrapped dye was the same as presented in **Figure 3.1**. For mass production of the dye loaded microspheres by EHD/TIPS method, a 20 ml volume syringe (BD Plastic™, VWR International, Lutterworth, UK) was fully loaded with the prepared PLGA solution containing dye. Since, the main aim of this study was to produce microspheres with size distribution of 150-300 µm, the polymer concentration for producing the required size range of dye loaded carriers was increased from 15 wt% to 17.5 wt% in the solution. This change was highly related to the environmental variations such as higher humidity, higher ambient temperature and atmospheric pressure.

For transferring the polymer-dye solution to the needle, the flow rate was set at 400 µl/min and the voltage was varied between 6.5 and 8.5 kV depending on the polymer-dye solution. To develop the near monodisperse microspheres, the single-needle EHD process for the PLGA solution containing each dye was carried out at the stable cone-jet mode into the metallic beaker that contained liquid nitrogen. The collection vessel was placed 80 mm below the exit of the nozzle with the ground electrode directly connected to it for attraction and deposition of the charged microspheres at the bottom of the metallic container. After 2700 s of collection in the container filled with liquid nitrogen, the samples were immediately placed in a freeze dryer (LTE Scientific Ltd, Oldham, UK) and lyophilized for 20 hours. After freeze drying, the free flowing lyophilized microspheres were collected into vials and stored for morphological and *in-vitro* release studies.

3.7.2 Modified Single Needle EHD/TIPS Process

In our initial experiments during the process of single needle electrospray, the products were scattered to the peripheral environment, due to the cloud of nitrogen gas that formed at ambient temperature above the collection beaker. Therefore, a smaller quantity of products was collected in the metallic beaker and consequently the percentage yield of the process and the drug entrapment efficiency could not be accurately calculated. **Figure 3.2** shows how this issue was overcome with the modifications applied to the single needle EHD/TIPS method for enhancing the efficiency of the process.

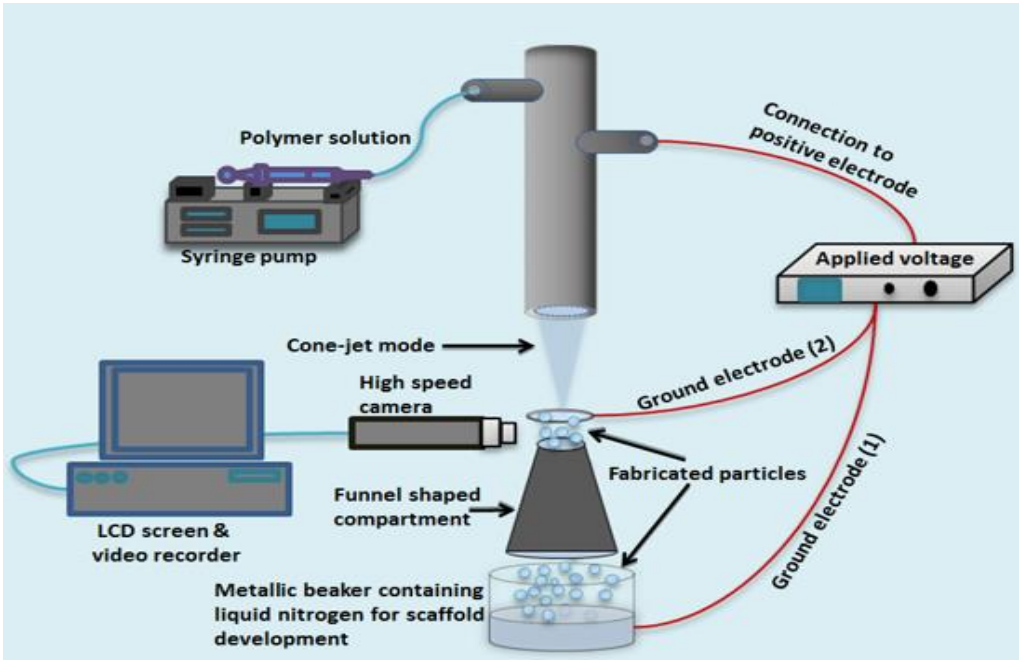

Figure 3.2: Schematic diagram of the modified single needle EHD/TIPS process

A funnel shaped compartment, a metallic beaker with wider opening and a second ground electrode (a ring with inner diameter 15 mm and outer diameter 20 mm) were adopted for optimization. The second ground electrode, which was placed between the tip of the nozzle and the metallic beaker, provided further stability of the cone-jet mode and also directing the products to the metallic beaker. The funnel shaped compartment made of non-conductive material created an area to prevent the particles from scattering to the peripheral environment. The funnel was 120 mm high and it was placed at 5 mm below the second ground electrode and 10 mm gap above the beaker (**Fig. 3.2**). It was necessary to have the gap between the metallic beaker and the funnel in order to allow the nitrogen gas to escape and facilitate the direction of the formed microspheres towards the collection vessel. A metallic beaker connected to a ground electrode with a wider opening that the funnel also provided a broader area for more attraction of oppositely charged particles to the collection vessel. The electrospraying of the polymer-dye solutions was also carried out by the modified single needle process with the similar processing parameters and the same duration (2700 s) as described in **Section 3.7.1**. The frozen products were then lyophilized for 20 hours.

3.7.3 Modified Co-axial Needle EHD/TIPS Process

In order to obtain the higher percentage yield of the process and the entrapment efficiency, the co-axial needle was also modified according to the modifications of the single needle process by a second ground electrode, a funnel shaped non-conductive compartment and a metallic collector with wider opening than the funnel (**Fig. 3.3**).

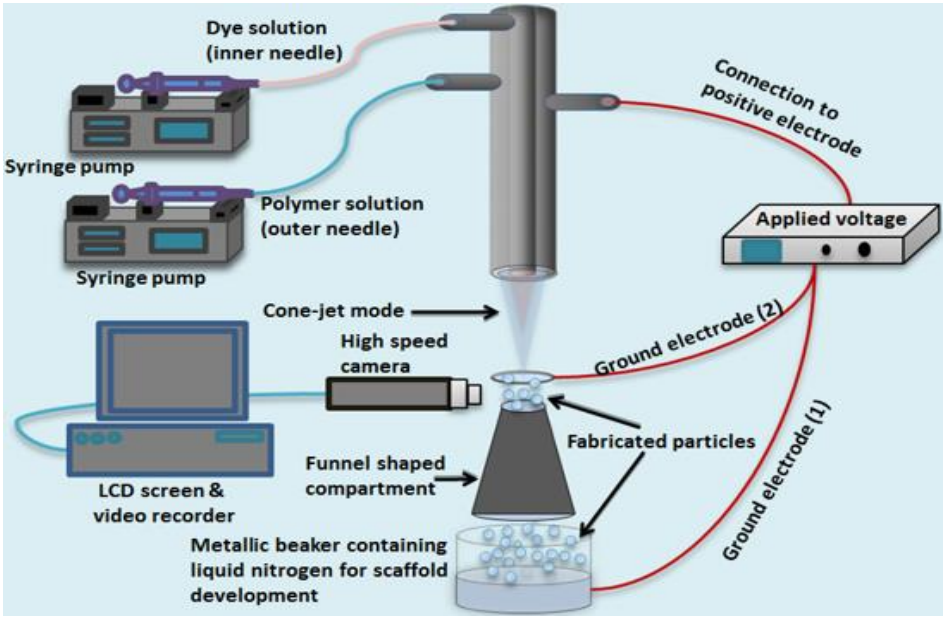

Figure 3.3: Schematic diagram of the modified co-axial needle EHD/TIPS process

The experimental setup for the co-axial needle EHD/TIPS process was similar to the single needle setup, but a two needles stainless steel co-axial device (Stainless tube & Needle Co. Ltd, Staffordshire, UK) was coupled to a high-power voltage supply. The central needle with 0.65 mm inner diameter was used to carry the agent-loaded solution, whereas the outer needle with 1.18 mm orifice (inner diameter) perfused with the prepared 17.5 wt% PLGA solution to produce the spherical polymeric shell. The flow rate for the inner needle was set at 80 µl/min while for the outer needle it was 400 µl/min. The applied voltage to provide the stable cone-jet for the microspheres fabrication was set at 6.8–7.4 kV over the period of collection depending on the physical properties (such as conductivity, surface tension and viscosity) of the two flowing solutions. The strategic method of microspheres collection, the collection distance and the period of products collection were similar to the modified single needle setup. The lyophilisation of the products collected from the co-axial EHD/TIPS process was also carried out as before.

3.8 Characterization of Generated Particles

3.8.1 Optical Microscopy

Five drops of each sample after collection in 10 ml glass vials were dispersed on a glass slide by a pipette and then placed in a desiccator for 12 hours (apart from microspheres collected in liquid nitrogen and lyophilized by freeze dryer) in order to dry and become ready for optical microscopy. An optical microscope (Nikon Eclipse ME 600, Nikon, Japan) was extensively used for all the investigations described in particle formation for EHD mode mapping and size distribution studies. The diameter measurements of the produced microspheres were carried out by means of Image Pro-Insight software (Media Cybernetics, UK).

3.8.2 Scanning Electron Microscopy

The morphology and detailed structure of the fabricated spherical particles were investigated using scanning electron microscopy (JEOL, JSM-630 field emission SEM). It was equipped with an emitter which can have a resolution up to 1.5 nm. The accelerating voltage was set at 5kV and the working distance between the emitter and the sample was fixed at 20 mm. The SEM studies were used extensively for all the investigations described in agent loaded microspheres fabrication for *in vitro* release studies.

The produced microspheres collected from both the single needle and the co-axial needle EHD/TIPS processes were completely dry due to collection in liquid nitrogen and long hours of freeze drying. Therefore, they could be taken for SEM studies immediately.

Since the polymers adopted for the preparation of spherical particles are non-conductive, the dried samples for the SEM studies were initially glued onto aluminium stud via adhesive carbon tabs, and then sputtered coated (Edwards sputter coater S 1 50B) with gold for 180 s prior to placing in SEM chamber for further analysis. This enables the samples to be more visual in SEM chamber and avoid charging which can cause damage to the samples. For determining the size distribution of particles, 100 spheres were randomly selected and analysed from each sample. The diameter of the microspheres from SEM studies was also measured by Image Pro-Insight software (Media Cybernetics, UK).

Since the fabricated microspheres were quite large with an internal solid structure, focused ion beams (FIB) could not be adopted for investigation of the internal structure. Therefore, for analysis by SEM machine (Hitachi S-3400N), they were randomly sectioned with a surgical blade after sputter gold coating.

SEM was also applied for further morphological analysis of the produced microspheres used in the release studies. A small quantity from each pack of loaded microspheres in the relevant release media at ambient (22 ± 2 ^{o}C) and physiological (37 ± 1^{o}C) temperatures after 2 and 12 days were prepared on glass slides, and placed in desiccator for 24 hours for complete drying under ambient conditions before SEM examination. This part of SEM studies was conducted in order to observe the effect of release medium on the degradation process of the loaded PLGA microspheres during the early and later stages of release studies. SEM preparation of these samples was similar as explained above.

3.8.3 Energy-Dispersive X-Ray Spectroscopy

Energy-dispersive X-ray (EDX) spectroscopy was used to confirm the presence of the dye in the PLGA microsphere-scaffolds. This study was performed for the modified single needle samples containing the PLGA microspheres with each of the entrapped dyes. For this study, a batch of the lyophilized microspheres (~0.01g) was gold-coated at argon atmosphere and then placed in the system comprised of a field emission SEM column (Gemini SEM), with an Oxford instrument of energy dispersive spectroscopy (EDS) (Spectro XLab 2000 Pro (P)ED-

XRF) for the analysis. The applied voltage was set at 20 kV. Sample preparation for EDX studies was similar to the SEM studies.

3.8.4 Fourier Transform Infrared (FTIR) Spectroscopy

Fourier transform infrared (FTIR) was adopted to illustrate the presence of different functional groups of the agents encapsulated in the polymeric particles. A Perkin-Elmer Spectrum 2000 spectrophotometer (Cambridge, UK) was adopted for this investigation. A resolution of 4 cm^{-1} and 32 scans were selected. FTIR spectra window was obtained by the Potassium bromide (KBr) disk method. In this method, 200 mg of the dried spectrophotometric-grade KBr powder was completely mixed with 10 mg of the dye loaded microspheres, and then fused into a transparent disk using a hydraulic press. The prepared KBr disk contained the sample was then placed in FTIR spectroscopy for analysis.

3.9 *In Vitro* Release Measurement

3.9.1 UV Spectroscopy

Release of the encapsulated materials (dyes) from their polymeric shell (microsphere) was determined by UV spectroscopy. In this section, a brief description is provided on how the UV absorption spectra can be used to identify the compounds as well as measuring the concentrations of the encapsulated dye in a solution. In UV spectroscopy, light in the ultra-violet rays is transmitted through a sample containing the encapsulated materials. Different components in the sample may absorb certain wavelength of the transmitted light. The intensity of the light which is absorbed at a given wavelength will then be related to the concentration of the component in the measured sample. At appropriately low concentration of the absorbing component detected in sample, a linear relationship exists between the absorbance and the concentration of materials. This linear relationship is expressed by the beer-lambert law in physics (Calloway, 1997; Mitschele, 1996) as follows:

$$A = \log_{10} \frac{I_0}{I} \quad \textbf{(3.5)}$$

$$\log_{10} \frac{I_0}{I} = \varepsilon\, l\, c \quad \textbf{(3.6)}$$

$$A = \varepsilon\, l\, c \quad \textbf{(3.7)}$$

Where A is the absorbance, I_0 is the incident intensity, I is the transmitted light intensity (dB), ε is the coefficient of the material in the sample (L mole^{-1} cm^{-1}), l is the path length through the sample (cm) and C is the concentration of the species under investigation (mole L^{-1}).

Release profiles of the encapsulated dyes were measured by using Perkin Elmer Lambda 35-vis spectrophotometer (Cambridge, UK). This system has the following specifications: optical system with double beam, spectral bandwidth of 0.1, 0.2, 0.5, 1, 2 and 5nm, wavelength ranging from 190 to 900 nm, accuracy of ± 0.3 nm, repeatability of ± 0.1 nm, and photometric readout for absorbance % and transmittance % reflectance. In *in vitro* release studies, the first step for drug release calculation and entrapment efficiency is to determine the calibration curve and the second step is finding the linear relationship between the concentration of the encapsulated materials and the corresponding absorbance. These steps will be descried in the next sections.

Calibration curve, which is based on the quantity of light absorbed by a solution against the solution concentration, must be prepared for finding the concentration of an unknown solution. For plotting a calibration curve, a number of standard solutions with various known concentrations of the agent compound need to be measured by the UV spectrophotometer (Barreiro-Iglesias et al., 2003; Cavrini et al., 1989; Thompson et al., 2005). A sample of an UV calibration curve is given in **Figure 3.4.**

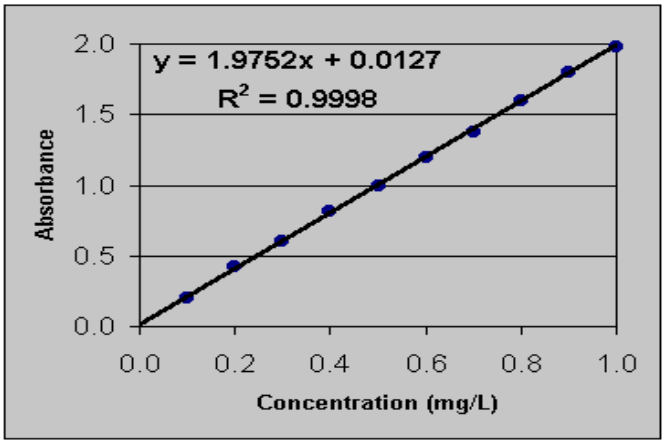

Figure 3.4: A sample of an UV calibration curve with the indicated error (R^2=0.9998)

3.9.2 Measuring Dye Encapsulation

3.9.2.1 Erythrosin B and Pyronin B

Erythrosin B absorbs light at three different wavelengths, 309 nm, 351 nm and another one between 450 nm and 550 nm; however, the wavelength 351 nm was selected as the reference

due to much stronger and clearer absorbance signal (**Fig. 3.5**). Pyronin B has light absorption at four various wavelengths of 261 nm, 348 nm, 398 nm and another one within the range of 450-550 nm, but only wavelength 348 was selected as a reference owing to much stronger light absorption and easily detection by UV spectroscopy (**Fig. 3.6**). Different samples with known concentrations of each dye in SBF was prepared, and the absorbance of the sample was then measured using UV spectrophotometer. Calibration curves of erythrosin B and pyronin B were respectively prepared for the different known concentrations ranging 0.001-0.5 mg/ml (1-500 ppm) and 0.001-0.35 mg/ml (1-350 ppm) dissolved in SBF (**Fig. 3.8**). All measurements were repeated in triplicate.

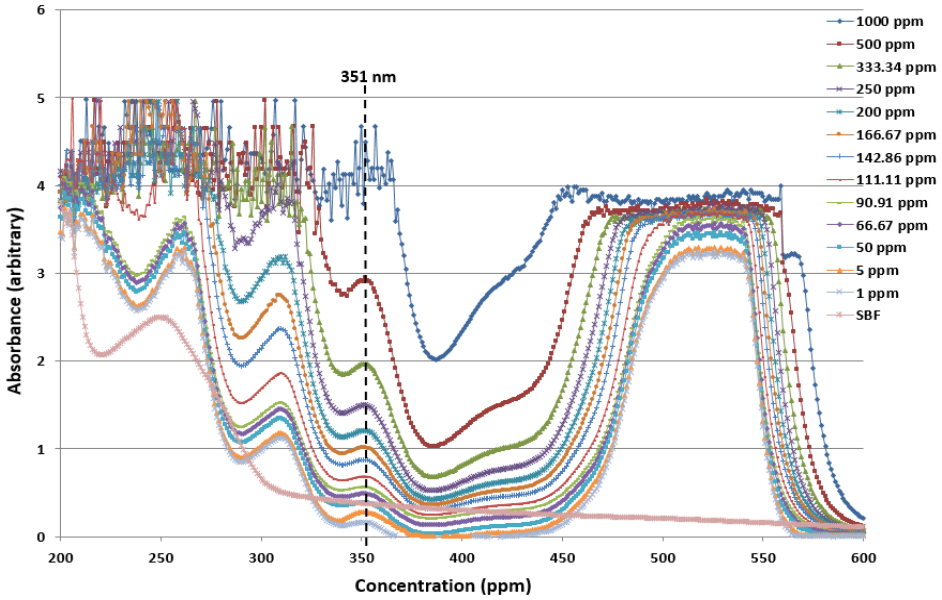

Figure 3.5: UV spectra of SBF media with different known concentrations of erythrosin B

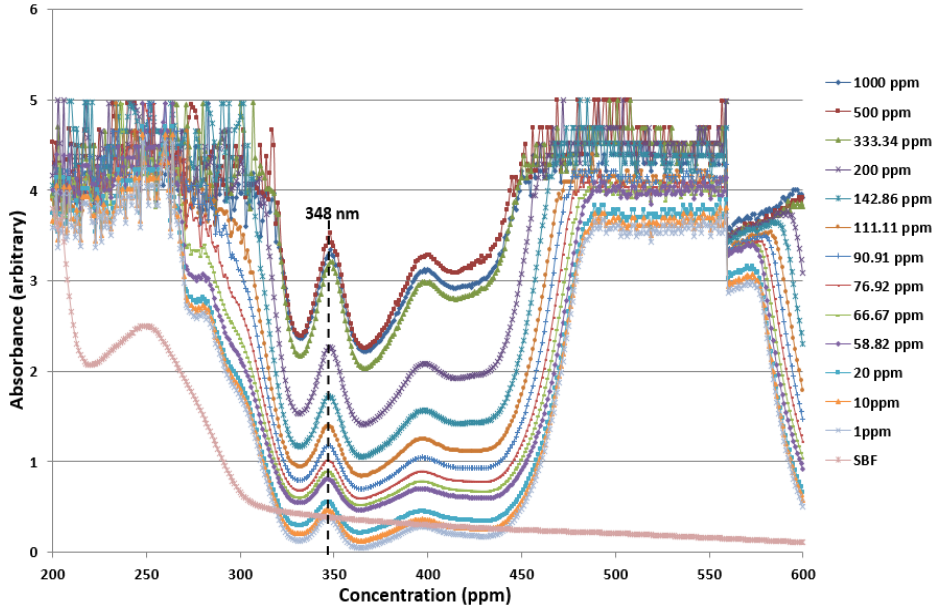

Figure 3.6: UV spectra of SBF media with different known concentrations of pyronin B

3.9.2.2 Reichardt's Dye

Wavelength 308 nm was selected as a reference for Reichardt's as it absorbs signal only at this wavelength. Different samples with known concentrations of this dye were dissolved in 80:20 SBF:ethanol (v/v) and the absorbance of each sample was measured with UV spectroscopy. The calibration curve was then prepared for the different known concentrations ranging 0.001-0.05 mg/ml (1-50 ppm) (**Fig. 3.8**). Since, Reichardt's is a hydrophobic material with no water solubility, ethanol in minimum volume was added to the SBF release medium for release rate studies. UV spectra of Reichardt's dye are shown in **Figure 3.7**. All measurements were repeated in triplicate.

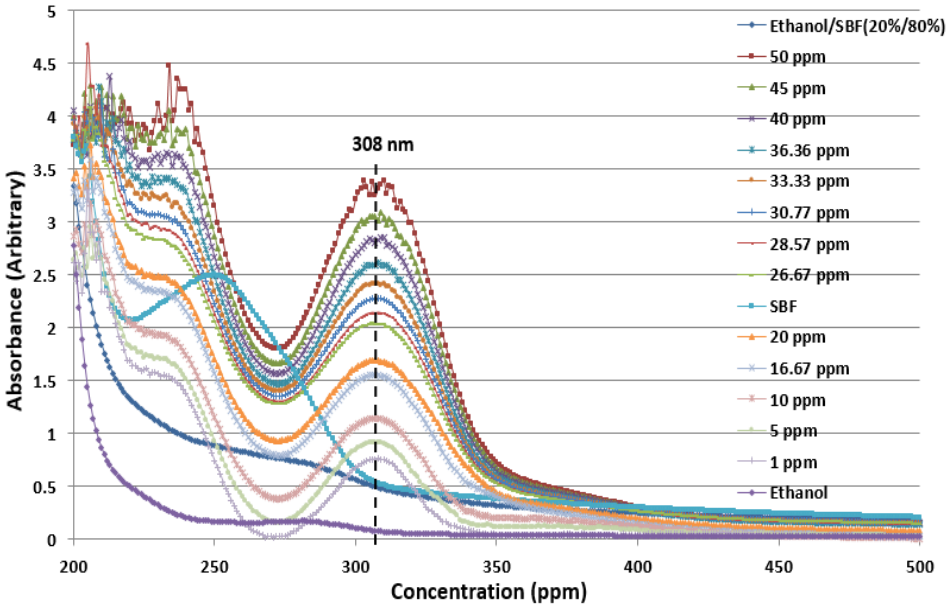

Figure 3.7: UV spectra of SBF:ethanol (80:20 v/v) media with different known concentrations of Reichardt's dye

The linear relationship between the concentration of each dye and the absorbance is shown in **Figure 3.8**. The correlation coefficient (R^2) of each dye, which is related to either experimental or calculation errors, and the equation between the concentration of the dye and the absorbance were also determined from this graph.

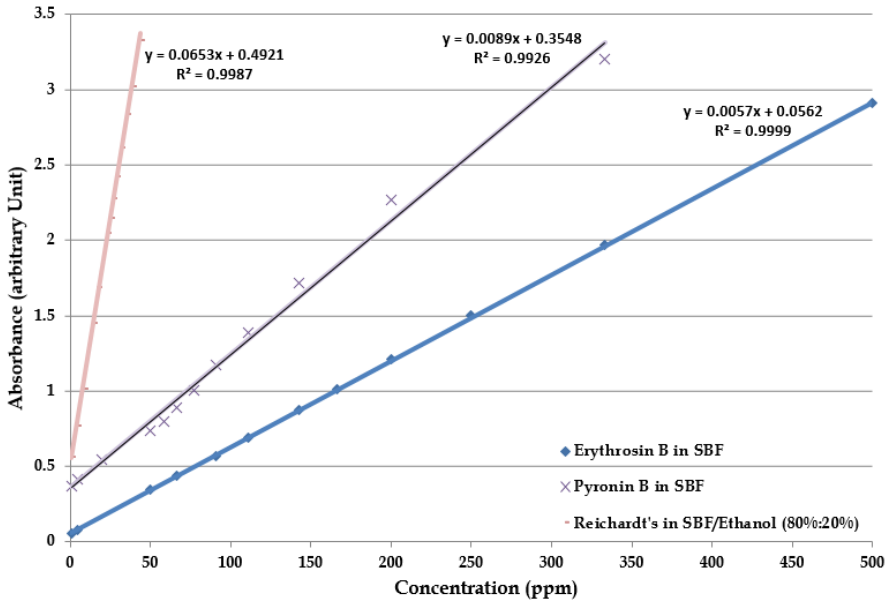

Figure 3.8: Linear relation between concentration of each dye and their absorbance at wavelength: 308 nm for Reichardt's, 348 nm for pyronin B and 351 nm for erythrosin B

3.9.2.3 Sample Preparation for Release Studies

In vitro release studies were carried out on all the samples collected from both the modified single needle and the modified co-axial needle EHD/TIPS processes. For erythrosin B and Pyronin B release studies, 0.1 g of the microspheres with dye encapsulated after freeze drying were collected in glass vials and then 10 ml of SBF was added. For Reichardt's release profile, 0.05 g of the fabricated microspheres were prepared in a glass vial with addition of 50 ml SBF:ethanol (80:20 v/v).

The release studies for each dye were carried out on at five different conditions including: ambient condition (22 ± 2^{o}C), physiological temperature (37 ± 1^{o}C), physiological temperature with fresh SBF and physiological temperature with sonication at 20 kHz for 30 s and also 40 kHz for 20 s. In total 5 batches of the loaded microspheres for the release studies of each dye were prepared in the explained media for the five different conditions. This part of the investigation using various external stimuli, such as sonication exposure and temperature variations, was to determine their effects on the release rate of the dyes from the microspheres. The main purpose was to obtain more suitable release rate of the incorporated agents. At discrete time intervals, 2 ml of each sample was extracted to measure the absorbance of the entrapped dye using the UV spectrophotometer and subsequently returned to the same vial after measurement. The *in vitro* release studies were conducted up to the time when the release had plateaued. In order to eliminate contamination and excessive unwanted PLGA in the measuring

solution, a 0.5 µm cellulose acetate membrane was adopted to filter the solution before each UV measurement was taken. For the samples in physiological temperature with fresh media, 2 ml of the solution extracted from each sample was replaced with a 2 ml new release media after each UV measurement. The amount of dye released in each media from the pack of microspheres was determined by interpolation of absorbance value from the calibration curve (**Fig. 3.8**). This study was performed for both the modified single needle and the modified co-axial needle EHD/TIPS methods in triplicate for each dye and the average values and standard deviations were calculated.

In order to normalize the results for the control at all time, 8 batches of only PLGA microspheres with no dye loaded were prepared. 2 of them were used for normalization of the samples at ambient temperature, whereas the other 6 were for normalization of the samples kept in the incubator at physiological temperature. 2 of them were used for the normalization of the samples replaced with fresh media by having 2 ml of them substituted with a new fresh media every time when measuring the relevant samples, whereas the other 2 was used for normalization of the samples in physiological temperature without the fresh SBF replacement. The last 2 control samples were adopted for normalization of the samples in physiological temperature with the application of sonication at different frequencies. Throughout the process of dye release studies, the controlled samples were also measured accordingly at pre-determined time intervals by UV spectrophotometer.

3.9.2.4 Dye Entrapment

To determine the concentration of pyronin B and erythrosin B entrapped in packs of microspheres, 0.1 g of the products after freeze drying was added to glass vial which was first filled with 5 ml DMC to dissolve the polymeric microspheres and release the dye, and then addition of 5 ml SBF to dissolve the dye. For determination of Reichardt's dye concentration, 0.05 g of the relevant microspheres was added to a solution containing 5 ml DMC and 45 ml SBF:ethanol (80:20 v/v). The solutions were stirred for 120 s and then 2 ml from the vials was filtered with 0.5 µm cellulose acetate membrane before the UV measurements. According to the absorbance measured with UV spectroscopy for each sample, the dye entrapment efficiency was then calculated based on the yield of the process. In fact, the entrapment efficiency is the ratio between the weight of the agent incorporated into the microspheres and that which was used in the electrosprayed solutions (Equation 3.9).

Based on the assumption that the solvent is all evaporated during the freeze drying process, the percentage yield of the process can be determined by measuring the weight of the materials collected in the metallic beaker (Equation 3.8). The dye entrapment efficiency, the dye loading percentage and the actual percentage of dye loaded in the process were calculated using the following equations:

$$\text{Yield (\%)} = \left[\frac{\text{Weight of the products after freeze drying}}{\text{weight of of PLGA+weight of dye}}\right] \times 100 \quad \textbf{(3.8)}$$

$$\text{Dye entrapment efficiency (\%)} = \left[\frac{\text{Weight of dye in the microspheres}}{\text{Yield of the process} \times \text{weight of drug in the solution}}\right] \times 100 \quad \textbf{(3.9)}$$

$$\text{Dye loading (\%)} = \left[\frac{\text{Weight of dye in the microspheres}}{\text{weight of the microspheres loaded with dye}}\right] \times 100 \quad \textbf{(3.10)}$$

$$\text{Actual dye loaded in the process (\%)} = \left[\frac{\text{Weight of dye in the total microspheres}}{\text{weight of dye in the electrosprayed solution}}\right] \times 100 \quad \textbf{(3.11)}$$

The actual percentage of dye loaded in the process (Equation 3.11) is the ratio between the weight of dye encapsulated in the total microspheres collected from each process and the weight of dye used in the electrosprayed solution. This equation is really important for mass production by the EHD/TIPS methods as it shows the capability of the process in preserving the amount of the dye encapsulated based on the collection of the total microspheres.

3.10 Sonication Exposure Setup

The effect of sonication on the release profile of the encapsulated materials was discussed in **Section 2.12.2.** This part of the investigation incorporating sonication was to determine the influence of different parameters such as duty cycle and exposure time on the release rate of the dyes from the microspheres. For this part of experimental work, a preliminary study was carried out on the release profile of PLGA particles fabricated via the modified single needle and co-axial needle EHD/TIPS processes. As explained in **Section 3.9.2.3,** two samples from each dye encapsulated in the produced microspheres were exposed to sonication using an ultrasonic cell disruptor (XL2000 Misonix Inc. Farmingdale, NY, USA; probe diameter 3mm) with operating frequencies of 20 kHz for 30 seconds and 40 kHz for 20 seconds. To avoid any damage or local heating to the dye loaded microspheres, they were gently poured into a water proof elastic latex tube which was relatively transparent to sonicator (Fatemi and Greenleaf, 1998). The tube and the sonicator probe were immersed in a beaker contained water with an

estimated 40 mm distance between them. The probe was kept with an angle of approximately 45^{o} respect to the vertical line so that the microspheres were not directly in line with the probe axis and thus introduced to relatively small intensity of sonication[1]. Ultrasonic wavelengths with 20 kHz and 40 kHz were applied for 30 s and 20 s respectively, and the sample was returned to the vial for the UV spectroscopy measurements. As described earlier, control measurements were also conducted to confirm that there was no change in the UV spectroscopy readings due to transfer of the microspheres between vial and the tube.

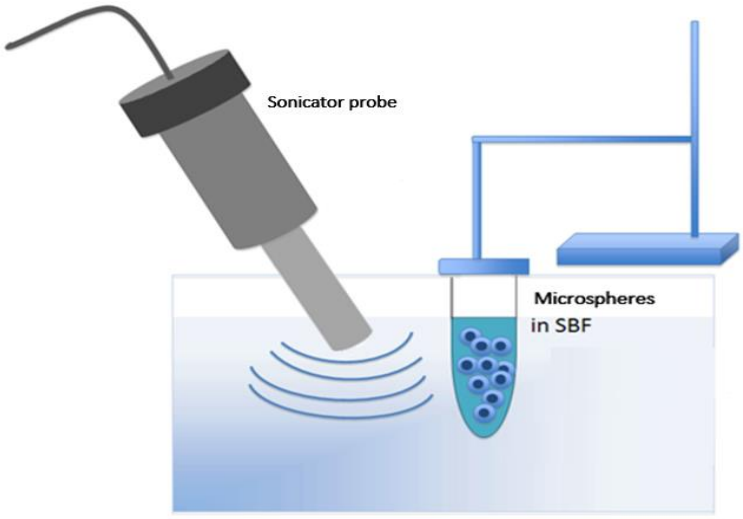

Figure 3.9: Schematic diagram of the sonicator exposure to a prepared sample

3.11 *In Situ* Deposition

The *in situ* deposition study was carried out in conjunction with the discussion in **Section 2.13.1** to empirically investigate the ability of the prepared microspheres for transferring through the syringe needle and their formation into scaffold after injection. For this purpose, a pack of microspheres with 0.3 g weight and 10 ml SBF were prepared (**Fig. 3.10b**). For this investigation, a piece of pig meat (150 mm, 50 mm and 12 mm) with the skin cover was also prepared and placed on a worktop (**Fig. 3.10a**). To find out how microspheres would form into scaffold within an infected tissue, an irregular-shaped cavity was created with 5 mm depth from the surface of the meat. Afterwards, 0.3 g of the microspheres was added to the 10 ml SBF and shaken for 60 s on the vortex machine to form a suspension. The suspended solution was then injected by a syringe and a needle through the cavity created in the meat (**Figs. 3.10c, 3.10d**

[1] Based on the available apparatus in this study, it was not viable to control the sonicator intensity. The only point of this investigation was to observe the influence of sonication on the release rate of encapsulated materials

and **3.10e**). After 600 s interval, waiting for the injected materials to dehydrate, the area around the cavity was sectioned with a surgical blade (**Figs. 3.10f** and **3.10g**).

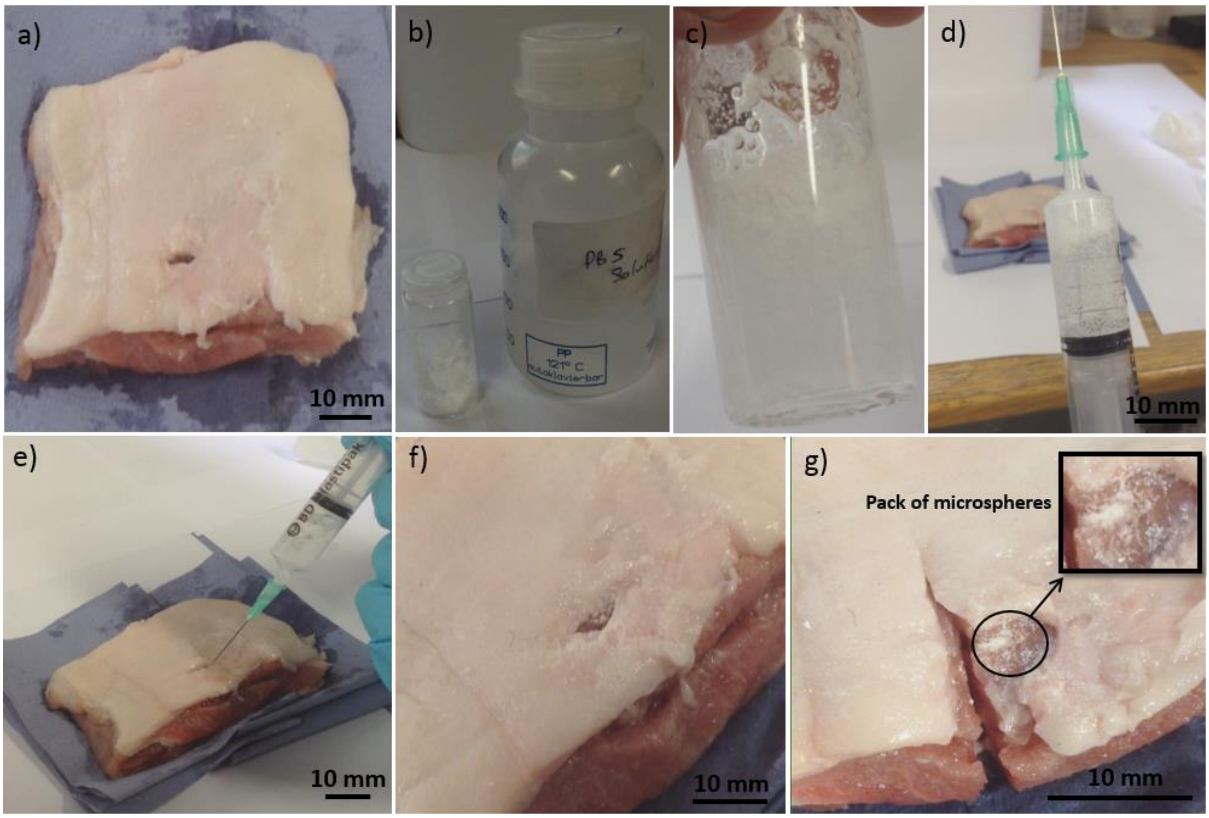

Figure 3.10: *In-situ* deposition protocol: a) Piece of meat, b) SBF solution and the microspheres, c) Microspheres suspended in SBF, d) Syringe filled with SBF and the suspended microspheres, e) Injection process of the suspended solution, f) Dehydration of the injected materials and g) Incision by surgical blade

As shown in **Figure 3.10g**, the pack of free flowing microspheres after injection and dehydration formed into a scaffold structure that deposited inside the created cavity within the tissue.

Chapter 4

Results and Discussion

Overview

This chapter of the thesis has two main parts: 1) the EHD mode mapping and size distribution studies, and 2) the *in vitro* release studies. In the first part of this chapter, the single needle EHD method was used to explore its ability for preparing polymeric drug spheres with different size ranges. The aim was to optimise the combination of several key processing parameters in order to achieve the stable cone-jet and subsequently producing spherical polymeric carriers with narrow size distribution. Then, according to the EHD mode mapping and size distribution studies, further experiments were conducted to investigate the capability of single needle EHD processing for fabricating the porous microspheres with the required size distribution (150-300 µm) and assembly of them into scaffold by TIPS and freeze-dryer for the purpose of chronic wounds therapy.

In the second part of this chapter, the results of process modifications and the improvements on the yield for obtaining more accurate entrapment efficiency of the incorporated materials were discussed. The morphological studies were also carried out investigating the differences between the loaded products of the single needle and the co-axial needle EHD/TIPS methods. Moreover, the results of *in vitro* release studies were investigated to show the capability of the loaded PLGA microspheres in providing controlled release of the active agents in a sustainable dosage over the release period. The advanced treatment of chronic wound requires the porous surface microspheres with great ability of delivering their payload with a high initial burst release followed by a sustained period. Therefore, in the *in vitro* release studies, the effects of different temperatures, addition of fresh media and sonication exposure upon the dye release were investigated, aiming to modify the release rate of the incorporated materials by external stimuli for an optimum control release. Finally, it was attempted to predict the release profile of immunosuppressive agents such as cyclosporine A and Tacrolimus based on the *in vitro* release profiles of the dyes adopted. In this second part of this chapter, the results of further investigations such as FTIR and EDX studies were also discussed in order to provide more information on the presence of the encapsulated dyes in the produced microspheres and the effect of the procedures on the biofunctionality of the processing materials.

4.1 EHD Mode Mapping and Size Distribution Studies for Controlling the Size of Spheres via Systematic Processing Parameter Variations

One of the most important characteristics of drug delivery systems is, selecting the appropriate size of the constituent particles (Panyam and Labhasetwar, 2003). This factor has a substantial influence on different *in vivo* functions of drug carriers such as circulation time, immunogenicity, internalization, extravasation, targeting, intercellular trafficking and degradation as well as flow properties, clearance and uptake mechanisms (Mitragotri and Lahann, 2009). For example, particles with micrometre size are important in passive drug targeting such as in pulmonary drug delivery and chronic wound therapy, whereas nano-sized particles have the ability to penetrate small capillaries, allowing enhanced accumulation of nano-particles at target sites (Lanza et al., 2002).

4.1.1 Characteristics of PCL and PLGA Solutions with Various Concentrations

The EHD process by which the spherical particles are generated is governed by the physical properties of solutions such as surface tension, viscosity, density and electrical conductivity as well as the processing parameters (the flow rate and the applied voltage). Different combinations of these variables lead to generation of various jetting modes (Cloupeau and Prunet-Foch, 1990). Therefore, to reach the ideal jetting mode for production of the required microspheres, the first step was to characterise the properties of the solutions adopted in this investigation (**Table 4.1**).

Increasing the polymer concentration of the solutions enhances the surface tension, density and viscosity, but decreases the electrical conductivity (**Table 4.1**). These changes in the solution properties due to changes in the polymer concentration lead to different EHD jetting modes, and hence the ranges of flow rate and the applied voltage to achieve the stable cone-jets change for each polymer solution.

An increase in the polymer concentration of the solution which was corresponded to an increase in the viscosity and the surface tension (**Table 4.1**) meant that a stronger electrostatic force (the applied voltage) was required to form a cone-jet for a solution of a higher polymer concentration. For example, PLGA/DMF and PLGA/DMAc solutions had higher viscosity and surface tension compared with PCL/toluene and PLGA/DMC solutions. Thus, higher applied voltages were found to be necessary to obtain the cone-jet during the EHD processing. However, in the case of PCL solutions, in particular PCL45,000, due to the very low electrical

conductivity and dielectric constant of the toluene, a much higher applied voltage was required to facilitate the stable cone-jet formation for generating spherical particles (**Fig. 4.3**).

Table 4.1: Properties of the polymer solutions adopted in the microspheres formation

Solution	Viscosity (mPa s)	Surface Tension (mN m^{-1})	Conductivity (µS m^{-1})	pH	Density (kg m^{-3})
5% PLGA in DMAc	4.5 ± 0.2	37.5 ± 0.9	2.8 ± 0.3	7.5	950 ± 10
10% PLGA in DMAc	6.1 ± 0.3	39.1 ± 0.7	1.5 ± 0.3	7.5	960 ± 10
20% PLGA in DMAc	12.9 ± 0.5	54.17 ± 1.2	0.90 ± 0.2	7.5	1000 ± 10
5% PLGA in DMF	4.0 ± 0.2	36.9 ± 0.7	2.5 ± 0.3	7.5	960 ± 10
10% PLGA in DMF	4.15 ± 0.3	40.9 ± 1.0	1.3 ± 0.2	7.5	980 ± 10
20% PLGA in DMF	11.5 ± 0.5	49.1 ± 0.8	1.0 ± 0.2	7.5	1050 ± 10
5% PLGA in DMC	3.7 ± 0.3	28.5 ± 0.5	0.20 ± 0.1	6.5	1100 ± 10
10% PLGA in DMC	4.18 ± 0.5	32.8 ± 0.6	0.10 ± 0.1	6.5	1110 ± 10
15% PLGA in DMC	12 ± 0.3	34.4 ± 0.9	0.10 ± 0.1	6.5	1110 ± 10
5% PCL45000 in toluene	3.0 ± 0.4	26.5 ± 0.6	-[2]	7.0	900 ± 10
7% PCL45000 in toluene	6.7 ± 0.4	28.0 ± 0.6	-	7.0	1000 ± 10
10% PCL45000 in toluene	11 ± 0.6	29.5 ± 0.7	-	7.0	1100 ± 10
15% PCL10000 in toluene	6.0 ± 0.5	28.4 ± 0.5	-	7.0	900 ± 10

[2] Electrical conductivity of the PCL solutions were out of the measurement range of the conductivity meter. Therefore, they could not be measured

Solution	Viscosity (mPa s)	Surface Tension (mN m^{-1})	Conductivity (µS m^{-1})	pH	Density (kg m^{-3})
20% PCL10000 in toluene	**16 ± 0.7**	**29.6 ± 0.8**	**-**	**7.0**	**940 ± 10**
25% PCL10000 in toluene	**25 ± 0.8**	**32.8 ± 0.6**	**-**	**7.0**	**960 ± 10**

Solution	Viscosity (mPa s)	Surface Tension (mN m^{-1})	Conductivity (µS m^{-1})	pH	Density (kg m^{-3})	Dielectric Constant
DMF	**1.0 ± 0.2**	**37.1 ± 0.8**	**4 ± 0.3**	**7.5**	**944 ± 10**	**37.8** (Smallwood, 1996)
DMAc	**2.1 ± 0.3**	**36.1 ± 0.6**	**4.6 ± 0.3**	**6.0**	**940 ± 10**	**36.7** (Smallwood, 1996)
DMC	**0.60 ± 0.2**	**30.7 ± 0.4**	**0.20 ± 0.1**	**6.0**	**1070 ± 10**	**3.1** (Tundo and Selva, 2002)
Toluene	**0.60 ± 0.1**	**28.5 ± 0.5**	**$8.0x10^{-8}$** (Luo et al., 2012)	**7.0**	**867 ± 10**	**2.38** (Smallwood, 1996)

Unlike the electrical conductivity that directly influences the EHD cone-jet mode, dielectric constant (relative permittivity) is a parameter that has very less effect on the cone-jet formation; however, it has a direct influence on the size distribution of particles. Experimentally, it has been demonstrated that the liquids with greater value of dielectric constant produce relatively small size of particles under cone-jet mode compared with those obtained lower value of dielectric constant (Luo et al., 2012).

4.1.2 Classifications of EHD Jetting Modes of the Polymer Solutions

Geometrical features of the jet and the various types encountered in this study as a function of the operating parameters for the generation of the spherical particles have been classified in **Figure 4.1**. According to Jaworek & Krupa, they include dripping, unstable cone-jet, stable cone-jet, multi-jet and irregular instabilities modes (Jaworek and Krupa, 1999b).

In the EHD technique, the cone-jet is the most stable and used atomization mode, as it generates a nearly uniform and near monodisperse spherical particles. In this study, dripping mode occurred when there was no voltage applied or either the applied voltage was not high enough to break the surface tension of the solution. In this mode, the drops form the shape of regular droplet detaching from the needle capillary as the gravitational force overcomes the surface tension (**Fig. 4.1b**). An increase in the applied voltage led to either unstable or the stable cone-jet mode. This rise in the voltage stabilised and shaped the cone-jet which results in a balance of liquid pressure, liquid surface tension, gravity, electric stresses at the liquid surface, the liquid inertia and the liquid viscosity (Hartman et al., 2000). When a balance between all these applied forces occurred, stable cone-jet was obtained (**Fig. 4.1d**); otherwise unstable cone-jet was generated (**Fig. 4.1c**).

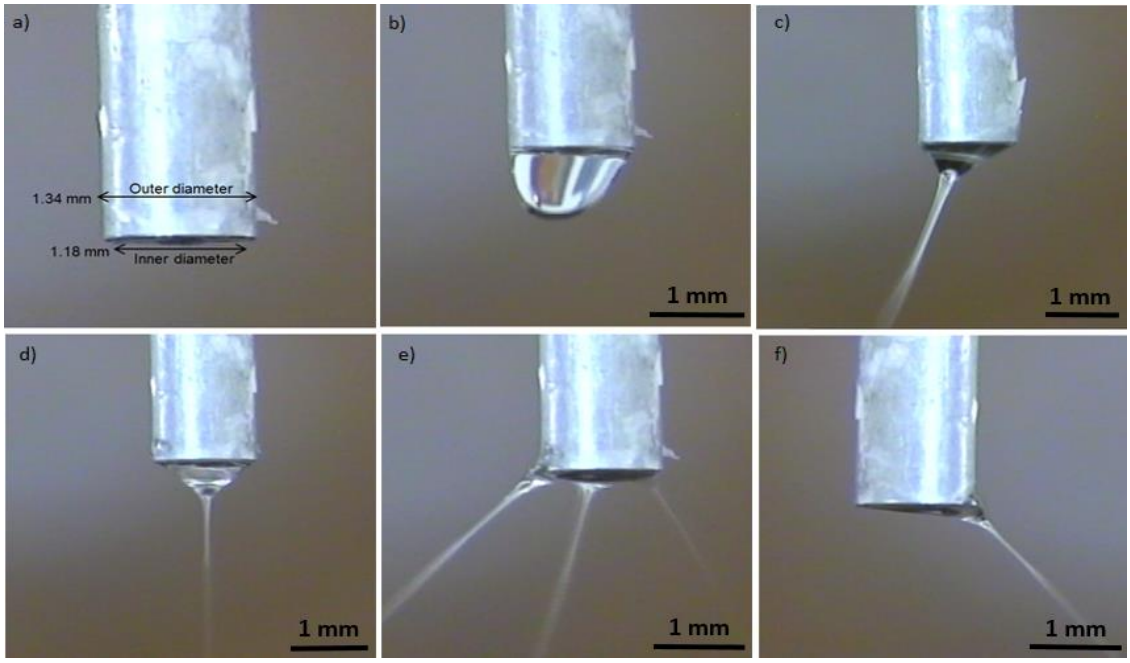

Figure 4.1: Geometrical features of different jet modes: a) No dripping, b) Dripping, c) Unstable cone-jet, d) Stable cone-jet, e) Multi-jet and f) Irregular instabilities

Further increase of the applied voltage caused multi-jet mode to evolve. This mode of jet occurred at applied voltage well above the range of applied voltage obtained for the stable cone-jet (**Fig. 4.1e**). Irregular instabilities mode which is another possible form of EHD jetting, encountered when intermittent droplet formation occurs (**Fig. 4.1f**).

4.1.3 Effect of Flow Rate and Applied Voltage on the Size Distribution

In this section, the effect of applied voltage and flow rate on the size and size distribution of spherical particles was studied. These two variables (flow rate and applied voltage) along with

different concentrations of polymer solutions were the significant parameters in determining the size distribution of the spherical particles collected at the stable cone-jet mode. The size of the spherical particles was increased by enhancement of the flow rates and polymeric concentration of the solutions (**Figs. 4.2-4.6**). This phenomenon occurred for all the polymer solutions with various concentrations. However, increase in the applied voltage led to reduction in size of particles collected at the stable cone-jet. Since, all the particles were tried to be collected at the stable con-jet mode, voltage was applied in a range to keep the cone-jet mode stable for the period of collection. However, sometimes due to the physical properties of the solutions and their interactions with the applied electric field, the cone-jet mode could not be very stable at varying flow rates **(Fig. 4.3)**.

4.1.3.1 Parametric Mode Mapping of PCL Solutions

Different concentrations of the PCL solutions dissolved in toluene were electrosprayed at different flow rates and the ranges of applied voltage, and the size distribution of the spherical particles produced were plotted against these two variables. **Figure 4.2** shows the results acquired from the electrospray of PCL10,000 solutions, whereas **Figure 4.3** is related to the findings collected from different concentrations of PCL45,000 solutions.

The solution with 15 wt% concentration of PCL10,000 dissolved in toluene provided a range of particle size varied from 100 µm up to 380 µm (**Fig. 4.2a**) depending on the flow rates and the range of applied voltage, whereas this range (size distribution of particles) with 20 wt% concentration of PCL10,000 were broadened changing from 200-600 µm (**Fig. 4.2b**). By increasing the concentration of this PCL type to 25 wt%, the particle size distribution extended slightly wider between 180-600 µm (**Fig. 4.2c**). This shows the direct effect of polymeric concentration and the flow rate on the size and size distribution of the spherical particles. Electrospray of PCL10,000 solutions with 20 and 25 wt% concentrations in general provided narrower size distribution of particles at each flow rate compared with the 15 wt% concentration. This was attributed to the higher viscosity of the more concentrated polymer solutions **(Table 4.1)** that provided more charges on the surface to break the surface tension upon the application of voltage. Therefore, it led to more stability of the cone-jet mode in production of the spherical particles.

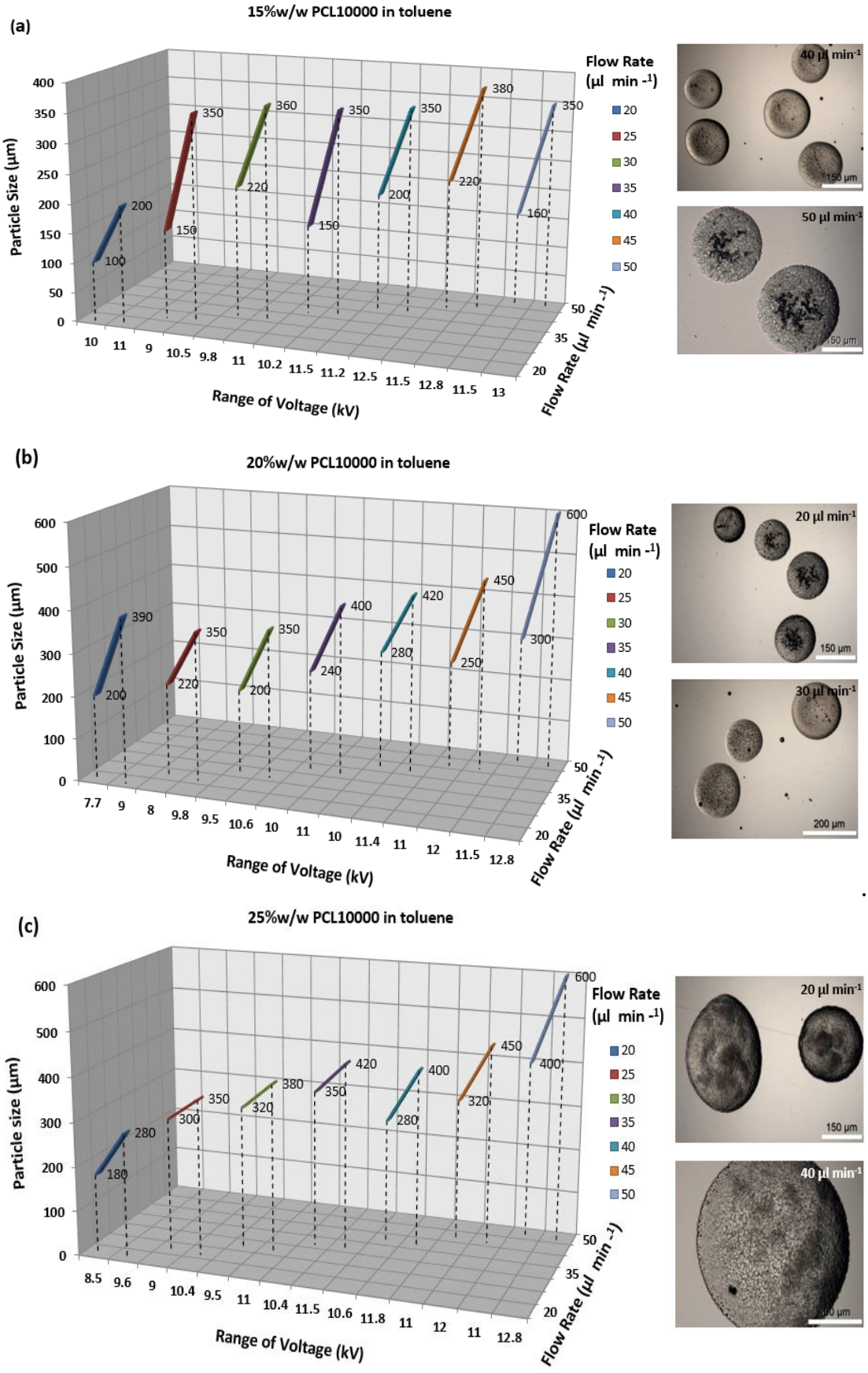

Figure 4.2: Parametric mode mapping of particles obtained from PCL10,000/toluene solution: a) 15 wt% concentration, (b) 20 wt% concentration and (c) 25 wt% concentration

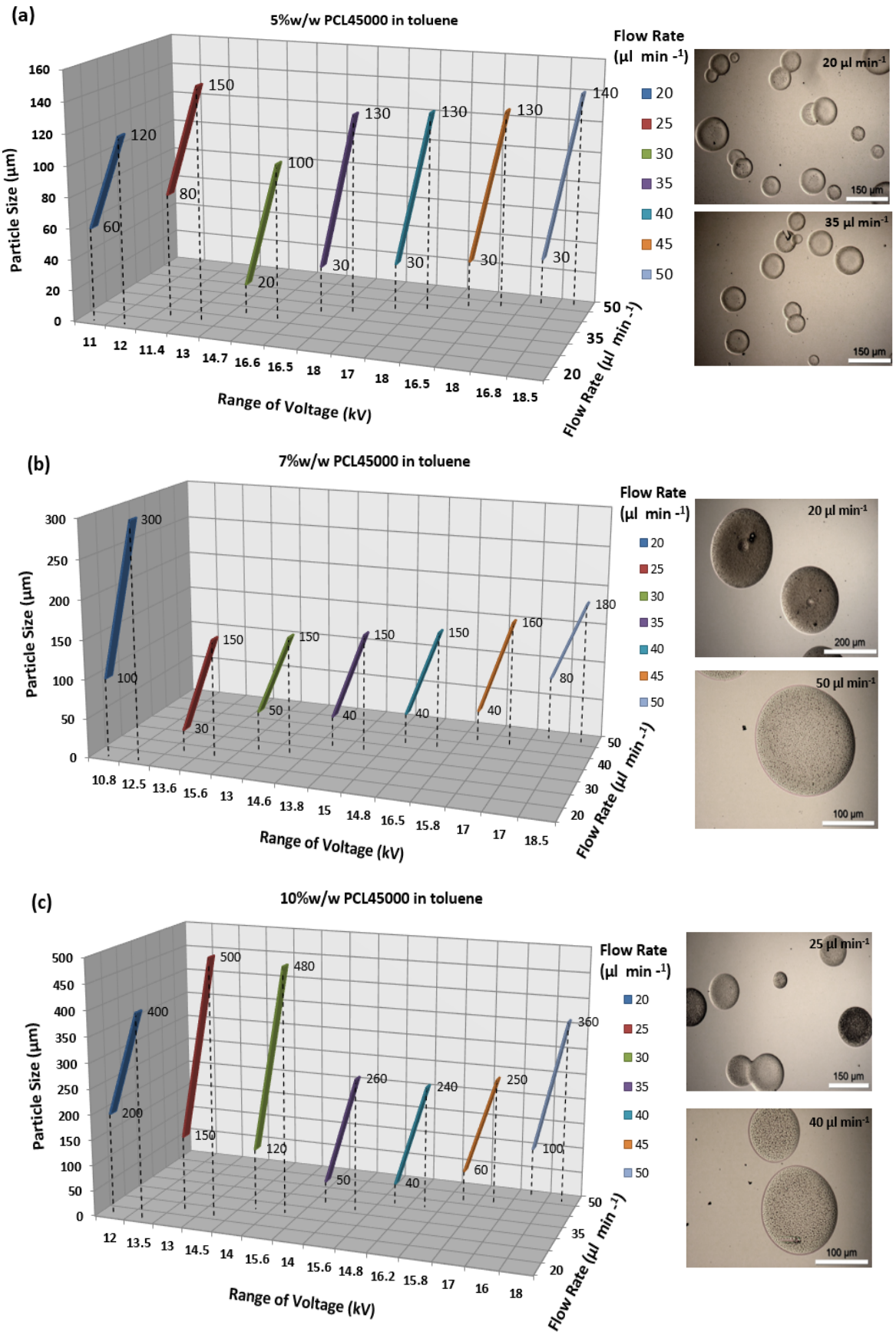

Figure 4.3: Parametric mode mapping of particles obtained from PCL45,000/toluene solution: (a) 5 wt% concentration, (b) 7 wt% concentration and (c) 10 wt% concentration

The solution with 5 wt% concentration of PCL45,000 in toluene provided a range of particle size varied from 20 µm up to 150 µm (**Fig. 4.3a**), depending on varying flow rates and the ranges of applied voltage. With this concentration, the size distribution of particles increased as the flow rate increased. The size range of particles with 7 wt% concentration of PCL45000 was broadened varying between 30 and 300 µm (**Fig. 4.3b**), and by increasing the concentration of this polymer to 10 wt%, the size distribution increased further ranging from 40 to 500 µm (**Fig. 4.3c**). As **Figure 4.3c** show, the 10 wt% of PCL45,000 solution could not provide stable cone-jet at low flow rates (less than 30 µl/min) compared with other two PCL 45,000 solutions. This was related to the very low electrical conductivity of this polymer solution (10 wt%) that could not provide enough charges on the liquid surface for formation of stable cone-jet mode. Therefore, it resulted in large size distribution of particles at low flow rates.

In general, toluene is a low viscous, highly volatile and almost non-conductive solvent (ε = 2.38 at 20°C; $\sigma = 8.0 \times 10^{-8}$ µS m^{-1} at 20°C) (Smallwood, 1996), and the combination of this solvent with a polymer such as PCL provided the solutions with very low conductivity that do not have enough capability to interact with an electric field. Therefore, high applied voltage was found to be necessary to achieve the stable cone-jet at different flow rates. Due to the very low electrical conductivity, the polymer solutions at low flow rates had difficulty to provide the stable cone-jet, but as the flow rate increased, the range of voltage was also elevated in order to compensate the low conductivity of the polymer solutions for obtaining the stable cone-jet for collection of the spherical particles.

4.1.3.2 Parametric Mode Mapping of PLGA Solutions

The findings from the electrospray of different concentrations (5, 10 and 20 wt%) of PLGA solutions dissolved in the two highly conductive solvents (DMF and DMAc) at different flow rates and the ranges of applied voltage are provided in **Figure 4.4**. As it shows, the size distribution of the spherical particles was significantly effected based on the variations of these two processing parameters.

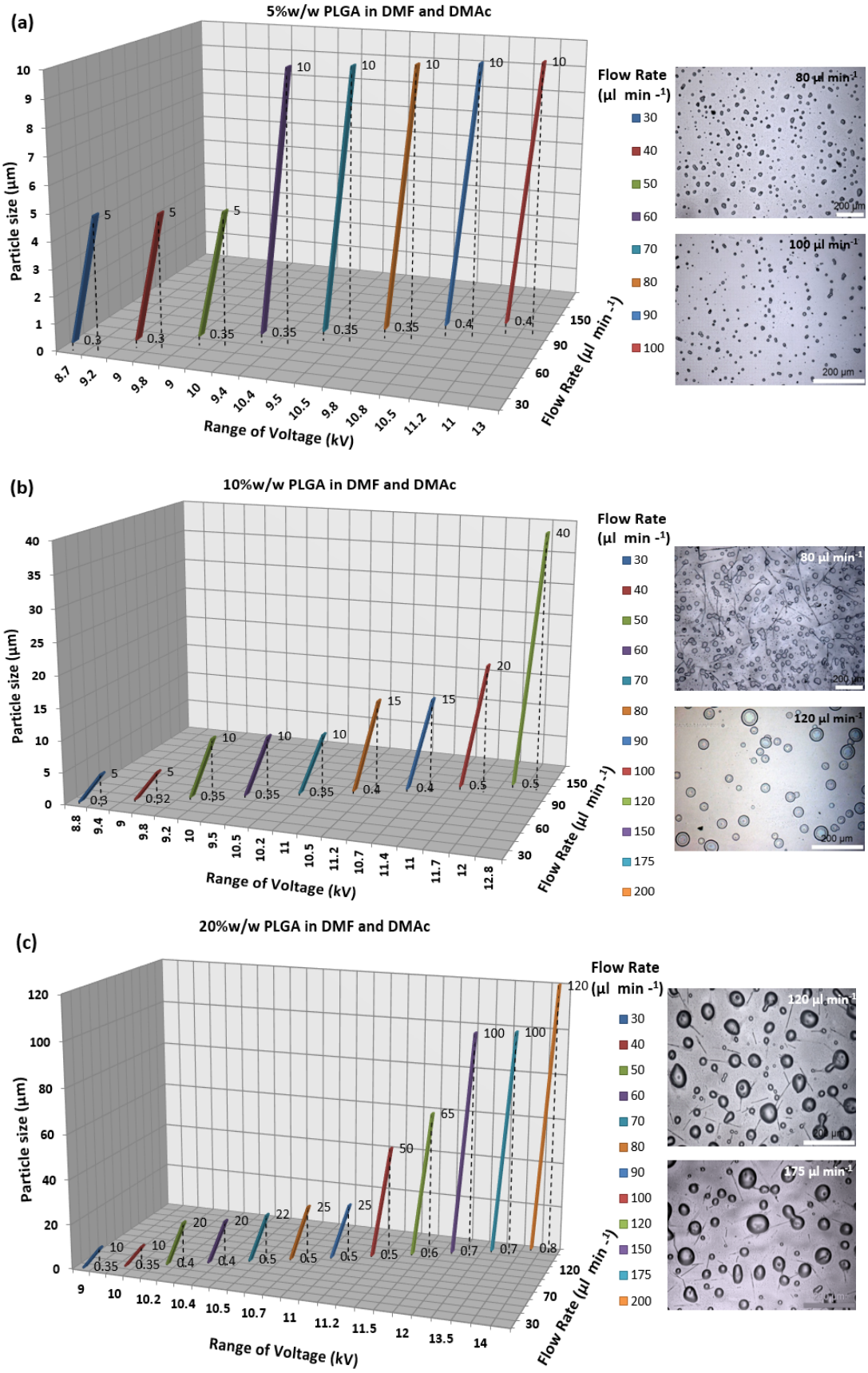

Figure 4.4: Parametric mode mapping of particles obtained from (a) 5 wt% concentration of PLGA in DMAc and DMF (b) 10 wt% concentration of PLGA in DMAc and DMF and (c) 15 wt% concentration of PLGA in DMAc and DMF

PLGA Solutions with 5 wt% concentration in DMF and DMAc provided particles with size distribution varying from 0.3 µm up to 10 µm (**Fig. 4.4a**) depending on different flow rates. By increasing the concentration of these two polymer solutions to 10 wt%, the particle size distribution increased between 0.3-40 µm (**Fig. 4.4b**). This range of particle size was extended wider up to 120 µm by enhancing the concentration of the two polymer solutions to 20 wt% (**Fig. 4.4c**). The wider range in the size distribution of particles with higher flow rates as well as higher concentration of the polymer solution is attributed to the high values of dielectric constant, conductivity, surface tension **(Table 4.1)** and the applied voltage that provided less stability of the cone-jet mode in production of the spherical particles.

In general, the two solvents of DMF (σ = 4.0 µS m^{-1}; ε = 37.8 at 20°C) and DMAc (σ = 4.6 µS m^{-1}; ε = 36.7 at 20°C) (Smallwood, 1996) are highly conductive with low volatility rate, and their combinations with PLGA co-polymer provided solutions with great ability to interact with the applied electric field. Therefore, these types of solutions required lower applied voltage to break the surface tension of the liquid solution for production of microspheres compared with the PCL solutions. However, due to high surface tension, high conductivity and high dielectric constant of the polymer solutions, they had difficulty to provide the stable cone-jet at high flow rates. Therefore, PLGA in DMF and DMAc generated small particles with a broad range of particle size. For the same reason (high conductivity and dielectric constant of the polymer solutions) no samples could be collected at flow rates above 100 µl/min and 120 µl/min, respectively, for 5wt% and 10 wt% concentrations of the polymer solutions. Since, the higher concentration of polymer led to reduction of electrical conductivity, the cone-jet was obtained with 20 wt% concentration of the two solutions (PLGA/DMAc and PLGA/DMF) at higher flow rates for production of particles, but still was not stable enough to produce monodisperse particles.

Different concentrations (5, 10 and 15 wt%) of PLGA co-polymer dissolved in DMC were electrosprayed at different flow rates and the size distribution of the produced particles were arranged in **Figure 4.5**. At various flow rates, distinct ranges of voltage were applied in order to obtain the stable cone-jet, and hence various ranges of particle size were collected.

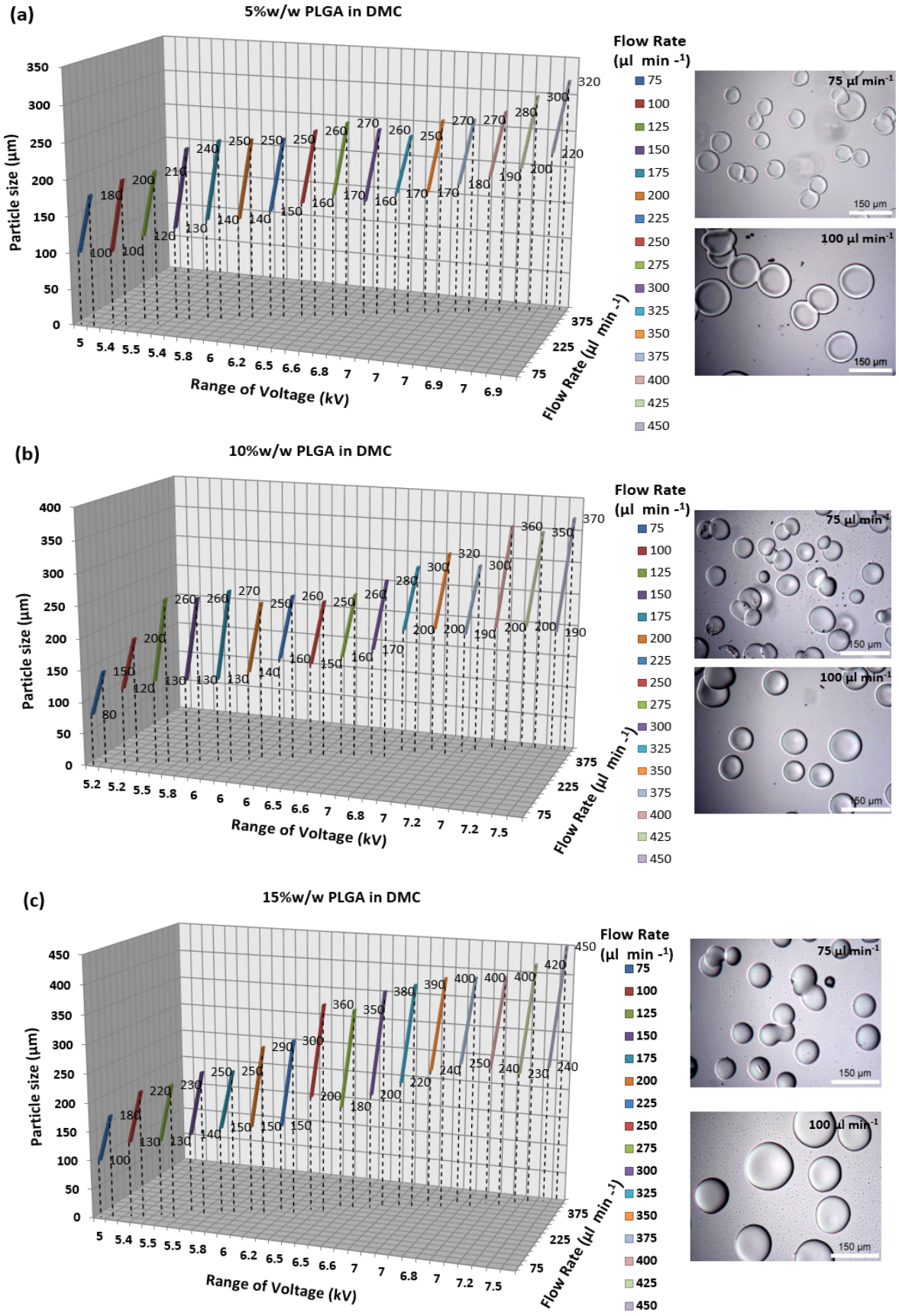

Figure 4.5: Parametric mode mapping of particles obtained from PLGA/DMC solutions: (a) 5 wt% concentration, (b) 10 wt% concentration and (c) 15 wt% concentration

PLGA solution with 5 wt% concentration in DMC provided a range of particles size varying from 100 µm up to 320 µm (**Fig. 4.5a**) depending on different flow rates and the ranges of applied voltage. By increasing the concentration of PLGA solution to 10 wt%, the size distribution of spherical particles varied between 80-370 µm (**Fig. 4.5b**). This range with 15 wt% concentration of PLGA was broadened, changing from 100-450 µm (**Fig. 4.5c**). As the three graphs in **Figure 4.5** demonstrate, by increasing the concentration of polymer and the flow rate, the range of particle size also enhances. This increase in the size distribution is due to the reduced ability of the higher concentrations of polymer at higher flow rates for obtaining the stable cone-jet in production of near monodisperse microspheres.

In general, DMC is a solvent with relatively low viscosity, low dielectric constant and moderate electrical conductivity ($\sigma = 2 \times 10^{-5}$ Sm^{-1}; $\varepsilon = 3.1$) (Tundo and Selva, 2002), and its combination with PLGA provided solutions which have less ability to interact with the applied electric field (potential). Therefore, electrospray of this solution at various flow rates was found to have less applied voltage compared with the other polymer solutions adopted in this study. This was attributed to the inherent physical properties of the solvent such moderate electrical conductivity and surface tension under ambient temperature. The unique property of this solvent led to better stability of the cone-jet throughout different flow rates with various concentrations of the polymer solution compared with the other PLGA solutions (PLGA/DMAc and PLGA/DMF) in this study.

4.1.4 Polydispersity Index

Polydispersity index (ratio of standard deviation to mean size) (PDI) is another factor to assess the EHD cone-jet mode and the size distribution of particles. Since, the collection of particles in this study is carried out at the stable cone-jet mode, values of PDI for each polymer solution with different concentrations indicates the stability of the cone-jet mode as well as the monodispersity of the generated particles at various flow rates. PDI in terms of percentage is calculated by taking the standard deviation divided by the average mean value of the particles' size and then multiply the total value by 100. PDI was calculated for each specific flow rate based on measuring the diameters of randomly 70 particles collected from electrospray of each processing sample.

4.1.4.1 Polydispersity of PCL Particles

Figure 4.6 is plotted based on the graphs provided in **Figures 4.2** and **4.3**. This figure shows the polydispersity index of particles' size obtained from electrospray of both PCL types in toluene. In general, PDI of PCL45,000 for all concentrations is greater compared with the values calculated for PCL10,000. This is attributed to the higher range of voltage applied to the PCL45,000 polymer solutions to compensate the relatively low electrical conductivity compared with the PCL10,000 for obtaining the stable cone-jet mode in production of the spherical particles. At flow rates above 35 µl/min, by increasing the concentration of polymer solution the PDI decreases. For example, the PDI of 5 wt% PCL45000 above this specific flow rate is approximately 45%, whereas by increasing the concentration of polymer to 10 wt%, this value drops to less than 40%. Also, the PDI of PCL10000 solution with low concentration (15 wt%) is above 22%, and this value by enhancing the polymeric concentration to 25 wt%, drops to less than 16%. This decrease in the PDI with respect to the higher concentration of polymer is attributed to the changes in the physical properties of the solution and also the lower value of the applied voltage that provided more stability of the cone-jet in production of the spherical particles.

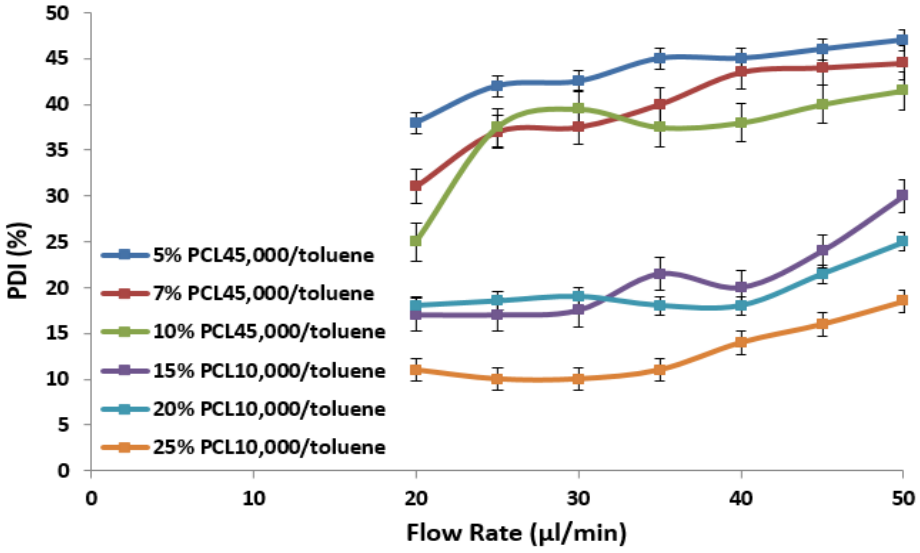

Figure 4.6: PDI of Particles' size obtained from PCL10000 and PCL45000 dissolved in toluene

4.1.4.2 Polydispersity of PLGA Particles

Figure 4.7, which is related to the results provided on the three graphs in **Figure 4.4**, shows the polydispersity of particles' size from the PLGA/DMF and PLGA/DMAc solutions

electrosprayed at different flow rates. In all concentrations of these two polymer solutions, the PDI increases with respect to enhancement of the flow rates. This phenomenon is more noticeable by comparing the low concentrations (5 wt% and 10 wt%) of solutions with the highest one (20 wt%). This figure also states that by decreasing the polymeric concentration, more monodisperse particles were obtained. However, the polydispersity of the particle size at low concentrations is still incredibly high to generate near monodisperse particles as drug carriers. The high values of polydispersity show the instability of the cone-jet for production of particles due to high conductivity and dielectric constant as well as high surface tension of the polymer solutions.

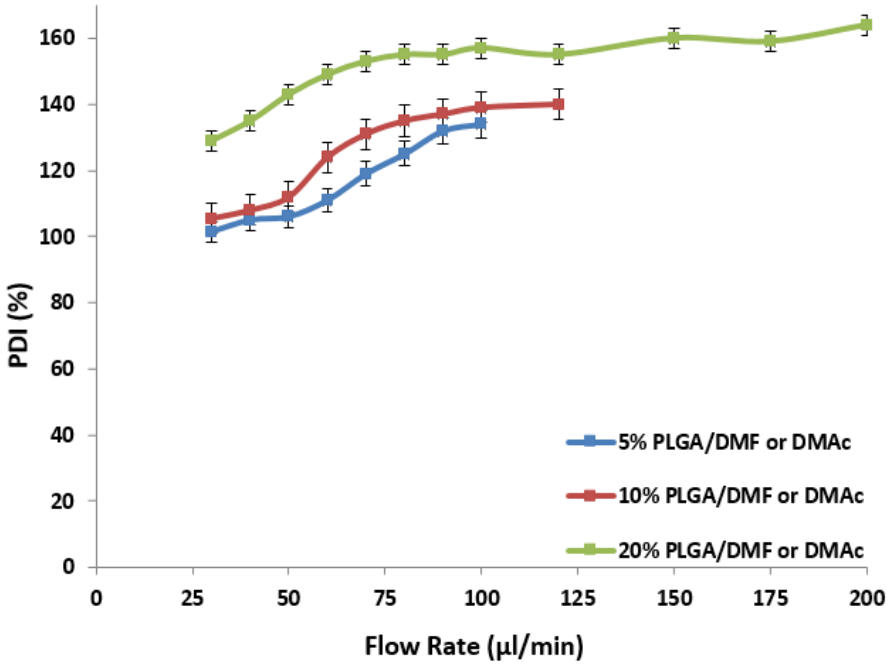

Figure 4.7: PDI of particles' size obtained from PLGA dissolved in DMF and DMAc

Figure 4.8 shows the polydispersity of particles' size of PLGA solutions in DMC which is arranged based on the results illustrated on the three graphs in **Figure 4.5**. This graph shows that the PDI of PLGA/DMC with 10 wt% concentration never exceeded 40%. However, this value for the two other concentrations, 5 wt% and 15 wt%, of the polymer solution drops to less than 33% and 30% respectively. This graph also demonstrates an increase trend of PDI values as the flow rate increased which in turn indicates less stability of the cone-jet in production of near monodisperse particles. PDI of the polymer solutions also shows that the combination of PLGA/DMC provided more stable cone-jet compared with the two other PLGA polymer solutions for production of spherical particles with the required size (150-300 µm). However, this combination (PLGA/DMC) provided poorer stability of cone-jet mode compared with the PCL10,000 solutions dissolved in toluene.

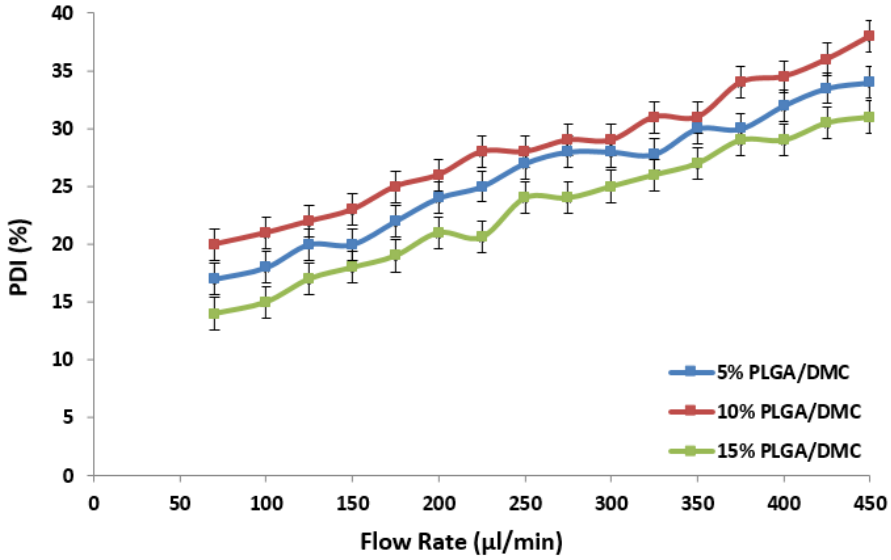

Figure 4.8: PDI of Particles' size obtained from PLGA dissolved in DMC

4.2 Optical Microscopy Analysis

Figure 4.9 shows an overview of typical microspheres generated from EHD processing of various polymer solutions. The three images in **Figures 4.9a(i), 4.9a(ii)** and **4.9a(iii)** demonstrate the small-sized microspheres obtained from the electrospray of different concentrations of PLGA solutions in DMAc and DMF. Detailed analysis using higher magnification (**Fig. 4.9a(iii)**) showed that all particles were spherical with a smooth outer surface and were small compared with those obtained from electrospray of the other polymer solutions in this study. The other three images in **Figures 4.9b(i), 4.9b(ii)** and **4.9b(iii)** illustrate the relatively large size distribution of microspheres collected from the electrospray of both PCL types in toluene. Optical microscopy analysis using higher magnification (**Figs. 4.9b(ii)** and **4.9c(iii)**) shows the porosity on the outer surface of particles, owing to quick evaporation of the solvent. Finally, **Figures 4.9c(i), 4.9c(ii)** and **4.9c(iii)** demonstrate the microspheres collected from electrospraying of PLGA in DMC. Further analysis of these samples at higher magnification shows spherical particles with smooth outer surface structure (**Fig. 4.9c(iii)**).

Placing the microspheres on the glass slides results in loss of their spherical shape, and the products appears concave (flattened) under optical microscope. This is because the polymer particles are not fully solidified as the melting point of the water is well above to that of the solvents used in this study. Therefore, the diameters recorded show a 10-15% higher value (depending on the viscosity of the polymer solution) compared with the actual diameter of the microspheres produced and stored in the vials.

Different polymer solutions (PLGA and/or PCL, in different solvents) have different inherent physical properties, which required different ranges of applied voltage and flow rate in order to obtain the stable cone-jet for generation of microspheres. Solutions with different concentrations will generate different size distributions regardless of the flow rate and applied voltage. In general, when flow rate was increased from 20 µl min^{-1} to 450 µl min^{-1} during the single nozzle EHD processing, the readiness of the liquid to form the cone-jet decreased and the microsphere diameter distribution broadened with increasing the flow rate for all polymer solutions at all the concentrations tested.

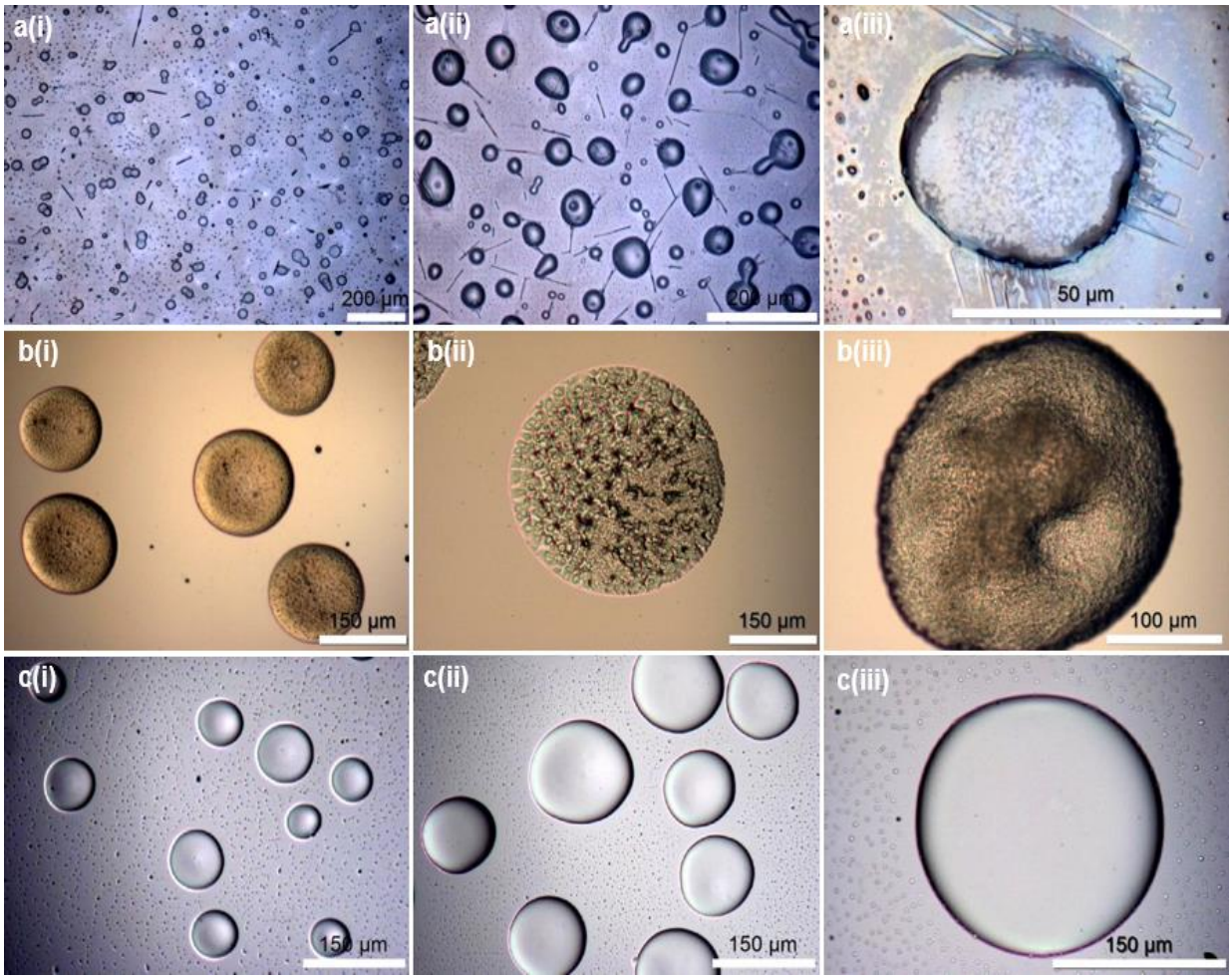

Figure 4.9: Size distribution of a(i) 10 wt% PLGA in DMAc at 150 µl min^{-1} (magnified x5), a(ii) 20 wt% PLGA in DMF at 200 µl min^{-1} (magnified x5), a(iii) 20 wt% PLGA dissolved in DMAc at 150 µl min^{-1} (magnified x50), b(i) 5 wt% PCL45000 in toluene at 25 µl min^{-1} (magnified x5), b(ii) 10 wt% PCL45000 in toluene at 30 µl min^{-1} (magnified x50), b(iii) 20 wt% PCL10000 in toluene at 50 µl min^{-1} (magnified x50), c(i) 5 wt% PLGA in DMC at 150 µl min^{-1} (magnified x5), c(ii) 10 wt% PLGA in DMC at 250 µl min^{-1} (magnified x5) and c(iii) 10 wt% PLGA in DMC at 300 µl min^{-1} (magnified x50)

For each liquid in the process of single needle EHD, a critical flow rate was observed, above which, the liquid showed difficulty achieving stable cone-jets, or the cone-jets remained stable for less than 5 minutes, and intermittent instability occurred. This critical flow rate was observed at 60 µl min^{-1} for 5 wt% PLGA in DMF and DMAc, 120 µl min^{-1} for 10 wt% and 15 wt% PLGA in DMF and DMAc, at 40 µl min^{-1} for PCL in toluene, and 400 µl min^{-1} for PLGA in DMC. This is attributed to the solvent properties, in particular, the collective influence of conductivity and dielectric constant **(Table 4.1)**. Electrical conductivity showed a stronger influence on the stable cone-jet formation than dielectric constant of the solvents; whereas dielectric constant showed a greater influence on the particle diameter distribution profile than the electrical conductivity of the solvent.

4.3 Particulate Scaffold

PLGA in DMF and DMAc: Although combination of PLGA with DMF and DMAc (high σ, high ε) is widely acceptable for clinical use at low dosage (New Jersey department health senior services, 2011), the polymer solutions did not generate near monodisperse microspheres with the required size distribution (**Fig. 4.4**). Therefore, this combination was discarded further in the development of particulate scaffold structure and encapsulation of pharmaceuticals. Failure was attributed to high dielectric constant of the PLGA/DMAc and PLGA/DMF solutions in generating the desirable size distribution of microspheres. Besides, high electrical conductivity and surface tension of the polymer solutions did not lead to obtaining the stable cone-jet for producing near monodisperse spherical particles.

PCL10,000 and PCL45,000 in toluene: Failure of PLGA in DMF and DMAc, led to using the combination of PCL and toluene. Although electrospray of PCL in toluene (low σ, low ε) provided the desirable size distribution of microspheres with surface porosity for formation of particulate scaffold (**Figs. 4.2** and **4.3**), toluene has high toxicity which makes it unsuitable for clinical use. The side effects include symptoms such as tiredness, confusion, weakness, memory loss, nausea, loss of appetite, and hearing and colour vision loss (Foxall, 2007). Besides, PCL has low rate of biodegradability which takes longer time to hydrolytically biodegrade inside the human body compared with PLGA co-polymer (Chen, 2010). Therefore, this combination was not investigated further for development of particulate scaffold for clinical use in treatment of chronic wounds.

PLGA in DMC: PLGA solution in DMC (moderate σ, low ε), a low toxicity solvent (Tundo and Selva, 2002), produced the appropriate size of microspheres over a broad range of processing parameters for all of the concentrations tested (5, 10 and 15 wt%, **Fig. 4.5**). This combination apart from producing the appropriate size of spheres, it could also overcome the problems of toluene toxicity and biodegradability of PCL polymer. The required size of microspheres for the formation of particulate scaffold was fabricated using 15 wt% PLGA in DMC at flow rate of 225 µl min^{-1} and the applied voltage ranging 6.0-7.0 kV (**Figs. 4.10** and **4.11**). Collection in liquid nitrogen followed by freeze drying generated the solid spherical particles **(Figs. 4.10a** and **4.11a)** with surface porosity (**Figs. 4.10c** and **4.11c**).

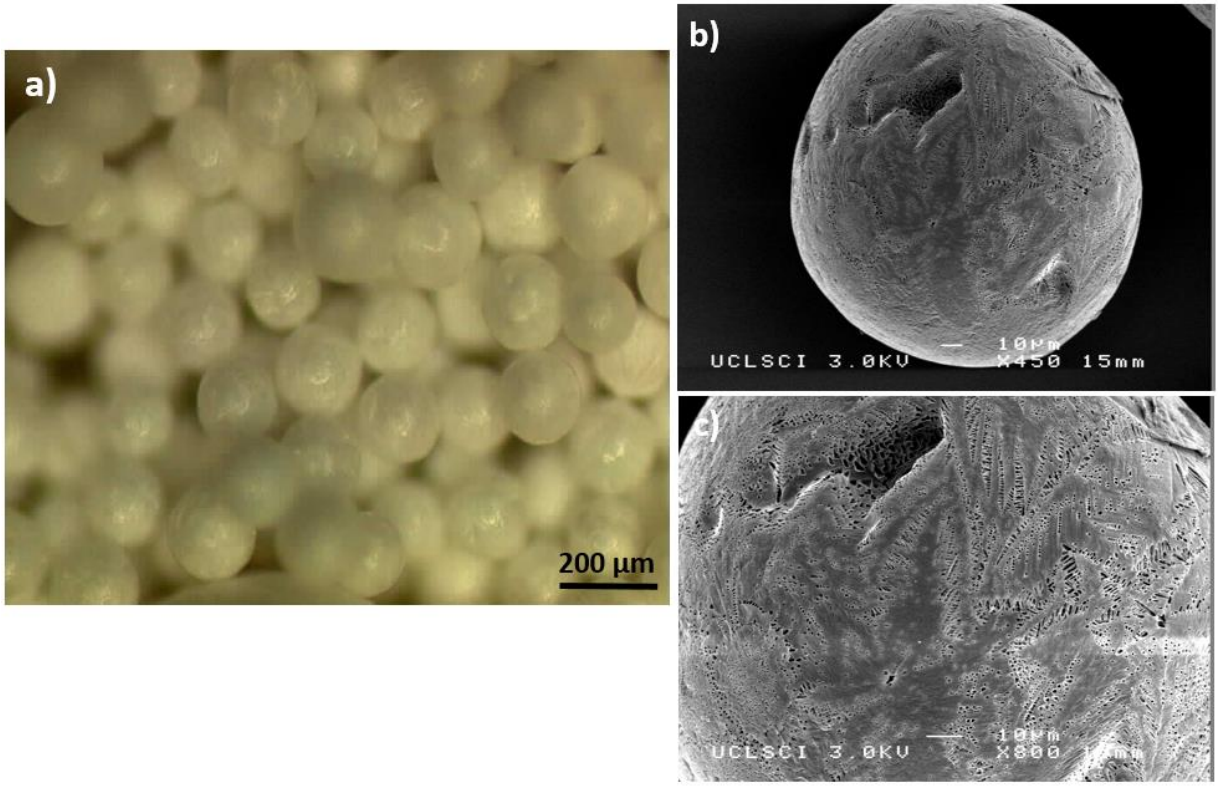

Figure 4.10: Particulate scaffold: a) Free flowing scaffold structure, b) SEM image of the microsphere and c) Surface porosity

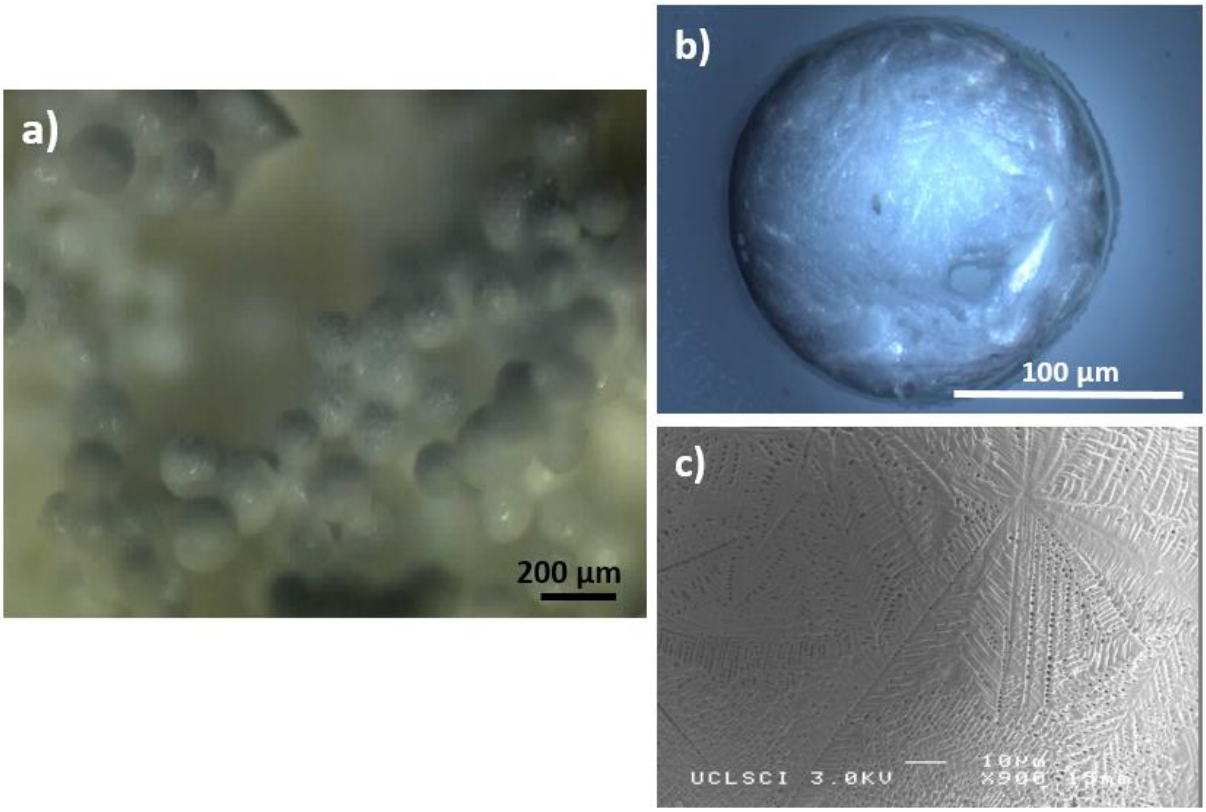

Figure 4.11: Particulate scaffold: a) Non-free flowing (rigid) structure, b) Optical microscopy of a microsphere and c) SEM image of surface porosity

Collection of microspheres from PLGA/DMC solutions with different concentrations in water provided smooth surface (**Fig. 4.9c(iii)**). However, as the two images in **Figures 4.10c** and **4.11c** present, collection in liquid nitrogen followed by freeze drying provided production of solid microspheres with porosity on the outer surface. Since, liquid nitrogen has very lower melting point (-210^{o}C) compared to that of DMC (between 2-4^{o}C), this is attributed to thermally induced liquid-liquid phase separation of the polymer solution upon quenching in liquid nitrogen and subsequent sublimation of the solvent via freeze drying of the sample.

Chronic wounds such as fistulae induce irregular shaped cavities on the epidermis and dermis or the tissue all the way to the fascia. Therefore, free flowing scaffold would be more suitable to fill in these irregular cavities, having minimal invasion of the scaffold and also allowing cell migration for tissue regeneration. This porous type of microspheres in the form of free flowing scaffold structure would be further investigated for *in vitro* release studies.

4.4 Characterizations of the Polymer and Dye Solutions Used for Encapsulation

The electrohydrodynamic process by which the microspheres are produced is controlled by the physical properties such as surface tension, viscosity, density and electrical conductivity of the solutions as well as the processing parameters (flow rate and applied voltage). Various combinations of these parameters enable the generation of various EHD jetting modes (Cloupeau and Prunet-Foch, 1990). Therefore, the first step was to characterise the properties of the solutions used for fabricating the dye loaded microspheres.

Table 4.2: Physical properties of the solutions adopted for encapsulation via the single needle and the co-axial needle EHD/TIPS processes

Solution	Viscosity (mPa s)	Surface Tension ($mN\ m^{-1}$)	Electrical Conductivity ($\mu S\ m^{-1}$)	pH	Density ($kg\ m^{-3}$)
DMC	**0.60 ± 0.2**	**30.7 ± 0.5**	**0.20 ± 0.1**	**6**	**1070 ± 10**
17.5% PLGA in DMC	**14.5 ± 0.2**	**34.16 ± 0.9**	**0.10 ± 0.1**	**7**	**1130 ± 10**
DMC with Reichardt's	**0.60 ± 0.4**	**30.7 ± 0.8**	**1 ± 0.2**	**6**	**1070 ± 10**
DMC with erythrosin B	**0.60 ± 0.3**	**30.7 ± 0.6**	**0.20 ± 0.1**	**6**	**1070 ± 10**
DMC with pyronin B	**0.60 ± 0.2**	**30.7 ± 0.5**	**0.6 ± 0.2**	**6**	**1070 ± 10**
17.5% PLGA in DMC mixed with Reichardt's	**14.5 ± 0.2**	**34.16 ± 0.5**	**0.9 ± 0.2**	**6.5**	**1130 ± 10**
17.5% PLGA in DMC mixed with erythrosin B	**14.5 ± 0.5**	**34.16 ± 0.7**	**0.1 ± 0.1**	**7**	**1130 ± 10**
17.5% PLGA in DMC mixed with pyronin B	**14.5 ± 0.4**	**34.16 ± 0.8**	**0.5 ± 0.2**	**7**	**1130 ± 10**

Since, the main aim of this study was to produce microspheres with size distribution of 150-300 µm, the polymer concentration for producing dye loaded carriers was increased from 15

wt% to 17.5 wt% in the solutions adopted for both the single needle and the co-axial needle encapsulation processes. This change in the polymer concentration was mainly related to the environmental variations such as higher humidity and increased ambient temperature during the encapsulation process.

Table 4.2 provides the characterization results of the polymer solution mixed with the different dyes. Since, only one polymer solution with same concentration (17.5 wt%) was adopted throughout the single needle EHD/TIPS experiments, the physical properties of the polymer solution such as viscosity, surface tension and density were similar; however due to use of different dyes, the electrical conductivity of the polymer solutions varied during the process depending on the used dye. Therefore, the applied voltage as one of the important factors for controlling the stable cone-jet mode was varied more during this set of experiments. This change in the applied voltage interfered with the size distribution of the collected microspheres. The ranges of applied voltage for electrospraying the polymer solutions with erythrosin B and pyronin B were 6.5-7 kV and 6.8-7.3 kV, respectively. However, this range for the polymer solution mixed with Reichardt's dye was increased between 7.8 and 8.5 kV, due to the higher electrical conductivity of the liquid (**Table 4.2**).

In the case of co-axial needle EHD/TIPS process, the physical properties of the liquid in the inner needle changed due to the use of solutions mixed with different dyes. Since, same concentrated polymer solution (17.5 wt%) was adopted for all the three dyes experiments, the changes in the inner needle had smaller influence on the fabrication of the microspheres with payload compared to that of the single needle experiments. Therefore, the range of applied voltage was reduced between 6.8 and 7.4 kV for all the three dyes in the co-axial needle encapsulation experiments.

4.5 Fabrication of Loaded Microspheres by the Single Needle and the Co-axial Needle EHD/TIPS Processes

The polymeric microspheres with surface porosity were produced based on the combination of EHD and TIPS process at ambient temperature (~20-25^{o}C). This technique consists of two stages: EHD stage for the microsphere fabrication, and TIPS stage for producing surface porosity. The main purpose of process optimization was to minimize the waste of the

processing materials and enhance the total dye entrapment efficiency by collecting more loaded particles.

In the EHD process, the stable cone-jet mode was adopted for fabrication of the required size range of loaded microspheres. In the case of the single needle process, since only one liquid is flowing through the needle, the stable cone-jet mode could be achieved by carefully selecting the applied voltage in a range to satisfy the electrical conductivity and the surface tension of the flowing liquid. However, in the case of co-axial needle, this jetting mode can be obtained for liquids satisfying the conditions $\sigma_i > \sigma_o$ where σ is the liquid-conductivity atmosphere surface tension (σ_i refers to conductivity of inner needle solution, whereas σ_o refers to conductivity of outer needle liquid) (Ku and Kim, 2002). Therefore, the key parameters should be selected carefully in a range to satisfy the requirements for the electrical conductivity and surface tension of the inner liquid which is sometimes referred to as a driving medium (López-Herrera et al., 2003).

4.5.1 Morphology of the Loaded Microspheres Collected from both EHD/TIPS Processes

The surface morphology of the fabricated microspheres was studied by SEM. **Figure 4.12** shows the SEM micrographs of the control microspheres with no load produced by the single needle EHD/TIPS process under different magnifications. These polymeric microspheres were used in the *in vitro* release studies as control for normalization of the loaded products obtained from the single needle and the co-axial needle methods. The SEM micrographs in **Figures 4.13** and **4.14** are respectively related to the products collected from the single needle and the co-axial needle EHD/TIPS processes for erythrosin B encapsulation. **Figures 4.15** (the single needle EHD/TIPS method) and **4.16** (the co-axial needle EHD/TIPS process) exhibits the SEM micrographs of the fabricated microspheres loaded with pyronin B under various magnifications. Finally, the SEM micrographs of the produced microspheres with Reichardt's dye encapsulation are provided in **Figures 4.17** and **4.18.**

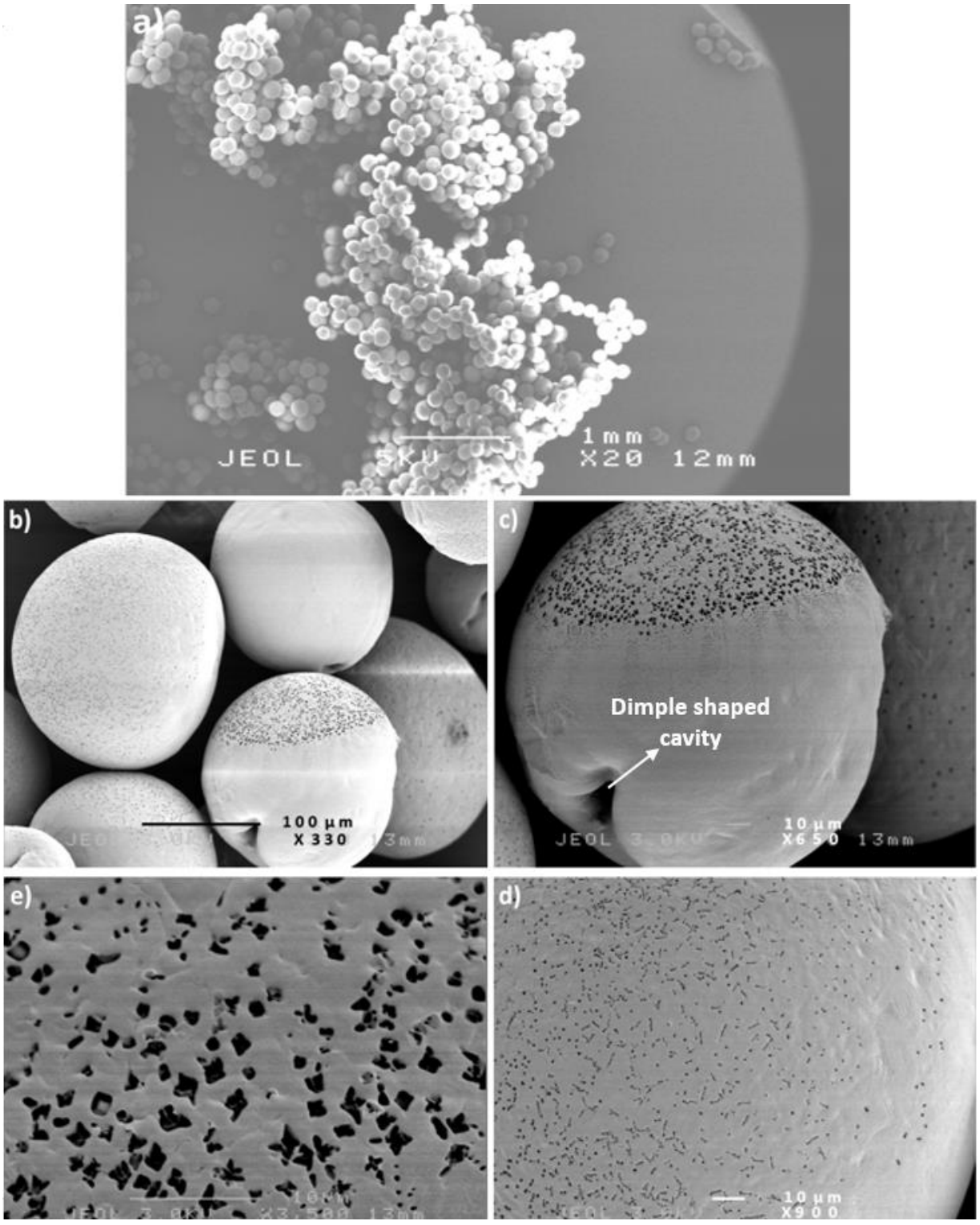

Figure 4.12: Unloaded microspheres collected from the single needle EHD/TIPS process

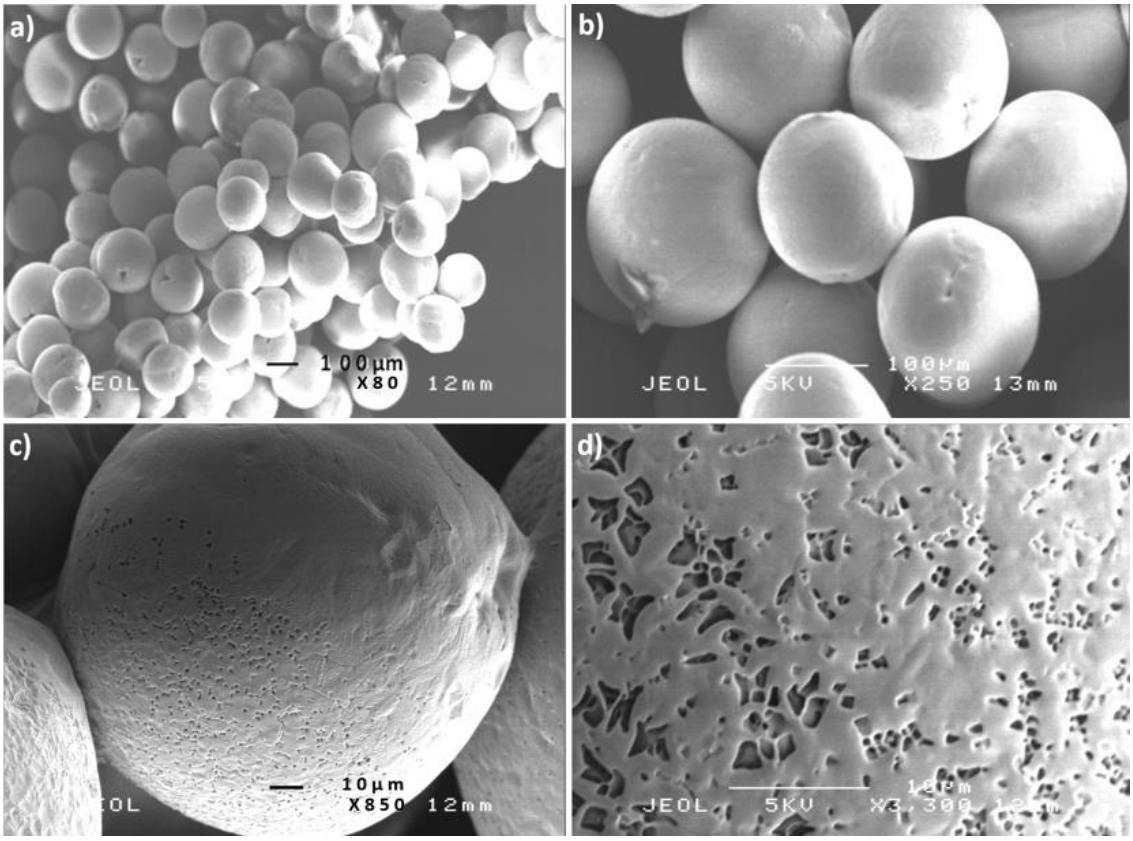

Figure 4.13: Microspheres loaded with erythrosin B collected from single needle EHD/TIPS process

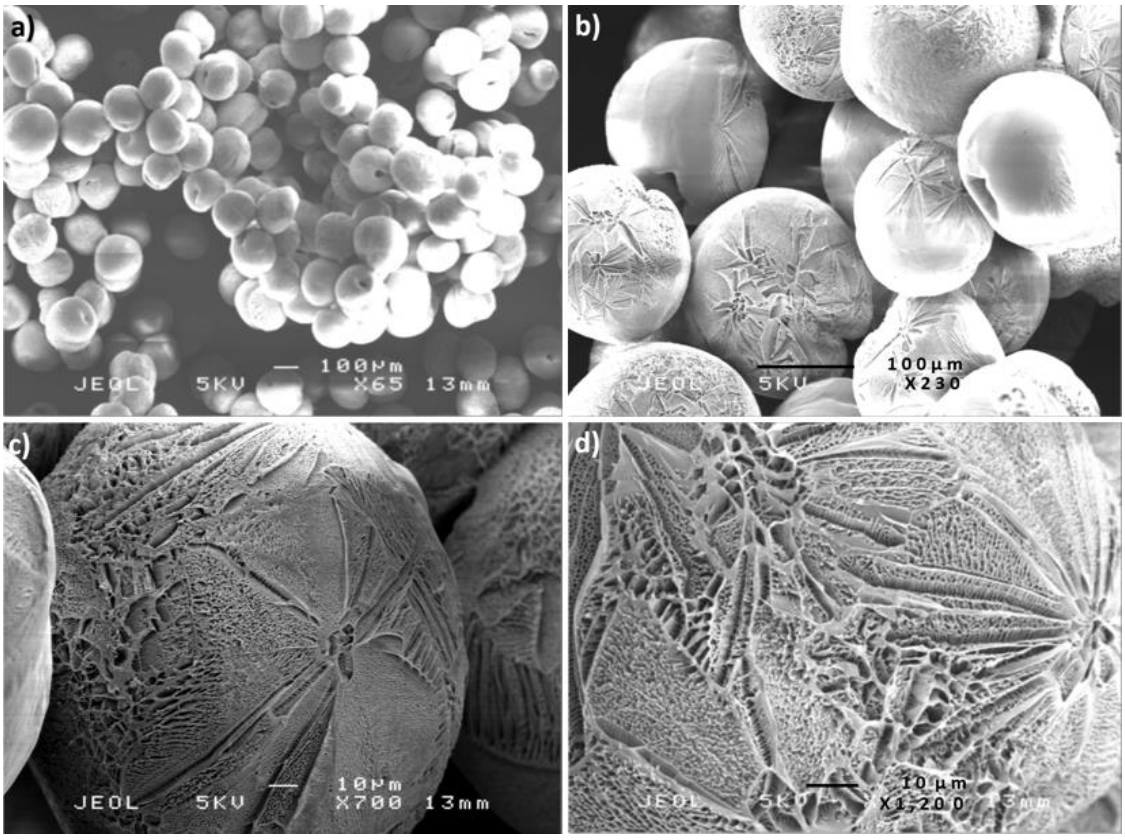

Figure 4.14: Microspheres loaded with erythrosin B collected from co-axial needle EHD/TIPS process

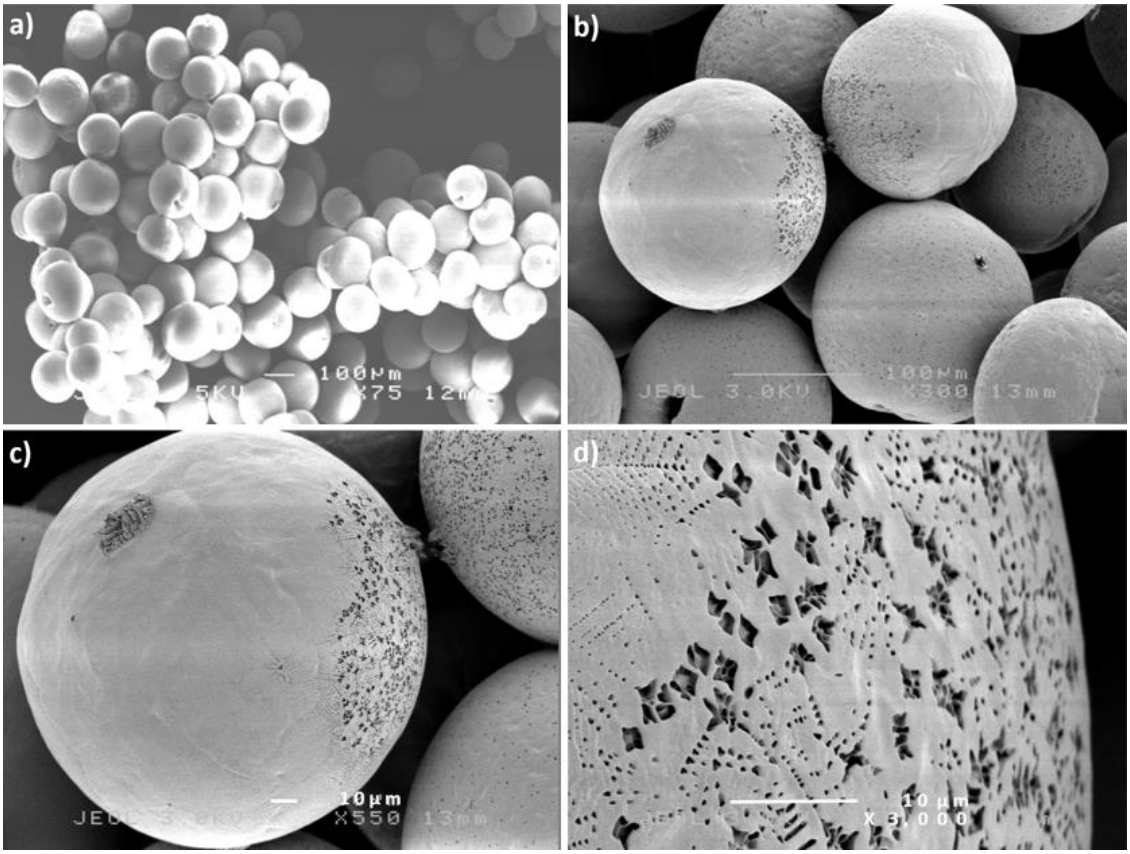

Figure 4.15: Microspheres loaded with pyronin B collected from single needle EHD/TIPS process

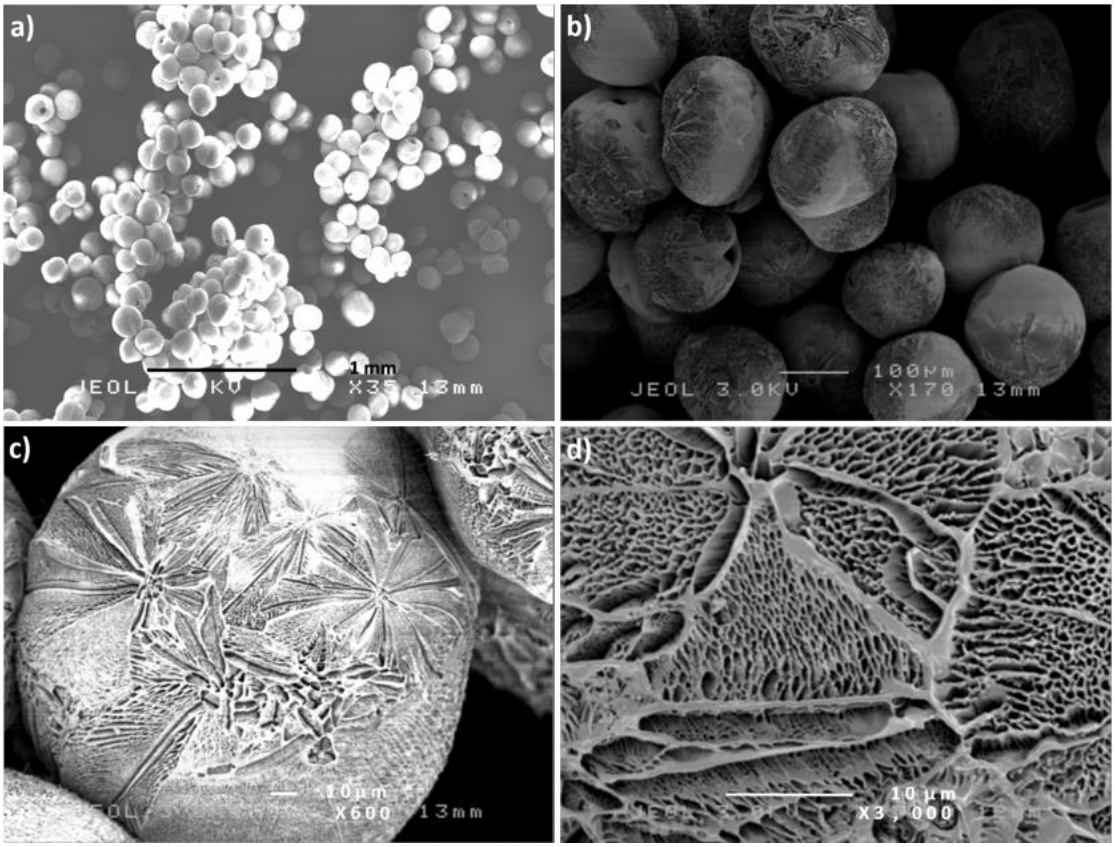

Figure 4.16: Microspheres loaded with pyronin B collected from co-axial needle EHD/TIPS process

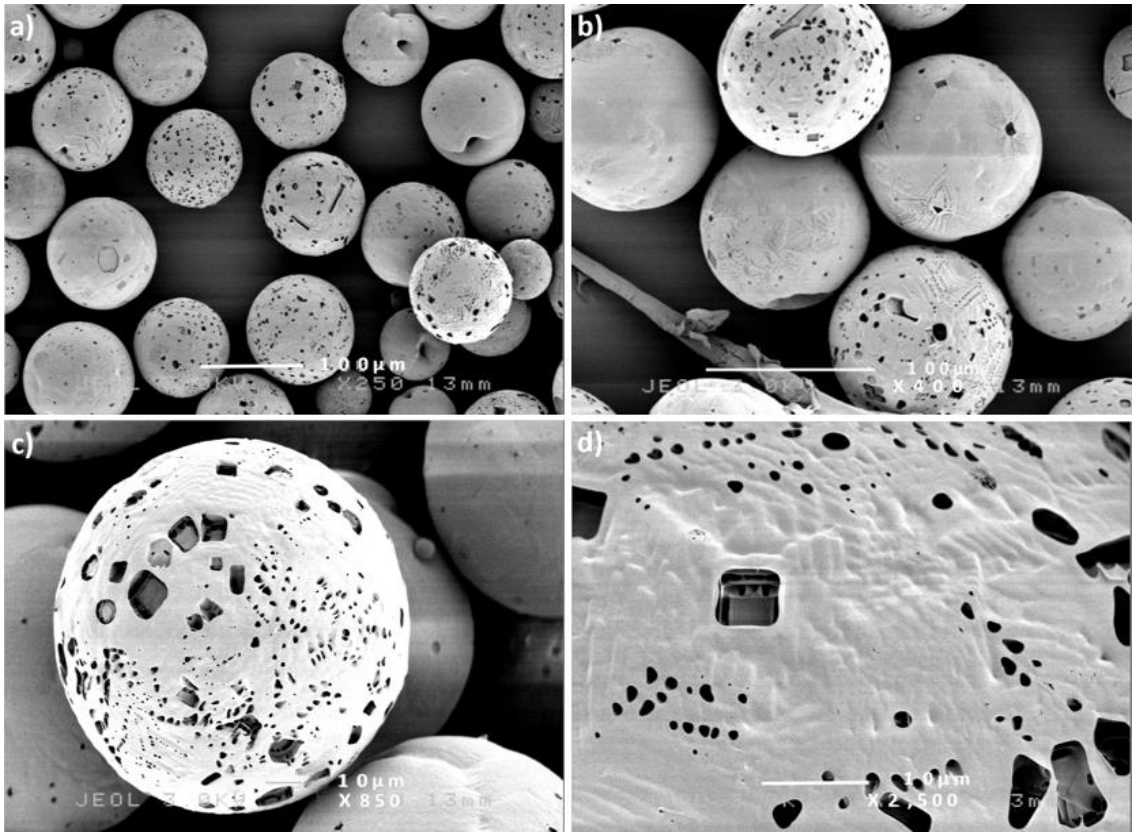

Figure 4.17: Microspheres loaded with Reichardt's collected from single needle EHD/TIPS process

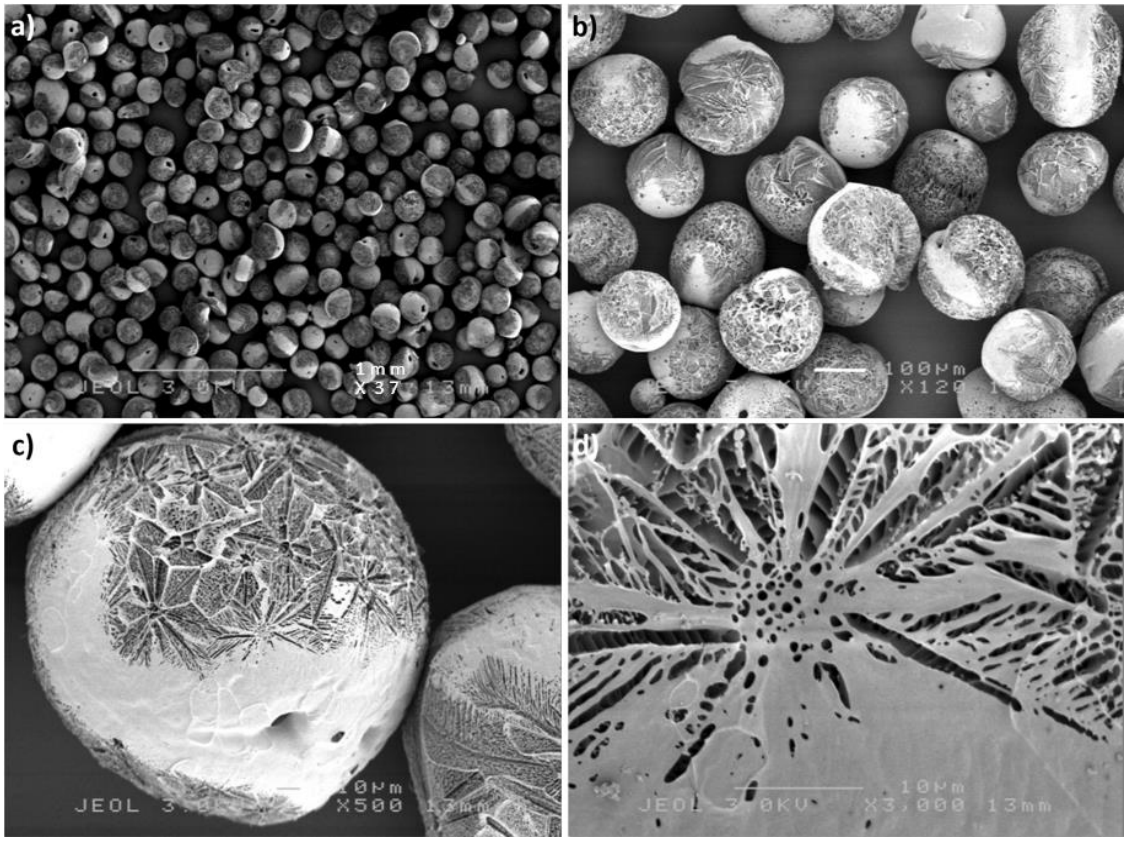

Figure 4.18: Microspheres loaded with Reichardt's collected from co-axial needle EHD/TIPS process

The SEM micrographs showed that the surface porosity is generated on all the fabricated microspheres based on using the EHD/TIPS process. However, evidence shows that the co-axial needle EHD/TIPS processing led to higher surface porosity of the products (**Figs. 4.14c, 4.14d, 4.16c, 4.16d, 4.18c** and **4.18d**) compared with those produced by the single needle process (**Figs. 4.12d, 4.12e, 4.13c, 4.13d, 4.15c, 4.15d, 4.17c** and **4.17d**). Surface porosity in the microspheres are due to the solvent extraction during the lyophilisation. Since, dimethyl carbonate was used in both the inner needle (polymer solution) and the outer needle (dye encapsulation) for the co-axial needle experiments, more sublimation of the solvent occurred during lyophilisation and consequently resulted in higher surface porosity in the products collected from the co-axial needle compared to those obtained from the single needle method.

The Small dimple shaped cavity on the surface (**Fig. 4.12**) which is observed in some of the fabricated microspheres is related to the detachment point of particles from the cone-jet followed by immediate solidification in liquid nitrogen. As the SEM micrographs show, the size, shape and dispersals of the surface porosity are not uniformly distributed over the surface area of the fabricated microspheres. This is most likely to be caused by differences in the local concentration of the polymer and the solvent. Therefore, more solvent extraction occurred from one region compared to the other during lyophilisation, and consequently led to heterogeneous surface porosity.

The diameter of the dye loaded microspheres and also the control products produced by the single needle and the co-axial needle EHD/TIPS processes were measured from the SEM images using Image Pro-Insight software (Media Cybernetics, UK). 100 microspheres from each sample were measured, and then size distribution, mean size, standard deviation and also polydispersity were calculated. **Table 4.3** demonstrates the details of these measurements.

The overall size distribution of the products collected from the co-axial needle products are slightly larger compared to those obtained from the single needle EHD/TIPS process. The control microspheres and the two batches of erythrosin B loaded microspheres produced by the two different methods had almost similar size distribution (**Table 4.3**). This was related to the similar physical properties of the solutions and the processing parameters applied in fabricating the products. However, the pyronin B loaded microspheres collected from the single needle process have slightly smaller size distribution compared to the erythrosin B loaded products and their counterparts collected from the co-axial needle setup. The smaller diameter of the single needle products with pyronin B encapsulation was due to higher electrical conductivity

of the solution and consequently higher application of voltage supply in fabricating the relevant particles during the EHD process.

Table 4.3: Size characteristics of the loaded microspheres prepared by the two different EHD/TIPS processes

Sample	Single needle EHD/TIPS			
	Number of particles studied	Mean size (μm)	Standard deviation (μm)	Polydispersity (%)
Unloaded PLGA microspheres	100	180	25	15
Erythrosin B encapsulated microspheres	100	180	30	16
Pyronin B encapsulated microspheres	100	165	25	14
Reichardt's encapsulated microspheres	100	100	30	29
	Co-axial needle EHD/TIPS			
Erythrosin B encapsulated microspheres	100	185	30	16
Pyronin B encapsulated microspheres	100	180	33	18
Reichardt's encapsulated microspheres	100	175	30	17

Finally, the Reichardt's loaded PLGA microspheres obtained from the single needle setup had the smallest size distribution of the produced particles (100 ± 30 μm) among all the particles fabricated. This was surely related to the higher applied voltage in production of the relevant microspheres due to the higher electrical conductivity of the single needle solution mixed with this dye (**Table 4.2**). However, in the co-axial needle setup, since, the polymer and the dye solutions were flowing separately through different needles, the applied voltage for fabricating the products were lower compared to that of the single needle. Therefore, the co-axial needle products with Reichardt's dye encapsulation were quite larger compared to their counterparts from the single needle method (**Table 4.3**).

As the calculated polydispersity in **Table 4.3** shows, the cone-jet mode for producing the microspheres loaded with erythrosin B and pyronin B was more stable compared to that of producing the Reichardt's loaded microspheres with the single needle process. This was highly related to the higher application of voltage with the Reichardt's dye-polymer solution, due to the higher electrical conductivity of this solution compared to that of the other polymer solutions.

Further analysis of the loaded PLGA microspheres was carried out using Hitachi SEM. This enabled the investigation of the internal structure of the products after freeze drying**. Figure 4.19** shows the internal structure of the porous surfaced- microspheres collected from the single needle method, whereas **Figure 4.20** exhibits the internal structure of products produced by the co-axial needle setup.

The images in **Figure 4.19** suggest that the single needle EHD/TIPS process forms microspheres with internal and surface porosity. However, the internal structure of the microspheres is denser with PLGA, therefore less porosity has occurred internally compared to the surface area. However, comparison with the images in **Figure 4.20** shows that the co-axial needle EHD/TIPS process has fabricated the required size distribution of the microspheres with more surface and internal porosities compared to that of the single needle products. **Figure 4.20** also demonstrates the internal cavities of the co-axial needle EHD/TIPS products which can be related to the phase separation of the payload from the polymer shell that occurred during the EHD processing before lyophilisation.

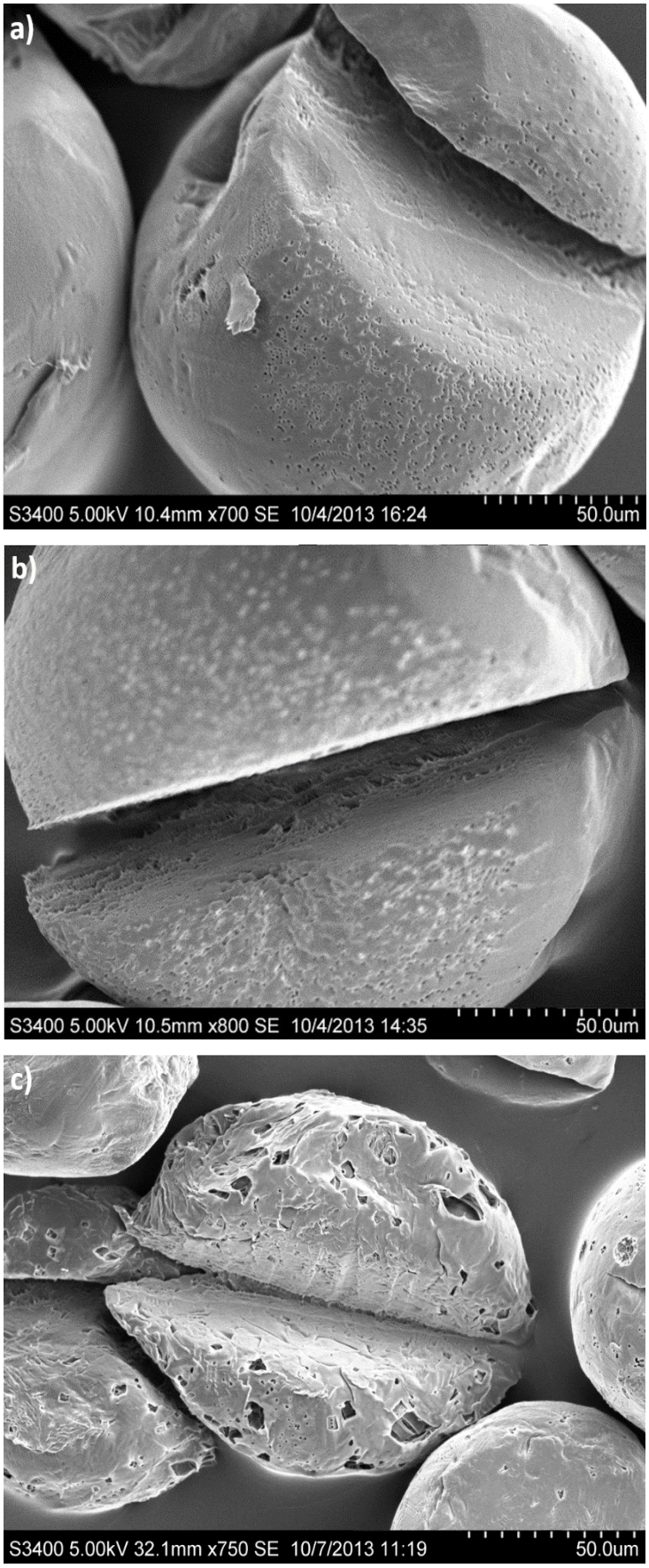

Figure 4.19: Cross-section studies of the single needle EHD/TIPS microspheres with: a) Erythrosin B entrapment, b) Pyronin B entrapment and c) Reichardt's dye entrapment

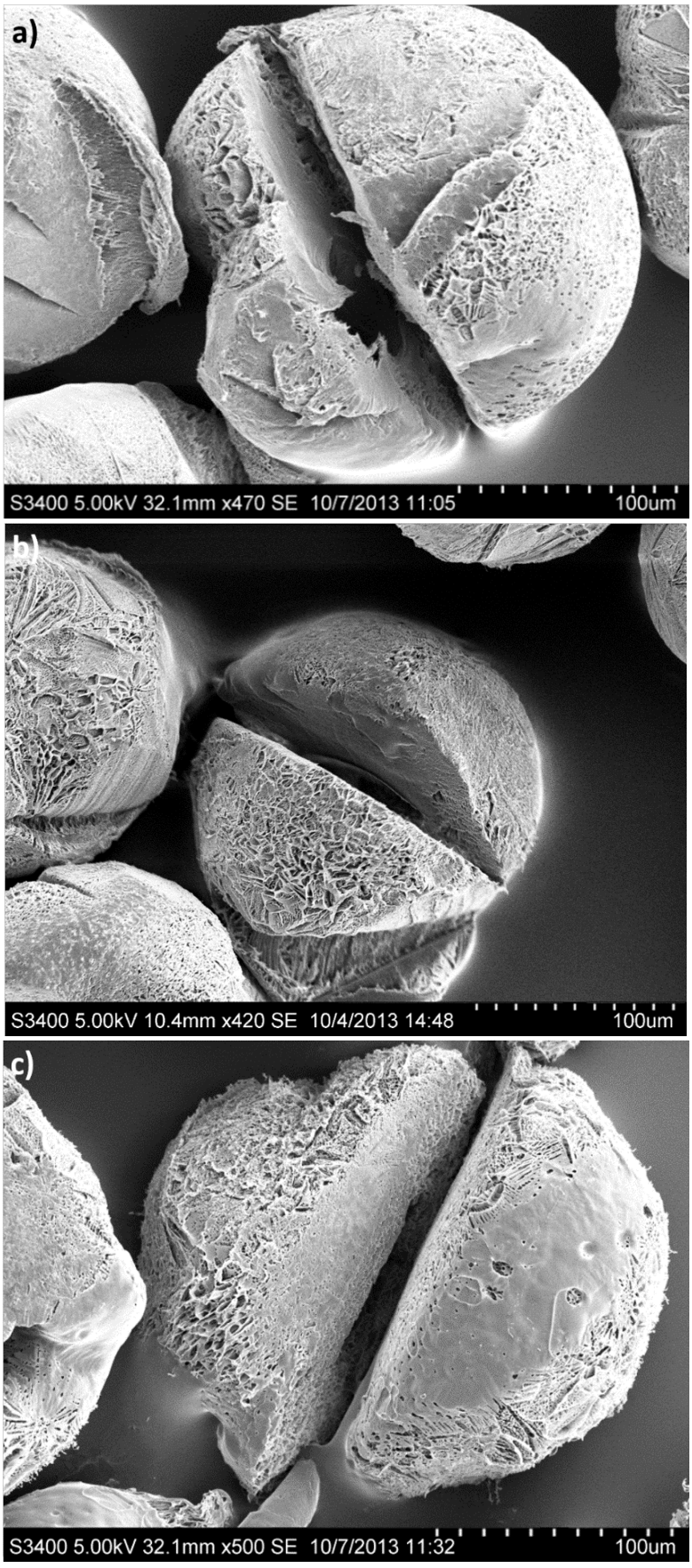

Figure 4.20: Cross-section studies of the co-axial needle EHD/TIPS microspheres with: a) Erythrosin B encapsulated, b) Pyronin B encapsulated and c) Reichardt's dye encapsulated

4.6 Energy-Dispersive X-Ray (EDX) Spectroscopy Studies

EDX spectroscopy was an additional investigation for determining the presence of dyes in the fabricated microspheres. Since, SEM imaging did not show evidence of the dyes entrapped in the fabricated microspheres, EDX studies were carried out to examine the presence of the dye in the produced microspheres. This semi quantitative method was used to verify the element(s) of the dye entrapped in the microspheres. The samples for EDX studies were randomly sectioned by a surgical blade before analysis for two main reasons; 1) the EDX spectroscopy did not detect the elements of the encapsulated materials on the surface, and 2) the X-rays could not pass through the particles shell due to the solid internal structure. The results obtained from the EDX studies were organised in **Figure 4.21**. This study was only carried out on the loaded microspheres obtained from the single needle process.

EDX analysis of the microspheres with entrapped erythrosin B showed that this dye was presented in the sample as indicated by iodine (I) in the structure of this dye (**Fig. 4.21a**). Chlorine (Cl) (**Fig. 4.21b**) in the structure of pyronin B was identified by EDX, indicating the presence of this dye in the relevant sample. The presence of nitrogen (N), in the molecular structure of Reichardt's dye was also detected by EDX, indicating the existence of this dye loaded in the PLGA TIPS microspheres (**Fig. 4.21c**).

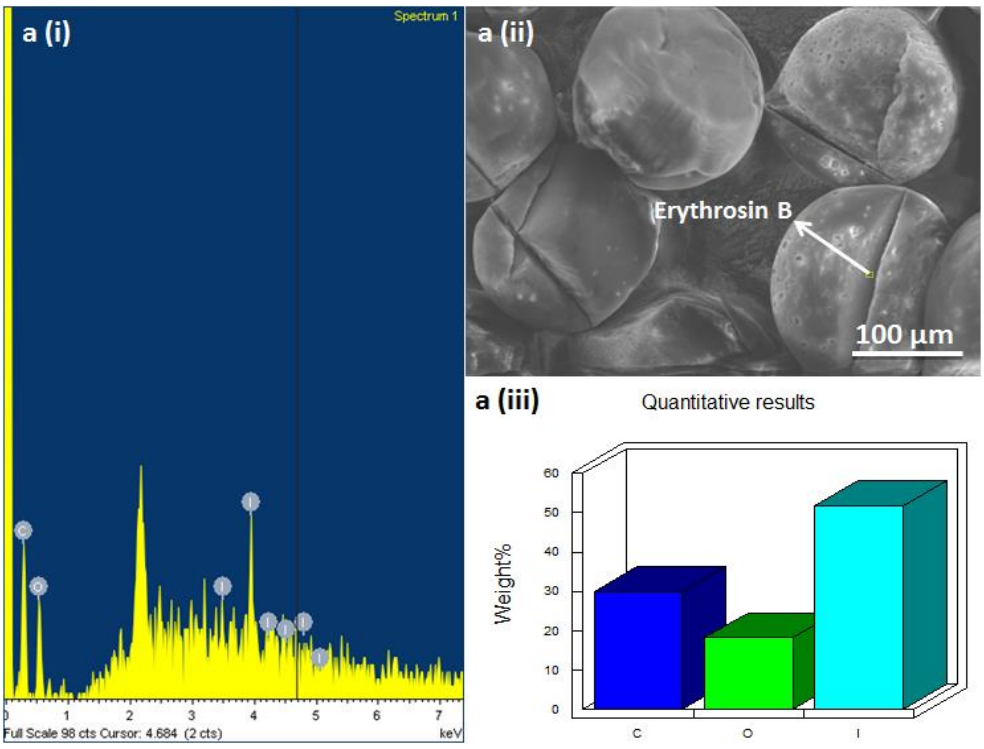

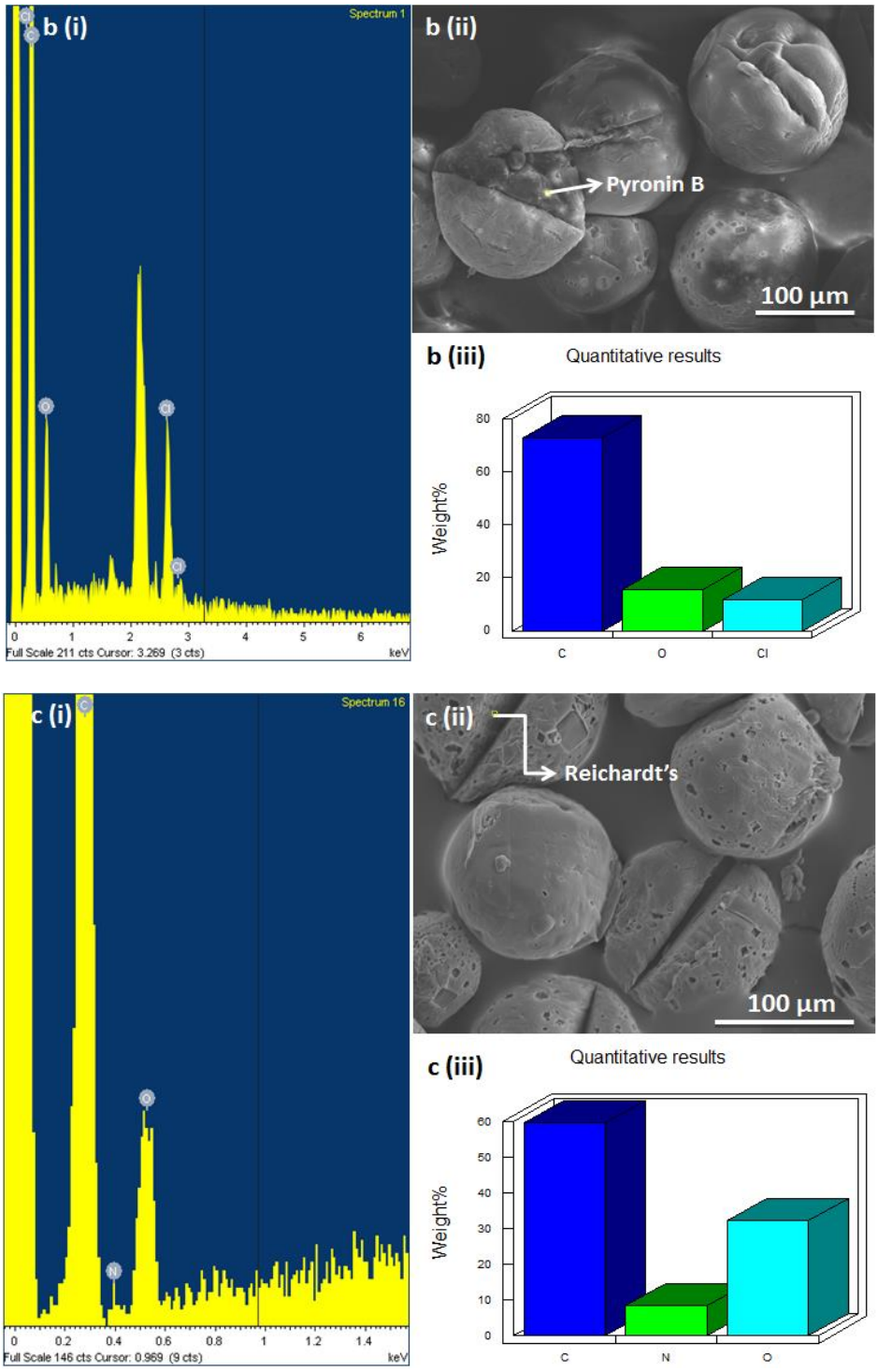

Figure 4.21: EDX studies of the dyes encapsulated in microspheres produced by the single needle EHD/TIPS process: a) Erythrosin B: a(i) Peaks of the detected elements, a(ii) Image of the loaded microspheres, a(iii) Semi-quantitative results of the detected elements; b) Pyronin B: b(i) Peaks of the detected elements, b(ii) Image of the loaded microspheres, b(iii) Semi-quantitative results of the detected elements; c) Reichardt's: c(i) Peaks of the detected elements, c(ii) Image of the loaded microspheres and c(iii) Semi-quantitative results of the detected elements

The EDX studies showed that the dyes were entrapped in the matrix of the microspheres, as it could not find the elements of the dyes on the surface of the loaded microspheres. The results from the combination of EDX and SEM studies also indicates that the dyes were entrapped in the matrix of the polymer microspheres produced by the single needle rather than the phase separation of drug encapsulation. The potential advantage of the matrix encapsulation over the phase separation of drug encapsulation which was observed in the co-axial needle products (**Fig. 4.20**) is to have a more controlled release of the encapsulated agent over a longer period of time (**Figs. 4.25-4.27**).

4.7 Fourier Transform Infrared (FTIR) Studies

Since SEM studies could not provide any evidence to demonstrate the dyes incorporated into the generated microspheres and the EDX studies were only carried out on the single needle products, FTIR was conducted on the products obtained from both the single needle and the co-axial needle EHD/TIPS methods in order to investigate the structural characteristics of the polymeric carriers and the dyes. FTIR spectra were recorded of the individual components followed by the PLGA microspheres with the dye to confirm the entrapment of the active agent.

Figure 4.22 shows a comparison of the FTIR spectra of PLGA, erythrosin B and erythrosin B-PLGA microspheres obtained from both the single needle and the co-axial needle EHD/TIPS methods. The chemical structure of PLGA and erythrosin B are also shown in **Figures 4.22a** and **4.22b**. The spectral features that distinguish the dye from PLGA is the presence of aromaticity in erythrosin B, whilst PLGA is aliphatic in nature with the presence of a carbonyl ester group. As expected, the typical bands for the ester carbonyl stretching (C=O) at 1750, 1423 (C-C stretch), 1390 (C-H stretch), C-O stretch at 1270 and 1087 cm^{-1} (C-O-C) group were observed in the FTIR spectra of PLGA. The characteristic peak due to the deformation modes of the substituted benzene ring appear at 962 cm^{-1} in the spectrum of erythrosin B. The aromatic ring substitution sensitive modes appear in the 1000-1350 cm^{-1} with prominent benzene ring C-C stretching vibrations in the 1440-1544 cm^{-1} regions. The comparison of spectra in **Figure 4.22c** also clearly indicate that the PLGA microspheres obtained by either the co-axial needle or the single needle process contained erythrosin B and as there were no large shifts in the majority of the characteristic peaks of PLGA, indicated that there was no chemical interaction between erythrosin B and the polymer.

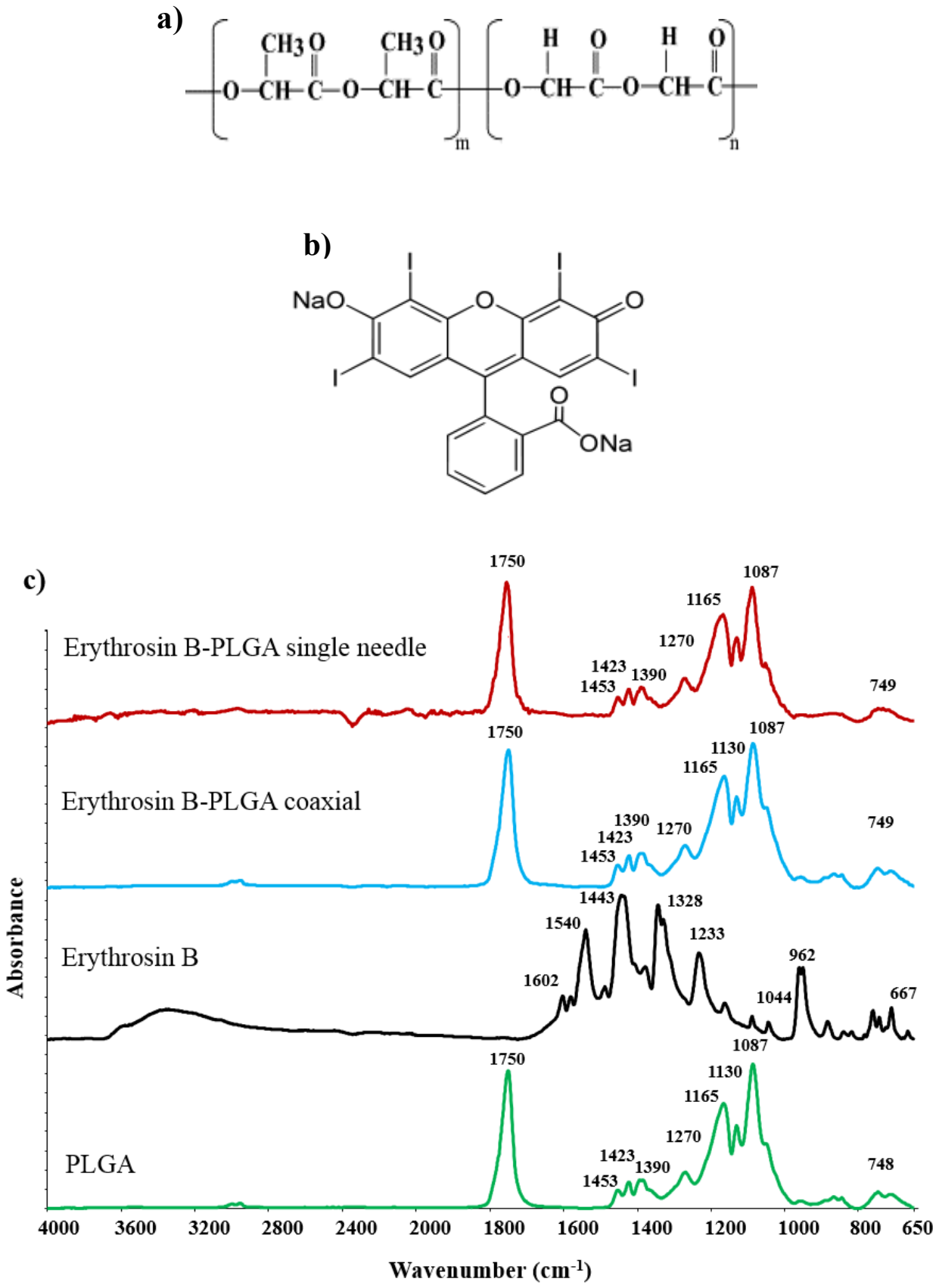

Figure 4.22: a) Structure of PLGA, b) Structure of erythrosin B and c) The FTIR spectra of erythrosin B and the PLGA samples contained this dye

The chemical structure of pyronin B along with the FTIR spectra of the samples obtained from encapsulation of this dye by the single needle and the co-axial needle EHD/TIPS methods are presented in **Figure 4.23**.

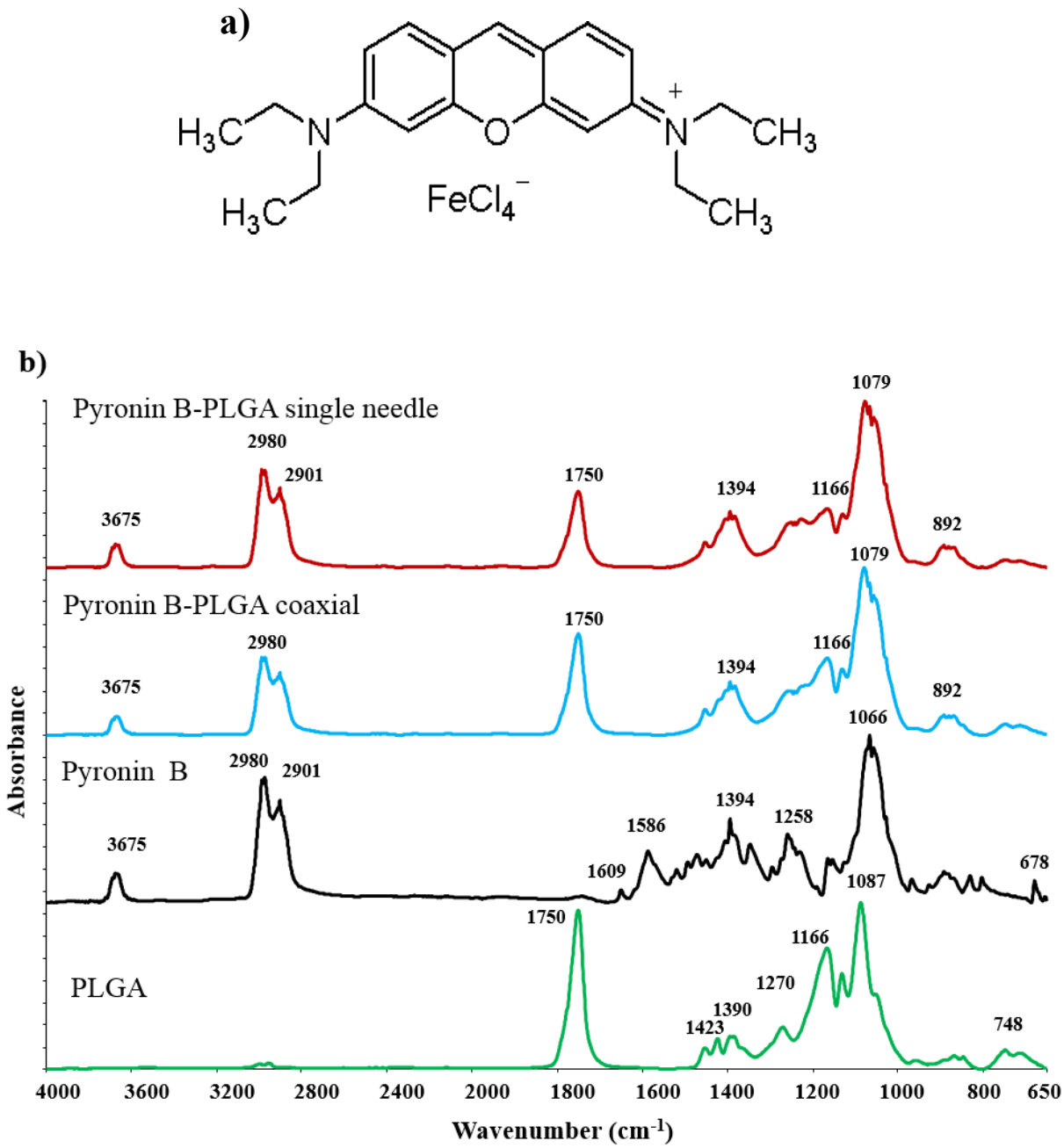

Figure 4.23: a) Structure of pyronin B and b) The FTIR spectra of pyronin B and the PLGA samples contained this dye

Pyronin B is a water soluble dye and the chemical structure is shown in **Figure 4.23a** which indicates that the stretching frequencies of its aromatic functional group can be used to detect its presence. Although, there are overlapping peaks in the region 1100-1200 cm^{-1} and the intensity of the peaks of the PLGA masks the low intensity peaks arising due to the presence of the shoulder appearing at 1609 cm^{-1} in the PLGA containing pyronin B, the presence of the dye in the loaded microspheres can be confirmed. The strong absorption peak due to carbonyl group is present in all the dye loaded PLGA particles and there is no observable shift, indicating no intermolecular interaction between the dye and the polymer. The stretching bands due to C-N are clearly strong in the PLGA containing the dye which further affirms the loading of this active agent in the microspheres (**Fig. 4.23b**).

Finally, a comparison of the spectra of Reichardt's, PLGA and Reichardt's dye encapsulated PLGA microspheres is illustrated in **Figure 4.24**. The structure of Reichardt's (**Fig. 4.24a**) shows that the dye is aromatic in nature and the conjugated C=N stretching vibration can be used to identify the presence of the dye within the loaded microspheres. The two peaks arising at 2988 and 2901 cm^{-1} are associated with aromatic C=N stretching, which is clearly observed in the loaded PLGA microspheres with the dye obtained by the two different EHD/TIPS processes (**Fig. 4.24b**).

According to the evidence provided by the FTIR spectra of the samples (**Figs. 4.22c, 4.23b** and **4.24b**), the single needle and the co-axial needle EHD/TIPS processes could successfully encapsulate the active agents into the polymeric microspheres without effecting their chemical structures throughout the process. Moreover, the FTIR results demonstrates the capability of the EHD/TIPS process to produce stable products for storage in certain period of time before usage for different applications.

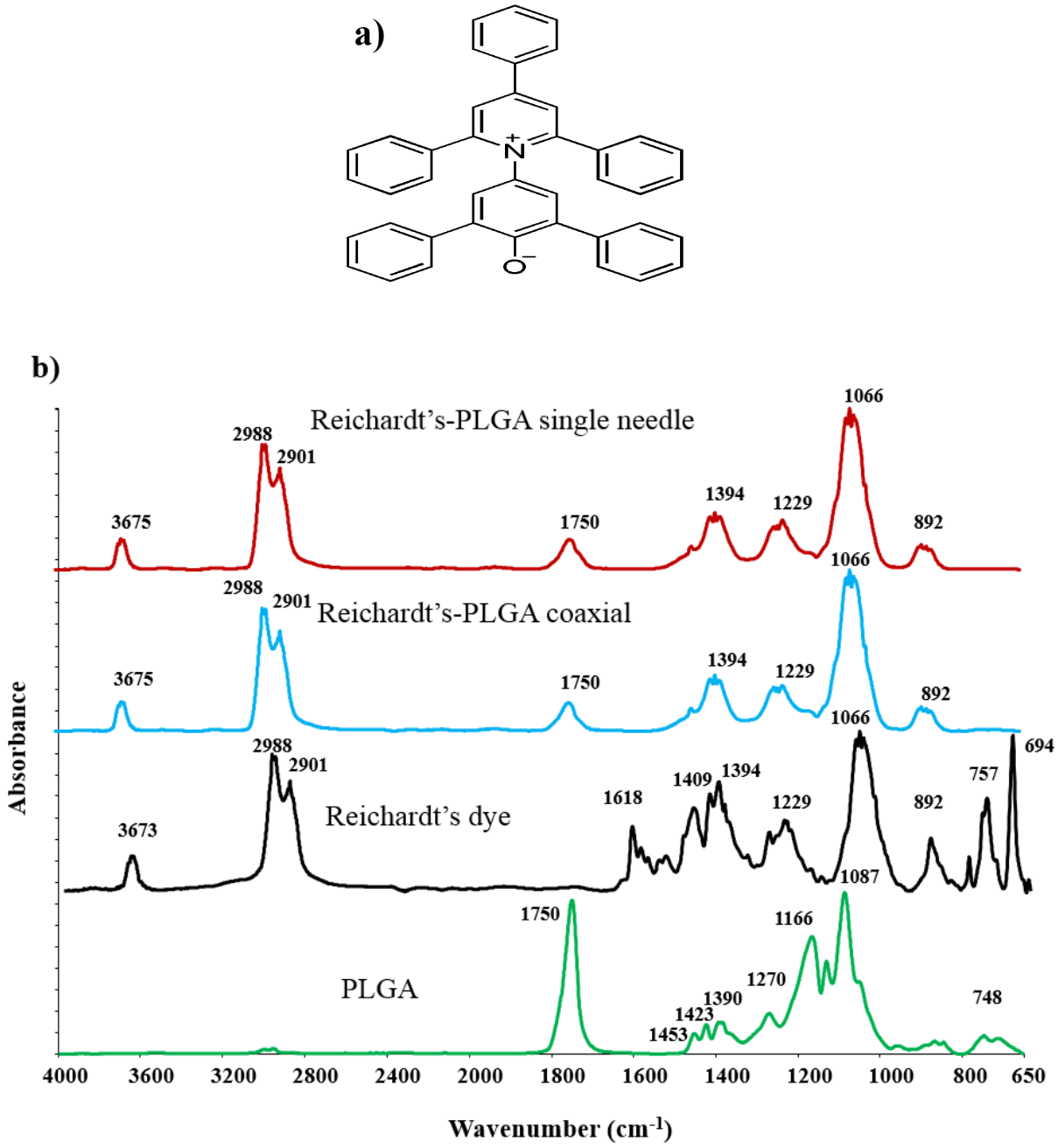

Figure 4.24: a) Structure of Reichardt's dye and b) The FTIR spectra of Reichardt's and the PLGA samples contained this dye

4.8 Yield of the EHD/TIPS Processes

In this section, further investigations were carried out on the yield of the single needle process. The main aim was to improve the percentage yield of the process. For this part, the yield of the conventional single needle EHD/TIPS process conducted in **Section 3.7.1** was discussed, and then it was compared to that of the modified process carried out in **Section 3.7.2** for producing

the required size of the loaded microspheres. Since, it was demonstrated that the modified single needle EHD/TIPS method led to higher percentage yield of the process, the co-axial needle EHD/TIPS setup was also modified for the encapsulation process. This helped for better comparison between the two different EHD methods (the single needle and the co-axial needle). The details for the modifications of the co-axial needle setup is described in **Section 3.7.3**.

4.8.1 The Conventional and the Two Modified EHD/TIPS Processes

The percentage yield of the process which is calculated according to equation 3.8 in dye entrapment section (**3.9.2.4**), was based on measuring the weight of the materials collected after the experimental process. The average percentage yield of the conventional single needle EHD/TIPS process was found to be 55% ± 2%, indicating a large portion of the starting materials was lost during the process. This is likely to have been caused by two main reasons. Firstly, liquid nitrogen vapour escaping from the collection vessel prevented the products being deposited in the collecting beaker. Secondly, the cone-jet mode was unstable during the mass production process. These issues were addressed by adopting a funnel-shaped compartment for directing the products into the beaker and also adding a second ground electrode for generating a more stable cone-jet. As a result, the average yield of the modified single needle process was increased to 92% ± 2% (Equation 3.8, **Section 3.9.2.4**). This value for the co-axial needle procedure based on the same modification was calculated 85% ± 3% which indicates lesser quantity of the products collected compared to the modified single needle process.

4.9 *In Vitro* Release Studies of the Loaded Microspheres Produced by the Modified EHD/TIPS Processes

In this section, the *in vitro* release studies were carried out on the three dyes encapsulated separately in the produced PLGA/TIPS microspheres. The aims were to study the encapsulation efficiency and the actual percentage of the dye loaded in each process, to determine the capability of the TIPS microspheres for releasing their payload and also to measure the amount of dye released over an extended period of time.

4.9.1 Dye Entrapment of the Conventional and the Two Modified EHD/TIPS Processes

Table 4.4: Dye entrapment for the conventional and the modified EHD/TIPS systems

Dye entrapment	Conventional single needle		
	Erythrosin B	**Pyronin B**	**Reichardt's**
Dye loading percentage (%)	**2.86 ± 0.04**	**2.87 ± 0.03**	**2.8 ± 0.04**
Entrapment efficiency (%)	**92 ± 2**	**93 ± 2**	**91.5 ± 1.5**
Actual dye loaded in the process (%)	**53 ± 3**	**52.5 ± 2.5**	**52.5 ± 2.5**
	Modified single needle		
Dye loading percentage (%)	**2.83 ± 0.03**	**2.89 ± 0.03**	**2.78 ± 0.02**
Entrapment efficiency (%)	**92 ± 1.5**	**94 ± 1**	**91 ± 1**
Actual dye loaded in the process (%)	**86 ± 2**	**87.5 ± 2.5**	**85 ± 3**
	Modified co-axial needle		
Dye loading percentage (%)	**2.35 ± 0.05**	**2.40 ± 0.04**	**2.15 ± 0.05**
Entrapment efficiency (%)	**73 ± 2**	**74 ± 2**	**68 ± 2**
Actual dye loaded in the process (%)	**67 ± 3**	**66 ± 3**	**61 ± 3**

The absorbance signal of the dyes encapsulated in the weighed TIPS microspheres was measured using UV spectroscopy. The total amount of dye was then calculated based on the linear relationship between the absorbance and the dye concentration from the standard calibration curves (**Fig. 3.8**). By calculating the total amount of dye in each sample, the entrapment efficiency was then computed according to equation 3.9. **Table 4.4** shows in detail how much dye was loaded in the microspheres according to the UV measurements. This table also demonstrates the loading efficiency (Equation 3.10) and the actual percentage (Equation

3.11) of the dyes loaded in the microspheres collected from the conventional and the two modified (the single needle and the co-axial needle) EHD/TIPS processes.

The close values of dye entrapment and dye loading efficiencies for the conventional and the modified single needle methods show the success of the EHD process in encapsulation. However, the difference in the actual percentage of the dye loaded demonstrate the feasibility of the modified single needle EHD/TIPS process in preserving more dye compared to the conventional method by collecting more dye loaded microspheres. **Table 4.4** also illustrates the higher loading percentage, entrapment efficiency, and actual percentage of dye loaded with the modified single needle EHD/TIPS process compared to that of the modified co-axial needle method. As it shows, the former method (single needle) is capable of producing microspheres with more dye encapsulated compared to the co-axial needle process. Since, the modified single needle method provided higher percentage yield of the process based on collecting more dye loaded microspheres, the *in vitro* release studies were conducted only on the samples collected from the modified single needle and the modified co-axial needle methods.

Release of encapsulated compounds from polymeric carriers can occur through various mechanisms, including diffusion, surface and bulk erosion, disintegration and desorption. For PLGA carriers, the release often occurs initially by diffusion from the polymer matrix, and then it is mediated via drug diffusion combined with degradation of polymer matrix by hydrolysis (Schliecker et al., 2003). Since, PLGA degrades by means of hydrolysis (Schliecker et al., 2003), the inward diffusion of the aqueous phase leads to degradation of the polymer chains, which in turn facilitates outwards diffusion of incorporated agent (Zhang et al., 2008).

The purpose of the *in vitro* release studies was to investigate the release behaviour of the encapsulated agent from the PLGA microspheres. The clear absorbance peaks for erythrosin B, pyronin B and Reichardt's dye were achieved at expected wavelengths of 351, 348 and 308 nm respectively (**Figs. 3.7-3.9**), indicating that they were not damaged or affected during the encapsulation processes. The *in vitro* release of the dyes from the porous PLGA microspheres collected from the two modified methods (single needle and co-axial needle) occurred in a time dependent manner with biphasic release patterns, with an initial burst release followed by a period of sustained release (**Figs. 4.25-4.27**). The initial burst release in this work is defined as the quick burst release of the active dye during the first 24 hours.

The *in vitro* release profiles of erythrosin B from the microspheres produced by the modified single needle and the modified co-axial needle EHD/TIPS processes are presented in **Figures 4.25a** and **4.25b,** respectively. As **Figure 4.25a** shows, the initial burst release occurred within 4 hours and it resulted in more than 40-60% of the dye release depending on the five different conditions. This shows that the temperature and sonication did not have any major effect on the duration of the initial burst release phase of erythrosin B from the single needle TIPS microspheres. The complete release of this dye occurred in 360 hours at ambient condition (22 ± 2^{o}C), in 250 hours at physiological temperature (37 ± 1^{o}C) with/without fresh media and in 200 hours at physiological temperature with sonicator exposure. The change in the pattern of dye release in biological temperature which occurred with the single needle products after 200 hours was likely related to be caused by the deformation of PLGA microspheres due to biodegradation and/or bulk erosion of the polymer shell, and consequently releasing more quantity of the entrapped agent via outward diffusion.

Figure 4.25b indicates that the burst release of erythrosin B from the co-axial needle products occurred within the first 5 hours and it resulted in dye release between 35% and 60%, depending on the five different conditions. This indicates that external stimuli such as the temperature and the sonication exposure only had influence on the release rate of this dye, but not on the duration of this release phase. The complete release of erythrosin B from the modified co-axial needle products occurred in 180 hours at the three conditions of physiological with/without fresh media and normal (22 ± 2^{o}C) temperatures, and in 155 hours with the application of sonication using various frequencies (20 kHz and 40 kHz).

Comparison between these two graphs (**Figs. 4.25a** and **4.25b**) shows that the release of erythrosin B from the single needle products occurred at higher rate, in particular in normal and physiological temperatures, compared to that of the co-axial needle products. The release of this dye from the modified single needle products also resulted in longer period of time with more controlled release compared to that of the co-axial needle microspheres. This advantage was likely related to less surface and internal porosities of the microspheres produced by the single needle method (**Figs. 4.13c, 4.13d** and **4.19a**) compared to those collected from the co-axial needle setup (**Figs. 4.14c, 4.14d** and **4.20a**).

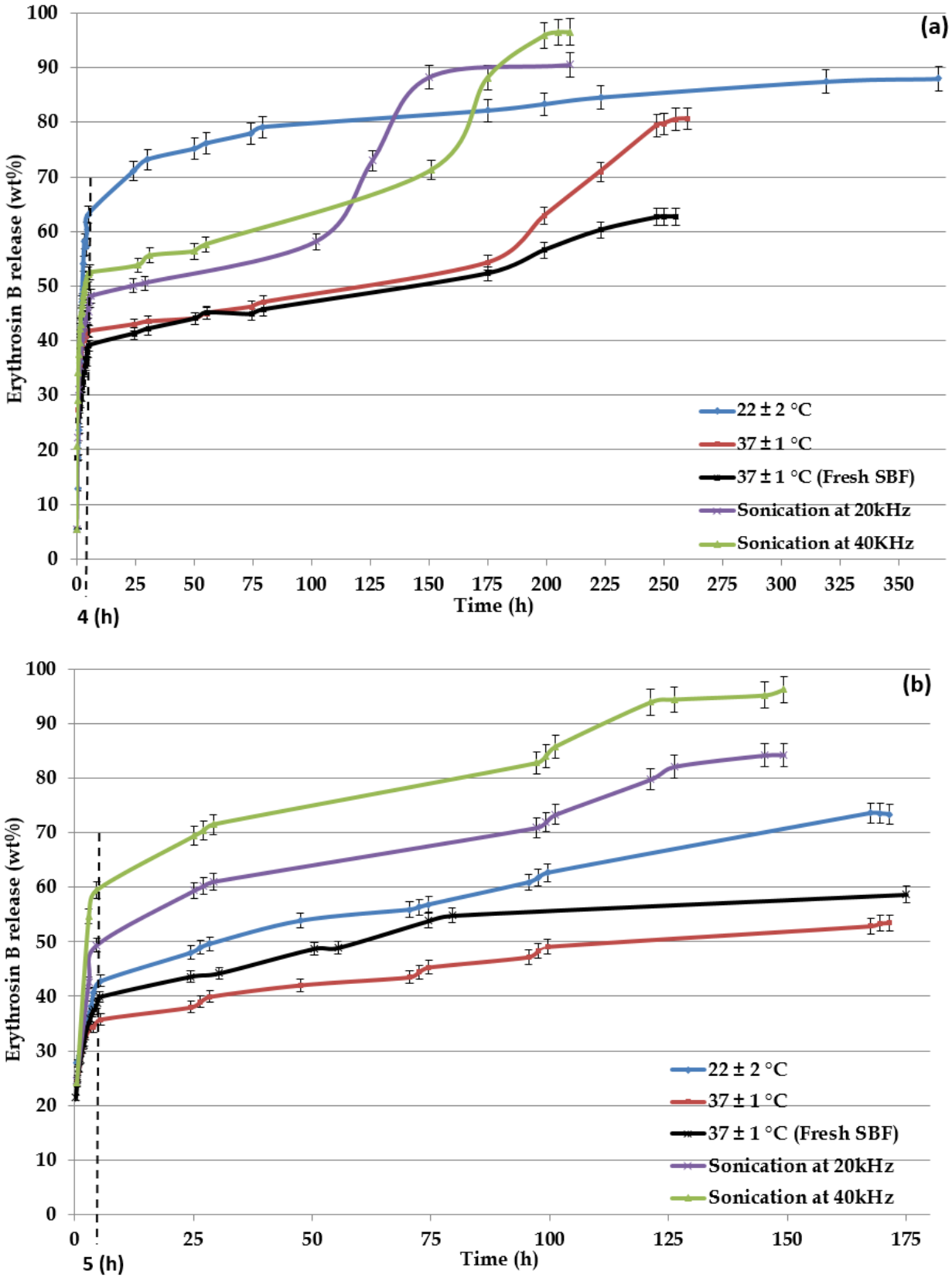

Figure 4.25: The *in vitro* release profiles of erythrosin B in SBF: a) The modified single needle EHD/TIPS process and b) The modified co-axial needle EHD/TIPS process

Figures 4.26a and **4.26b** are related to the release profiles of pyronin B from the microspheres produced by the two modified EHD/TIPS systems (single needle and co-axial needle). The initial burst release of this dye from the single needle products occurred within 3.5 hours (**Fig. 4.26a**) that led to more than 40-75% of the dye release, depending on the five different conditions. It suggests that temperature variations and sonication with various frequencies did not influence the duration of the initial burst release phase, but only affected the release rate of this dye from the produced microspheres. Pyronin B was completely released in 98 hours with more than 94% release at normal temperature, in 78 hours with 60% overall release at physiological temperature, and in 56 hours with over 82-85% dye release using sonication with different frequencies.

The initial burst release of pyronin B from the microspheres produced by the modified co-axial needle process occurred in 5.5 hours and as the graph in **Figure 4.26b** shows, 40-85% of the dye was released during this phase, depending on the five different conditions investigated in this study. This shows that the changes in temperature and other external stimuli such as fresh media or the sonication exposure did not have any effect on the duration of the burst release of this dye from their carriers, but only affected the release rate. Pyronin B was fully released from the co-axial needle products for the period of 32 hours with overall 50% and 70% dye release in physiological and normal temperatures, respectively (**Fig. 4.26b**). The complete release of pyronin B with application of sonication occurred in 30 hours with approximately 88% and 94% release using different frequencies (**Fig. 4.26b**).

Comparison between two graphs in **Figure 4.26** shows that the release of pyronin B from the single needle products occurred at higher rate, in particular in the conditions of ambient and physiological (with/without fresh media) temperatures, compared to that of the co-axial needle products. It also shows the advantage of the single needle products for releasing their payload (pyronin B) in longer period of time with more controllable behaviour compared to their counterparts obtained from the co-axial needle setup. The shorter period of dye release based on the co-axial needle setup encapsulation was attributed to higher surface and internal porosities of the prepared TIPS microspheres (**Figs. 4.16c, 4.16d** and **4.20b**) compared to those collected from the single needle method (**Figs. 4.15c, 4.15d** and **4.19b**).

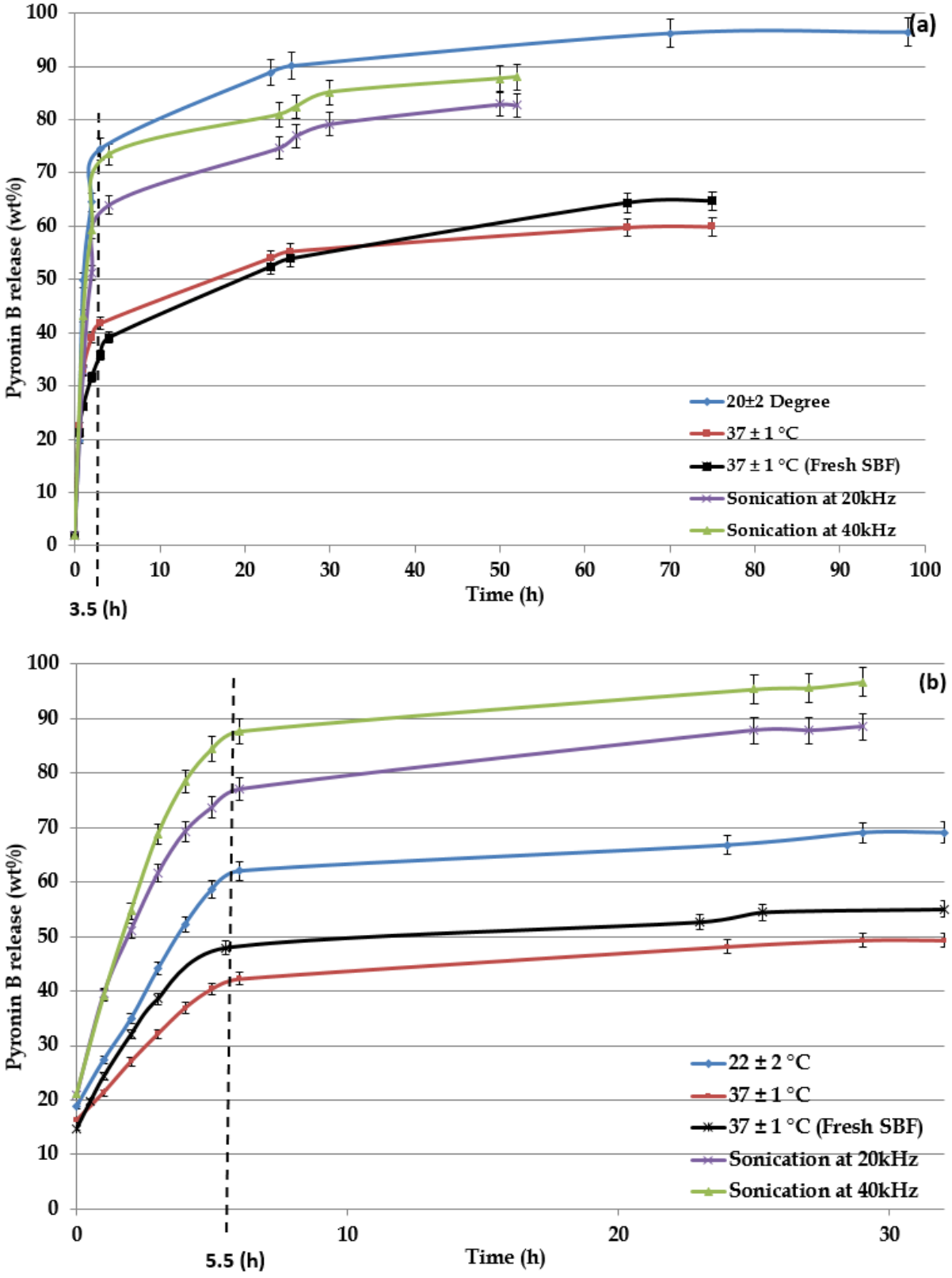

Figure 4.26: The *in vitro* release profiles of pyronin B in SBF: a) The modified single needle EHD/TIPS process and b) The modified co-axial needle EHD/TIPS process

The *in vitro* release profiles of Reichardt's from the polymeric microspheres collected from the two modified EHD/TIPS methods are provided in **Figure 4.27**. The initial burst release of this dye from the single needle products occurred in 4 hours. As **Figure 4.27a** shows, more than 60-72% of the incorporated dye was released during the initial burst release depending on the five different conditions investigated in this study. The high value of initial burst release was likely attributed to the small amount (20% v/v) of ethanol added to the SBF media for measuring the released dye. **Figure 4.27a** also indicates that the external stimuli such as temperature and/or sonication exposure did not have any influence on the duration of the initial burst release of the dye. The complete release of Reichardt's occurred in 170 hours with overall dye release of 79% and 85% at the ambient and physiological temperatures respectively, whereas with application of sonication it occurred in shorter period of time (130 hours) with approximately 92% (20 kHz) and 95% (40 kHz) dye release in total.

The initial burst release of Reichardt's dye from the co-axial needle products occurred in 5 hours that led to more than 60-85% of dye release depending on the five different conditions investigated in this study **(Fig. 4.27b**). This shows that external stimuli such as temperatures, fresh media and sonication did not affect the duration of this phase, but only influenced the release rate of this dye. As explained above, the high value of initial burst release with the co-axial needle products was likely due to the small amount (20% v/v) of ethanol added to the SBF media for measuring the released dye. The complete release of Reichardt's from the products of the co-axial needle setup occurred in 50 hours at physiological and normal temperatures, and in 35 hours with applied acoustic pressure (sonication). However, the complete release of the dye in physiological temperature with fresh media occurred in slightly longer period of time (55 hours) compared to the system without fresh media (**Fig. 4.27b**).

The high release rate, which was attributed to the use of ethanol in release media, was observed in the *in vitro* release profiles of Reichardt's from the microspheres obtained from both encapsulation methods. However, comparison between **Figures 4.27a** and **4.27b** shows that the single needle products were able to release the dye in a longer period with more controllable manner compared to those produced by the co-axial needle setup. As discussed with the other two dyes (erythrosin B and pyronin B), this benefit was related to the less surface porosity and more solid internal structure of the single needle products (**Figs. 4.17c, 4.17d** and **4.19c)** compared to those obtained from the co-axial needle method (**Figs. 4.18c, 4.18d** and **4.20c**).

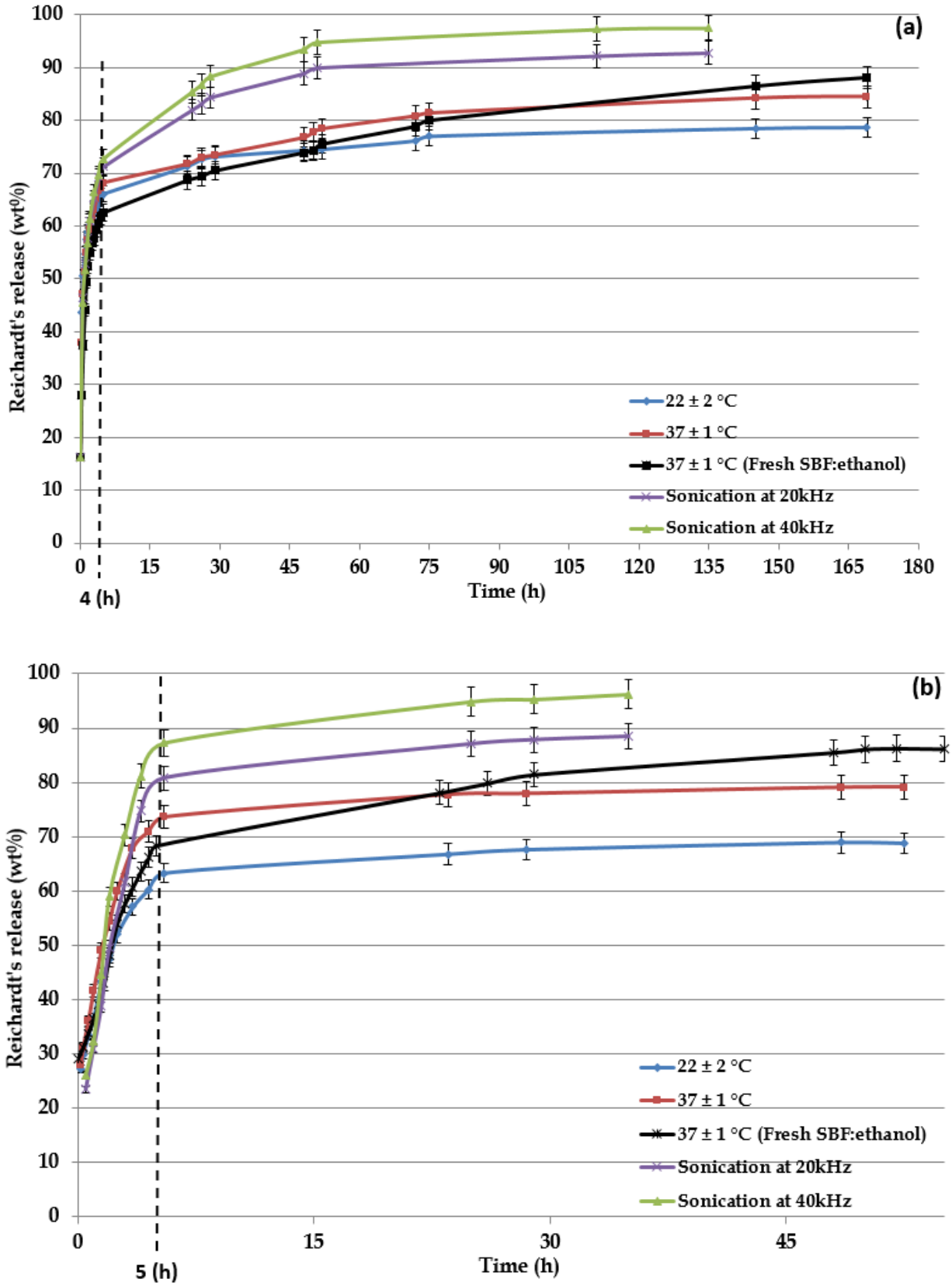

Figure 4.27: The *in vitro* release profiles of Reichardt's dye in SBF:ethanol: a) The modified single needle EHD/TIPS process and b) The modified co-axial needle EHD/TIPS process

Pyronin B and erythrosin B have similar chemical properties and they both are amphiphilic. However, pyronin B is heavier (M_w=1042.28 g/mole) and has higher water solubility (20 g/mole) compared to erythrosin B (M_w=839.85 g/mole and 1 g/mole water solubility). These factors led to quicker period of release for pyronin B (**Fig. 4.26**) compared to erythrosine B (**Fig. 4.25**) for both the single needle and the co-axial needle methods in all the five different conditions. However, Reichardt's dye (551.68 g/mole) has a different chemical structure (**Fig. 4.24a**) compared to the other two dyes (**Figs. 4.22b** and **4.23a)**. Since, it was completely hydrophobic, ethanol was used in the SBF media, and it resulted in higher initial burst release, but with a longer release period compared to pyronin B. The amount of ethanol in the release media had a major effect on the release rate of this dye. Therefore, by varying the volume concentration of ethanol in the SBF media, more optimum initial burst release with associated different periods of sustained release can be obtained. Comparison shows that the chemical properties of active agents such as hydrophobicity had a much more significant effect on the release rate compared to the physical properties such as molecular weight. Since, drugs such as Cyclosporine A and Tacrolimus with high molecular weight have very low water solubility, it is predicted that they would have a release profile pattern similar to erythrosin B or Reichardt's dyes.

The surface porosity led to high initial burst release of the loaded microspheres (single needle and co-axial needle) which was a required condition for the chronic wound therapy. After that long period of sustained release was obtained which was related to two main reasons: firstly decrease in inward diffusion rate of water for dye release due to the denser polymer matrix compared to the surface **(Figs. 4.19 and 4.20)** and secondly decrease in concentration gradient of the dye between the release media and the polymer matrix due to the high and quick initial burst release. However, analysis and comparison of the results collected from the experimental methods showed that the microspheres collected from the single needle EHD/TIPS process were capable of releasing the payload in a more controlled manner (longer period of sustained release) (**Figs. 4.25a, 4.26a** and **4.27a**) compared to their counterparts collected from the co-axial needle setup (**Figs. 4.25b, 4.26b** and **4.27b**). The longer period of sustained release was related to the less internal and surface porosities of the microspheres collected from the single needle (**Figs. 4.13, 4.15**, **4.17** and **4.19**) compared to their counterparts (**Figs. 4.14, 4.16, 4.18** and **4.20**) from the co-axial needle. This suggests that surface porosity up to a certain level can lead to a better agent release (Enayati et al., 2010a), however further porosity will results in faster release with less controllable manner.

4.9.2 Quantification of the *In Vitro* Release

Over the past few decades, number of different mathematical formulations have been developed, aiming to design a more and more effective controlled drug release system with reduction in the administration frequency and side effects connected to the dosing (Dash et al., 2010). Quantification is very useful for prediction of the release kinetics before the release systems are realized. More often, it allows the measurements of some important physical parameters such as drug diffusion and co-efficient, and restoring to model fitting on experimental release data. The release patterns can be divided into those that release the drug at slow zero or first order rate, and those that provide an initial rapid dose followed by slow zero or first order release of sustained component (Dash et al., 2010). The purpose of designing a controlled drug release system in this study was for the biomedical application in chronic wound therapy. Therefore, such drug delivery systems were required to initially release part of the dose rapidly in order to attain the effective therapeutic concentration of the drug, followed by a well-defined behaviour to supply the maintenance dose enabling the attainment of the desired drug concentration. Although, number of different mathematical formulations exists to evaluate the drug release mechanism, in this study only four of them were used for the assessment of the *in vitro* release profiles of the adopted dyes. The four applicable fundamental drug release equations in this study (**Table 4.5**) have been widely used for evaluation of the kinetics and the mechanism of the *in vitro* drug release from the polymeric drug carriers and they have been selected based on water solubility characteristics of the incorporated materials (Sharma et al., 2010).

Table 4.5: The equations used for quantification of the *in vitro* dye release studies (Dash et al., 2010)

Release mechanism	Mathematical formula	Release Constant (unit)	Description of drug release
Zero order	$Q_t = Q_o + K_0 t$	K_0 (1/h)	**Independent of its concentration dissolved in solution**
First order	$\text{Log } Q_t = \text{Log } Q_o + K_C t/2.303$	K_C (2.303/h)	**Dependent on its concentration**
Higuchi	$Q_t = K_H\ t^{1/2}$	K_H ($1/h^{1/2}$)	**Dependent on diffusion and also erosion (degradation) of drug shell**
Hixon-Crowell	$(Q_0)^{1/3} - (Q_t)^{1/3} = K_{HC}\ t$	K_{HC} (1/h)	**Dependent on the surface area or diameter of the drug carrier**

Q_t (mg) is the amount of drug released at time t (h)

Q_o (mg) is the initial amount of drug

The *in vitro* release profiles of the dyes adopted for prediction of Cys A and Tacrolimus were applied on the four kinetic models (zero order, first order, Higuchi and Hixon-Crowell) in order to find out the best fitted model for the *in vitro* dye release from the porous loaded microspheres. The details of the four release kinetics equations which applied to the *in vitro* dye release profiles obtained from the modified single needle and the modified co-axial needle EHD/TIPS methods are provided in **Tables 4.6** and **4.7**, respectively.

Table 4.6: The release parameters calculated from the *in vitro* release data of the single needle products

Samples contained the dye		Zero order		First order		Higuchi		Hixon-Crowell	
	Conditions	R^2	K_0	R^2	K_C	R^2	K_H	R^2	K_{HC}
Erythrosin B	22 ± 2ºC	0.44	0.16	0.24	-0.01	0.76	2.28	0.45	-0.05
	37 ± 1ºC	0.72	0.16	0.78	-0.01	0.88	2.60	0.80	-0.06
	37 ± 1ºC (Fresh media)	0.85	0.12	0.72	-0.01	0.95	2.1	0.85	-0.04
	Sonication at 20 kHz	0.86	0.26	0.69	-0.01	0.89	3.85	0.87	-0.09
	Sonication at 40 kHz	0.87	0.25	0.69	-0.01	0.88	3.81	0.86	-0.08
Pyronin B	22 ± 2ºC	0.44	0.64	0.21	-0.02	0.77	4.44	0.45	-0.21
	37 ± 1ºC	0.68	0.37	0.57	-0.01	0.83	3.91	0.68	-0.13
	37 ± 1ºC (Fresh media)	0.82	0.51	0.71	-0.01	0.95	5.18	0.82	-0.17
	Sonication at 20 kHz	0.71	0.78	0.60	-0.01	0.83	6.55	0.71	-0.25
	Sonication at 40 kHz	0.68	0.65	0.61	-0.01	0.80	4.187	0.68	-0.22
Reichardt's	22 ± 2ºC	0.35	0.18	0.19	-0.01	0.75	2.22	0.35	-0.06
	37 ± 1ºC	0.43	0.23	0.25	-0.01	0.75	2.90	0.43	-0.07
	37 ± 1ºC (Fresh media)	0.54	0.28	0.34	-0.01	0.80	3.66	0.54	-0.09
	Sonication at 20 kHz	0.45	0.34	0.27	-0.01	0.81	3.92	0.45	-0.11
	Sonication at 40 kHz	0.56	0.46	0.39	-0.01	0.81	4.180	0.57	-0.15

Table 4.7: The release parameters calculated from the *in vitro* release data of the co-axial needle products

Samples contained the dye		Zero order		First order		Higuchi		Hixon-Crowell	
	Conditions	**R^2**	**K_0**	**R^2**	**K_C**	**R^2**	**K_H**	**R^2**	**K_{HC}**
Erythrosin B	**22 ± 2ºC**	**0.82**	**0.22**	**0.81**	**-0.01**	**0.97**	**3.34**	**0.81**	**-0.07**
	37 ± 1ºC	**0.86**	**0.13**	**0.77**	**-0.01**	**0.95**	**1.90**	**0.86**	**-0.04**
	37 ± 1ºC (Fresh media)	**0.67**	**0.18**	**0.55**	**-0.01**	**0.87**	**2.58**	**0.67**	**-0.06**
	Sonication at 20 kHz	**0.80**	**0.28**	**0.83**	**-0.01**	**0.92**	**3.95**	**0.83**	**-0.09**
	Sonication at 40 kHz	**0.79**	**0.32**	**0.81**	**-0.01**	**0.88**	**4.52**	**0.79**	**-0.10**
Pyronin B	**22 ± 2ºC**	**0.60**	**1.13**	**0.48**	**-0.02**	**0.79**	**8.26**	**0.60**	**-0.37**
	37 ± 1ºC	**0.67**	**0.77**	**0.55**	**-0.02**	**0.85**	**4.167**	**0.68**	**-0.26**
	37 ± 1ºC (Fresh media)	**0.70**	**1.02**	**0.58**	**-0.03**	**0.87**	**7.75**	**0.71**	**-0.34**
	Sonication at 20 kHz	**0.62**	**1.50**	**0.45**	**-0.03**	**0.81**	**10.74**	**0.62**	**-0.50**
	Sonication at 40 kHz	**0.55**	**1.62**	**0.40**	**-0.03**	**0.75**	**11.90**	**0.55**	**-0.54**
Reichardt's	**22 ± 2ºC**	**0.52**	**0.60**	**0.44**	**-0.01**	**0.70**	**4.148**	**0.53**	**-0.20**
	37 ± 1ºC	**0.47**	**0.71**	**0.39**	**-0.01**	**0.65**	**6.45**	**0.48**	**-0.23**
	37 ± 1ºC (Fresh media)	**0.70**	**0.85**	**0.59**	**-0.01**	**0.85**	**7.40**	**0.70**	**-0.28**
	Sonication at 20 kHz	**0.58**	**1.42**	**0.47**	**-0.02**	**0.72**	**10.67**	**0.58**	**-0.47**
	Sonication at 40 kHz	**0.57**	**1.50**	**0.45**	**-0.02**	**0.70**	**11.30**	**0.57**	**-0.50**

The correlation coefficient (R^2) and the release constant are the two important parameters in each drug release mathematical equation. The former (R^2) is found from the graph plotted with the amount of drug release (Q_t for the Higuchi and Zero order, Log (Q_0 - Q_t) for First order and ($Q_0 - Q_t$)$^{1/3}$ for Hixson-Crowell) versus time (t for the Zero order, First order and Hixson-Crowell, $t^{1/2}$ for Higuchi) for each controlled release mathematical formulation, whereas latter (release constant) is found from the slope of line equation in each graph. The R^2 with highest value is then selected as the best fitted drug release model. **Tables 4.6** and **4.7** show that the highest correlation coefficient for the three dyes in all the five different conditions was obtained with Higuchi compared to that of the other formulations used for the controlled release quantification. This indicates that the amount of dye release from their polymer shell is mostly proportional to the square root of time. Thus, based on the description of this mathematical

formulation, the release of the incorporated dyes occurred through the combination of dye diffusion and polymeric shell (PLGA) biodegradation (**Table 4.5**). The high value of release constant for Higuchi compared to that of the other mathematical equations that occurred with the three dyes in all the five different conditions is related to the high initial burst release phase. The release profiles of the three dyes based on the Higuchi equation are provided in **Figures 4.28-4.30** which shows the percentage of dye release with respect to the square root of time.

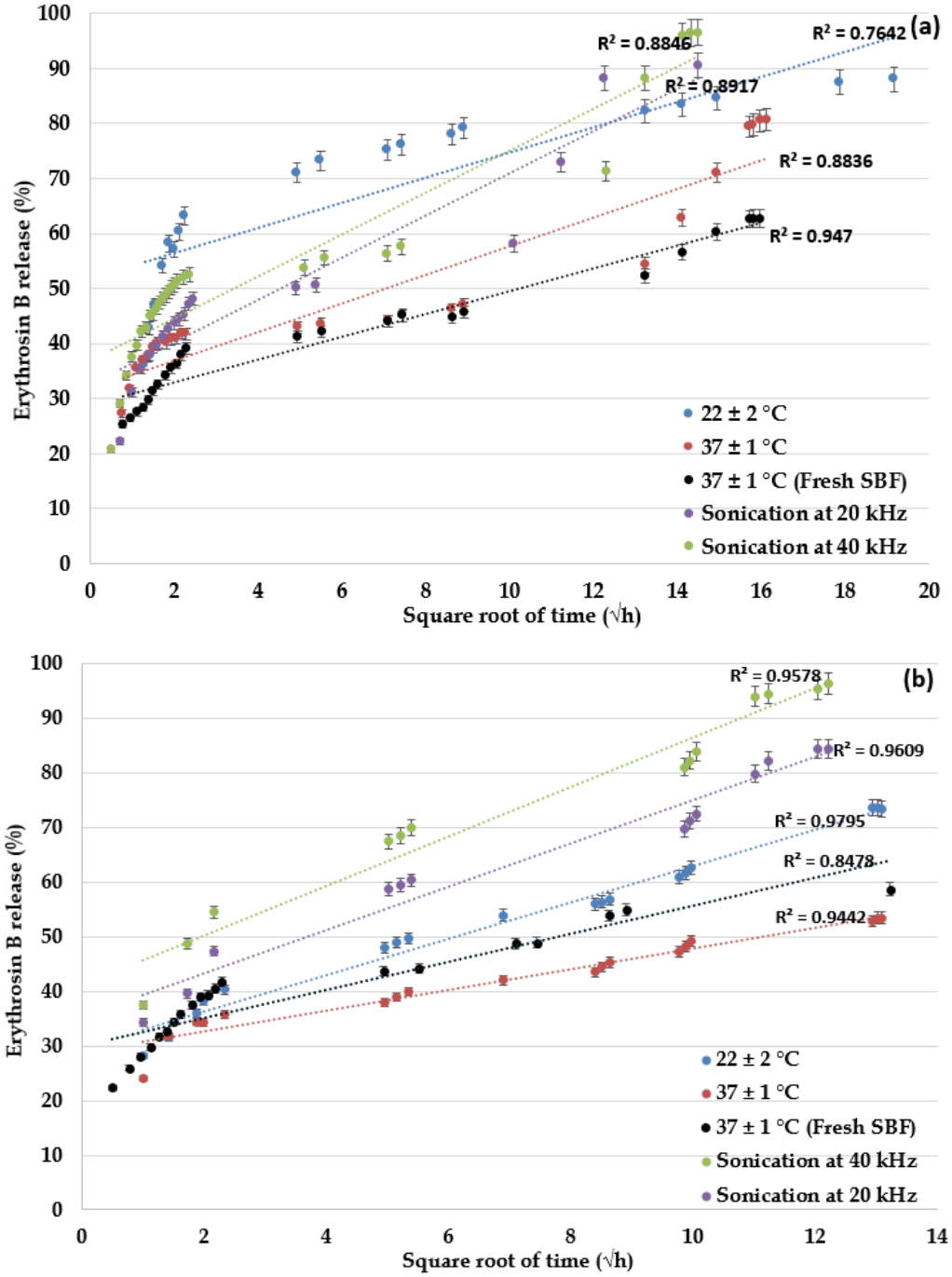

Figure 4.28: Release profiles of erythrosin B in SBF based on Higuchi equation: a) Single needle products and b) Co-axial needle products

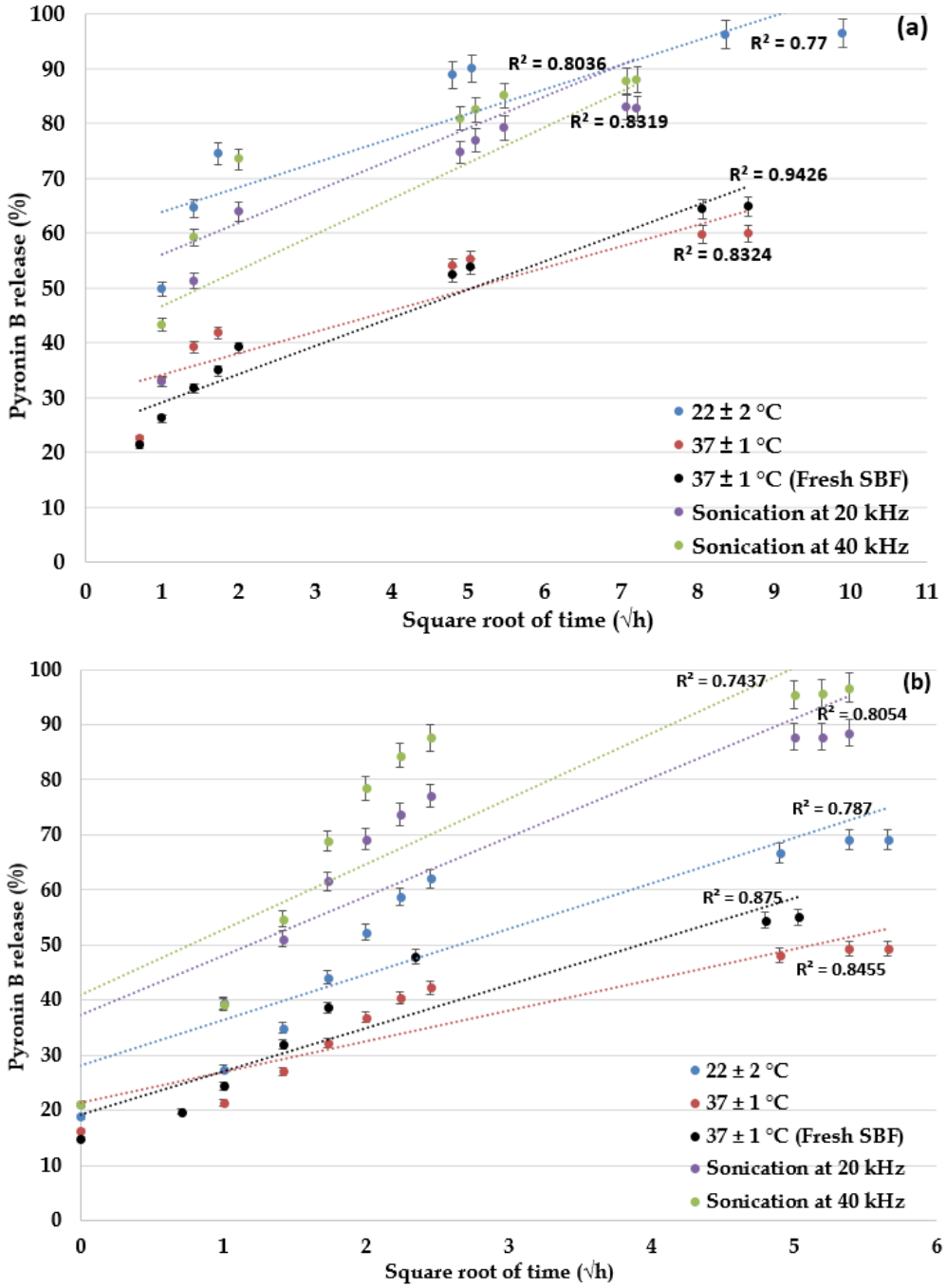

Figure 4.29: Release profiles of pyronin B in SBF based on Higuchi equation: a) Single needle products and b) Co-axial needle products

The results obtained from the EDX studies showed that the active dyes were entrapped in the matrix of the polymer microspheres rather than surface encapsulation. Thus, based on the morphological and the *in vitro* release studies, the high initial burst release was related to the surface porosity that led to quick diffusion of the dyes encapsulated close to the surface. Considering that the encapsulated dye is not uniformly distributed within the matrix of the polymeric particles, the long period of sustained release is related to two main factors: 1) decrease in inward diffusion rate of water for dye release due to the denser polymer matrix

compared to the surface **(Figs. 4.19 and 4.20),** and 2) decrease in concentration gradient of the dye between the release media and the polymer matrix due to the high and quick initial burst release. Therefore, the two phases of the dye release had different rates of diffusion. Quantification of the *in vitro* release data demonstrated that the Higuchi equation is more fitted model compared to the other mathematical equations, which further affirms that the release mechanism is based on the dye diffusion during the early stages and the combination of diffusion and polymer degradation through the latter stages.

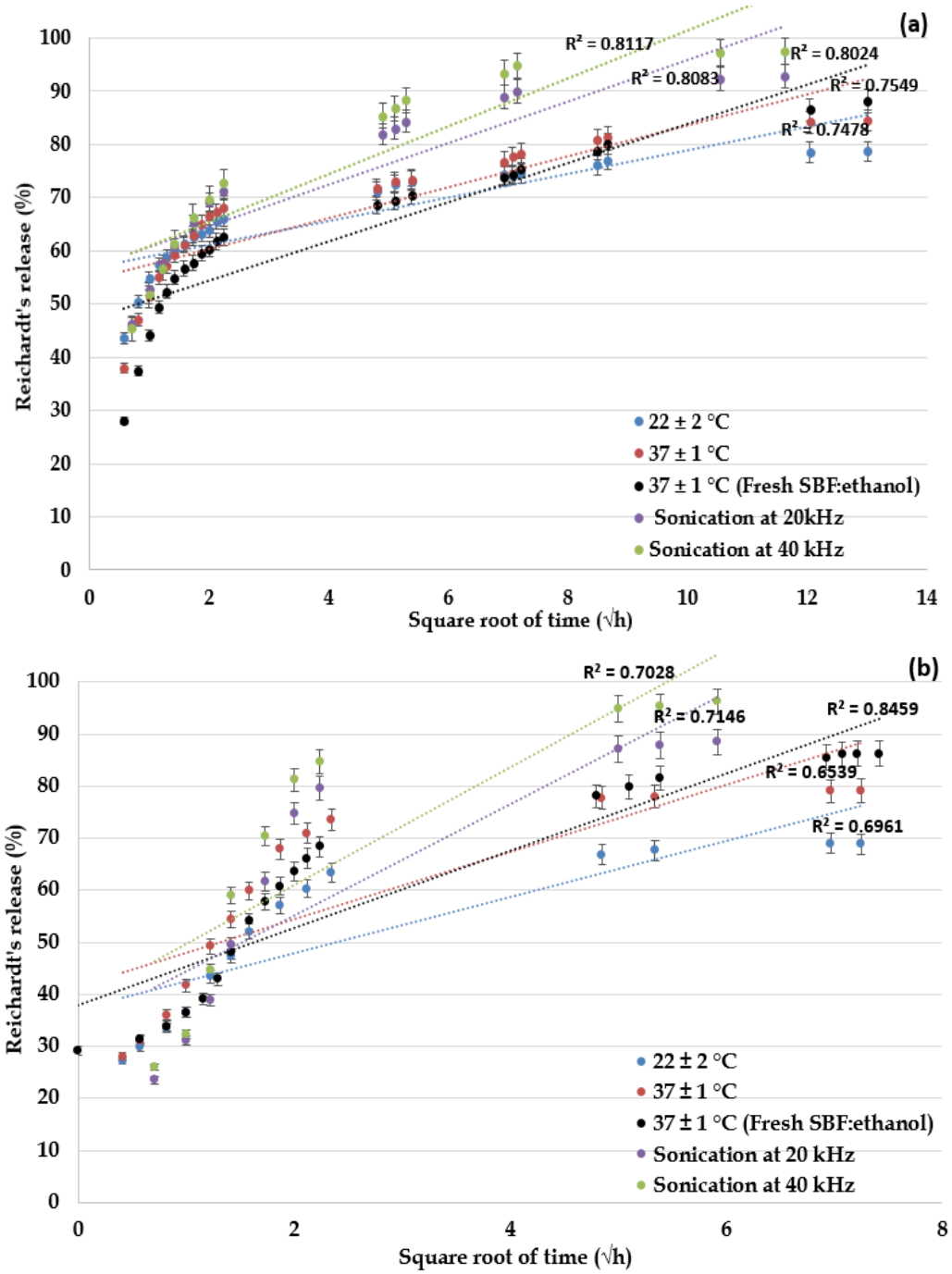

Figure 4.30: Release profiles of Reichardt's dye in SBF:ethanol based on Higuchi equation: a) Single needle products and b) Co-axial needle products

As **Figures 4.28-4.30** show, the release mechanism of the three selected dyes, particularly for erythrosin B and pyronin B, was mostly based on Higuchi, which further confirmed that the dye release was controlled through the combination of dye diffusion and polymer shell biodegradation (erosion). Therefore, it can be predicted that the release mechanisms of the immunosuppressants such as Cys A and Tacrolimus with high molecular weight and low water solubility would be based on Higuchi equation, releasing the encapsulated drug with square root of time via the combination of diffusion and the polymer degradation.

4.9.3 Effect of Microsphere Size and Morphology in Burst Release

The key feature in designing such drug delivery system in this study was to reduce the frequency of dosing and provide uniform drug release with high initial burst for treatment of chronic wounds such as fistulae. The total amount of dyes used in the release studies was the same for all formulations, and the PLGA formulations were prepared under same processing conditions. One factor, apart from the surface morphology, affecting the drug release kinetics is the microsphere dimension (Gaumet et al., 2007), as particles with different dimensions have different surface areas, and thus, providing different total surface area available for drug release. The initial burst release is commonly attributed to the release of encapsulated agent located close to the surface of the particles as well as the morphological structure of the products (Cohen et al., 1991; Pitt, 1990). The surface porosity led to high initial burst release of the loaded microspheres collected from the two different EHD/TIPS methods (**Figs. 4.25-4.27**) which is related to the quick diffusion of the dyes from the polymer matrix. However, the initial burst release of the dyes was faster from the single needle products compared to their counterparts from the co-axial needle method. This was highly related to more encapsulation of the dyes at the layers close to the surface area of the single needle microspheres and consequently the quicker diffusion of the incorporated materials.

Although the main goal in this study was to produce microspheres with the targeted size distribution (150-300 μm), in some cases, this required size range was not obtained due to the physical properties of the processing solutions and the environmental conditions such as humidity and temperature. Thus, this could have a significant effect on the release kinetics of the active agents. For example, the required size distribution of the microspheres was not achieved for Reichardt's loaded microspheres produced by the single needle method (**Table 4.13**). Moreover, based on the SEM images, the Reichardt's loaded microspheres had more surface porosity (**Fig. 4.17**) compared to the other loaded microspheres collected from the

single needle method. Therefore, the high initial burst release (**Fig. 4.27a**) of this dye compared to the other two dyes, apart from using ethanol in the release media, could also be related to the more surface porosity and greater encapsulation of the agent close to the surface due to the smaller surface area available in the microspheres fabricated (**Table 4.13**).

4.9.4 Effect of External Stimuli on Release Profile

In this chapter, further investigation of the results obtained from the *in vitro* release studies was carried out on the loaded microspheres fabricated by the modified single needle and the co-axial needle EHD/TIPS processes. The final objective of this study was to investigate the effects of external stimuli in order to tailor and control the payload release profile for producing more efficient drug delivery system. As mentioned in **Section 3.9.2.3**, the *in vitro* release studies were carried out at various temperatures, using sonication at different duty cycles and also fresh media to stimulate the dye release. The main reason behind this investigation was to have a more controlled release behaviour of the payloads from their polymeric carriers. In this part, the application of external stimuli on the *in vitro* dye release profiles of the single needle products was discussed in conjunction with those obtained from the co-axial needle method.

4.9.4.1 Fresh Media

As explained in **Section 3.9.2.3,** addition of the 2 ml fresh media to the release medium was carried out at the pre-determined times during UV measurements. The *in vitro* release studies showed that addition of fresh media (SBF for pyronin B and erythrosin B, and SBF:ethanol for Reichardt's dye) can in general lead to higher percentage release of the entrapped dyes compared to that of the physiological temperature without using the fresh media. This was observed on the release profiles of pyronin B and Reichardt's entrapped in the microspheres produced by the two EHD/TIPS methods (**Figs. 4.26** and **4.27**) and also the erythrosin B release profile from the co-axial needle products (**Fig. 4.25b**). When the release media is constant, a homeostatic level occurs between the amount of dye in the media and the remaining agent entrapped after a certain period of time (the concentration gradient of the dye decreases to zero). Therefore, the release rate will decrease due to PLGA resistance to absorb more water. However, by adding more fresh media, the homeostasis imbalance is induced and the dye concentration gradient increases again. PLGA starts to absorb more water, and consequently more dyes will be released by diffusion (Makadia and Siegel, 2011).

However, less percentage release of erythrosin B with fresh media compared to that of the physiological condition was recorded with the single needle products (**Fig. 4.25a**). Since, erythrosin B is less hydrophilic (lower water solubility) compared to pyronin B, this could be simply related to the dilution of the small amount of released dye in the new fresh media.

Comparison of the *in vitro* release studies with fresh media showed no significant difference in the release pattern of the dyes encapsulated by means of two different methods (the single needle and the co-axial needle). However, more percentage release of the dyes was in general achieved with the single needle encapsulation method (**Figs. 4.25a, 4.26a** and **4.27a**) compared to the co-axial needle setup (**Figs. 4.25b, 4.26b** and **4.27b**) due to longer period of dye release.

4.9.4.2 Temperature

The release profiles of the dyes encapsulated in TIPS microspheres were effected by variations in temperature. As discussed earlier in **Section 3.9.2.3,** the release studies of the loaded microspheres were carried out at two distinct temperature conditions, 22 ± 2^{o}C and 37 ± 1^{o}C.

The complete comparison of the *in vitro* dye release with the effect of temperature between the single needle and the co-axial needle EHD/TIPS products are given in **Table 4.8.** This table is provided based on the differences in the release rate of dyes between the ambient (22 ± 2^{o}C) and the physiological (37 ± 1^{o}C) temperatures from the point where the sustained release is started until the complete release of the agent. As this table shows, the higher temperature in general resulted in negative effect (decrease) in the release rate of the amphiphilic materials such as erythrosin B and pyronin B compared to the normal temperature. The lower release rate in physiological temperature was slightly compensated by using 2ml addition of fresh media in the release medium, but still lower release rate was observed compared to that of the normal temperature (22 ± 2^{o}C).

In case of Reichardt's, positive effect (increase) in the release rate was observed in physiological temperature (37 ± 1^{o}C) compared to the normal temperature (22 ± 2^{o}C) for both the single needle and co-axial needle products. Moreover, even higher release rate of the dye in physiological temperature was observed with the addition of fresh media compared to the normal condition (**Table 4.8**).

The lower release rate of erythrosin B and pyronin B in physiological temperature (37 ± 1^{o}C) compared with normal temperature (22 ± 2^{o}C) (**Figs. 4.25** and **4.26**) is related to the higher

degradation and evaporation rate of these two dyes, in particular iodine bonding in erythrosin B and chloride in pyronin B, in aqueous solution of 37 ± 1°C (Jane et al., 2010). Unlike the release profiles of these two dyes (erythrosin B and pyronin B), the temperature changes did not have any significant effect on the Reichardt's release rate (**Fig. 4.27**). This can be related to either using ethanol in the release media to facilitate the release, or Reichardt's dye does not evaporate and/or degrade with heat in aqueous solution.

Table 4.8: The release characteristics of the loaded microspheres effected by temperature during the sustained release phase

Samples of TIPS microspheres Containing	Modified single needle EHD/TIPS			
	Dye released differences with fresh media (%)		Dye released difference without fresh media (%)	
	Start	Finish	Start	Finish
Erythrosin B	- (24 ± 2)	- (22 ± 2)	- (22 ± 2)	- (7 ± 2)
Pyronin B	- (35 ± 2)	- (30 ± 2)	- (32 ± 2)	- (35 ± 2)
Reichardt's	- (3 ± 2)	+ (10 ± 2)	+ (2 ± 2)	+ (7 ± 2)
	Modified co-axial needle EHD/TIPS			
Erythrosin B	- (2 ± 2)	- (15 ± 2)	- (7 ± 2)	- (20 ± 2)
Pyronin B	- (14 ± 2)	- (15 ± 2)	- (20 ± 2)	- (20 ± 2)
Reichardt's	+ (5 ± 2)	+ (16 ± 2)	+ (10 ± 2)	+ (10 ± 2)

- The positive sign shows the increase in release rate, whereas the negative sign shows the decrease in the release rate as the temperature increased from 22 ± 2°C to 37± 1°C

4.9.4.3 Sonication

A systematic investigation using sonication (**Section 3.10**) was carried out to determine the effect of various exposure parameters such as duty cycle and exposure time on the release rate of the dyes from the loaded microspheres.

The comparison of the *in vitro* dye release studies with the influence of sonication exposure between the single needle and the co-axial needle products is presented in **Table 4.9**. Since, sonication was carried out on samples in physiological temperature, the difference in the release rate of the encapsulated dyes is compared to that of the physiological temperature

without fresh media. The comparison is for the period of sustained release (from the point where the burst release is finished until the complete period of agent release).

Table 4.9: The release characteristics of the loaded microspheres exposed to sonication during the sustained release phase

Samples of TIPS microspheres contained	Modified single needle EHD/TIPS			
	Dye released differences with 20 kHz (%)		Dye released difference with 40 kHz (%)	
	Start	Finish	Start	Finish
Erythrosin B	+ (5 ± 2)	+ (10 ± 2)	+ (10 ± 2)	+ (15± 2)
Pyronin B	+ (20 ± 2)	+ (23 ± 2)	+ (30 ± 2)	+ (27 ± 2)
Reichardt's	+ (3 ± 2)	+ (7 ± 2)	+ (4 ± 2)	+ (10 ± 2)
	Modified co-axial needle EHD/TIPS			
Erythrosin B	+ (12 ± 2)	+ (30 ± 2)	+ (20 ± 2)	+ (40 ± 2)
Pyronin B	+ (35 ± 2)	+ (38 ± 2)	+ (45 ± 2)	+ (45 ± 2)
Reichardt's	+ (7 ± 2)	+ (8 ± 2)	+ (10 ± 2)	+ (15 ± 2)

- The positive sign shows the increase in release rate, whereas the negative sign shows the decrease in the release rate with application of sonication compared to the dye release rate in physiological temperature

The release profiles were noticeably affected by having the prepared loaded PLGA/TIPS microspheres exposed to sonication. The sonicator has been adopted for various drug delivery applications in order to increase the release rate of pharmaceuticals in target tissues (Mitragotri, 2005). The formation of gas or vapour filled bubbles in the medium exposed to sonicator is the main mechanism for increasing the release rate of the incorporated dyes (Larina et al., 2005). Such bubbles can violently collapse and deform the structure of microspheres due to high shear stresses in the region of collapse and/or the shock waves produced by the collapse of the bubbles towards the microsphere surface (Nyborg, 2001). In this study, an increase in the release rate was observed for all the samples exposed to sonicator in physiological temperature (**Figs. 4.25-4.27**). The results also showed that sonicator with higher frequency led to more increase of dye release compared to that at lower frequency with longer period of application (**Table 4.9**). This is due to more intensive bubbles produced by higher frequency which in turn damaged the microsphere surface and its structure, leading to more dye release.

As **Table 4.9** shows, sonication provided higher rate of dye release from all the loaded microspheres produced by the two different EHD/TIPS methods. This table also indicates that the sonication had a greater effect on the co-axial needle products in releasing their payload compared to that of the single needle system. This was highly related to higher surface and internal porosities of the products produced by the co-axial needle system compared to that of the single needle method.

4.10 Biodegradation Studies of PLGA

PLGA co-polymer is insoluble in water. However, it is hydrolytically unstable and degrades by hydrolysis of its ester bond. Thus, random chain scission occurs through this hydrolysis, leading to degradation into two different monomers of lactic and glycolic acids.

The interesting feature for this part of the investigation was to observe the variations in the surface morphology and internal structure of the loaded microspheres during the degradative hydrolysis as a function of time. The SEM studies for this part were only carried out for the packs of loaded microspheres in the release media kept at two different conditions of ambient and physiological temperatures.

The microspheres produced by the two different EHD/TIPS methods had the required surface and internal porosities for the particular biomedical application in chronic wound therapy (**Figs. 4.13-4.20**). However, as the SEM images show, these loaded microspheres lost their surface integrity and became less porous during the initial degradative hydrolysis of the polymer (within 2 days) when placed in the release media (**Figs. 4.31a, 4.31c, 4.32a, 4.32c, 4.33a** and **4.33c**). These products were spongy and flexible to form into any shape.

The packs of loaded microspheres in their release media started to aggregate after a certain period of time and formed into a relatively large lump shape. They became quite brittle and rough on the surface (**Figs. 4.31b(i), 4.31d(i), 4.32b(i)**, **4.32d(i)** and **4.33d(i)**). The SEM of the loaded microspheres also show that the surface pores of the products is considerably decreased by 12 days in the release media (**Figs. 4.31b(ii), 4.31d(ii), 4.32b(ii)**, **4.32d(ii)** and **4.33d(ii)**), whereas, their internal structure has obtained more porosity (**Figs. 4.31b(iii), 4.31d(iii), 4.32b(iii)**, **4.32d(iii)** and **4.33d(iii)**) compared to the start point of the release studies.

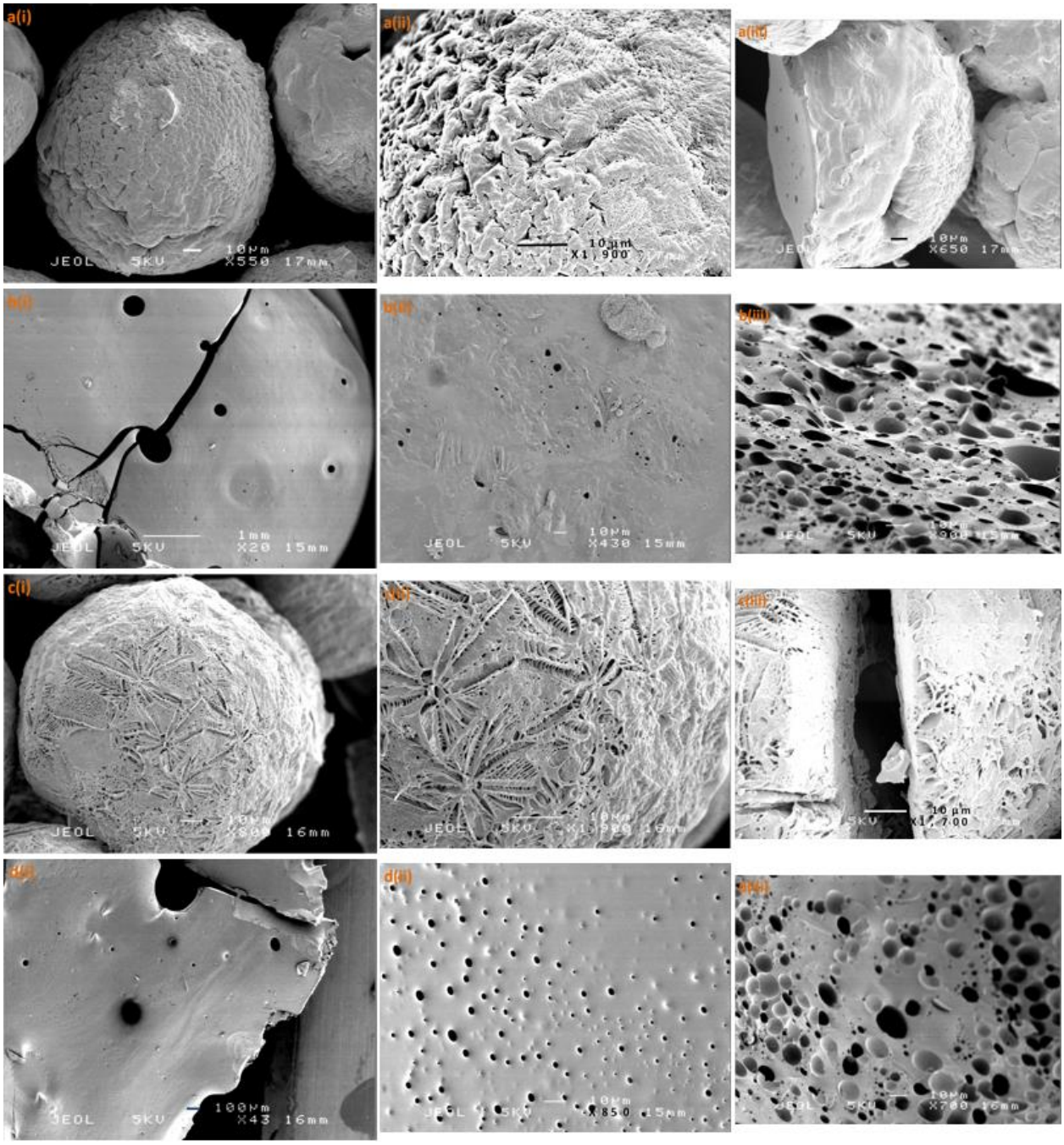

Figure 4.31: Surface morphology of the erythrosin B loaded microspheres in SBF: a) Single needle after 2 days, b) Single needle after 12 days, c) Co-axial needle after 2 days and d) Co-axial needle after 12 days

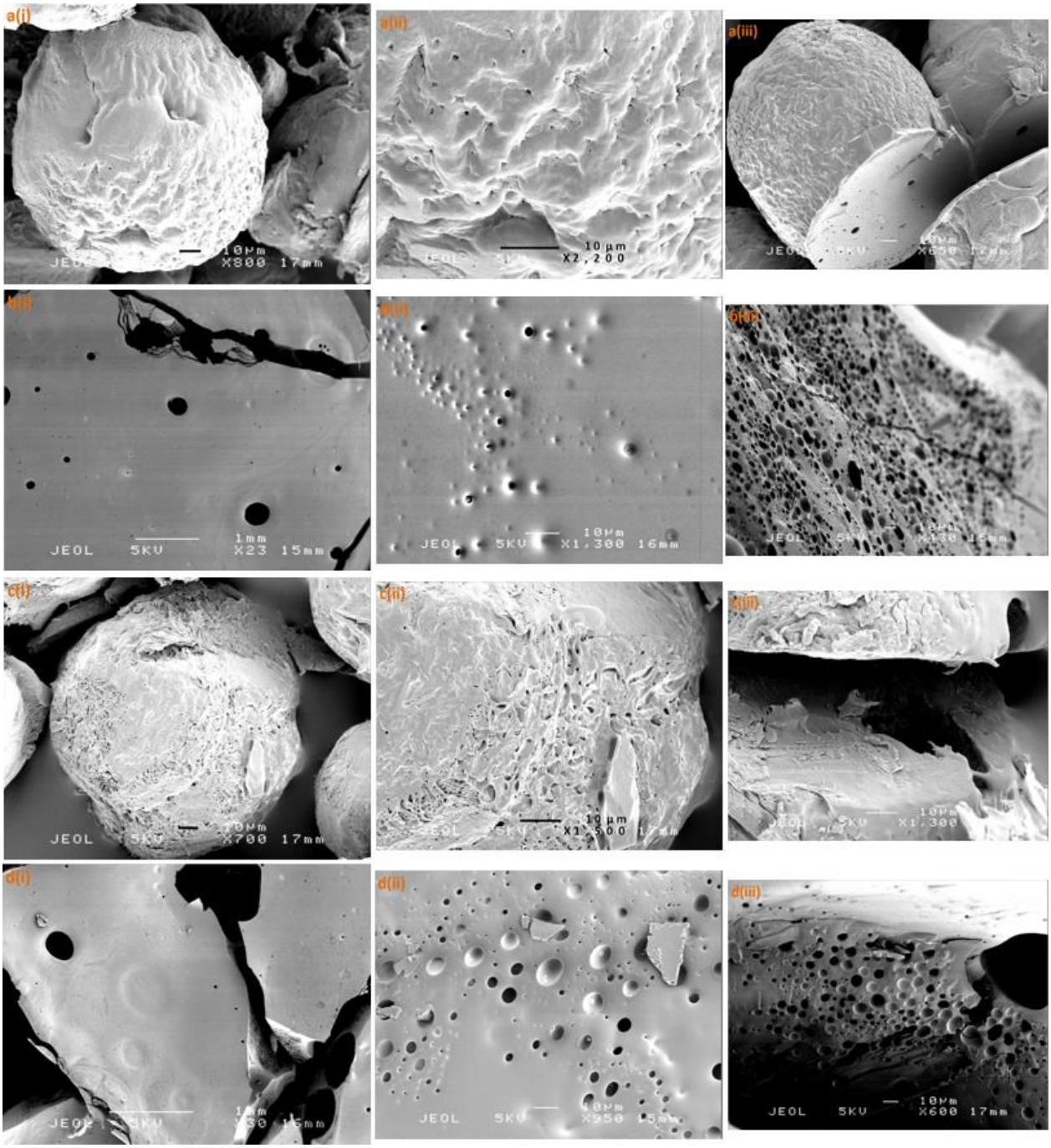

Figure 4.32: Surface morphology of the pyronin B loaded microspheres in SBF: a) Single needle after 2 days, b) Single needle after 12 days, c) Co-axial needle after 2 days and d) Co-axial needle after 12 days

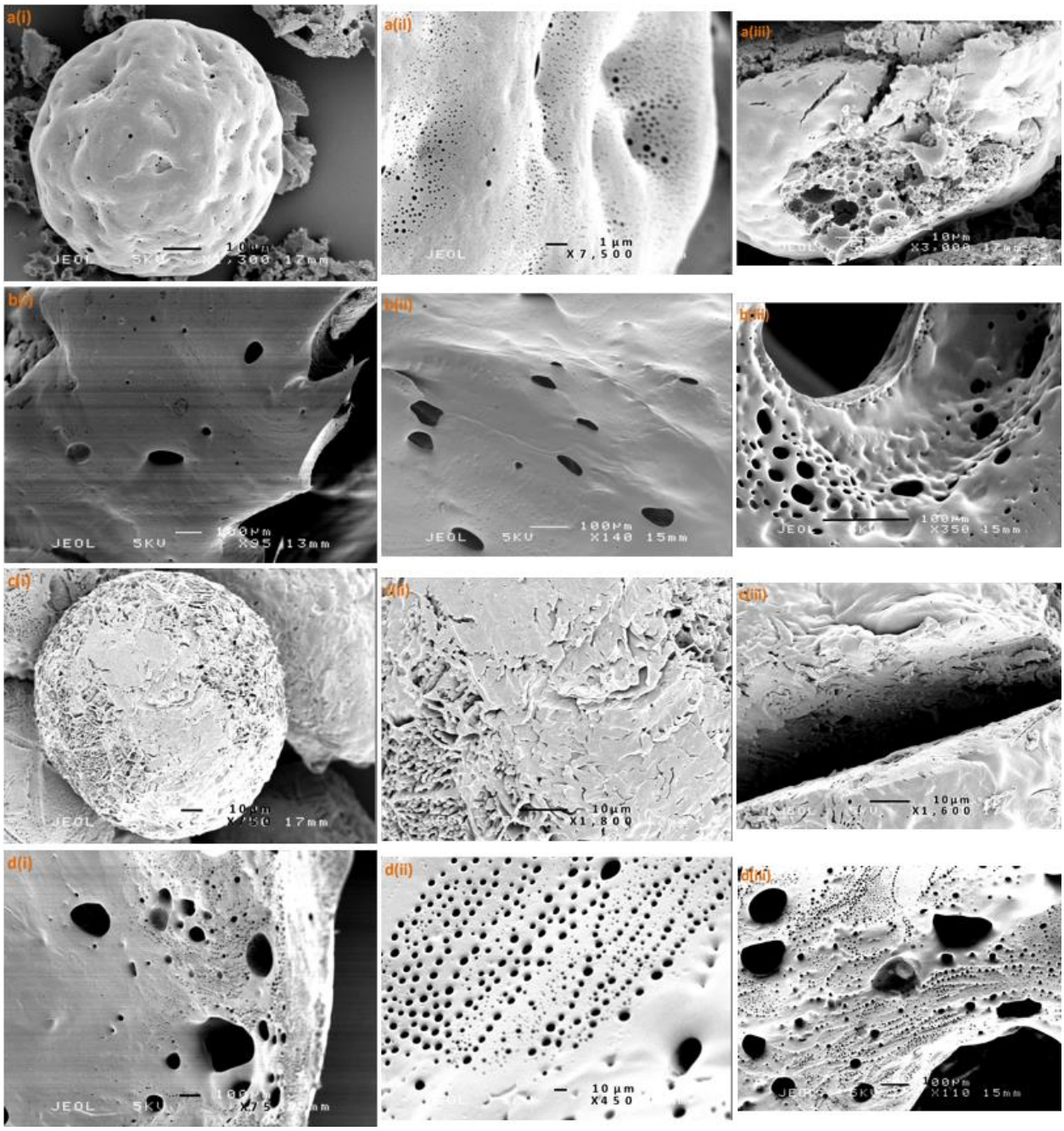

Figure 4.33: Surface morphology of the Reichardt's loaded microspheres in SBF/Ethanol (80:20 v/v): a) Single needle after 2 days, b) Single needle after 12 days, c) Co-axial needle after 2 days and d) Co-axial needle after 12 days

As the SEM images of the loaded microspheres in the release media showed, the variations in the temperature up to 12 days did not have any significant difference on the morphology of the drug carriers. Therefore, based on the *in vitro* release studies, the changes in the release rate at various temperatures were mainly attributed to chemical properties such as the evaporation and degradation rate of the active agents in aqueous solutions.

Summary

This chapter of the thesis demonstrated the successful preparation of micro-scale polymeric particles as drug carriers using the single needle EHD method. This method overcame some of the disadvantages of other conventional methods such as the need for elevated temperature, multiple processing and the use of surfactants and other additives for producing the required polymeric drug carriers.

In **Section 4.1**, the key processing parameters (flow rate and applied voltage) and the physical properties of the processing solutions were modified to obtain a stable cone jet mode. The cone-jet mode was of particular interest, as it could result in near-monodisperse particles upon jet break-up. The flow rate and the applied voltage were varied in a wide range depending on the physical properties of the processing solutions for production of the near monodisperse required size (150-300 µm) of the microspheres. It was illustrated that the particle sizes were reduced at higher applied voltages which was more noticeable at higher flow rates. The polydispersity index (PDI) of the particles was found to increase by enhancing the flow rates. This showed the instability of the cone-jet mode which was directly related to combination of the processing parameters as well as the physical properties of the solutions. This phenomenon was more noticeable with the processing solutions (PLGA/DMF and PLGA/DMC) that obtained high electrical conductivity, high dielectric constant and high surface tension.

Section 4.3 showed that the PLGA/DMC solution at specific processing parameters (the flow rate of 225 µl/min, and the applied voltage 6.0-7.0 kV) successfully fabricated the required size range (150-300 µm) of the polymeric microspheres using the single needle EHD method combined with TIPS. This combination not only led to the required size distribution, it also provided surface porosity in the microspheres. The key factor in producing surface porosity was related to thermally induced liquid-liquid phase separation of the polymer solution in liquid nitrogen, followed by sublimation of the solvent via lyophilisation of the sample.

This chapter also demonstrated that the dye loaded polymeric microspheres fabricated by the two different EHD/TIPS methods are able to release their payload in a controllable manner with high initial burst release for the purpose of targeted delivery and chronic wound therapy. The *in vitro* release studies of the produced spherical particles were conducted at five different conditions: normal and physiological temperatures, physiological temperature with fresh media and with sonication exposure using two various duty cycles (20 kHz and 40 kHz). The purpose of this investigation was to monitor their payload release in order to achieve a suitable initial

burst release followed by a more regulated and sustained release profile. This chapter also showed that the percentage yield of the process was improved in order to minimise the waste of the initial materials for more accurate calculation of the entrapment efficiencies.

Section 4.5 of this chapter demonstrated that different morphological structures can be obtained using two different EHD/TIPS processes. The SEM images exhibited more surface porosity of the co-axial needle microspheres with hollow internal structure compared to the single needle products. This was attributed to use of DMC in the inner and the outer needles of the co-axial EHD/TIPS system, and consequently more extraction of the solvent during lyophilisation. The EHD/TIPS process does not have any control over the size and shape of the pores on the surface or internally. However, comparison of the results between the two different EHD/TIPS process (single needle and Co-axial needle) concludes that the changes in the concentration of polymer solution can result in different size and shape of surface pores (more concentrated polymer solution provides less surface porosity and vice versa).

The results obtained from the EDX studies (**Section 4.6**) showed that the active dyes were entrapped in the matrix of the polymer microspheres rather than surface encapsulation. Thus, based on the morphological and *in vitro* release studies, the high initial burst release was related to the surface porosity that led to quick diffusion of the dyes encapsulated close to the surface. Considering that the encapsulated dye is not uniformly distributed within the matrix of the polymeric particles, the long period of sustained release is related to two factors: 1) decrease in the inward diffusion rate of water for dye release due to the denser polymer matrix compared to the surface area **(Figs. 4.19 and 4.20),** and 2) decrease in the concentration gradient after a high initial burst release. Therefore, each phase (burst and sustained) of the dye release had different rates of diffusion.

In **Section 4.7**, the FTIR results demonstrated the feasibility of the both EHD/TIPS methods (single needle and co-axial needle) in encapsulating the active agents and their success in not affecting biofunctionality of the materials throughout the process.

Section 4.9 of this chapter shows that the release of the encapsulated dyes from the two different fabricated products had profiles which began with a burst release phase followed by a sustained release. However, the sustained release of materials from the single needle products occurred in longer period of time compared to that of the co-axial needle products. In this section, it was found that the size distribution of particles and morphological structure (surface porosity) are the two key factors in controlling the release of the encapsulated agent. Moreover,

it was also provided that the chemical structure of the encapsulated agents play more crucial role in the release rate compared to the physical properties. Therefore, it was predicted that immunosuppressive drugs such as Cyclosporine A and Tacrolimus with high molecular weight would have release pattern similar to that of erythrosin B and/or Reichardt's due to their high resistance to absorb water. The quantification of the release studies as a part of this section provided the evidence to show that the release mechanisms of the three selected dyes, particularly for erythrosin B and pyronin B, were mostly based on Higuchi model. Therefore, it can be further predicted that the release mechanisms of Cys A and Tacrolimus with high molecular weight and very low water solubility would be based on Higuchi equation, releasing the encapsulated drug from the porous PLGA microspheres with square root of time via the combination of diffusion and the polymer degradation.

Section 4.9 also showed that the temperature can have a negative effect on the release rate of amphiphilic materials such as erythrosin B and pyronin B, and positive effect on the release rate of Reichardt's dye. Furthermore, this section demonstrated that sonication can lead to an increase in release rate of all the incorporated agents regardless of the method used for encapsulation process. The evidence provided in this section also indicated that the addition of fresh media can in general have positive affect on the release rate, leading to more dye release. Although, the application of external stimuli led to different release rates of the dyes through the course of release, it did not change the duration of the initial burst release phase.

The final part of this chapter (**Section 4.10**) indicated that the loaded microspheres lost their surface integrity and became less porous during the degradative hydrolysis of the polymer shell in their release media. However, the internal pores start to grow through the course of release studies by means of hydrolysis due to more SBF absorption of PLGA carrier.

Chapter 5

Conclusions and Future Work

5.1 Conclusions

The main objective of the research described in this thesis was to demonstrate the feasibility of the electrohydrodynamic processing as an alternative and viable technique for preparing the microspheres with the required size distribution of 150-300 µm for biomedical application, in particular, in chronic wound therapy. The next objective was to stimulate the *in vitro* release profiles of the encapsulated agents from the prepared microspheres in order to predict the release profile of toxic immunosuppressive agents such as Cyclosporine A and Tacrolimus. To fulfil this objective, three different dyes (erythrosin B, pyronin B and Reichardt's) with various chemical and physical properties were selected in order to cover the high molecular weight and low water solubility of the drugs. The *in vitro* release studies were carried out at various conditions using external stimuli such as temperature and sonication to provide an optimum release profile for this particular biomedical application. The following conclusions are drawn from the extensive investigations carried out to achieve these objectives.

5.1.1 Mode Mapping of PCL and PLGA Particles Using Single Needle EHD Processing

Biodegradable PCL and PLGA polymeric microspheres with various size distributions were produced using single needle EHD technique. A method of microsphere fabrication providing systematic variation of size and size distribution has been demonstrated at ambient temperature and pressure, with adjusting applied voltage, flow rate and polymeric concentrations serving as the process control parameters. The range of operating parameters in terms of flow rate (for PCL/toluene varied from 20 to 50 µl/min, for PLGA/DMF and PLGA/DMAc varied from 30 to 200 µl/min and for PLGA/DMC changed from 75 to 450 µl/min) and the applied voltage (7.5-18 kV for the PCL solutions, 8.5-14 kV for PLGA/DMAc, and PLGA/DMF, and 5-7.5 kV for PLGA/DMC) along with the inherent properties of the solutions such as viscosity, surface tension and electrical conductivity were identified for the ideal processing window in obtaining the stable cone-jet. As it was stated earlier, in general, reduction in polymeric concentration of solution leads to high electrical conductivity and lower value of surface tension; therefore, less force in form of applied voltage is needed to break the surface tension of the flowing liquid to

obtain the more stable cone-jet for production of near monodisperse polymeric spheres. However, for fabrication of the required size distribution of the microspheres, more concentrated polymer solutions with higher flow rates and applied voltage were needed which in some cases led to high polydispersity of the produced particles.

Polydispersity index (PDI) was another parameter for validation of the EHD jetting modes. This parameter determines the capability of the polymer solutions in generation of near monodisperse microspheres at the stable cone-jet mode. High PDI of PLGA/DMF and PLGA/DMAc solutions demonstrate poor ability of the flowing liquids in obtaining the stable cone-jet for productions of near monodisperse particles. The high value of PDI also shows the large range of particles' size. This index with the other processed polymer solutions drops to less than 50% which in turn determines the great capability of those solutions (PLGA/DMC and PCL/toluene) for achieving the stable cone-jet mode in generating the near monodisperse microspheres. The noticeable reduction in the PDI of PLGA/DMC and PCL/toluene is attributed to the lower electrical conductivity, lower dielectric constant, moderate surface tension and viscosity of DMC and toluene compared with those of DMAc and DMF. This shows the significant impact of the physical properties on providing the stable EHD cone-jet mode for production of near monodisperse particles.

This investigation also demonstrated that the single-axial EHD technique combined with TIPS process was successful for the production of near monodisperse, porous polymeric microspheres and also developing them into particulate scaffold as drug carriers under ambient conditions (**Figs. 4.10** and **4.11**). Out of the five different types of polymer solutions (PLGA in DMF, PLGA in DMAc, PLGA in DMC, PCL10000 in toluene and PCL45000 in toluene), the combination of PLGA and DMC finally produced the required size of microspheres ranging 150-300 μm for the formation of scaffold in clinical use. Owing to the inherent properties of the solvent, the PLGA/DMC solution also overcame the undesired effects of toluene toxicity and slow biodegradation of PCL in PCL/toluene blends. The appropriate size distribution of particles with 15 wt% PLGA in DMC solution was obtained at flow rate 225 μl min^{-1} with range of voltage 6.0-7.0 kV **(Fig. 4.5c)**. Electrospray of this polymer solution in liquid nitrogen generated the desirable size distribution (150-300 μm) of microspheres for formation of the particulate scaffold, and by freeze drying the sample porous surface of the products was yielded for the purpose of better drug release. These products in the form of particulate scaffold were adopted further for drug encapsulation and the *in vitro* release studies.

5.1.2 Preparing Loaded Polymeric Carriers with the Required Size Distribution

Simple manipulation of the voltage, flow rate, collecting distance and varying polymeric concentrations during electrohydrodynamic jetting were demonstrated to provide a means of producing biodegradable PLGA drug carriers with size distribution of 150-300 µm and porous surface morphology. As it was shown, in addition to the solution properties and the processing parameters (applied voltage and flow rate), the environmental conditions such as humidity and temperature have significant impact on the size of the generated microspheres. Previously in **Sections 4.1** and **4.3**, the required size distribution of microspheres were collected with 15 wt% PLGA/DMC solution. However, due to environmental changes, the required size range of the products could not be obtained for further investigation. Increasing the viscosity of the polymer solution was found to be essential in order to obtain the required size range of the microspheres. Therefore, in **Section 4.4**, the same single needle EHD setup combined with TIPS was carried out on 17.5 wt% PLGA/DMC solutions with different processing parameters (flow rate of 400 µl/min and applied voltage of 6.5-8.5 kV) to produce the required size range of products.

5.1.3 Modification of the EHD/TIPS Processes

Based on the percentage yield of the process which was calculated 55% ± 2%, the conventional single needle EHD method combined with TIPS led to waste of approximately half the processing materials adopted during the encapsulation process. Therefore, modification was conducted in order to minimize the waste of the initial material and also enhance the accuracy in calculation of the entrapment efficiency. The percentage yield of the process after modifications was increased to 92% ± 2%, indicating small amount of initial materials loss. The co-axial needle EHD/TIPS process, which was also modified according to the single needle method, had the average percentage yield of 85% ± 3%.

Actual percentage of the dye loaded parameter was defined in **Section 3.9.2.4** in order to show the effect of modification on preserving the encapsulated materials based on the total collection of the loaded microspheres. The actual percentage of the dye loaded before optimization was found to be 53% ± 3% in average, indicating large amount of drug lost throughout the process; however, this value after modifications of the single needle and the co-axial needle EHD/TIPS processes was averaged to be 86% ± 4% and 65% ± 5%, respectively. This modification as described earlier is found to be really important in mass production for preserving the initial processing materials.

5.1.4 Production of the Loaded Microspheres by the Modified EHD/TIPS Processes

The modified single needle and the modified co-axial needle EHD/TIPS methods were carried out for production of the encapsulated polymeric microspheres. The aim was to encapsulate a second material in the polymeric carrier and stimulate the *in vitro* release profile. For the modified single needle encapsulation process, the three different polymer solutions that mixed separately with erythrosin B, pyronin B and Reichardt's were electrosprayed for production of the required size distribution of microspheres. It was found that the erythrosin B loaded microspheres had size distribution of 180 ± 30 µm, whereas the size distribution of the pyronin B loaded particles and Reichardt's loaded microspheres were 165 ± 25 µm and 100 ± 30 µm respectively. The size distribution of the produced microspheres were directly related to the physical properties of the solutions and the processing parameters.

For the modified co-axial needle process, a second solution (DMC) mixed with each dye and the polymer solution (PLGA/DMC) with same concentration as used in the modified single needle process (17.5 wt%) were adopted for encapsulation of the active agents. The average size distribution of the loaded products from the modified co-axial needle was found to be 180 ± 35 µm, which shows that the produced microspheres were slightly larger compared to their counterparts obtained from the modified single needle method.

The SEM images showed that the single needle and the co-axial needle EHD/TIPS methods produced microspheres with internal and surface porosities. As the SEM images showed, the internal structure of the single needle products was denser with the PLGA polymer compared to their surface. Comparison of the morphological structure between the products of the two methods showed that the co-axial needle EHD/TIPS process resulted in higher surface and internal porosities compared to their counterparts collected from the single needle method.

Stability of the produced microspheres loaded with various materials was carried out using FTIR. Based on the evidence provided by the FTIR spectra of the samples (**Figs. 4.22c, 4.23b** and **4.24b**), the single needle and the co-axial needle EHD/TIPS methods could successfully encapsulate the active agents (erythrosin B, pyronin B and Reichardt's) into the polymeric microspheres without affecting their chemical structures throughout the process. Moreover, the FTIR results demonstrated the capability of the EHD/TIPS process in producing stable products for long period of storage before use.

Encapsulation is a method of enclosing the therapeutic agent in protective polymeric carriers. This study confirmed the successful encapsulation of the three different model drugs in the required size distribution of the polymeric microspheres. The successful encapsulation was shown in the products obtained from both the single needle and the co-axial needle EHD/TIPS methods. In number of studies, encapsulation of various therapeutic agents were reported in PLGA particles, and in most of the cases the solvent evaporation method has been adopted as the fabrication technique. This method has some definitive disadvantages such as relatively low encapsulation efficiency, particularly in preparation of drug loaded particles in nano scale, defunctionalisation of drug under extreme processing conditions and multistep processing (**Section 2.7.1**). However, these disadvantages were minimised and bio-safe products with complete extraction of solvent were obtained with using the EHD method combined with TIPS.

5.1.5 *In Vitro* Release Studies of the Loaded Microspheres Produced by the Modified EHD/TIPS Methods

The *in vitro* release profiles of the three model drugs (erythrosin B, pyronin B and Reichardt's) loaded in the TIPS microspheres were studied. It was observed that the release of the model drugs was time-dependant and all the release profiles started with an initial burst release followed by a period of sustained release. During the sustained release, the release rate for all the samples increased as biodegradation of the polymer particles took place via hydrolysis and the internal structure would be expected to contain higher concentration of the incorporated materials. Release of the encapsulated materials from the PLGA matrix occurs with diffusion of dye during the early phases, and then it is mediated through both diffusion of the therapeutic agents and degradation of the polymer carrier at the later stages.

The results from the EDX studies showed that the active dyes were entrapped in the matrix of the polymer microspheres rather than surface encapsulation. Thus, the high initial burst release was related to the surface porosity that led to quick diffusion of the dyes encapsulated close to the surface. Since, the encapsulated dye is not uniformly distributed within the matrix of the polymeric particles, the long period of sustained release is related to two main factors: 1) decrease in the inward diffusion rate of water for dye release due to the denser polymer matrix compared to the surface area **(Figs. 4.19 and 4.20),** and 2) decrease in the concentration gradient after a high initial burst release. Therefore, each phase (burst and sustained) of the dye release had different rates of diffusion. The *in vitro* release studies showed that the loaded microspheres produced by the modified single needle process had longer period of sustained

release compared to that of their counterparts obtained from the modified co-axial needle setup. According to the SEM images, this was attributed to the less surface and internal porosity of the produced microspheres from the modified single needle EHD/TIPS method compared to their counterparts collected from the modified co-axial EHD/TIPS setup. Moreover, the SEM combined with EDX studies provided the evidence that incorporation of the dyes by the single needle process occurred in the polymer matrix and the layers near the surface of the microspheres **(Fig. 4.19)**, whereas with the co-axial needle method, internal cavity was obtained that indicates the phase separation of the agent encapsulation from the polymer matrix **(Fig. 4.20)**.

Use of three different model drugs was to predict the stimulation release of immunosuppressive agents such as Cyclosporine A and Tacrolimus. The selection of these three dyes was based on the chemical property of their water solubility and physical properties such as molecular weight similar to the actual drugs. Comparison of the *in vitro* release studies showed that chemical properties of active agents such as water solubility (hydrophobicity) have much greater effect on the release profile compared to the physical properties such as molecular weight. Therefore, it was predicted that the release profile of the actual drugs would be similar to that of the erythrosin B or Reichardt's dyes. The quantification of the release studies provided the evidence to show that the release mechanisms of the three selected dyes, particularly for erythrosin B and pyronin B, were mostly based on Higuchi equation. Therefore, it can be further predicted that the release mechanisms of the immunosuppressants such as Cys A and Tacrolimus with high molecular weight and low water solubility would be based on Higuchi equation, releasing the encapsulated drug from such porous polymeric microspheres with square root of time via the combination of diffusion and the polymer degradation.

5.1.6 Studying the Effect of Particles Size and Morphology on the Burst Release

The particle size and the surface morphology are the two key factors in initial burst release phase. Particles with different dimensions will have different surface areas and thus have different total surface available for drug release. Moreover, this phase of release is also related to the surface porosity, as the initial burst release is commonly attributed to the release of the drug loaded close to the surface of particles. The initial burst release of the dyes was faster from the single needle products compared to the co-axial needle products. This was highly related to the quicker diffusion of the dyes incorporated in the layers close to the surface area of the microspheres.

In case of Reichardt's, the required size distribution of the microspheres was not achieved for the dye loaded microspheres obtained from the single needle method. Moreover based on the SEM images, the Reichardt's loaded microspheres had greater surface porosity compared to the other loaded microspheres from the single needle products. Therefore, the high initial burst release of this dye compared to that of the other two dyes, apart from using ethanol in the release media, could also be related to the higher surface porosity and greater surface encapsulation of Reichardt's due to the smaller surface area available in the produced microspheres.

5.1.7 Studying the Effect of Fresh Media on Release Profile

Based on the *in vitro* release studies conducted, the release profiles of pyronin B and Reichardt's entrapped in the microspheres produced by the single needle and the co-axial needle methods and also the erythrosin B release profile from the modified co-axial needle products showed higher release rate with fresh media at physiological temperature. This was due to the increase in concentration gradient that occurred between the amount of dye in the media and the remaining agent entrapped by addition of fresh media, and consequently led to more release of the dye via diffusion. However, less percentage release of erythrosin B from the single needle product with addition of fresh media was recorded compared to that of the physiological temperature without fresh media. Since, erythrosin B has lower water solubility compared to other hydrophilic materials such as pyronin B, this could be simply related to the dilution of the small amount of released dye with the new fresh media.

Comparison of the *in vitro* release studies at physiological temperature with fresh media showed no significant difference in the release pattern of the dyes encapsulated by means of two different methods (the single needle and the co-axial needle). However, more percentage release of the dyes was in general achieved with the single needle encapsulation method compared to the co-axial needle setup due to longer period of release.

5.1.8 Studying the Effect of Temperature on Release Profile

Effect of temperature was investigated on the release profiles of the encapsulated agents in order to stimulate an optimum profile with more controlled release. It was shown that increase in temperature in general resulted in lower release rate of the amphiphilic materials (erythrosin B and pyronin B) compared to that of the normal conditions. This was highly related to number

of factors such as quicker degradation and/or higher evaporation of the dyes in aqueous solutions at physiological temperature (37 ± 1^{o}C) over the course of release studies. However, the lower release rate in biological temperature was slightly compensated by using 2ml addition of fresh media in the release media, but still lower release rate was observed compared to that of the normal temperature. In case of Reichardt's dye, since it is hydrophobic, it could not be degraded in aqueous solution (release media) and/or evaporated by heat as observed throughout the *in vitro* release studies. Therefore, the positive effect of release rate was observed in physiological temperature (37 ± 1^{o}C) compared to the normal condition (22 ± 2^{o}C) in both the single needle and co-axial needle products. Moreover, the higher release rate was even observed with addition of fresh media in physiological temperature.

5.1.9 Studying the Effect of Sonication on Release Profile

This further investigation was carried out to study the effect of the different sonication parameters such as duty cycle and exposure time with the purpose of obtaining more efficient release profile. The sonication systematic exposure was conducted on the loaded PLGA microspheres at two different frequencies of 20 kHz for 30 s and 40 kHz for 20 s. The release profiles were noticeably affected by having the loaded microspheres exposed to the sonicator. It was related to the formation of the gas or vapour filled bubbles in the medium exposed to the sonication as the main mechanism for increasing the release rate of the incorporated dyes. This increase was observed for all the samples exposed to sonication in physiological temperature. The effect of sonication on release rate of the dyes from the co-axial needle microspheres was greater compared to that of the single needle products. The *in vitro* release studies also showed that exposure of samples to sonication did not influence the duration of the initial burst release but it led to higher release rate with shorter period of sustained release (**Figs. 4.25-4.27**). Moreover, the results demonstrated that the sonication with higher frequency led to more increase of dye release compared to less frequency with longer period. This is due to more intensive bubbles produced by higher frequency which in turn damage the microsphere surface and its structure, inducing more dye release (Enayati et al., 2010a; Nyborg, 2001).

5.2 Future Work

The synthesised polymeric particles should ideally have the following features: high loading efficiency, controlling drug distribution and release characteristics, uniform size and shape. The applied processing technique should be able to produce these features, and also be efficient in terms of time and material usage, convenient and easily scalable. The EHD forming techniques have demonstrated great promise in terms of these criteria offering a versatile capability for the generation of nearly uniform loaded microspheres. In this thesis, it was demonstrated that the EHD methods can achieve near uniform dispersion of drug within a polymer matrix of the products with high loading capacity and minimal drug loss. However, there are several aspects of future work recommended as follows:

5.2.1 Effect of Needle Geometry on the EHD Processing

The geometry of a needle is one of the important factors for the applied electric field in the EHD processing. However, to the best of the author's knowledge, there are only few documents to systematically demonstrate the influence of needle geometry within the research work of EHD spraying as a vital factor for the applied electric field which is a driving force for the liquid to form the cone-jet mode. Most of the previously discussed investigations were based on the regular geometry of the capillary with brief explanation of its influence on the cone-jet domain (Chen et al., 1999). Therefore, further investigations are required to be conducted to assess the effects of irregular needle geometry such as tip angle, length and shape on the stable cone-jet domain, in which the cone-jet mode can be achieved and maintained for long period of mass production.

5.2.2 Encapsulation of Different Therapeutic Agents

Effective drug delivery strategies for different biomedical applications are becoming more significant as more specific drugs become available with growing knowledge about diseases from human and genome project. All therapeutic agents would require tailored drug delivery system and targeting mechanisms to deliver them to their specific target tissue without influencing their therapeutic efficacy. In this research, it was demonstrated that biodegradable spherical particles could be prepared with high encapsulation efficiency for chronic wound therapy. The encapsulation process was conducted on various model drugs with different physical and chemical properties, aiming to predict the *in vitro* release profile of actual drugs. Since, working with immunosuppressive drugs can be hazardous, this investigation should be

conducted in a wider range of model drugs to cover the variety of the existing immunosuppressive agents for different biomedical applications.

5.2.3 Cell Study for the Prepared Microspheres

Spheres are a potential useful drug delivery system with ability of delivering the therapeutic agent in a sustained release profile. These particles can be used for different applications in biomedicine depending on their dimensions. For example, nano size particles are very important for their great efficiency of arterial uptake (Song et al., 1998) and cellular entry (Desai et al., 1997), whereas micro size particles are useful for targeted delivery (Monsky et al., 1999) and wound therapy within tissue (Keshaw et al., 2010). In this study, loaded PLGA microspheres with size distribution of 150-300 μm were successfully produced and the *in vitro* release studies showed an efficient drug release profile for this particular biomedical application. However, the mechanism of enhanced therapeutic efficacy of the drug loaded microspheres should be conducted at tissue level. For instance, further research can be conducted on the behaviour of the packs of microspheres and their reactions at tissue level, their trafficking and sorting into different intracellular compartment.

5.2.4 Effect of Morphology on Various *In Vitro* Parameters

Recently, there has been growing recognitions that particles with surface porosity play an important role in various applications such as chronic wound therapy. The surface morphology influence the effectiveness of drug delivery system. In this thesis, it was shown that the drug carriers of this particular morphology could be obtained through different combinations of processing parameters and physical properties of the solutions. This specific morphological structure was different between the two types of produced microspheres obtained from the various EHD/TIPS methods (the single needle and the co-axial needle). Also, it was shown that this morphological structure (surface porosity) influenced the *in vitro* release profiles of the encapsulated dyes. A more systematic investigation should be carried out assessing the effectiveness of the surface porosity on the release profile of the incorporated materials and discover an optimum surface porosity on the required size distribution of particles for an optimum drug delivery with more sustained release phase. Apart from the *in vitro* release studies, other *in vitro* investigations such as biocompatibility, clearance and targeting of these particles are required to fully understand the factors determining the effectiveness of these

particles. For instance, the dependence of phagocytosis by macrophages on shape and aspect ratio, the internalisation of spherical particles and their bio distribution should be studied.

5.2.5 Effect of Dimensions in Tissue Engineering

Tissue engineering has emerged as a viable alternative to the problem of organ and tissue shortage. The use of the fabricated PLGA microspheres in this study within the required size distribution and surface porosity as scaffold materials for the growth of cells for tissue engineering is an emerging area for applications in medial engineering (Botchwey et al., 2004). As the *in situ* deposition study (**Section 3.11**) showed, the produced microspheres had tendency of settling down at the bottom of the created irregular shaped cavity within tissue. Further research is required to investigate the *in situ* deposition of the microspheres similar to the *in vitro* and *in vivo* cases for the chronic wound therapy.

5.2.6 Preparation of Multilayer Microspheres

The potential capability of EHD processing has attracted the researchers in this field for preparation of multi-layered micro- and nano-particles for various applications in food engineering, drug delivery and biomedicine research. The multi-layered structure can enhance the capability of the products for successful penetrating the body's immune system and efficiently carrying the therapeutic agents to their intended sites. Each layer can be systematically designed for a specific reason, which can meet and overcome the physiological barriers encountered as it moves through the body.

The produced microspheres in this study can be prepared in multi-layered structure with each layer loaded for a particular purpose. The four layered structure which was carried out for the first time by Labbaf et al. (2014) can be further improved based on more appropriate selection of materials for better encapsulation of the active agents with more controlled release. The further work can be related to preparation of multi-layered porous surface micro- and/or nano-spheres for a wider range of biomedical applications.

5.2.7 Targeted Drug Delivery via Bioconjugation

The EHD processing can be employed to produce bioconjugated polymeric carriers for targeted drug delivery. One of the more important applications of such targeted drug delivery system is for cancer therapy. For cancer drug delivery, experience, skill and knowledge from various

technologies such as nanotechnology and advanced polymer chemistry are required to bring together new ways of developing such drug delivery system. Using monoclonal antibodies (MAbs) is one of the methods which can be applied for development of such drug delivery. PLGA polymeric particles can be used for site-specific drug delivery by incorporation of appropriate targeting groups of antitumor monoclonal antibodies. Therefore, further research can be conducted for delivering the anticancer such as radionucleotides, toxins and chemotherapeutic agents to the tumour and also preventing damage to the normal surrounding tissue.

5.2.8 Sonicator Safety

In this study, sonication was used in combination with the model drugs release. It was shown that the acoustic pressures with different applied frequencies (20 and 40 kHz) enhanced the drug release. However, understanding the safety of therapeutic sonication and the development of generalised rules that account for sonication health and safety is a crucial topic for future research activities (Madersbacher and Marberger, 2003; Nyborg, 2001).

The problem of biological response in the use of sonication for stimulating drug release should be addressed. It is likely that sonication frequencies which optimize membrane permeability are different to the frequencies that optimize drug release. Therefore, the response of cells and their membranes to sonication must be carefully considered in order to minimize or avoid the damages to the target or adjacent tissues.

Ultrasound frequencies ranged from 19.5 kHz to 10 MHz is used for various medical applications. Some applications of ultrasound with low frequencies are in angioplasty at 19.5 kHz, ocular drug delivery at 20 kHz, lipoplasty at 20-50 kHz and transdermal delivery of insulin, low-molecular weight heparin and vaccines at 20-100 kHz (Mitragotri, 2005). However, the significant clustering of applications is found in frequencies ranging from 1 to 3 MHz. This range frequencies are mostly used for medical imaging. At this range of frequencies, focusing and targeting treatments are better. Therefore, it is beneficial to develop a research area to investigate the exposure of drug carriers at higher frequencies and study their release characteristics.

5.2.9 Quantifying the *In Vitro* Release

In this study, quantification of the release studies was conducted to find and predict the release mechanism of the incorporated materials from the PLGA particles. As it was shown, the mechanism of dye release from the porous polymeric particles was based on Higuchi equation. However, the correlation coefficient for this modelling equation was not high enough to satisfy the *in vitro* release data, due to different diffusional rates for the two release phases. Therefore, more accurate mathematical modelling equations are required to consider the significant effect of surface porosity of such microspheres on the release rate, particularly on the initial burst release phase, and dissolution of the encapsulated materials into the release media.

5.2.10 Commercial Viability

A full assessment of commercial and clinical viability of the utilised techniques in this study is a crucial problem which should be considered in future work. The EHD processing has some definitive advantages compared to other existing particle fabrication techniques in terms of simplicity, efficiency, cleanliness and ambient conditions. Although in this study, it was tried to electrospray for mass production, there is still the issue of scaling up and associated cost to address, where it should be noted that EHD with single needle is a low-volume throughput process and it is not suitable or efficient for traditional industrial spraying processes. Approaches that address this problem are to use multi-nozzle or slit-nozzle systems (Almekinders and Jones, 1999; Regele et al., 2002; Snarski and Dunn, 1991). Therefore, further research can be conducted on scaling up and commercialisation via two methods: 1) scaling up the production through multiplexed microfabricated sources of spraying and 2) fabrication of miniaturised portable devices for encapsulation and delivery of drug for patient-specific needs.

References

Ahmad, Z., Zhang, H.B., Farook, U., Edirisinghe, M., Stride, E., Colombo, P., 2008. Generation of multilayered structures for biomedical applications using a novel tri-needle coaxial device and electrohydrodynamic flow. J. R. Soc. Interface 5, 1255–1261.

Almekinders, J.C., Jones, C., 1999. Multiple jet electrohydrodynamic spraying and applications. J. Aerosol Sci. 30, 969–971.

Amsden, B.G., Goosen, M.F.A., 1997. An examination of factors affecting the size, distribution and release characteristics of polymer microbeads made using electrostatics. J. Control. Release 43, 183–196.

Arshady, R., 1989. Microspheres and microcapsules: A survey of manufacturing techniques. Part 1: Suspension cross-linking. Polym. Eng. Sci. 29, 1746–1758.

Arshady, R., 1990. Microspheres and microcapsules, a survey of manufacturing techniques: Part III: Solvent evaporation. Polym. Eng. Sci. 30, 915–924.

Arshady, R., 1991. Preparation of biodegradable microspheres and microcapsules: 2. Polyactides and related polyesters. J. Control. Release 17, 1–21.

Arya, N., Chakraborty, S., Dube, N., Katti, D.S., 2009. Electrospraying: a facile technique for synthesis of chitosan-based micro/nanospheres for drug delivery applications. J. Biomed. Mater. Res. B. Appl. Biomater. 88, 17–31.

Asiyanbola, B., Soboyejo, W., 2008. For the surgeon: an introduction to nanotechnology. J. Surg. Educ. 65, 155–161.

Augustin, M., Maier, K., 2003. Psychosomatic Aspects of Chronic Wounds. Dermatology Psychosom. / Dermatologie und Psychosom. 4, 5–13.

Avgoustakis, K., 2004. Pegylated poly(lactide) and poly(lactide-co-glycolide) nanoparticles: preparation, properties and possible applications in drug delivery. Curr. Drug Deliv. 1, 321–333.

Bangham, A.D., Standish, M.M., Watkins, J.C., 1965. Diffusion of univalent ions across the lamellae of swollen phospholipids. J. Mol. Biol. 13, 238–252.

Barisci, J.., Liu, L., Strounina, E.., Wallace, G.., 2000. Factors affecting the yield of polypyrrole colloids produced under electrohydrodynamic conditions. Colloids Surfaces A Physicochem. Eng. Asp. 167, 201–208.

Barnett, S.B., ter Haar, G.R., Ziskin, M.C., Nyborg, W.L., Maeda, K., Bang, J., 1994. Current status of research on biophysical effects of ultrasound. Ultrasound Med. Biol. 20, 205–218.

Barreiro-Iglesias, R., Alvarez-Lorenzo, C., Concheiro, A., 2003. Controlled release of estradiol solubilized in carbopol/surfactant aggregates. J. Control. Release 93, 319–330.

Batycky, R.P., Hanes, J., Langer, R., Edwards, D.A., 1997. A theoretical model of erosion and macromolecular drug release from biodegrading microspheres. J. Pharm. Sci. 86, 1464–1477.

Benoit, M.-A., Baras, B., Gillard, J., 1999. Preparation and characterization of protein-loaded poly(ε-caprolactone) microparticles for oral vaccine delivery. Int. J. Pharm. 184, 73–84.

Berkland, C., Pack, D.W., Kim, K.K., 2004. Controlling surface nano-structure using flow-limited field-injection electrostatic spraying (FFESS) of poly(D,L-lactide-co-glycolide). Biomaterials 25, 5649–5658.

Bertling, J., Blömer, J., Kümmel, R., 2004. Hollow Microsperes. Chem. Eng. Technol. 27, 829–837.

Bhargava, P., Zheng, J.X., Li, P., Quirk, R.P., Harris, F.W., Cheng, S.Z.D., 2006. Self-Assembled Polystyrene- b lock -poly(ethylene oxide) Micelle Morphologies in Solution. Macromolecules 39, 4880–4888.

Blaker, J., Knowles, J., Day, R., 2008a. Novel fabrication techniques to produce microspheres by thermally induced phase separation for tissue engineering and drug delivery. ACTA BIOMATER 4, 264–272.

Blaker, J., Pratten, J., Ready, D., Knowles, J., Forbes, A., Day, R.M., 2008b. Assessment of antimicrobial microspheres as a prospective novel treatment targeted towards the repair of perianal fistulae. Aliment. Pharmacol. Ther. 28, 614–622.

Blanco-Príeto, M.J., Campanero, M.A., Besseghir, K., Heimgatner, F., Gander, B., 2004. Importance of single or blended polymer types for controlled in vitro release and plasma levels of a somatostatin analogue entrapped in PLA/PLGA microspheres. J. Control. Release 96, 437–448.

Boas, U., Heegaard, P.M.H., 2004. Dendrimers in drug research. Chem. Soc. Rev. 33, 43–63.

Botchwey, E.A., Pollack, S.R., Levine, E.M., Johnston, E.D., Laurencin, C.T., 2004. Quantitative analysis of three-dimensional fluid flow in rotating bioreactors for tissue engineering. J. Biomed. Mater. Res. A 69, 205–215.

Brannon-peppas, L., 1997. Polymers in Controlled Drug Delivery. Med. Plast. magezine, 35-45.

Brazel, C.S., Peppas, N.A., 1999. Recent studies and molecular analysis of drug release from swelling-controlled devices. STP Pharma Sci. 9, 473–485.

Brennen, C.E., 1995. Cavitation and Bubble Dynamics. Oxford University Press, New York, 282-300.

Buchanan, G.N., Bartram, C.I., Phillips, R.K.S., Gould, S.W.T., Halligan, S., Rockall, T.A., Sibbons, P., Cohen, R.G., 2003. Efficacy of Fibrin Sealant in the Management of Complex Anal Fistula. Dis. Colon Rectum 46, 1167–1174.

Bungenburg de Jong, H.G., Kaas, A.J., 1931. Zar Kennetus komplex koazeration, V. Mitteilung: relative verschiebumer im elektrischen gleichstromfeide von fllussigkeits-einschliebungen in komplex-kooazervat-tropfehen. Biochem. Z. 232, 338–345.

Burke, P.A., Klumb, L.A., Herberger, J.D., Nguyen, X.C., Harrell, R.A., Zordich, M., 2004. Poly(lactide-co-glycolide) microsphere formulations of darbepoetin alfa: spray drying is an alternative to encapsulation by spray-freeze drying. Pharm. Res. 21, 500–506.

Burlak, G., Koshevaya, S., Sanchez-Mondragon, J., Grimalsky, V., 2001. Electromagnetic eigenoscillations and fields in a dielectric microsphere with multilayer spherical stack. Opt. Commun. 187, 91–105.

Burton, K.W., Shameem, M., Thanoo, B.C., DeLuca, P.P., 2000. Extended release peptide delivery systems through the use of PLGA microsphere combinations. J. Biomater. Sci. Polym. Ed. 11, 715–729.

Cai, Q., Bei, J.Z., Wang, S.G., 2000. Study on the biocompatibility and degradation behaviour of poly(l-lactide-co-glycolide) in vitro and in vivo. Chinese J. Funct. Polym. 13, 249–254.

Calloway, D., 1997. Beer-Lambert Law. J. Chem. Educ. 74, 744.

Cantor, S., 1997. Kernels of Truth. Weeks Publ. Co. Available at: http://www.foodproductdesign.com/articles/1997/04/kernels-of-truth.aspx (accessed 12.27.13).

Carrasquillo, K.G., Stanley, A.M., Aponte-Carro, J.C., De Jésus, P., Costantino, H.R., Bosques, C.J., Griebenow, K., 2001. Non-aqueous encapsulation of excipient-stabilized spray-freeze dried BSA into poly(lactide-co-glycolide) microspheres results in release of native protein. J. Control. Release 76, 199–208.

Cavrini, V., Di Pietra, A.M., Gatti, R., 1989. Analysis of miconazole and econazole in pharmaceutical formulations by derivative UV spectroscopy and liquid chromatography (HPLC). J. Pharm. Biomed. Anal. 7, 1535–1543.

Challen, G.A., Boles, N., Lin, K.K.-Y., Goodell, M.A., 2009. Mouse hematopoietic stem cell identification and analysis. Cytometry. A 75, 14–24.

Champion, J.A., Mitragotri, S., 2006. Role of target geometry in phagocytosis. Proc. Natl. Acad. Sci. U. S. A. 103, 4930–4934.

Chang, M.-W., Stride, E., Edirisinghe, M., 2009. A novel process for drug encapsulation using a liquid to vapour phase change material. Soft Matter 5, 5029-5036.

Chang, M.-W., Stride, E., Edirisinghe, M., 2010. A new method for the preparation of monoporous hollow microspheres. Langmuir 26, 5115–5121.

Chang, R.-K., Price, J.C., Whitworth, C.W., 1986. Dissolution Characteristics of Polycaprolactone-Polylactide Microspheres of Chlorpromazine. Drug Dev. Ind. Pharm. 12, 2355–2380.

Chen, C.H., Emond, M.H.J., Kelder, E.M., Meester, B., Schoonman, J., 1999. Electrostatic sol-spray deposition of nanostructured ceramic thin films. J. Aerosol Sci. 30, 959–967.

Chen, G., 2010. Degradation behavior of aliphatic biodegradable polyesters. Soc. Plast. Eng.

Chen, J., McLellan, J.M., Siekkinen, A., Xiong, Y., Li, Z.-Y., Xia, Y., 2006. Facile synthesis of gold-silver nanocages with controllable pores on the surface. J. Am. Chem. Soc. 128, 14776–14777.

Chen, X., Jia, L., Yin, X., Cheng, J., Lu, J., 2005. Spraying modes in coaxial jet electrospray with outer driving liquid. Phys. Fluids 17, 2101-2108.

Chiellini, F., Piras, A.M., Errico, C., Chiellini, E., 2008. Micro/nanostructured polymeric systems for biomedical and pharmaceutical applications. Nanomedicine (Lond). 3, 367–393.

Ciach, T., 2007. Encapsulation of proteins by Electro Hydro Dynamic Atomization. Macromol. Symp. 253, 98–102.

Clark, A.R., 1995. Medical Aerosol Inhalers: Past, Present, and Future. Aerosol Sci. Technol. 22, 374–391.

Cloupeau, M., Prunet-Foch, B., 1990. Electrostatic spraying of liquids: Main functioning modes. J. Electrostat. 25, 165–184.

Cloupeau, M., Prunet-Foch, B., 1994. Electrohydrodynamic spraying functioning modes: a critical review. J. Aerosol Sci. 25, 1021–1036.

Cohen, S., Yoshioka, T., Lucarelli, M., Hwang, L.H., Langer, R., 1991. Controlled delivery systems for proteins based on poly(lactic/glycolic acid) microspheres. Pharm. Res. 8, 713–720.

Crotts, G., Park, T.G., 1998. Protein delivery from poly(lactic-co-glycolic acid) biodegradable microspheres: release kinetics and stability issues. J. Microencapsul. 15, 699–713.

Crovetti, G., Martinelli, G., Issi, M., Barone, M., Guizzardi, M., Campanati, B., Moroni, M., Carabelli, A., 2004. Platelet gel for healing cutaneous chronic wounds. Transfus. Apher. Sci. 30, 145–151.

Dalecki, D., 2004. Mechanical bioeffects of ultrasound. Annu. Rev. Biomed. Eng. 6, 229–248.

Dash, S., Murthy, P.N., Nath, L., Chowdhury, P., 2010. Kinetic modeling on drug release from controlled drug delivery systems. Acta Pol. Pharm. 67, 217–223.

De La Mora, J.F., Loscertales, I.G., 1994. The current emitted by highly conducting Taylor cones. J. Fluid Mech. 260, 155-184.

De San Ildefonso Pereira, A., Maruri Chimeno, I., Facal Alvarez, C., Torres, J., Casal, J.E., 2002. Bacteriology of anal fistulae. Rev. Esp. Enferm. Dig. 94, 533–536.

Demir, H., Menku, P., Kirnap, M., Calis, M., Ikizceli, I., 2004. Comparison of the effects of laser, ultrasound, and combined laser + ultrasound treatments in experimental tendon healing. Lasers Surg. Med. 35, 84–89.

Deng, K.L., Zhong, H.B., Tian, T., Gou, Y.B., Li, Q., Dong, L.R., 2010. Drug release behavior of a pH/temperature sensitive calcium alginate/poly(N-acryloylglycine) bead with core-shelled structure. eXPRESS Polym. Lett. 4, 773–780.

Desai, M.P., Labhasetwar, V., Walter, E., Levy, R.J., Amidon, G.L., 1997. The Mechanism of Uptake of Biodegradable Microparticles in Caco-2 Cells Is Size Dependent. Pharm. Res. 14, 1568–1573.

Diamond Foods, 2007. Diamond Foods - Investor Relations - Press Releases. Available at: http://phx.corporate-ir.net/phoenix.zhtml?c=189398&p=irol-newsArticle&ID=1020240&highlight (accessed 3.26.14).

Ding, L., Lee, T., Wang, C.-H., 2005. Fabrication of monodispersed Taxol-loaded particles using electrohydrodynamic atomization. J. Control. Release 102, 395–413.

Edwards, J.V., Howley, P., Cohen, I.K., 2004. In vitro inhibition of human neutrophil elastase by oleic acid albumin formulations from derivatized cotton wound dressings. Int. J. Pharm. 284, 1–12.

Ekemen, Z., Ahmad, Z., Stride, E., Kaplan, D., Edirisinghe, M., 2013. Electrohydrodynamic bubbling: an alternative route to fabricate porous structures of silk fibroin based materials. Biomacromolecules 14, 1412–1422.

Enayati, M., Ahmad, Z., Stride, E., Edirisinghe, M., 2010a. One-step electrohydrodynamic production of drug-loaded micro- and nanoparticles. J. R. Soc. Interface 7, 667–675.

Enayati, M., Ahmad, Z., Stride, E., Edirisinghe, M., 2010b. Size mapping of electric field-assisted production of polycaprolactone particles. J. R. Soc. Interface 7 Suppl 4, S393–402.

Farook, U., Stride, E., Edirisinghe, M.J., 2009a. Controlling size and size distribution of electrohydrodynamically prepared microbubbles. Bubble Sci. Eng. Technol. 1, 53–57.

Farook, U., Stride, E., Edirisinghe, M.J., 2009b. Preparation of suspensions of phospholipid-coated microbubbles by coaxial electrohydrodynamic atomization. J. R. Soc. Interface 6, 271–277.

Farook, U., Stride, E., Edirisinghe, M.J., Moaleji, R., 2007. Microbubbling by co-axial electrohydrodynamic atomization. Med. Biol. Eng. Comput. 45, 781–789.

Fatemi, M., Greenleaf, J.F., 1998. Ultrasound-stimulated vibro-acoustic spectrography. Science 280, 82–85.

Ferrara, K.W., 2008. Driving delivery vehicles with ultrasound. Adv. Drug Deliv. Rev. 60, 1097–1102.

Finkel, R., Cubeddu, L.X., Clark, M.A., 2009. Pharmacology. Lippincott Williams & Wilkins, Philadelphia, 1–15.

Folkman, J., Long, D.M., 1964. The use of silicone rubber as a carrier for prolonged drug therapy. J. Surg. Res. 4, 139–142.

Foxall, K., 2007. Toluene toxicological overview, Health protection agency. Available at: http://www.hpa.org.uk/webc/hpawebfile/hpaweb_c/1194947395545 (accessed 3.26.14).

Freitas, S., Merkle, H.P., Gander, B., 2005. Microencapsulation by solvent extraction/evaporation: reviewing the state of the art of microsphere preparation process technology. J. Control. Release 102, 313–332.

Fu, K., Pack, D.W., Klibanov, A.M., Langer, R., 2000. Visual Evidence of Acidic Environment Within Degrading Poly(lactic-co-glycolic acid) (PLGA) Microspheres. Pharm. Res. 17, 100–106.

Fujiwara, M., Shiokawa, K., Kubota, T., 2012. Direct encapsulation of proteins into calcium silicate microparticles by water/oil/water interfacial reaction method and their responsive release behaviors. Mater. Sci. Eng. C 32, 2484–2490.

Fukushima, S., Kishimoto, S., Takeuchi, Y., Fukushima, M., 2000. Preparation and evaluation of o/w type emulsions containing antitumor prostaglandin. Adv. Drug Deliv. Rev. 45, 65–75.

Gañán-Calvo, A.M., 1997. On the theory of electrohydrodynamically driven capillary jets. J. Fluid Mech. 335, 165–188.

Gañán-Calvo, A.M., Dávila, J., Barrero, A., 1997. Current and droplet size in the electrospraying of liquids. Scaling laws. J. Aerosol Sci. 28, 249–275.

Gaponik, N., Radtchenko, I.L., Sukhorukov, G.B., Rogach, A.L., 2004. Luminescent Polymer Microcapsules Addressable by a Magnetic Field. Langmuir 20, 1449–1452.

Gaumet, M., Gurny, R., Delie, F., 2007. Fluorescent biodegradable PLGA particles with narrow size distributions: preparation by means of selective centrifugation. Int. J. Pharm. 342, 222–230.

Gilbert, W., 1600. De Magnete, Magneticisque Corporibus, et de Magno Magnete Tellure (On the Magnet and Magnetic Bodies, and on That Great Magnet the Earth), 1st editio. ed. Peter Short, London, 1544-1603.

Göpferich, A., 1996. Mechanisms of polymer degradation and erosion. Biomaterials 17, 103–114.

Gratton, S.E.A., Pohlhaus, P.D., Lee, J., Guo, J., Cho, M.J., Desimone, J.M., 2007. Nanofabricated particles for engineered drug therapies: a preliminary biodistribution study of PRINT nanoparticles. J. Control. Release 121, 10–18.

Green, B.K., 1955. Pressure sensitive record material, US Pat. 2,712,507.

Green, B.K., Schleicher, L., 1957. Oil-containing microscopic capsules and method of making them, US Pat. 2,800,457.

Grossman, J., 1994. The evolution of inhaler technology. J. Asthma 31, 55–64.

Guan, G., Zhang, Z., Wang, Z., Liu, B., Gao, D., Xie, C., 2007. Single-Hole Hollow Polymer Microspheres toward Specific High-Capacity Uptake of Target Species. Adv. Mater. 19, 2370–2374.

Gupta, S., Zhang, Q., Emrick, T., Russell, T.P., 2006. "Self-corralling" nanorods under an applied electric field. Nano Lett. 6, 2066–2069.

Hartman, R.P.., Borra, J.-P., Brunner, D.., Marijnissen, J.C.., Scarlett, B., 1999. The evolution of electrohydrodynamic sprays produced in the cone-jet mode, a physical model. J. Electrostat. 47, 143–170.

Hartman, R.P.A., Brunner, D.J., Camelot, D.M.A., Marijnissen, J.C.M., Scarlett, B., 2000. Jet break-up in electrohydrodynamic atomization in the cone-jet mode. J. Aerosol Sci. 31, 65–95.

Hartman, R.P.A., Brunner, D.J., Marijnissen, J.C.M., Scarlett, B., 1998. Scaling laws for droplet size and current produced in the cone-jet mode. J. Aerosol Sci. 29, S977–S978.

Hawley, P.R., 1975. Anorectal fistula. Clin. Gastroenterol. 4, 635–649.

Hayati, Bailey, Tadros, 1987a. Investigations into the mechanisms of electrohydrodynamic spraying of liquids. Pt. I. Effect of electric field and the environment on pendant drop and factors affecting the formation of stable jets and atomisation. J. Colloid Interface Sci. 117, 205–221.

Hayati, Bailey, Tadros, 1987b. Investigations into the mechanisms of electrohydrodynamic spraying of liquids. Pt. II. Mechanism of stable jet formation and electrical forces acting on a liquid cone. J. Colloid Interface Sci. 117, 222–230.

Hilder, T.A., Hill, J.M., 2008. Carbon nanotubes as drug delivery nanocapsules. Curr. Appl. Phys. 8, 258–261.

Hombreiro Pérez, M., Zinutti, C., Lamprecht, A., Ubrich, N., Astier, A., Hoffman, M., Bodmeier, R., Maincent, P., 2000. The preparation and evaluation of poly(ϵ-caprolactone) microparticles containing both a lipophilic and a hydrophilic drug. J. Control. Release 65, 429–438.

Hou, S., Man, K.Y.K., Chan, W.K., 2003. Nanosized Micelles Formed by the Self-assembly of Amphiphilic Block Copolymers with Luminescent Rhenium Complexes. Langmuir 19, 2485–2490.

Huang, X., Brazel, C.S., 2001. On the importance and mechanisms of burst release in matrix-controlled drug delivery systems. J. Control. Release 73, 121–136.

Hughes, L.E., 1978. Surgical pathology and management of anorectal Crohn's disease. J. R. Soc. Med. 71, 644–651.

Ijsebaert, J.C., Geerse, K.B., Marijnissen, J.C., Lammers, J.W., Zanen, P., 2001. Electro-hydrodynamic atomization of drug solutions for inhalation purposes. J. Appl. Physiol. 91, 2735–2741.

Jain, R.A., 2000. The manufacturing techniques of various drug loaded biodegradable poly(lactide-co-glycolide) (PLGA) devices. Biomaterials 21, 2475–2490.

Jalil, R., Nixon, J.R., 1990. Biodegradable poly(lactic acid) and poly(lactide-co-glycolide) microcapsules: problems associated with preparative techniques and release properties. J. Microencapsul. 7, 297–325.

Jamshidi, K., Hyon, S.-H., Ikada, Y., 1988. Thermal characterization of polylactides. Polymer (Guildf). 29, 2229–2234.

Jane, G., Carlos, D.J., Corso, R., Campos, A. De, Martins, S.M., 2010. Biodegradation of Erythrosin B Dye by Paramorphic Neurospora crassa 74A. An Int. J. Biol. Technol. 53, 473–480.

Jaworek, A., Krupa, A., 1999a. Jet and drops formation in electrohydrodynamic spraying of liquids. A systematic approach. Exp. Fluids 27, 43–52.

Jaworek, A., Krupa, A., 1999b. Classification of the modes of EHD spraying. J. Aerosol Sci. 30, 873-893.

Jayasinghe, S., Edirisinghe, M., Wilde T. De, 2002. A novel ceramic printing technique based on electrostatic atomization of a suspension. Mater. Res. Innov. 6, 92–95.

Jayasinghe, S.N., Edirisinghe, M.J., 2002. Effect of viscosity on the size of relics produced by electrostatic atomization. J. Aerosol Sci. 33, 1379–1388.

Jayasinghe, S.N., Edirisinghe, M.J., 2004. Electrostatic atomisation of a ceramic suspension. J. Eur. Ceram. Soc. 24, 2203–2213.

Jenne, J., 2001. Cavitations in biological tissues. Ultraschall Med. 22, 200–207.

Jeong, U., Im, S.H., Camargo, P.H.C., Kim, J.H., Xia, Y., 2007. Microscale fish bowls: a new class of latex particles with hollow interiors and engineered porous structures in their surfaces. Langmuir 23, 10968–10975.

Jiang, P., Hwang, K.S., Mittleman, D.M., Bertone, J.F., Colvin, V.L., 1999. Template-Directed Preparation of Macroporous Polymers with Oriented and Crystalline Arrays of Voids. J. Am. Chem. Soc. 121, 11630–11637.

Johnson, E.K., Gaw, J.U., Armstrong, D.N., 2006. Efficacy of anal fistula plug vs. fibrin glue in closure of anorectal fistulas. Dis. Colon Rectum 49, 371–376.

Jones, D., 2004. Pharmaceutical Applications of Polymers for Drug Delivery. iSmithers Rapra Publishing, Belfast. pp. 34–36.

Kalra, V., Lee, J.H., Park, J.H., Marquez, M., Joo, Y.L., 2009. Confined assembly of asymmetric block-copolymer nanofibers via multiaxial jet electrospinning. Small 5, 2323–2332.

Kaparissides, C., Alexandridou, S., Kotti, K., Chaitidou, S., 2006. Recent Advances in Novel Drug Delivery Systems. J. Nanotech. 2, 1–11.

Kawashima, Y., Serigano, T., Hino, T., Yamamoto, H., Takeuchi, H., 1998. A new powder design method to improve inhalation efficiency of pranlukast hydrate dry powder aerosols by surface modification with hydroxypropylmethylcellulose phthalate nanospheres. Pharm. Res. 15, 1748–1752.

Keshaw, H., Thapar, N., Burns, A.J., Mordan, N., Knowles, J.C., Forbes, A., Day, R.M., 2010. Microporous collagen spheres produced via thermally induced phase separation for tissue regeneration. Acta Biomater. 6, 1158–1166.

Kim, S., Kim, J.-H., Jeon, O., Kwon, I.C., Park, K., 2009. Engineered polymers for advanced drug delivery. Eur. J. Pharm. Biopharm. 71, 420–430.

Kirkegaard, T., Hansen, A., Bruun, E., Brynskov, J., 2004. Expression and localisation of matrix metalloproteinases and their natural inhibitors in fistulae of patients with Crohn's disease. Gut 53, 701–709.

Kishida, A., Murakami, K., Goto, H., Akashi, M., Kubota, H., Endo, T., 1998. Polymer Drugs and Polymeric Drugs X: Slow Release of 5-Fluorouracil from Biodegradable Poly({gamma}-Glutamic Acid) and its Benzyl Ester Matrices. J. Bioact. Compat. Polym. 13, 270–278.

Kissel, T., Li, Y.X., Volland, C., Görich, S., Koneberg, R., 1996. Parenteral protein delivery systems using biodegradable polyesters of ABA block structure, containing hydrophobic poly(lactide-co-glycolide) A blocks and hydrophilic poly(ethylene oxide) B blocks. J. Control. Release 39, 315–326.

Kohane, D.S., Tse, J.Y., Yeo, Y., Padera, R., Shubina, M., Langer, R., 2006. Biodegradable polymeric microspheres and nanospheres for drug delivery in the peritoneum. J. Biomed. Mater. Res. A 77, 351–361.

Kokubo, T., Kushitani, H., Sakka, S., Kitsugi, T., Yamamuro, T., 1990. Solutions able to reproduce in vivo surface-structure changes in bioactive glass-ceramic A-W. J. Biomed. Mater. Res. 24, 721–734.

Konishi, Y., Okubo, M., Minami, H., 2003. Phase separation in the formation of hollow particles by suspension polymerization for divinylbenzene/toluene droplets dissolving polystyrene. Colloid Polym. Sci. 281, 123–129.

Körber, M., Bodmeier, R., 2008. Development of an in situ forming PLGA drug delivery system I. Characterization of a non-aqueous protein precipitation. Eur. J. Pharm. Sci. 35, 283–292.

Kost, J., Leong, K., Langer, R., 1989. Ultrasound-enhanced polymer degradation and release of incorporated substances. Proc. Natl. Acad. Sci. U. S. A. 86, 7663–7666.

Krause, A.W., Carley, W.W., Webb, W.W., 1984. Fluorescent erythrosin B is preferable to trypan blue as a vital exclusion dye for mammalian cells in monolayer culture. J. Histochem. Cytochem. 32, 1084–1090.

Ku, B.K., Kim, S.S., 2002. Electrospray characteristics of highly viscous liquids. J. Aerosol Sci. 33, 1361–1378.

Kwon, I.C., Bae, Y.H., Kim, S.W., 1991. Electrically erodible polymer gel for controlled release of drugs. Nature 354, 291–293.

Labbaf, S., Ghanbar, H., Stride, E., Edirisinghe, M., 2014. Preparation of multilayered polymeric structures using a novel four-needle coaxial electrohydrodynamic device. Macromol. Rapid Commun. 35, 618–623.

Langer, R., 1990. New methods of drug delivery. Science 249, 1527–1533.

Langer, R., 1998. Drug delivery and targeting. Nature 392, 5–10.

Langer, R., Folkman, J., 1976. Polymers for the sustained release of proteins and other macromolecules. Nature 263, 797–800.

Lanza, G.M., Yu, X., Winter, P.M., Abendschein, D.R., Karukstis, K.K., Scott, M.J., Chinen, L.K., Fuhrhop, R.W., Scherrer, D.E., Wickline, S.A., 2002. Targeted antiproliferative drug delivery to vascular smooth muscle cells with a magnetic resonance imaging

nanoparticle contrast agent: implications for rational therapy of restenosis. Circulation 106, 2842–2847.

Larina, I. V, Evers, B.M., Ashitkov, T. V, Bartels, C., Larin, K. V, Esenaliev, R.O., 2005. Enhancement of drug delivery in tumors by using interaction of nanoparticles with ultrasound radiation. Technol. Cancer Res. Treat. 4, 217–226.

Lazar, D.A., Curra, F.P., Mohr, B., McNutt, L.D., Kliot, M., Mourad, P.D., 2001. Acceleration of recovery after injury to the peripheral nervous system using ultrasound and other therapeutic modalities. Neurosurg. Clin. N. Am. 12, 353–357.

Lee, C.C., MacKay, J.A., Fréchet, J.M.J., Szoka, F.C., 2005. Designing dendrimers for biological applications. Nat. Biotechnol. 23, 1517–1526.

Lee, J.S., Chae, G.S., Kim, M.S., Cho, S.H., Lee, H.B., Khang, G., 2004. Degradation behaviour in vitro for poly(D,L-lactide-co-glycolide) as drug carrier. Biomed. Mater. Eng. 14, 185–192.

Lee, Y., Kim, C., Jang, W., Choi, H., Jhon, M., 2001. Synthesis and electrorheological characteristics of microencapsulated polyaniline particles with melamine–formaldehyde resins. Polymer (Guildf). 42, 8277–8283.

Lentacker, I., Geers, B., Demeester, J., De Smedt, S.C., Sanders, N.N., 2010. Design and evaluation of doxorubicin-containing microbubbles for ultrasound-triggered doxorubicin delivery: cytotoxicity and mechanisms involved. Mol. Ther. 18, 101–108.

Li, S., Vert, M., 1999. Biodegradable polymers: polyesters, in: Mathowitz, E. (Ed.), Biodegradable Polymers: Polyesters. New York: John Wiley and Sons, New York, pp. 71–93.

Li, Z.-Z., Wen, L.-X., Shao, L., Chen, J.-F., 2004. Fabrication of porous hollow silica nanoparticles and their applications in drug release control. J. Control. Release 98, 245–254.

Lim, D.W., Hwang, S., Uzun, O., Stellacci, F., Lahann, J., 2010. Compartmentalization of Gold Nanocrystals in Polymer Microparticles using Electrohydrodynamic Co-Jetting. Macromol. Rapid Commun. 31, 176–182.

Lim, Y.T., Kim, J.K., Noh, Y.-W., Cho, M.Y., Chung, B.H., 2009. Multifunctional silica nanocapsule with a single surface hole. Small 5, 324–328.

Lin, D.., Kalachandra, S., Valiyaparambil, J., Offenbacher, S., 2003. A polymeric device for delivery of anti-microbial and anti-fungal drugs in the oral environment: effect of temperature and medium on the rate of drug release. Dent. Mater. 19, 589–596.

Lin, G.H.Y., Brusick, D.J., 1986. Mutagenicity studies on FD&C Red No.3. Mutagenesis 1, 253–259.

Liu, D., Yang, S., Lee, S.-T., 2008. Preparation of Novel Cuprous Oxide−Fullerene[60] Core−Shell Nanowires and Nanoparticles via a Copper(I)-Assisted Fullerene-Polymerization Reaction. J. Phys. Chem. C 112, 7110–7118.

López-Herrera, J., Barrero, A., López, A., Loscertales, I., Márquez, M., 2003. Coaxial jets generated from electrified Taylor cones. Scaling laws. J. Aerosol Sci. 34, 535–552.

Loscertales, I.G., Barrero, A., Guerrero, I., Cortijo, R., Marquez, M., Gañán-Calvo, A.M., 2002. Micro/nano encapsulation via electrified coaxial liquid jets. Science 295, 1695–1698.

Lou, X.W., Archer, L.A., Yang, Z., 2008. Hollow Micro-/Nanostructures: Synthesis and Applications. Adv. Mater. 20, 3987–4019.

Luan, X., Skupin, M., Siepmann, J., Bodmeier, R., 2006. Key parameters affecting the initial release (burst) and encapsulation efficiency of peptide-containing poly(lactide-co-glycolide) microparticles. Int. J. Pharm. 324, 168–175.

Luo, C.J., Loh, S., Stride, E., Edirisinghe, M., 2011. Electrospraying and Electrospinning of Chocolate Suspensions. Food Bioprocess Technol. 5, 2285–2300.

Luo, C.J., Stride, E., Edirisinghe, M., 2012. Mapping the Influence of Solubility and Dielectric Constant on Electrospinning Polycaprolactone Solutions. Macromolecules 45, 4669–4680.

Luo, L., Eisenberg, A., 2001. Thermodynamic Size Control of Block Copolymer Vesicles in Solution. Langmuir 17, 6804–6811.

Lyday, P.A., 2005. Iodine and Iodine Compounds, in: Ullmann's Encyclopedia of Industrial Chemistry. Wiley-VCH Verlag GmbH & Co. KGaA, Weinheim, Germany.

Madan, P.L., 1978. Microencapsulation I. Phase Separation or Coacervation. Drug Dev. Ind. Pharm. 4, 95–116.

Madersbacher, S., Marberger, M., 2003. High-energy shockwaves and extracorporeal high-intensity focused ultrasound. J. Endourol. 17, 667–672.

Mainardes, R.M., Urban, M.C.C., Cinto, P.O., Chaud, M.V., Evangelista, R.C., Gremião, M.P.D., 2006. Liposomes and micro/nanoparticles as colloidal carriers for nasal drug delivery. Curr. Drug Deliv. 3, 275–285.

Makadia, H.K., Siegel, S.J., 2011. Poly Lactic-co-Glycolic Acid (PLGA) as Biodegradable Controlled Drug Delivery Carrier. Polymers (Basel). 3, 1377–1397.

Mallapragada, S.K., Peppas, N.A., Colombo, P., 1997. Crystal dissolution-controlled release systems. II. Metronidazole release from semicrystalline poly(vinyl alcohol) systems. J. Biomed. Mater. Res. 36, 125–130.

Mallardé, D., Boutignon, F., Moine, F., Barré, E., David, S., Touchet, H., Ferruti, P., Deghenghi, R., 2003. PLGA–PEG microspheres of teverelix: influence of polymer type on microsphere characteristics and on teverelix in vitro release. Int. J. Pharm. 261, 69–80.

Marmottant, P., Hilgenfeldt, S., 2003. Controlled vesicle deformation and lysis by single oscillating bubbles. Nature 423, 153–156.

Martínez-Pérez, C.A., Olivas-Armendariz, I., Castro-Carmona, J.S., García-Casillas, P.E., 2011. Advances in Regenerative Medicine. InTech, mesico, Shanghai, 275-290.

Mathiowitz, E., Jacob, J.S., Jong, Y.S., Carino, G.P., Chickering, D.E., Chaturvedi, P., Santos, C.A., Vijayaraghavan, K., Montgomery, S., Bassett, M., Morrell, C., 1997. Biologically erodable microspheres as potential oral drug delivery systems. Nature 386, 410–414.

Mei, F., Chen, D.-R., 2007. Investigation of compound jet electrospray: Particle encapsulation. Phys. Fluids 19, 103303–103313.

Mitragotri, S., 2005. Healing sound: the use of ultrasound in drug delivery and other therapeutic applications. Nat. Rev. Drug Discov. 4, 255–260.

Mitragotri, S., Blankschtein, D., Langer, R., 1995. Ultrasound-mediated transdermal protein delivery. Science 269, 850–853.

Mitragotri, S., Lahann, J., 2009. Physical approaches to biomaterial design. Nat. Mater. 8, 15–23.

Mitschele, J., 1996. Beer-Lambert Law. J. Chem. Educ. 73, A260–261.

Miyazaki, S., Yokouchi, C., Takada, M., 1988. External control of drug release: controlled release of insulin from a hydrophilic polymer implant by ultrasound irradiation in diabetic rats. J. Pharm. Pharmacol. 40, 716–717.

Mizushige, K., Kondo, I., Ohmori, K., Hirao, K., Matsuo, H., 1999. Enhancement of ultrasound-accelerated thrombolysis by echo contrast agents: dependence on microbubble structure. Ultrasound Med. Biol. 25, 1431–1437.

Modi, S., Jain, J.P., Kumar, N., 2005. Synthesis, characterization, and degradation of poly(ester-anhydride) for particulate delivery. Isr. J. Chem. 45, 401–409.

Monsky, W.L., Fukumura, D., Gohongi, T., Ancukiewcz, M., Weich, H.A., Torchilin, V.P., Yuan, F., Jain, R.K., 1999. Augmentation of transvascular transport of macromolecules and nanoparticles in tumors using vascular endothelial growth factor. Cancer Res. 59, 4129–4135.

Moon, G.D., Jeong, U., 2008. Decoration of the Interior Surface of Hollow Spherical Silica Colloids with Pt Nanoparticles. Chem. Mater. 20, 3003–3007.

Moore, C., Promes, S.B., 2004. Ultrasound in pregnancy. Emerg. Med. Clin. North Am. 22, 697–722.

Murillo, M., Gamazo, C., Goñi, M., Irache, J., Blanco-Príeto, M., 2002. Development of microparticles prepared by spray-drying as a vaccine delivery system against brucellosis. Int. J. Pharm. 242, 341–344.

Murthy, R.S.R., 1997. Biodegradable polymers, in: Biodegradable Polymers. CBS Publisher, New Dehli, India, pp. 27–51.

Mustoe, T., 2005. Tissue repair and ulcer/wound healing: molecular mechanisms, therapeutic targets and future directions, Dermal ulcer healing: Advances in understanding. EUROCONFERENCES, Paris, France.

New Jersey department health senior services, 2011. Right to know hazerdious substance fact sheet. Available at: http://nj.gov/health/eoh/rtkweb/documents/fs/0759.pdf (accessed 3.26.14).

Nicholls, G., Heaton, N.D., Lewis, A.M., 1990. Use of bacteriology in anorectal sepsis as an indicator of anal fistula: experience in a distinct general hospital. J. R. Soc. Med. 83, 625–626.

Nihant, N., Grandfils, C., Jérôme, R., Teyssié, P., 1995. Microencapsulation by coacervation of poly(lactide-co-glycolide) IV. Effect of the processing parameters on coacervation and encapsulation. J. Control. Release 35, 117–125.

Nishiyama, N., Kataoka, K., 2003. Polymeric micelle drug carrier systems: PEG-PAsp(Dox) and second generation of micellar drugs. Adv. Exp. Med. Biol. 519, 155–177.

Nyborg, W.L., 2001. Biological effects of ultrasound: development of safety guidelines. Part II: general review. Ultrasound Med. Biol. 27, 301–333.

O'Donnell, P.B., McGinity, J.W., 1997. Preparation of microspheres by the solvent evaporation technique. Adv. Drug Deliv. Rev. 28, 25–42.

Ohtsuki, C., Aoki, Y., Kokubo, T., BANDO, Y., Neo, M., Nakamura, T., 1995. Transmission and Apatite Electron Layer Microscopic Formed Observation of Glass-Ceramic Body Fluid on Its Surface in a Simulated bonds to living bone through an apatite layer which is formed on the surface of the glass-ceramic in the body . J. Ceram. Soc. Japan 103, 449–454.

Okada, H., Toguchi, H., 1995. Biodegradable microspheres in drug delivery. Crit. Rev. Ther. Drug Carrier Syst. 12, 1–99.

Okochi, H., Nakano, M., 2000. Preparation and evaluation of w/o/w type emulsions containing vancomycin. Adv. Drug Deliv. Rev. 45, 5–26.

Okubo, M., Konishi, Y., Minami, H., 1998. Production of hollow polymer particles by suspension polymerization. Colloid Polym. Sci. 276, 638–642.

Oyane, A., Kim, H.-M., Furuya, T., Kokubo, T., Miyazaki, T., Nakamura, T., 2003. Preparation and assessment of revised simulated body fluids. J. Biomed. Mater. Res. A 65, 188–195.

Paik, N.-J., Cho, S.-H., Han, T.R., 2002. Ultrasound therapy facilitates the recovery of acute pressure-induced conduction block of the median nerve in rabbits. Muscle Nerve 26, 356–361.

Paine, M.D., Alexander, M.S., Stark, J.P.W., 2007. Nozzle and liquid effects on the spray modes in nanoelectrospray. J. Colloid Interface Sci. 305, 111–123.

Pancholi, K.P., Farook, U., Moaleji, R., Stride, E., Edirisinghe, M.J., 2008. Novel methods for preparing phospholipid coated microbubbles. Eur. Biophys. J. 37, 515–520.

Panyam, J., Labhasetwar, V., 2003. Biodegradable nanoparticles for drug and gene delivery to cells and tissue. Adv. Drug Deliv. Rev. 55, 329–347.

Pareta, R., Brindley, A., Edirisinghe, M.J., Jayasinghe, S.N., Luklinska, Z.B., 2005. Electrohydrodynamic atomization of protein (bovine serum albumin). J. Mater. Sci. Mater. Med. 16, 919–925.

Pareta, R., Edirisinghe, M.J., 2006. A novel method for the preparation of biodegradable microspheres for protein drug delivery. J. R. Soc. Interface 3, 573–582.

Park, T.G., Yong Lee, H., Sung Nam, Y., 1998. A new preparation method for protein loaded poly(D, L-lactic-co-glycolic acid) microspheres and protein release mechanism study. J. Control. Release 55, 181–191.

Parks, A.G., 1961. Pathogenesis and treatment of fistuila-in-ano. Br. Med. J. 1, 463–469.

Peng, X., Zhang, L., 2005. Surface fabrication of hollow microspheres from N-methylated chitosan cross-linked with glutaraldehyde. Langmuir 21, 1091–1095.

Pitt, C., 1990. The controlled parenteral delivery of polypeptides and proteins. Int. J. Pharm. 59, 173–196.

Pitt, W.G., Husseini, G.A., Staples, B.J., 2004. Ultrasonic drug delivery--a general review. Expert Opin. Drug Deliv. 1, 37–56.

Poliachik, S.L., Chandler, W.L., Mourad, P.D., Bailey, M.R., Bloch, S., Cleveland, R.O., Kaczkowski, P., Keilman, G., Porter, T., Crum, L.A., 1999. Effect of high-intensity focused ultrasound on whole blood with and without microbubble contrast agent. Ultrasound Med. Biol. 25, 991–998.

Prausnitz, M.R., Mitragotri, S., Langer, R., 2004. Current status and future potential of transdermal drug delivery. Nat. Rev. Drug Discov. 3, 115–124.

Ptachcinski, R.J., Venkataramanan, R., Burckart, G.J., 1986. Clinical pharmacokinetics of cyclosporin. Clin. Pharmacokinet. 11, 107–132.

Pushkar, S., Philip, A., Pathak, K., Pathak, D., 2006. Dendrimers : Nanotechnology Derived Novel Polymers in Drug Delivery. Indian J. Pharm. Educ. Res. 40, 153–158.

Rajput, M., Sharma, R., Kumar, S., Jamil, F., Sissodia, N., 2012. Pulsatile Drug Delivery System : A Review 3, 118–124.

Rangkupan, R., Reneker, D.H., 2003. Electrospinning Process of Molten Polypropylene in Vacuum. J. Met. Mater. Miner. 12, 81–87.

Rasiel, A., Sheskin, T., Bergelson, L., Domb, A.J., 2002. Phospholipid coated poly(lactic acid) microspheres for the delivery of LHRH analogues. Polym. Adv. Technol. 13, 127–136.

Rasve, G., Borade, G., Deshmukh, S., Tagalpallwar, A., 2011. Pulsatile drug delivery system: current scenario. Int. J. Pharma Bio Sci. 2, 332–343.

Ravivarapu, H.B., Lee, H., DeLuca, P.P., 2000. Enhancing initial release of peptide from poly(d,l-lactide-co-glycolide) (PLGA) microspheres by addition of a porosigen and increasing drug load. Pharm. Dev. Technol. 5, 287–296.

Rayleigh, J.W.S., 1882. On the equilibrium of liquid conducting masses charged with electricity. Philos. Mag. Ser. 5 14, 184–186.

Reddy, M., Gill, S.S., Wu, W., Kalkar, S.R., Rochon, P.A., 2012. Does this patient have an infection of a chronic wound? JAMA 307, 605–611.

Regele, J., Papac, M., Rickard, M.J., Dunn-Rankin, D., 2002. Effects of capillary spacing on EHD spraying from an array of cone jets. J. Aerosol Sci. 33, 1471–1479.

Reichardt, C., 1994. Solvatochromic Dyes as Solvent Polarity Indicators. Chem. Rev. 94, 2319–2358.

Roh, K.-H., Martin, D.C., Lahann, J., 2006. Triphasic nanocolloids. J. Am. Chem. Soc. 128, 6796–6797.

Rooney, J.A., 1970. Hemolysis Near an Ultrasonically Pulsating Gas Bubble. Science. 169, 869–871.

Salamone, J.C., 1996. Controlled Drug delivery system, in: Claypool, J. (Ed.), Polymeric Materials Encyclopedia, Twelve Volume Set. CRC Press, Florida, USA, pp. 1510–1512.

Samarasinghe, S.R., Balasubramanian, K., Edirisinghe, M.J., 2007. Encapsulation of silver particles using co-axial jetting. J. Mater. Sci. Mater. Electron. 19, 33–38.

Savic, R., Luo, L., Eisenberg, A., Maysinger, D., 2003. Micellar nanocontainers distribute to defined cytoplasmic organelles. Science 300, 615–618.

Schliecker, G., Schmidt, C., Fuchs, S., Wombacher, R., Kissel, T., 2003. Hydrolytic degradation of poly(lactide-co-glycolide) films: effect of oligomers on degradation rate and crystallinity. Int. J. Pharm. 266, 39–49.

Schmidt, W., Roessling, G., 2006. Novel manufacturing process of hollow polymer microspheres. Chem. Eng. Sci. 61, 4973–4981.

Schreier, H., Gonzalez-Rothi, R.J., Stecenko, A.A., 1993. Pulmonary delivery of liposomes. J. Control. Release 24, 209–223.

Schuppan, D., Freitag, T., 2004. Fistulising Crohn's disease: MMPs gone awry. Gut 53, 622–624.

Schwartz, D.A., Herdman, C.R., 2004. Review article: The medical treatment of Crohn's perianal fistulas. Aliment. Pharmacol. Ther. 19, 953–967.

Seow-Choen, F., Hay, A.J., Heard, S., Phillips, R.K., 1992. Bacteriology of anal fistulae. Br. J. Surg. 79, 27–28.

Setterstrom, J.A., Tice, T.R., Myers, W.E., 1984. Development of Encapsulated Antibiotics for Topical Administration to Wounds. Recent Adv. Drug Deliv. Syst. 185–198.

Sharma, R., Walker, R.B., Pathak, K., 2010. Evaluation of the Kinetics and Mechanism of Drug Release from Econazole nitrate Nanosponge Loaded Carbapol Hydrogel. Indian J. Pharm. Educ. Res. 45, 25–31.

Sheng-Tanner, X., McKerlie, C., Spaner, D., 2000. Characterization of graft-versus-host disease in SCID mice and prevention by physicochemical stressors. Transplantation 70, 1683–1693.

Shi, J., Alves, N.M., Mano, J.F., 2006. Drug release of pH/temperature-responsive calcium alginate/poly(N-isopropylacrylamide) semi-IPN beads. Macromol. Biosci. 6, 358–363.

Singh, J., Roberts, M.S., 1989. Transdermal delivery of drugs by iontophoresis: a review. Drug Des. Deliv. 4, 1–12.

Sinha, R., Kim, G.J., Nie, S., Shin, D.M., 2006. Nanotechnology in cancer therapeutics: bioconjugated nanoparticles for drug delivery. Mol. Cancer Ther. 5, 1909–1917.

Sinha, V.R., Trehan, A., 2003. Biodegradable microspheres for protein delivery. J. Control. Release 90, 261–280.

Sinha, V.R., Trehan, A., 2005. Biodegradable microspheres for parenteral delivery. Crit. Rev. Ther. Drug Carrier Syst. 22, 535–602.

Smallwood, I.M., 1996. Handbook of Organic Solvent Properties. John Wiley & Sons Inc; Spiral edition, New York, pp. 245-251.

Smith, D.P.H., 1986. The Electrohydrodynamic Atomization of Liquids. IEEE Trans. Ind. Appl. IA-22, 527–535.

Snarski, S.R., Dunn, P.F., 1991. Experiments characterizing the interaction between two sprays of electrically charged liquid droplets. Exp. Fluids 11, 268–278.

Song, C., Labhasetwar, V., Cui, X., Underwood, T., Levy, R.J., 1998. Arterial uptake of biodegradable nanoparticles for intravascular local drug delivery: results with an acute dog model. J. Control. Release 54, 201–211.

Suzuki, R., Takizawa, T., Negishi, Y., Utoguchi, N., Maruyama, K., 2007. Effective gene delivery with liposomal bubbles and ultrasound as novel non-viral system. J. Drug Target. 15, 531–537.

Swain, B.P., Pattanayak, D.K., 2008. Simulated body fluid (SBF) adsorption onto a-SiC:H thin films deposited by hot wire chemical vapor deposition (HWCVD). Mater. Lett. 62, 3484–3486.

Tamada, J.A., Langer, R., 1993. Erosion kinetics of hydrolytically degradable polymers. Proc. Natl. Acad. Sci. U. S. A. 90, 552–556.

Tang, K., Gomez, A., 1994. On the structure of an electrostatic spray of monodisperse droplets. Phys. Fluids 6, 2317-2332.

Tang, K., Gomez, A., 1995. Generation of Monodisperse Water Droplets from Electrosprays in a Corona-Assisted Cone-Jet Mode. J. Colloid Interface Sci. 175, 326–332.

Tang, K., Gomez, A., 1996. Monodisperse Electrosprays of Low Electric Conductivity Liquids in the Cone-Jet Mode. J. Colloid Interface Sci. 184, 500–511.

Taylor, G., 1964. Disintegration of Water Drops in an Electric Field. Proc. R. Soc. A Math. Phys. Eng. Sci. 280, 383–397.

Taylor, G., 1969. Electrically Driven Jets. Proc. R. Soc. A Math. Phys. Eng. Sci. 313, 453–475.

Thompson, D.R., Kougoulos, E., Jones, A.G., Wood-Kaczmar, M.W., 2005. Solute concentration measurement of an important organic compound using ATR-UV spectroscopy. J. Cryst. Growth 276, 230–236.

Tundo, P., Selva, M., 2002. The chemistry of dimethyl carbonate. Acc. Chem. Res. 35, 706–716.

Uhrich, K.E., Cannizzaro, S.M., Langer, R.S., Shakesheff, K.M., 1999. Polymeric systems for controlled drug release. Chem. Rev. 99, 3181–3198.

Umamaheswara Reddy, C., Arun, A., Amalraj, A., Reddy, B.S.R., 2007. Polymeric drug based on sulfanilamide: synthesis, antimicrobial and drug releasing studies. J. Pharm. Pharmacol. 59, 1207–1213.

Unger, E.C., Hersh, E., Vannan, M., Matsunaga, T.O., McCreery, T., 2001. Local drug and gene delivery through microbubbles. Prog. Cardiovasc. Dis. 44, 45–54.

Valo, H., Peltonen, L., Vehviläinen, S., Karjalainen, M., Kostiainen, R., Laaksonen, T., Hirvonen, J., 2009. Electrospray encapsulation of hydrophilic and hydrophobic drugs in poly(L-lactic acid) nanoparticles. Small 5, 1791–1798.

Vandervoort, J., Ludwig, A., 2002. Biocompatible stabilizers in the preparation of PLGA nanoparticles: a factorial design study. Int. J. Pharm. 238, 77–92.

Vert, M., Feijen, J., Albertson, A., Scott, G., Chiellini, E., 1992. Degradable Polymers and Plastics. Melksham Redwood Press Ltd. 73-92.

Vonarbourg, A., Passirani, C., Desigaux, L., Allard, E., Saulnier, P., Lambert, O., Benoit, J.-P., Pitard, B., 2009. The encapsulation of DNA molecules within biomimetic lipid nanocapsules. Biomaterials 30, 3197–3204.

Wang, J., Wang, B.M., Schwendeman, S.P., 2002. Characterization of the initial burst release of a model peptide from poly(D,L-lactide-co-glycolide) microspheres. J. Control. Release 82, 289–307.

Warden, S.J., 2003. A new direction for ultrasound therapy in sports medicine. Sports Med. 33, 95–107.

Weber, C., 1931. On the breakdown of a fluid jet. J. Mech. Appl. Math. 11, 136–159.

West, R.L., Van der Woude, C.J., Endtz, H.P., Hansen, B.E., Ouwedijk, M., Boelens, H.A.M., Kusters, J.G., Kuipers, E.J., 2005. Perianal fistulas in Crohn's disease are predominantly colonized by skin flora: implications for antibiotic treatment? Dig. Dis. Sci. 50, 1260–1263.

Williams, D., 2008. The relationship between biomaterials and nanotechnology. Biomaterials 29, 1737–1738.

Witschi, C., Doelker, E., 1998. Influence of the microencapsulation method and peptide loading on poly(lactic acid) and poly(lactic-co-glycolic acid) degradation during in vitro testing. J. Control. Release 51, 327–341.

Wu, J., Nyborg, W.L., 2008. Ultrasound, cavitation bubbles and their interaction with cells. Adv. Drug Deliv. Rev. 60, 1103–1116.

Wu, Y., Clark, R.L., 2007. Controllable porous polymer particles generated by electrospraying. J. Colloid Interface Sci. 310, 529–535.

Wu, Y., MacKay, J.A., McDaniel, J.R., Chilkoti, A., Clark, R.L., 2009. Fabrication of elastin-like polypeptide nanoparticles for drug delivery by electrospraying. Biomacromolecules 10, 19–24.

Wu, Y., Yu, B., Jackson, A., Zha, W., Lee, L.J., Wyslouzil, B.E., 2009. Coaxial electrohydrodynamic spraying: a novel one-step technique to prepare oligodeoxynucleotide encapsulated lipoplex nanoparticles. Mol. Pharm. 6, 1371–1379.

Xie, J., Lim, L.K., Phua, Y., Hua, J., Wang, C.-H., 2006a. Electrohydrodynamic atomization for biodegradable polymeric particle production. J. Colloid Interface Sci. 302, 103–112.

Xie, J., Marijnissen, J.C.M., Wang, C.-H., 2006b. Microparticles developed by electrohydrodynamic atomization for the local delivery of anticancer drug to treat C6 glioma in vitro. Biomaterials 27, 3321–3332.

Xie, J., Ng, W.J., Lee, L.Y., Wang, C.-H., 2008. Encapsulation of protein drugs in biodegradable microparticles by co-axial electrospray. J. Colloid Interface Sci. 317, 469–476.

Xu, Y., Hanna, M.A., 2007. Electrosprayed bovine serum albumin-loaded tripolyphosphate cross-linked chitosan capsules: synthesis and characterization. J. Microencapsul. 24, 143–151.

Xu, Y., Skotak, M., Hanna, M., 2006. Electrospray encapsulation of water-soluble protein with polylactide. I. Effects of formulations and process on morphology and particle size. J. Microencapsul. 23, 69–78.

Yamaguchi, Y., Takenaga, M., Kitagawa, A., Ogawa, Y., Mizushima, Y., Igarashi, R., 2002. Insulin-loaded biodegradable PLGA microcapsules: initial burst release controlled by hydrophilic additives. J. Control. Release 81, 235–249.

Yang, Y.Y., Chung, T.S., Ng, N.P., 2001. Morphology, drug distribution, and in vitro release profiles of biodegradable polymeric microspheres containing protein fabricated by double-emulsion solvent extraction/evaporation method. Biomaterials 22, 231–241.

Yao, J., Kuang Lim, L., Xie, J., Hua, J., Wang, C.-H., 2008. Characterization of electrospraying process for polymeric particle fabrication. J. Aerosol Sci. 39, 987–1002.

Yeo, L.Y., Gagnon, Z., Chang, H.-C., 2005. AC electrospray biomaterials synthesis. Biomaterials 26, 6122–6128.

Yin, W., Yates, M.Z., 2008. Effect of interfacial free energy on the formation of polymer microcapsules by emulsification/freeze-drying. Langmuir 24, 701–708.

Yoshida, M., Roh, K.-H., Lahann, J., 2007. Short-term biocompatibility of biphasic nanocolloids with potential use as anisotropic imaging probes. Biomaterials 28, 2446–2456.

Yoshii, H., Soottitantawat, A., Liu, X.-D., Atarashi, T., Furuta, T., Aishima, S., Ohgawara, M., Linko, P., 2001. Flavor release from spray-dried maltodextrin/gum arabic or soy matrices as a function of storage relative humidity. Innov. Food Sci. Emerg. Technol. 2, 55–61.

Yow, H.N., Routh, A.F., 2008. Colloidal buckets formed via internal phase separation. Soft Matter 4, 2080-2085.

Zbicinski, I., Smucerowicz, I., Strumillo, C., Crowe, C., 2000. Application of pulse combustion technology in spray drying process. Brazilian J. Chem. Eng. 17, 441–450.

Zeleny, J., 1917. Instability of Electrified Liquid Surfaces. Phys. Rev. 10, 1–6.

Zhang, H., Lu, Y., Zhang, G., Gao, S., Sun, D., Zhong, Y., 2008. Bupivacaine-loaded biodegradable poly(lactic-co-glycolic) acid microspheres I. Optimization of the drug incorporation into the polymer matrix and modelling of drug release. Int. J. Pharm. 351, 244–249.

Zhang, H., Zhang, J., Streisand, J.B., 2002. Oral mucosal drug delivery: clinical pharmacokinetics and therapeutic applications. Clin. Pharmacokinet. 41, 661–680.

Zhang, H.B., Jayasinghe, S.N., Edirisinghe, M.J., 2006. Electrically forced microthreading of highly viscous dielectric liquids. J. Electrostat. 64, 355–360.

Zhang, J.X., Chen, D., Wang, S.J., Zhu, K.J., 2005. Optimizing double emulsion process to decrease the burst release of protein from biodegradable polymer microspheres. J. Microencapsul. 22, 413–422.

Zhang, L., Eisenberg, A., 1996. Multiple Morphologies and Characteristics of "Crew-Cut" Micelle-like Aggregates of Polystyrene- b -poly(acrylic acid) Diblock Copolymers in Aqueous Solutions. J. Am. Chem. Soc. 118, 3168–3181.

Zhang, Y., Guan, Y., Yang, S., Xu, J., Han, C.C., 2003. Fabrication of Hollow Capsules Based on Hydrogen Bonding. Adv. Mater. 15, 832–835.

Zhu, G., Mallery, S.R., Schwendeman, S.P., 2000. Stabilization of proteins encapsulated in injectable poly (lactide- co-glycolide). Nat. Biotechnol. 18, 52–57.

Zimlich, W.C., Ding, J.Y., Busick, D.R., Moutvic, R.R., Placke, M.E., Hirst, P.H., Pitcairn, G.R., Malik, S., Newman, S.P., Macintyre, F., Miller, P.R., Shepherd, M., Lukas, T.M., 2000. The Development Of a Novel Electrohydrodynamic (EHD) Pulmonary Drug Delivery Device. Respir. Drug Deliv. VII 1, 241–246.